Functional Structure from Recycled Wind Turbine Blades

Final Report - DSE Spring 2024

25 June 2024

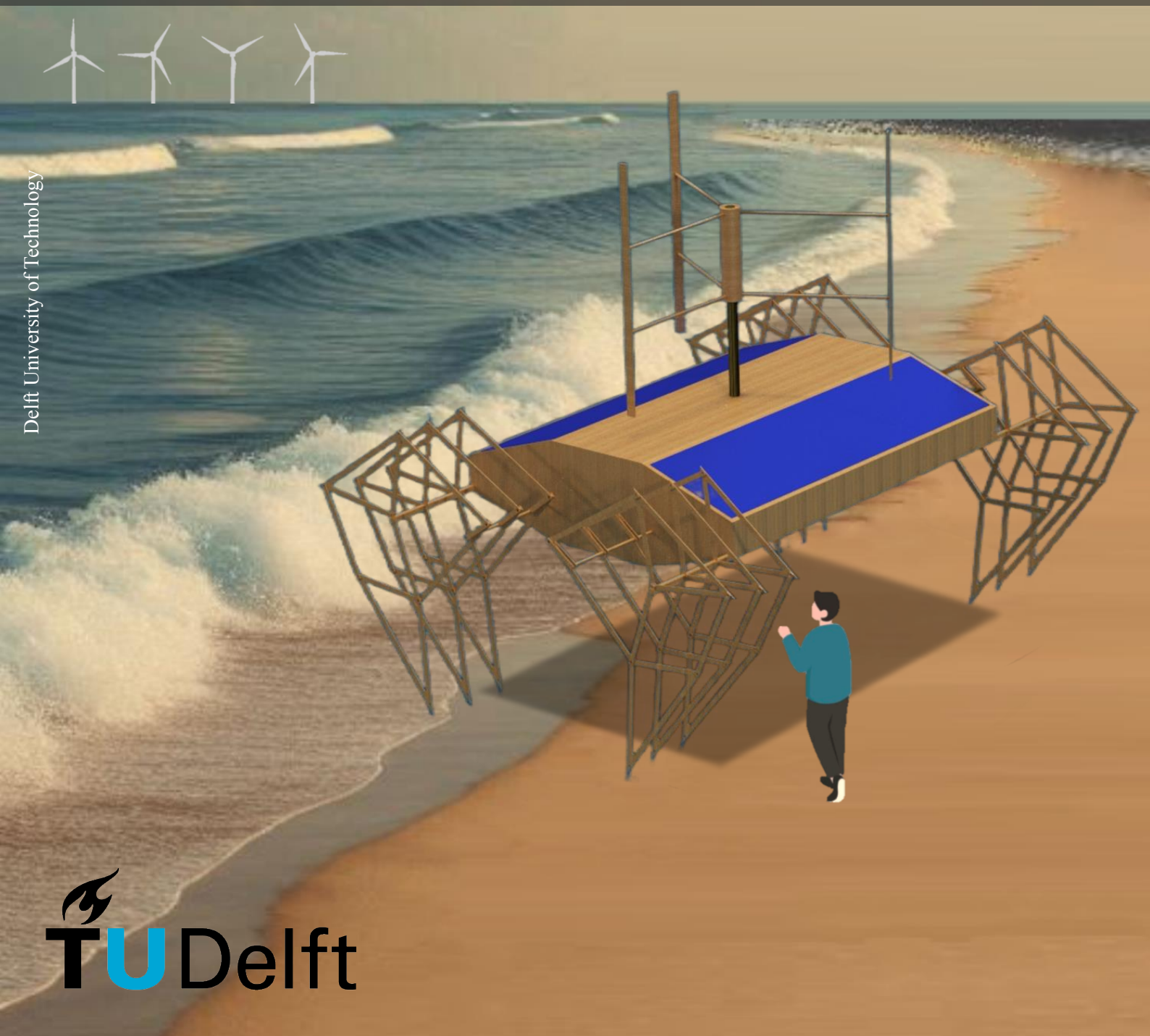

Delft University of Technology

TU Delft

This page is intentionally left blank

Functional Structure from Recycled Wind Turbine Blades

Final Report - DSE Spring 2024

Group 17

Student Name	Student Number
Thijmen God	5265762
Mariëtte de Groot	4771028
Paul Heijnen	5296447
Jedong Kim	5065488
Oliwia Książek	5582636
Alexandre Morland	5294053
Haanbee Park	5293367
Rithik Putatunda	5275105
Wei Wei	5489237
Mannes van de Winkel	5054885

Project Tutor:	Kunal Masania
Coach:	Sunyi Wang
Coach:	Hafiz Ghazali Bin Muhammad Amri
Teaching Assistent:	Al Farouk Khalil

Date:	June 25, 2024
Version:	2.0
Course:	Design Synthesis
Code:	AE3200
Faculty:	Aerospace Engineering

TU Delft

Executive Overview

Market Analysis

The increasing size of wind turbines, predicted to grow from 100 meters in 2016 to 150 meters by 2035, poses significant recycling challenges at their end of life. The use of composite materials, which are difficult and energy-intensive to recycle, exacerbates this issue. The EU is expected to produce 570 million tonnes of blade waste by 2030, and current solutions like landfill are inadequate and often banned by new legislation. Alternative solutions, such as repurposing blade sections, offer a sustainable approach but are underutilised.

The market analysis performed in this report presents the overlap of three markets, those being sustainability awareness, functional beach structures, and recycling wind turbine blades. One innovative way to raise awareness about the issues in each market is through tangible projects, such as Theo Jansen's Strandbeest, which captivates public interest.

The market for recycling wind turbine blades currently involves methods like mechanical processing, pyrolysis, and chemical processing, each with limitations. There is a growing push towards a circular economy in the wind industry, as seen with calls for a Europe-wide landfill ban by 2025. Despite that, a SWOT analysis revealed that while there is no existing market for repurposed turbine blade structures, which presents both a challenge and an opportunity.

Trade-off Summary

After the ideation phase and arriving at four straw man concepts, the team recognised that the ideas were not elegant. After consulting several professionals, the team returned to the component trade-offs to evaluate its reliability. Environmental effects were ignored, and this was considered the forefront reason for the initial doubts.

A revised trade-off method was proposed, focusing on better integration and performance in the operating environment. Previous criteria like mass, cost, and sustainability were evaluated, and new criteria emphasising the operational environment were introduced. Previous criteria were, however, not discarded, as it provided a suitable starting point for the next set of designs, whose subsystems flow from the component trade-offs. The final design trade-off considered five concepts, including a combination of the Strandbeest and Windcar, which ultimately was selected for detailed design due to its better performance across the newly defined criteria. An overview of the designs and criteria is presented in Table 1.

Table 1: Final design trade-off table. 'G' stands for good performance, 'A' for average and 'B' for bad.

Criteria / Designs	Harsh conditions	Terrain	Minimise power	Maximise material	Embodied intelligence
Sand Buggy	G	A	G	B (sail)	A
Strandbeest	A	G	B	G	G
Windcar	A	A	G	A	A
Mounted Concept	A	B (small wheels)	A (interference)	B (sail)	B
Strandbeest/Windcar	A	G	A	G	G

The selected straw man diagram under the new criteria is illustrated in Figure 1. It includes Jansen linkages for the kinematic motion, and a vertical axis wind turbine to provide power to the other subsystems, including those for movement.

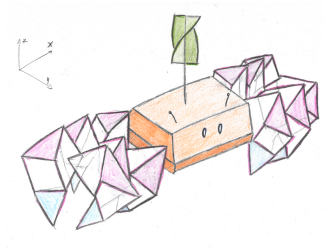

Figure 1: Selected straw man design.

Material Analysis

The objective of this material analysis is to identify the suitable material for manufacturing the next generation of wind turbine blades, focusing on its properties at the end of the blades' lifecycle.

Selecting Material for Next-Generation Wind Blades

Natural fibre-reinforced thermoplastics offer a sustainable alternative to CFRP and GFRP thermosets. They provide better end-of-life recyclability and utilise abundant natural fibres, contributing to significant CO2 reductions. Among several natural fibre options evaluated—hemp, flax, coir, and bamboo fibres—flax was chosen for its consistent mechanical properties across all criteria, as can be seen in Figure 2, making it the preferred choice for the composite.

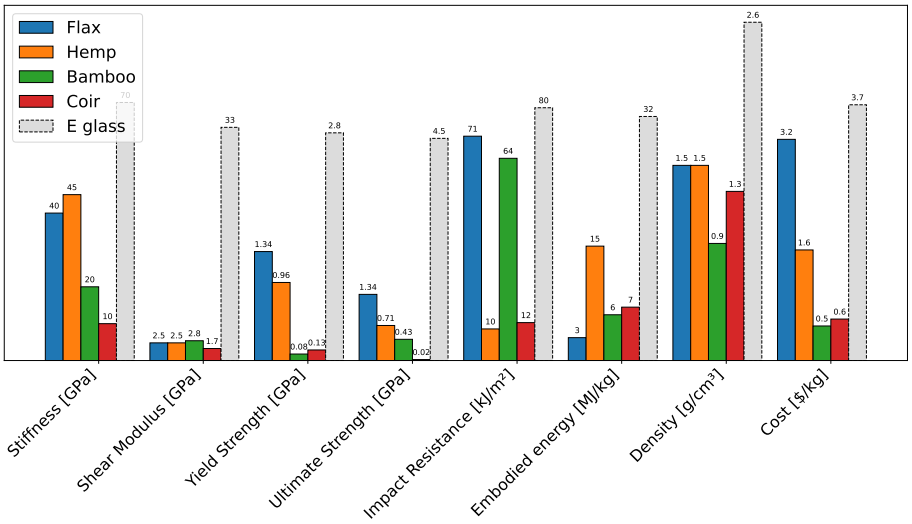

Figure 2: Properties of flax, hemp, bamboo, and coir fibres. The scales of each plot have been normalised to ensure readability. The glass fibres are shown in gray to allow for comparison although they are not natural fibres

The next step involves selecting the optimal thermoplastic. Thirteen different composites were evaluated based on criteria including melting temperature, density, water absorption properties, and mechanical strength. Polyoxymethylene (coPOM) emerged as the most favourable choice in this analysis, with a fibre fraction of 50%. This ratio is chosen because it balances the influence of both the fibres and the thermoplastic matrix on the composite's mechanical properties. It ensures proper impregnation of the fibres while maximising the overall performance of the composite.

To determine the EoL properties of the composite, the rule of mixture was first applied to establish the properties at BoL, which were then derived for EoL using regressions found in the literature.

Material Recovery and Manufacturing Techniques

This section describes the type of material that can be recovered from a wind blade as well as the manufacturing constraints associated with it.

Description of wind turbine blades

Wind turbine blades are constructed using various stacking sequences of composites tailored to specific properties. Figure 3 illustrates a typical cross-section, showcasing three common fibre orientations: unidirectional, bi-axial, and tri-axial. As a result, components extracted from wind blades retain these fibre orientations.

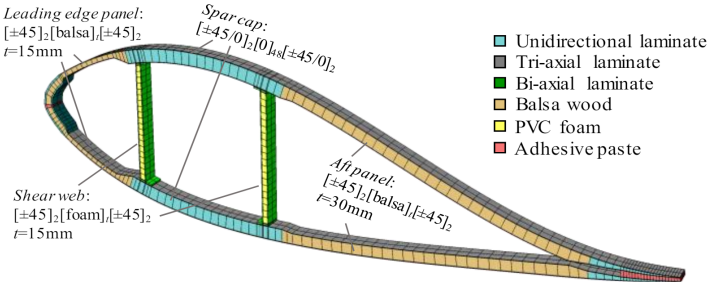

Figure 3: Cross-section of a commercially available large utility wind turbine rotor blade [1]

Parts that can be manufactured

From the extracted parts, three types of structures are sought: beams, flat panels, and airfoils. These can be produced by heating the thermoplastic to its melting temperature and then moulding it into the desired shape. To reduce thickness, panels can be cut lengthwise before moulding.

Once the manufacturable parts are determined, joining methods are investigated, encompassing both static and dynamic joints. For static joints, mechanical, adhesive, and other joining techniques are explored, weighing their respective advantages and disadvantages. The specific method to be employed remains undecided.

Regarding dynamic joints, compliant mechanisms were initially considered but were deemed unsuitable due to material constraints, significant loads, and potential fatigue issues. Instead, embedded inserts formed by melting the composite and reshaping the fibres are preferred.

Wind Model

Assuming wind speeds are normally distributed over a year, the mean velocity of $6.5 m/s$ was used to size the wind turbine. Current wind turbines are made increasingly large and positioned high above the ground. At those heights, atmospheric boundary layer effects can in large part be neglected. However, for turbines placed close to the ground such as the one in this design exercise, wind shear as a result of the ABL must be taken into account when sizing the rotors.

For the design space of the vertical axis wind turbine (3-6 m) the free stream velocity at a reference height of 10 m- the height at which most weather stations collect data- and that at the rotors can differ by as much as 23 %. The user requires a system that can operate year-long and under all weather conditions. For these reasons, it was decided to account for wind shear in the model to be sure of reliable, year-long operation as well as realistic shear and bending loads.

Wind Turbine Design

Wind turbine design was initialised with a set of trade-offs. These determined the rotor orientation (horizontal or vertical) and the rotor configuration. It was decided that a vertical axis wind turbine (VAWT) best fit the needs of the system for reasons related to sustainability including noise, maintenance, and efficiency. The high centre of gravity for horizontal axis wind turbines (HAWT) was another prominent reason for choosing a VAWT.

Concerning rotor configuration there were four options; those being V-rotor, phi-rotor, H-rotor, and helical-rotor. Manufacturability and space efficiency were deemed the most critical criteria, where the H-rotor performed the best out of all four options.

Next was the selection of the aerofoil. This was done based on literature where the DU17VAWT200 variable pitch aerofoil with a solidity of 0.1 provided the best trade-off between performance and safety.

The sizing of the turbine depended on the average wind speed and power requirement for all the subsystems. The latter derives from the user requirement stating that 60 % of power must be generated from wind energy, equalling 320 W. The sizing of the turbine follows from an iterative procedure of aspect ratio as the size depends on the height of the turbine due to wind shear effects. The sizes were determined for six different aspect ratios ranging from 0.5 to 5, all converging within 1 % in the fourth iteration.

For the same aspect ratios, the turbines were analysed for static loading; namely shear and bending moment. The wind shear phenomenon meant loads are greater closer to the tip of the turbine as illustrated in Figure 4, exemplified for the bending moments due to the addition of a moment arm. While large aspect ratio turbines require a smaller size to produce the required power, they also induce the largest loads in the supporting structure and thus do not directly translate to better overall performance.

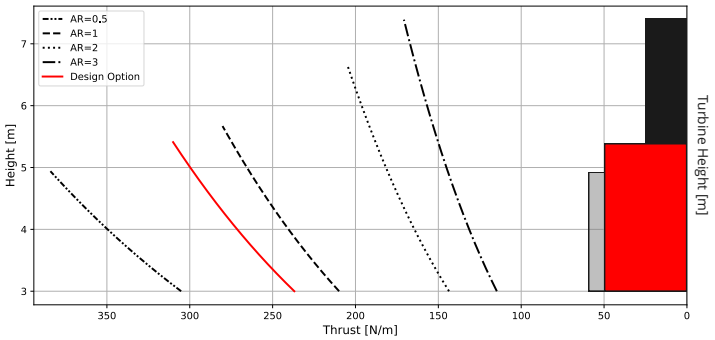

Figure 4: Internal thrust distribution at cut-out speed as a function of turbine height for different aspect ratios including the design option in red and turbine heights for illustration purposes, assuming constant thrust coefficient

The loading cases influenced the overall design of the entire structure. Determining the aspect ratio was therefore done considering the best structural performance, with aerodynamic performance considered secondary. The chosen aspect ratio was 0.8.

Rotor performance was discussed as a function of the wind speed. Several diagrams were included for the tip-speed ratio, power and thrust coefficients, power, thrust, rotational speed, and torque. The cut-in speed (3 m/s), rated speed (10 m/s), and cut-out speed (20 m/s) were important points of transition. At these points, the distribution of the power and thrust generated change as aerofoil pitch or rotational speed changes.

The aerofoil angle of attack is a function of rotational speed, incoming airspeed, and aerofoil pitch. To account for the atmospheric boundary layer, and thus non-uniform wind speeds, the aerofoil pitch had to vary over the rotor span to ensure the angle of attack remained constant. What resulted was a non-linear distribution, with a maximum relative twist of 10.4 deg. This completed the turbine design, an image of which can be found in Figure 13.

A cage for the turbine was added to ensure safety on the beach with bystanders around the system.

Kinematics

The original Jansen's linkage was modified to improve stability and step height for a walking robot. Next to that, both the crankshaft and the fixed point of the linkage are at the same height and this is beneficial when creating a platform as a body.

Steering of the structure will be done by differential steering. The structure has two electric

motors turning two crankshafts, on what the legs are attached, independently to create a turning motion. On each of the crankshafts, an electrically powered permanent magnet brake is installed to either brake in case of an emergency or to act as a parking brake.

The linkage was sized based on the step height of 30 *cm* which should be sufficient to prevent the structure from getting its legs stuck. With this step height, the crankshaft of the linkage, and thus the body, is at a height of 94 *cm* from the ground. This new sizing leads to a new power estimation for motion of 220 W.

Control and Navigation

The functional structure is required to navigate autonomously on the Dutch coast. The Dutch coast is divided into four sections by obstacles that the Strandbeest cannot traverse as shown in Figure 5. Each section would require at least one of the structures to cover the entire coastline.

To ensure that it can navigate completely autonomously, it performs path planning by using waypoints to plan a route as shown in Figure 6.

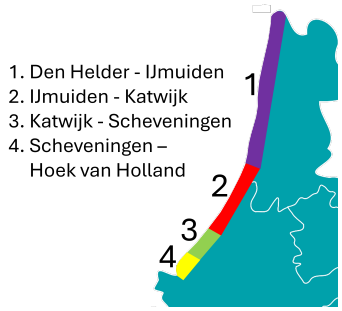

Figure 5: The Dutch coast split in four sections for deployment of the structure.

Figure 6: An example of route planning and simultaneously predetermined avoidance of the barrier.

Large and permanent obstacles can be avoided by the structure. However, it needs a live detection system for smaller temporary and mobile obstacles. For this, two LiDAR sensors are used that cover 360 degrees around the structure.

To monitor whether the weather conditions are safe and suitable to operate in, several sensors and a telecommunication system are included as well.

Power Transmission and Management

The power generated by the wind turbine and the solar panels is delivered to various output components. The list of the output components and estimated power requirement are tabulated in Table 2. The final power budget after iterations is shown in Table 3. The required power remains and the power division between power the wind turbine and solar panel stays constant, but the power available for the chosen function is increased.

Table 2: Required power per component.

Component		Power $[W]$
Control and Navigation	LiDAR	12
	GPS	0.25
	IMU	0.33
	PM brake	10
Weather data collection	Anemometer	0.03
	5G-receiver	6
Active cooling	Temperature control fan	3
	Thermometer	0.03
Motion		220

Table 3: Power budget of the entire system.

Element	Power $[W]$
Motion	210
Control and navigation	23
Weather data collection	6
Active cooling	3
Function to be performed	53
Subtotal with η_{elec} = 0.554	534
of which generated by wind turbine	320
of which generated by solar panel	213

Structural Analysis

The structural analysis is divided into three sections: analysing the body without considering the legs, analysing the legs, and evaluating the failure modes. Based on these analyses, the final structural design and manufacturing techniques were determined. Consequently, this section is organised into four parts: body analysis, leg analysis, failure mode analysis, and manufacturing.

Body Analysis

Before performing the body analysis, the structure must be idealized and the load case determined, as shown in Figure 7. With this setup, a stability analysis can be conducted to determine the necessary width of the structure to prevent tipping due to the force generated by the wind turbine. The sum of moments about the CG is plotted in Figure 8, taking into account both stability and logistic constraints. Based on this analysis, a width of 3.2 meters is chosen.

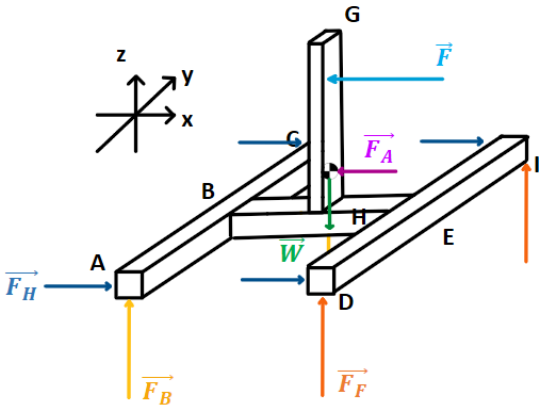

Figure 7: Free-body diagram of the body

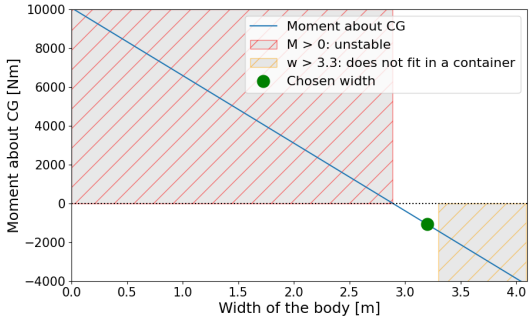

Figure 8: Sum of moments about the CG of the structure as a function of the body's width. Negative moments are stabilising.

Knowing the width of the structure allows for a detailed stress analysis. An initial analysis revealed that the configuration shown in Figure 7 is suboptimal, resulting in high bending stresses at the centre of beam BE. To better distribute the loading and reduce these stresses, the configuration depicted in Figure 9 is proposed. For this new configuration, the cross-sections of each beam were computed to ensure that the stresses in each element were adequately supported.

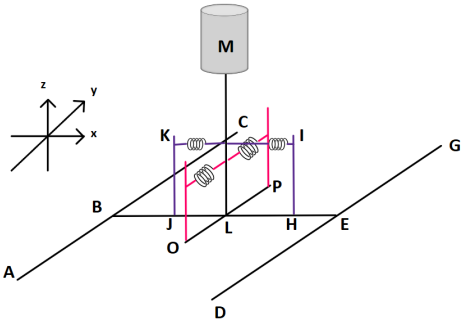

(a) New design option, including springs to damp vibrations and reduce the bending stress of beam BE. Note that the springs are not considered in this figure for clarity.

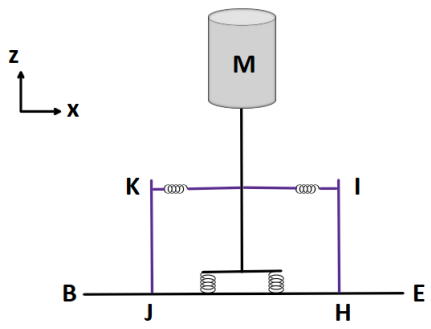

(b) Side view of the central view to display the platform used to dampen the vibrations. Note that the drawing is not to scale.

Figure 9: The new design option and its side view.

After determining the cross-sections of the beam and considering the material properties, the next step is to assess whether the configuration results in acceptable deflections. The initial deflection analysis revealed a deflection of 1.2 meters, which is not acceptable. Consequently, a maximum deflection requirement of 30 cm was established, as shown in Figure 10. Based on this requirement, a new cross-section for beam AC was found, as illustrated in Figure 11.

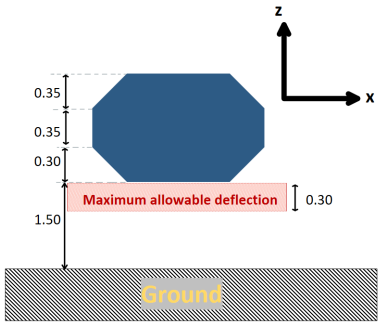

Figure 10: Free-body diagram of the body. The dimensions are provided in meters.

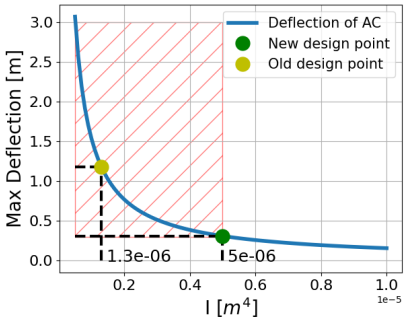

Figure 11: Sum of moments about the CG of the structure as a function of the body's width. Negative moments are stabilising.

Once all the cross-sections were determined, the tower supporting the wind turbine was designed to bear the mass of the turbine and withstand the wind loading.

Leg analysis

With the body fully sized, the next step was to analyze the legs. A stress analysis was performed on the leg model shown in Figure 12a, and a cross-section was selected to ensure that the stresses in the legs remained below the ultimate strength of 402 MPa, as demonstrated in Figure 12b. For those stresses, the joints were sized and it was demonstrated that a joint diameter of 10 mm was optimal. This concludes the design of the structure.

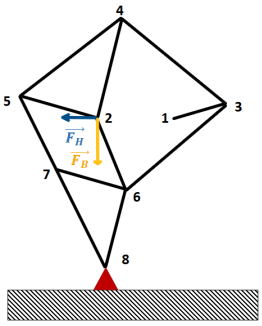

(a) Leg model with the constraints and the forces applied. The red triangle indicates a pinned connection.

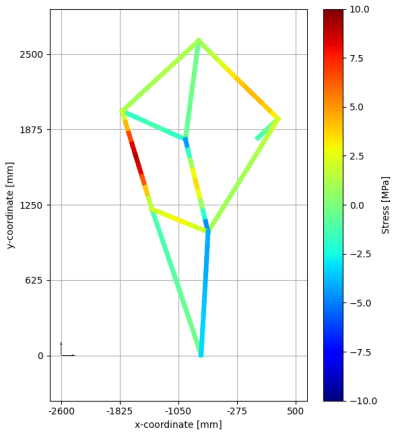

(b) Stresses in the legs.

Figure 12: Leg configuration and stresses

Failure Mode Analysis

The next step is to ensure the structure does not fail. Four potential failure modes were analyzed: buckling of structural elements, failure of adhesive bonds, failure of mechanical joints, and

exceeding the material's ultimate strength. It was demonstrated that the structure will not fail under any of these failure modes at the beginning of its operational life. However, it is known that material properties will degrade over time due to environmental exposure and fatigue. Considering these factors, the estimated lifetime of the structure is 2.5 years, with maintenance required every 1.1 years. To facilitate the determination of maintenance requirements, a weaker element is intentionally installed in the leg. This design choice enables quick and easy inspections of the structure. If a failure is detected in this weaker element, it serves as a clear indicator that maintenance is necessary.

Manufacturing

After analysing the body and leg, including investigating potential failure modes, all dimensions have been finalized confidently. The next step is to develop a production plan outlining every necessary step from decommissioning the wind blade to the final assembly of the structure.

Final Design

The final design is shown in Figure 13 and the external dimensions of the final design are presented in Table 13.1.

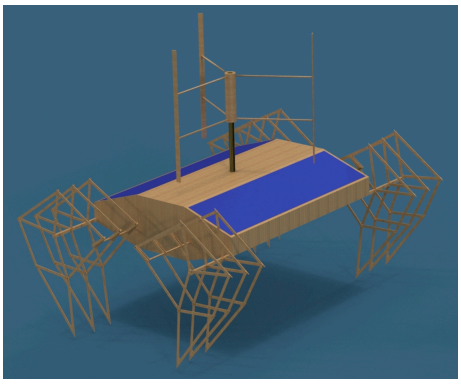

Figure 13: Final design of the B.F.G. (Bestia Functionis et Gaudii)

Table 4: External dimensions of the final design concept

Parameter	Value	Unit
WT diameter	3.025	m
Height of structure	5.1	m
Width of structure	6.2	m
Length of structure	3.2	m
Ground clearance	1.5	m
Leg height	2.6	m

Technical Risk Assessment

Similar to Theo Jansen's Strandbeests, various risks are encountered when bringing the designed structure to life. Those are divided into two main parts: production risks and operational risks. For the sake of brevity, only the top three critical risks will be summarised here. Overall, all high-likelihood severe-risk scenarios have been addressed.

Considering production risks, excessive damage to EoL wind turbine blade and therefore worse quality of the recycled composite may weaken the structure. This can be mitigated by using the damaged material for parts with a considerable safety margin. Another risk is the delamination of the composite during component extraction. As mitigation, suitable processing methods will be adapted for the potentially damaged composites. The third critical risk is cutting through fibres during the process of thickness reduction. To minimise the negative impact, a minimum thickness of 0.005 m is used for the non-load-bearing components.

For operational risks, collision with obstacles on the coastline was the most critical one. To mitigate it, an obstacle avoidance system capable of reacting to unexpected events is implemented. Another risk is being trapped by seawater (tide). To minimise the likelihood of this happening, the structure should be aware of tidal changes to plan its route accordingly. Finally, the structure

may generate insufficient energy in the absence of wind. To reduce the consequence of this risk, a battery system is implemented, allowing for energy storage.

Overall, no risk with high likelihood and severe consequences is left unadressed.

Verification and Validation of the Final Design

For the verification of the mission and system requirements, four different methods are used: test, analysis, demonstration and inspection. To all of the requirements, a method of verification is assigned. In the compliance matrix of the mission and system requirements, all the requirements received either a fully met, partially met, not met or to be investigated mark. Out of the 33 mission and system requirements, 25 received a fully met mark, one a partially met, none received a not met mark and seven requirements still have to be investigated.

The mission was validated by simulating the performance of the structure with a data set of two days with wind and solar data. It was found that the total operation time is 13 hrs in two days.

Sustainable Development

Sustainability is a driving factor in the system design for all five phases of the system lifecycle; material sourcing, manufacturing, logistics, operations and maintenance, and the end-of-life. This is most prevalent in the use of next-generation wind turbine blade material for the main structural elements. Reusing an already existing processed material eliminates the environmental impact and energy consumption from extracting raw materials and processing them into half fabricates. These elements are responsible for a high fraction of the total structure mass, and thus the overall impact due to used resources is greatly reduced.

Two end-of-life strategies of the system were investigated as the mechanical properties of the structure are expected to be drastically different depending on the duration of its operation. This plan is created for all used materials. An example of this for the composite material is as follows:

- *Short operation period* Cut into required sizes and use in load-bearing applications
- *Maximum operation period* Grind up into small particles and use in the production of new composite products. Heat up and reshape to form board, and use in non-load-bearing applications such as interior decoration, furniture backing, or signage.

Nomenclature

Abbreviations

ABL	Atmospheric Boundary Layer
AR	Aspect ratio
BLDC	Brushless DC
DMS	Double-multiple-streamtube
DoD	Depth of discharge
DOF	Degree of Freedom
EoL	End of Life
GFRP	Glass fibre-reinforced polymer
GPS	Global Positioning System
HAWT	Horizontal axis wind turbine
MCB	Miniature circuit breaker
NF	Natural fibre
PMA	Permanent Magnet Alternator
PV	Photovoltaic
SPD	Surge protection device
TSR	Tip speed ratio
VAWT	Vertical axis wind turbine
WDT	Watchdog timer

Greek Letters

α	Detected obstacle angle
β	Incoming flow angle
η	Efficiency
λ	Tip speed ratio
ω	Rotational speed
ϕ_r	Rolling resistance
Ψ	Inflow angle
ρ	Density
σ	Stress
τ	Shear strength
θ	Azimuth angle
θ_p	Pitch angle
φ	Aerofoil pitch angle

Latin Letters

a	Induction factor
C	Consequence
c	Chord length
C_D	Drag coefficient
C_L	Lift coefficient
C_p	Performance coefficient
h	Height
I	Moment of inertia
J	Polar moment of inertia
L	Likelihood
m	Mass
N	Normal force
P	Power
p	Pressure
R	Radius
r	Shaft radius
Re	Reynolds number
T	Torque
T_{2D}	Averaged thrust
U	Wind speed
V	Velocity
W	Weight
z_0	Surface roughness length
μ	Friction coefficient of sand
A	Area
C_T	Thrust coefficient
F	Force
g	Gravitational acceleration of Earth
N	Internal normal force
Q	First moment of area
T_p	Process temperature
V	Internal shear force

Contents

1

Introduction

Rising concerns over global warming, environmental pollution, and the challenges associated with securing a reliable energy supply have prompted governmental bodies to transition from fossil fuels to renewable energy sources. Among these, wind energy stands out as a promising field due to its distinct advantages. It is cost-effective [2], extensively available [3], and relies on mature technology that has been used for electricity production since the early 20th century, and for over 3500 years to power human activities [4].

Given these advantages, wind energy is expected to significantly increase its share in power generation in the coming decades. In Europe, wind energy is projected to account for a quarter of the continent's electricity production by 2050 [5]. This represents an 82% increase from current production levels, necessitating the production of larger wind turbines to meet the growing demand. This expansion is projected to generate approximately 325,000 tonnes of waste from wind turbine blades (WTBs) annually [5, 6]. Currently, these blades are primarily made of thermoset composites, posing significant end-of-life challenges due to limited and economically unviable recycling solutions. Consequently, decommissioned wind blades are often either incinerated or deposited in landfills [7–10], undermining the sustainability goals of the wind energy sector.

To address this issue, research has focused on replacing traditional GFRP thermoset composites with natural fibre (NF) thermoplastics. This combination addresses the sustainability challenge in two ways. First, NF have a negative carbon footprint, in contrast to the significant carbon emissions from the production of glass fibres. Second, thermoplastics enable reversible processing, allowing for re-moulding, unlike thermosets, which cannot be reshaped once chemically cross-linked. This remoulding capability opens new possibilities for recycling wind turbine blades.

Despite the acknowledged recycling potential of these new materials, to the best of team's knowledge, no case study has been conducted on this matter. Thus, this project was initiated to *"validate the viability of repurposing next-generation WTBs at the end of their life into an autonomous wind-powered structure capable of performing a societally meaningful mission"*. Significant milestones have already been achieved in this quest. The project framework was established in the initial weeks, providing a solid foundation for the preliminary design phase. This phase culminated in the selection of a final concept, which has been investigated in the past weeks.

This report, therefore, aims to present the final piece of the puzzle that will complete the design of the project, showcasing the final design. To convey this message, it is divided into four parts.

Firstly, the key points from previous milestones will be recapitulated, including the market analysis (Chapter 2), a summary of the trade-off process (Chapter 3), and the requirements (Chapter 4). Secondly, the material analysis is covered in Chapter 5, and the associated manufacturing constraints are detailed in Chapter 6. These chapters provide essential inputs for the third phase.

The third phase begins with power estimation (Chapter 7), followed by system analyses. Aerodynamics is detailed in Chapter 8, while motion is addressed in Chapter 9. Control strategies are then elucidated in Chapter 10, followed by the power distribution in Chapter 11. Finally, structural integrity is analyzed in Chapter 12. The fourth phase focuses on presenting the outcomes of these analyses and reflecting upon them. Beginning with the presentation of the final design in Chapter 13, the reflection is segmented into three aspects: technical risk assessment (Chapter 14), verification and validation (Chapter 15), and sustainability aspects (Chapter 16).

2

Market Analysis

2.1. Wind Turbine Problem

Bigger does not always mean better. One industry where this holds is the growing production and size of wind turbines and the immense challenge of recycling them at their end of life. Trends in the United States suggest that turbines will grow from 100 meters in 2016 to 150 meters in 2035, equivalent to the height of the Washington Monument [11]. Figure 2.1 illustrates this trend for on- and off-shore turbines. Projects in Europe follow this trend closely, with the Haliade X on the Maasvlakte in the Netherlands producing more than 12 MW of power with rotor blades of 107 m long [12]. While on the surface they seem like a positive development, there hides a significant problem.

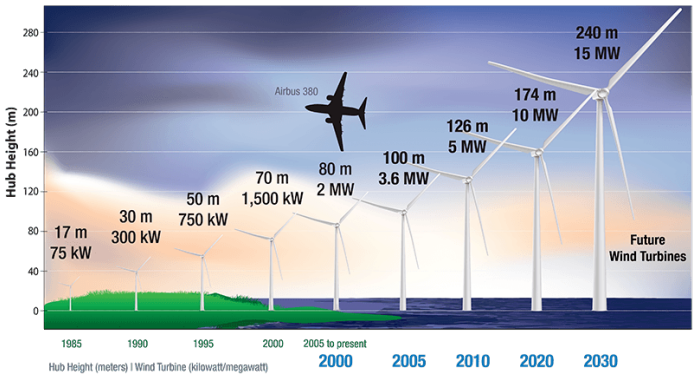

Figure 2.1: Growing size of wind turbines [11]

Composite materials have become the standard in wind turbine technology. Their high stiffness, high strength properties are directly responsible for the growing size of rotor blades. The problem: recycling composite materials is difficult and highly energy inefficient. Recent investigations performed by the European Commission in 2023 estimate that the EU alone will produce 570 million tonnes of blade waste by 2030 [13]. Current, and especially cheap, end-of-life solutions involve sending the blades to land fill, sometimes even in foreign countries.

New legislation on end of life solutions limits the possibility for rotor blades to end up in landfill. WindEurope, a Brussels-based wind energy association, called for ”a Europe-wide ban on landfilling decommissioned wind turbine blades” by 2025 at the Spanish Wind Energy Association’s 2021 Congress [14]. Legislation, however, does not eradicate the problem, and new end of life solutions such as re-powering or recycling fall behind the growth of turbine sizes [15]. Repurposing blade sections proves to be an elegant and sustainable solution to the problem. It is also the turbine end of life solution that is least applied today, presenting a market with little competition. Proving its feasibility, for example through a functional beach structure, will raise awareness of the issue to the general public. Despite there being more efficient (energy intensive) methods to perform beach related functions, none do so with full circularity in mind.

2.2. The Strandbeest

Theo Jansen is a prominent example of an artist capable of grabbing the public's attention through his Strandbeest collection, shown in Figure 2.2. It is a structure resembling an animal and built with simple PVC pipes. It moves with the help of wind and organic looking kinetic linkages optimised for smooth ground contact. Most importantly, it never fails to gather a large group of curious bystanders that wish to know more about the structure.

Figure 2.2: One of the many Strandbeest designed and constructed by Theo Jansen [16]

With the appropriate manufacturing methods, the wind turbine repurposing problem and the Strandbeest can be combined, resulting in a functional Strandbeest structure made of the NF composites found in wind turbine blades.

2.3. Market Introduction of Functional Strandbeest Structure

In response to the problem outlined in Section 2.1, this section will explore the market for recycling current WTBs, made of thermoset composites.

There are three main ways to recycle the current turbine blades: mechanical processing, pyrolysis, and chemical processing. The most common and budget-friendly is mechanical processing. It involves shredding the wind blade and reusing the raw materials in different products. Companies such as Global Fibreglass Solutions[1] or EURECUM[2] turn decommissioned wind blades into usable pellets, panels, and other raw constructing materials (see Figure 2.3). Although this may seem like an effective solution in a way, the mechanical properties of the original long continuous fibres of the blades cannot be preserved using this process.

Figure 2.3: Ground up blade composites turned into pellets (Global fibreglass Solutions)

Figure 2.4: Reclaimed glass fibre from pyrolysis on blades (Carbon Rivers)

Besides shredding, cutting is also a type of mechanical processing. It involves segmenting the blades into sheets and beams that can be used to manufacture different products. On one hand, this approach ensures better preservation of material properties compared to shredding. On the other hand, unlike shredding, the geometry of the cut pieces are constrained by the blade curvature and thus extensive segmentation plans need to be executed as the WTBs are made of thermoset composite and cannot be remoulded [17].

[1] Global Fibreglass Solutions, *URL* `https://globalfibreglass.com/applications/`, accessed 01 May 2024

[2] EURECUM, *URL* `https://www.eurecum-gmbh.de/en/recycling-of-wind-turbines/`, accessed 01 May 2024

Much effort is put into recycling the current wind turbine blades. However, due to the properties of thermoset composite, the recycling methods are limited; mechanical properties are downgraded, and recycling is often not profitable. With the next-generation thermoplastic blades, a vastly different set of recycling methods will be implemented. As thermoplastics can be remoulded, the new methods will pose fewer constraints on the geometry of the recycled parts.

There are various types of wind-powered vehicles available on the market today. Among them are racing cars designed to reach high speeds using only wind as their power source. For example, Chinook ETS Wind Powered Car was built to achieve the greatest efficiency in terms of vehicle speed compared to wind speed [3]. Another similar vehicle is Rick Cavallaro's Blackbird, which can even travel upwind [4].

Figure 2.5 illustrates the market gap between the three markets for sustainability awareness functional beach structures, and recycling wind turbine blades. This project aims to design a structure that can fill this gap.

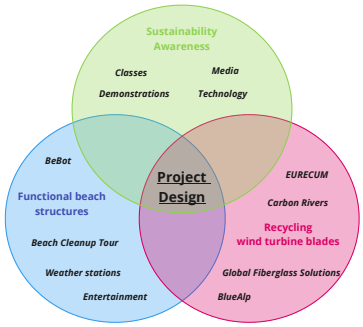

Figure 2.5: A Venn Diagram illustrating the market gap the designed structure will enhance

2.4. Stakeholder Analysis

Based on the market analysis, three stakeholder groups emerge (see Table 2.1): those related to materials and manufacturing, those involved during the operational life of the structure, mission stakeholders who will stay informed throughout the project and those related to funding .

Table 2.1: Project stakeholders are divided into three main categories: material-related stakeholders, operational stakeholders, and stakeholders involved in the overall mission, including funding

Material/Manufacturing	Operational	Mission
Research team on thermoplastics and NFs composite	Waste management company	Customer
Supplier of thermoplastics wind turbine blades	Beachgoers	Product design team
Manufacturing partner(s)	Coastal communities	European union for funding
Partner for the end-of-life of the structure	Municipal authorities	Dutch Government
Supplier of the electronics	UNESCO (for the coastal areas on its list)	Private investors
	Staatsbosbeheer	
	Royal Netherlands Institute for Sea Research	
	Customer for weather data	

[3] Lenovo StoryHub, URL: *https://news.lenovo.com/chinook-wind-powered-cars-future-of-travel/* accessed 17 June 2024

[4] BBC, URL: *https://www.bbc.com/future/article/20120727-the-wind-beneath-my-wheels* acessed 17 June 2024

3

Trade-off Summary and Lessons Learned

Reflecting on the designs presented at the end of the midterm phase, it is clear that the method of component trade-off could be improved [18]. Rather than producing a coherent system as the team intended, the design was a collection of subsystems which did not necessarily perform well together. Figure 3.1 presents these structures, with the left most structure the result of the previous trade-off method.

The intention of this chapter is to evaluate this process and suggest an improved method of comparison to arrive at a final concept. Section 3.1 will discuss the limitations of the previous trade-off and how the team handles them. Section 3.2 will repeat the criteria and design options from the midterm and discuss the revisions made ahead of the detailed design phase.

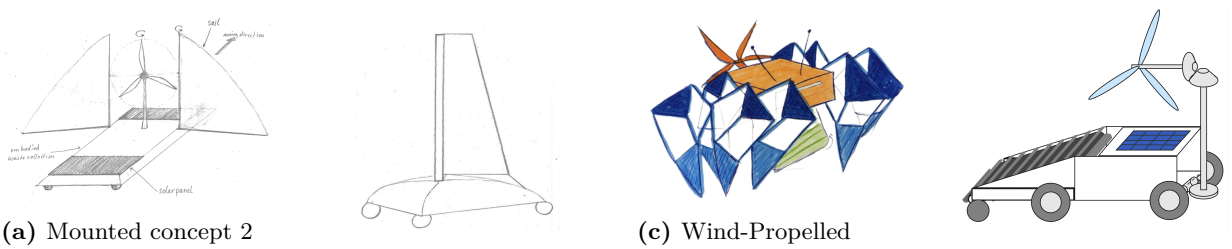

(a) Mounted concept 2 with a sail on each side

(b) Sand Buggy concept

(c) Wind-Propelled Strandbeest Concept

(d) Windcar Concept

Figure 3.1: Four design concepts in the final trade-offs

The selected straw man diagram under the new criteria is illustrated in Figure 3.2. It includes Jansen linkages for the kinematic motion, and a vertical axis wind turbine to provide power to the other subsystems, including those for movement.

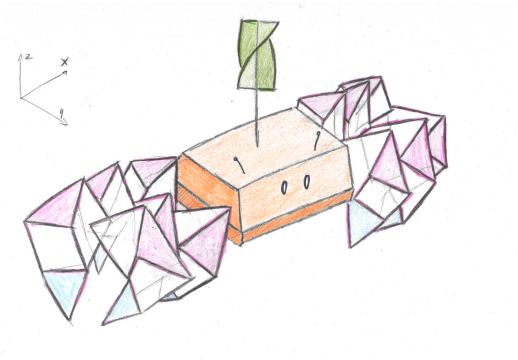

Figure 3.2: Selected straw man to enter detailed design

3.1. Limitations of Previous Component Trade-off

Having completed the straw man design phase, including the subsystem trade-offs, certain issues presented themselves. The main concern was the interference between the wind turbine and the sails of the mounted concept (illustrated in Figure 3.1a). The sizing of the two components was done separately, each with its own power requirement. Despite integrability being a criterion for each trade-off, its weight was not sufficiently high to significantly influence the outcome. The

limitations of the old criteria will be discussed in the following section. The interaction between the two subsystems was largely unknown, and could not be understood without professional insights or detailed analysis, the latter being unfeasible given the time constraints.

The team consulted several professors from the Faculty of Aerospace Engineering regarding this issue, including Dr. Julie Teuwen of the ASM department and Prof.dr.ir. Carlos Simão Ferreira of Wind Energy. Professor Ferreira identified several issues with the mounted concept. Firstly, the weight distribution would be difficult to manage with the placement of the wind turbine and sails. Secondly, Professor Ferreira stressed the importance of minimising the number of subsystems present on the structure. Given the harsh conditions and uneven terrain, more subsystems introduce more points of failure, making maintenance significantly more difficult. Dividing the aerodynamic surfaces into those for motion and those for power generation was a mistake that the team failed to identify before delivering the straw man concepts to the user.

It was noted that the component trade-off was the lacking verification for the method. The order in which the trade-offs were performed was reasoned at the beginning of the chapter; however, an alternative order was not discussed. The absence of a holistic trade-off of different straw man concepts resulted in a final design that resembled a Frankenstein design rather than a sound engineering solution.

3.2. Revised Trade-off After Midterm and Selected Design

The decision was made to revise the trade-off to better reflect the environment in which the structure will operate. Furthermore, system integration through the previous method could not be evaluated properly, focusing too much on subsystems in isolation. The criteria used in the previous trade-off method are listed below with indications as to whether it was weighed high or low.

Old criteria

- Mass (high)
- Cost (low)
- Size (low)
- Sustainability (low)
- Integrability (low)
- Reliability (high)
- Complexity (low)

With the previous criteria and their limitations established, it is worth restating the concepts that were tested against these criteria. This is done in Table 3.1, where each concept is listed in order of performance according to the previous trade-off.

The mounted concept of Figure 3.1a is a combination of the best performing options from each subsystem (sail + wheels + HAWT + battery). It is necessary to note that the design options found on the remaining three systems flow from the previous trade-offs. While not scoring the highest according to the criteria listed above, they must not be discarded when considered in combination with other subsystems. With these considerations, integrability can be ensured as designs are assessed as a complete system, rather than a combination of its parts.

Table 3.1: Subsystem concepts listed in order of trade-off performance

Aerodynamic surfaces for motion	**Kinematic mechanism**	**Power generation**	**Energy storage**
Sail [a,b]	Wheels [a, b, d]	HAWT [a, c]	Lead-acid battery
Kite	Caterpillar tracks	VIV enegy harvesting	Lithium-ion battery
HAWT [c, d]	Ski	VAWT	
VAWT	Jansen linkage [c]	Wave energy	
Wind turbine array		Wind turbine array	
Flapping wings		Kite	
		Solar [a, d]	
		Dynamo [b]	

Embodied intelligence is a concept that proved difficult to define in early stages due to its abstraction. To a certain extent it relates to the elegance of a structure, where its intended functions derive from mechanical properties on micro and macro scales. Embodied intelligence was never a criteria within the component trade off, but after the user, Dr. Masania, expressed his desire for the structure to display a level of embodied intelligence, it was included as a criteria for the revised trade off. The remaining criteria in Table 3.2 came from the conversations with Dr. Teuwen and Prof.dr.ir. Ferreira. For these criteria, more attention was given to the operational environment, that being the harsh conditions of the beach. The four concepts from Figure 3.1 are traded off with new criteria along with a fifth design representing a combination of the Strandbeest and Windcar concepts.

The combination concept makes use of the better qualities of the Strandbeest and Windcar concepts; performing better on the beach terrain, maximising the material and displaying embodied intelligence. This is ultimately the design that will be carried out for detailed design.

Table 3.2: Table showing the final design trade-off. 'G' stands for good performance, 'A' for average and 'B' for bad.

Criteria / Designs	**Harsh conditions**	**Terrain**	**Minimise power**	**Maximise material**	**Embodied intelligence**
Sand Buggy	G	A	G	B (sail)	A
Strandbeest	A	G	B	G	G
Windcar	A	A	G	A	A
Mounted Concept	A	B (small wheels)	A (interference)	B (sail)	B
Strandbeest/Windcar	A	G	A	G	G

4

Requirements Overview

This chapter describes the flow of requirements and the functional diagrams. In Section 4.1 the main stakeholders are defined and their high level requirements are shown. Section 4.2 shows the functional flow diagram and the functional breakdown structure. Then Section 4.3 and Section 4.4 shows the mission and system requirements respectively. Finally, the subsystems are described in Section 4.5 and the subsystem requirements that flow from Section 4.3 and Section 4.4 are described in Section 4.6.

4.1. Stakeholder Requirements

From the project description and market analysis, the project's stakeholders can be determined. The stakeholder requirements will come from the following stakeholders:

- **USER**: The customer for which the strandbeest is being designed: the Project Tutor and the faculty of Aerospace Engineering of TU Delft.
- **MAI**: The party that will perform maintenance of the structure.
- **MAN**: The manufacturer of the structure.
- **EoL**: The company that will process the structure at the end of its lifetime.
- **GOV**: Governmental institutions or NGO's.

The requirements flowing from these stakeholders are shown in Table 4.1

Table 4.1: Stakeholder Requirements

Identifier	Stakeholder Requirement
REQ-USER-01	Most structural components shall be produced from a single 100 m wind turbine blade manufactured from a natural fibre thermoplastic composite.
REQ-USER-02	The design shall operate in all weather conditions of the Dutch coastline.
REQ-USER-03	The structure shall perform its functions autonomously.
REQ-USER-04	The structure shall generate energy from wind to fulfill its functions.
REQ-USER-05	The structure shall not be hazardous to individuals interacting with it.
REQ-USER-08	The structure shall not require highly specialised tools to manufacture.
REQ-USER-09	The overall concept cost shall not exceed 50,000 EUR per unit in electronics and manufacturing.
REQ-USER-10	Sustainability shall be incorporated in the design process.
REQ-USER-12	The design shall be developed within 10 weeks.
REQ-USER-13	The design shall be developed by 10 bachelor's students.
REQ-USER-16	The structure shall demonstrate embodied intelligence.
REQ-USER-17	The structure shall allow for easy transportation.
REQ-MAI-01	The maintenance of the structure shall not require specialised tools.
REQ-MAI-03	The structure shall be designed in such a way that majority of the parts are easily accessible by the maintenance crew.

Continued on next page

Table 4.1 – continued from previous page

Identifier	Stakeholder Requirement
REQ-MAN-01	The system shall be manufacturable within 10 weeks.
REQ-MAN-02	The system shall be manufuctured under humane conditions.
REQ-EoL-01	Circularity shall be taken into account for the design of the structure.
REQ-EoL-02	The system shall be easy to disassemble.
REQ-GOV-01	The system shall legally operate on public beaches.
REQ-GOV-03	The system shall not harm nature.

From these stakeholder requirements, together with the project objective statement, the functions that the structure will have to perform are determined.

4.2. Project Logic Diagrams

Reflecting on the design exercise, the functional breakdown structure and flow diagram have changed considerably. This is no surprise as it is difficult to know precisely what the system will do. Throughout detailed design phases and analysing subsystems, the team encountered infeasibilities and opportunities that meant the functions must be re-evaluated. Most notable is the decision that instead of designing for the waste collection system specifically the structure shall be designed for a more general 'functional module' to allow for wider applications of the system.

Identifiers highlighted in red correspond to functions that are no longer designed for in the final design. Those in green have been added throughout the detailed design. The functional breakdown structure can be found in Table 4.4. Similarly, the functional flow diagram outlines the relationships between the functions throughout different phases. It can be found in Table 4.5.

4.3. Mission Requirements

Mission and system requirements are derived from the analysis of potential stakeholders, the funtional flow and breakdown, system reliability, and sustainability. The most important requirements are 'key' and 'driving' requirements. Within this report, 'key' requirements (green) represent the most important interests of stakeholders, while 'driving' requirements (yellow) heavily influence the design. Some requirements fall under both categories. They are highlighted in orange in the tables.

Table 4.2: Mission Requirements ('key'=green, 'driving'=yellow), both=orange

Identifier	Mission Requirement
REQ-USER-10-MIS-02	Sustainability shall have a trade-off weight of at least 10 %.
REQ-MAN-02-MIS-01	Machining tools used manufacturing of the system shall be inspected and certified by a third party in accordance with the EU machinery regulation.
REQ-MAN-02-MIS-02	The manufacturing process shall be regulated under the EU labour law.
REQ-GOV-01-MIS-02	The system shall meet all laws and regulations on operations of structures on public beaches.

4.4. System Requirements

Develop an end-of-life solution for future wind turbine blades in the form of an embodied intelligence wind-powered structure

- **Design** DES
  - **Define system and mission requirements** DES-REQ
    - **Analyse mission** DES-REQ-1
      - Analyse user requirements DES-REQ-1.1
      - Generate MNS and POS DES-REQ-1.2
    - **Perform market analysis** DES-REQ-2
    - **Generate technical requirements from user requirements** DES-REQ-3
  - **Perform trade-off** DES-TRO
    - **Determine trade-off criteria method** DES-TRO-1
    - **Determine trade-off criteria and weights** DES-TRO-2
  - **Create preliminary design** DES-PRE
    - **Illustrate layout of the design chosen from the trade-off** DES-PRE-1
    - **Determine design characteristics** DES-PRE-2
      - Estimate aerodynamic characteristics DES-PRE-2.1
      - Determine control characteristics DES-PRE-2.2
      - Determine material characteristics DES-PRE-2.3
        - Perform literature study on natural fibers and composite manufacturing DES-PRE-2.3.1
        - Determine theoretical material properties DES-PRE-2.3.2
        - Produce a sample material DES-PRE-2.3.3
        - Test the produced sample DES-PRE-2.3.4
      - Estimate power characteristics DES-PRE-2.4
  - **Generate design option tree** DES-DOT
    - **Perform operational environment literature study** DES-DOT-1
    - **Develop system and subsystem functions** DES-DOT-2
    - **Create functional flow diagram** DES-DOT-3
    - **Create functional breakdown structure** DES-DOT-4
    - **Generate design option per function** DES-DOT-5
  - **Create final design** DES-FIN
    - **Verify preliminary design** DES-FIN-1
    - **Validate preliminary design** DES-FIN-2
    - **Iterate preliminary design** DES-FIN-3
    - **Optimise preliminary design** DES-FIN-4
    - **Analyse the optimized design** DES-FIN-5
    - **Revise configuration and layout of the optimized design** DES-FIN-6
    - **Create operation and logistics description** DES-FIN-7
    - **Make a production plan** DES-FIN-8
      - Create CAD model of the design DES-FIN-8.1
      - Create technical drawings for manufacturing DES-FIN-8.2
    - **Generate cost breakdown structure** DES-FIN-9
    - **Investigate return on investment** DES-FIN-10
    - **Create H/W and S/W block diagrams** DES-FIN-11
    - **Create communication flow diagram** DES-FIN-12
- **Manufacturing** MAN
  - **Produce parts** MAN-PAR
    - **Recycle decommissioned wind turbine blade** MAN-PAR-1
      - Cut out the blade in the shape of necessary parts MAN-PAR-1.1
      - Reform the blade into re-shapeable material MAN-PAR-1.2
    - **Purchase necessary parts** MAN-PAR-2
  - **Assemble parts** MAN-ASB
    - **Manufacture subassemblies** MAN-ASB-1
      - Assemble body structure MAN-ASB-1.1
      - Assemble garbage collector MAN-ASB-1.2
      - Assemble other passive structures MAN-ASB-1.3
      - Integrate functional subsystem MAN-ASB-1.4
    - **Perform full assembly of the structure** MAN-ASB-2
      - Assemble subassemblies MAN-ASB-2.1
      - Perform wiring MAN-ASB-2.2
- **Operate** OP
  - **Perform functions** OP-FUNC
    - **Perform active function(s)** OP-FUNC-1
      - Collect garbage OP-FUNC-1.1
        - Pick up ground samples OP-FUNC-1.1.1
        - Separate garbage and sand OP-FUNC-1.1.2
        - Dispose sand OP-FUNC-1.1.3
        - Store garbage OP-FUNC-1.1.4
        - Dispose garbage locally OP-FUNC-1.1.5
      - Produce sound OP-FUNC-1.2
      - Shine lights OP-FUNC-1.3
      - Desalinate seawater OP-FUNC-1.4
      - Display entertainment OP-FUNC-1.5
    - **Perform passive function(s)** OP-FUNC-2
      - Collect data OP-FUNC-2.1
        - Measure UV exposure OP-FUNC-2.1.1
        - Measure wind direction and speed OP-FUNC-2.1.2
        - Measure humidity and precipitation OP-FUNC-2.1.3
        - Measure air quality OP-FUNC-2.1.4
      - Educate public OP-FUNC-2.2
        - Display infographics OP-FUNC-2.2.1
        - Play informational videos OP-FUNC-2.2.2
      - Provide garbage bin OP-FUNC-2.3
      - Include first aid services OP-FUNC-2.4
  - **Navigate** OP-NAV
    - **Follow trajectory** OP-NAV-1
      - Determine GPS location OP-NAV-1.1
      - Determine trajectory plan OP-NAV-1.2
        - Analyse navigational data OP-NAV-1.2.1
        - Assess position against data OP-NAV-1.2.2
        - Determine proceeding action OP-NAV-1.2.3
        - Adjust heading OP-NAV-1.2.4
      - Relay navigational data OP-NAV-1.3
    - **Avoid obstacles** OP-NAV-2
      - Detect waterline OP-NAV-2.1
      - Detect holes OP-NAV-2.2
      - Detect foreign objects OP-NAV-2.3
      - Detect people OP-NAV-2.4
      - Correct trajectory OP-NAV-2.5
        - Process obstacle data OP-POW-2.5.1
        - Activate trajectory system OP-POW-2.5.2
        - Execute trajectory feedback loop OP-POW-2.5.3
        - Deactivate trajectory system OP-POW-2.5.4
      - Relay information to control module OP-NAV-2.6
  - **Extract energy from wind and solar** OP-POW
    - **Generate power** OP-POW-1
      - Convert wind energy into electrical energy OP-POW-1.1
      - Store electrical energy in a battery OP-POW-1.2
      - Convert solar energy into electrical energy OP-POW-1.3
    - **Transfer energy to movement linkages** OP-POW-3
    - **Distribute power** OP-POW-2
      - Provide power to active systems OP-POW-2.1
      - Provide power to passive systems OP-POW-2.2
      - Provide power to navigation subsystem OP-POW-2.3
      - Provide power to the obstacle avoidance subsystem OP-POW-2.4
- **Perform maintenance** MAI
  - **Perform regular check-up on determined weakness spots** MAI-CHE
    - Perform visual inspections MAI-CHE-1
    - Perform stress tests MAI-CHE_2
    - Perform non-destructive tests MAI-CHE-3
  - **Detect damage** MAI-DET
  - **Analyse damage** MAI-ANA
  - **Repair damage** MAI-REP
    - Change damaged module MAI-REP-1
      - Replace the damaged module with a new trash collection module MAI-REP-1.1
      - Replace the damaged module with a new module with different functionalities MAI-REP-1.2
    - Change damaged part MAI-REP-2
- **Perform end-of-life procedures** EOL
  - **Repurposing the structure** EOL-REP
    - **Repurpose the structure as public installation art** EOL-REP-1
      - Remove non-structural parts EOL-REP-1.1
      - Find new uses for the non-structural parts EOL-REP-1.2
      - Find appropriate locations for installation EOL-REP-1.3
  - **Disassemble structure into parts** EOL-DIS
    - **Reuse parts in other structures** EOL-DIS-1
    - **Refurbish parts for other structures** EOL-DIS-2
      - Repair parts and repurpose EOL-DIS-2.1
    - **Recycle parts** EOL-DIS-3
      - Dispose material EOL-DIS-3.1

Key:

- Top Level
- Level 1 Function
- Level 2 Function
- Level 3 Function
- Level 4 Function

Table 4.4: Revised Functional Breakdown Structure

Top level flow:

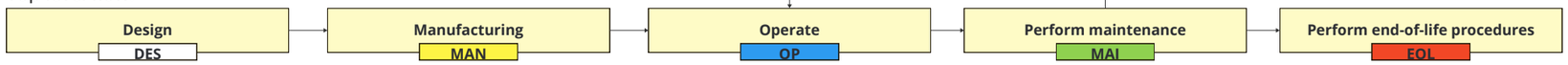

Key:

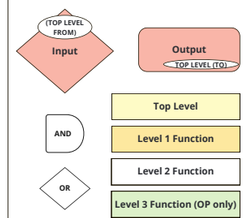

Color Legend:

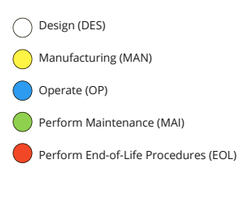

Lower level flow:

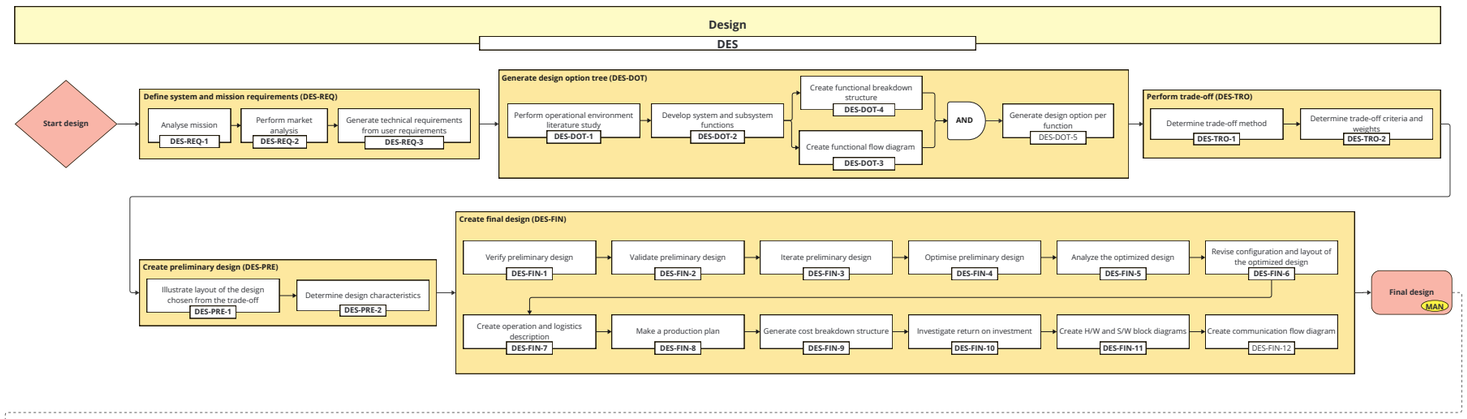

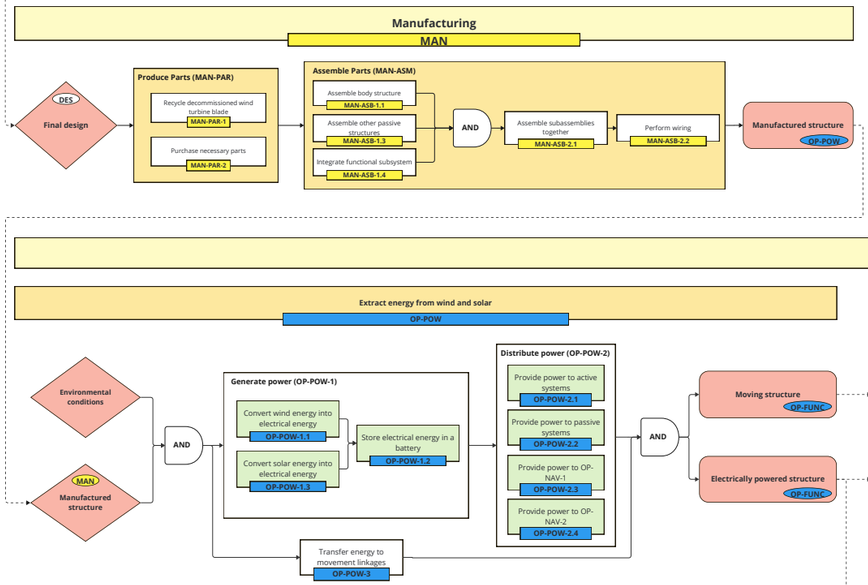

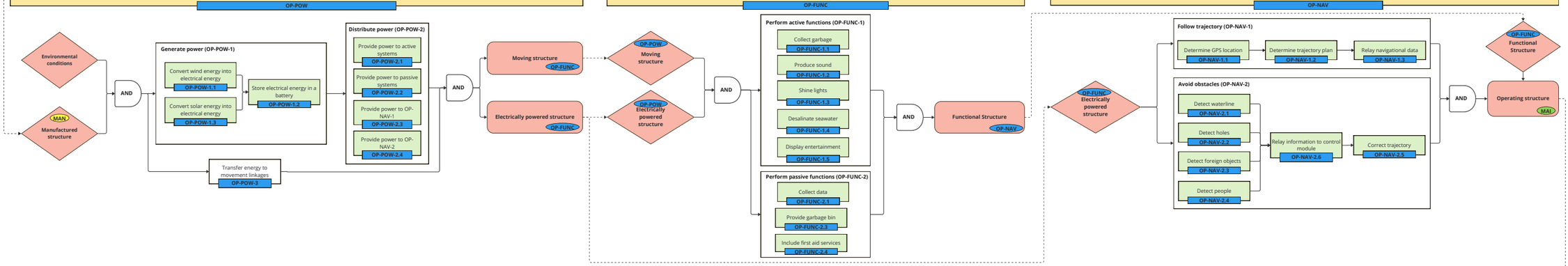

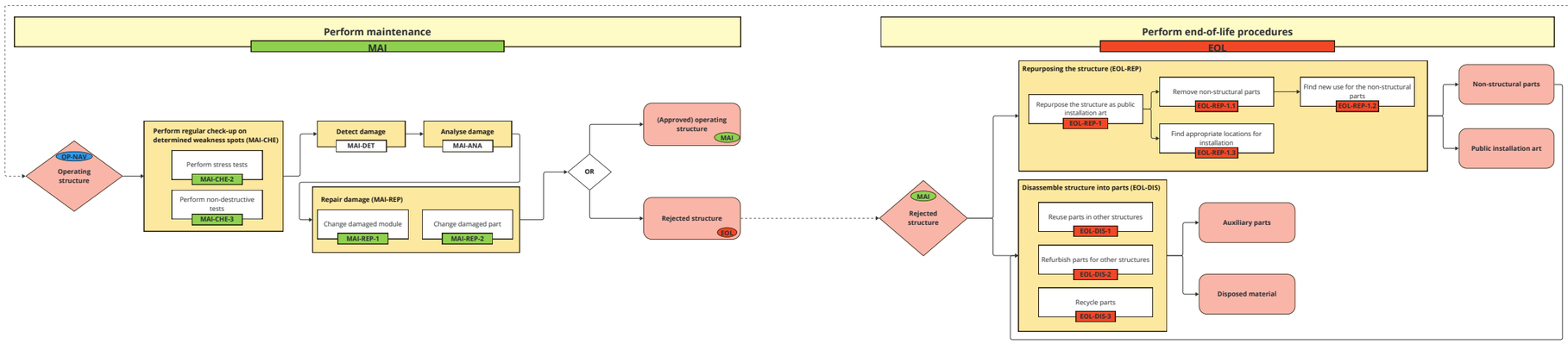

Table 4.5: Revised Functional Flow Diagram

Table 4.3: System Requirements. ('key'=green, 'driving'=yellow), both=orange

System REQ Identifier	System Requirement
REQ-USER-01-SYS-01	80% of the mass of the structural components shall be produced from a single 100 m wind turbine blade manufactured from a NF thermoplastic composite.
REQ-USER-02-SYS-01	The system shall withstand wind up to 100 km/h.
REQ-USER-02-SYS-02	The system shall withstand at least 5 mm/h of rain.
REQ-USER-02-SYS-03	The system shall withstand 3 mm of hail.
REQ-USER-02-SYS-04	The operation of system shall not be hindered by corrosion due to saline water for at least 52 weeks.
REQ-USER-02-SYS-05	The operation of system shall not be hindered by corrosion due to sand particles for at least 52 weeks.
REQ-USER-02-SYS-06	The operation of system shall not be hindered by photodegredation due to exposure to UV rays for at least 52 weeks.
REQ-USER-02-SYS-07	The system shall be able to operate in the presence of lightning.
REQ-USER-02-SYS-08	The system shall be able to travel at least 100 m in windless conditions.
REQ-USER-03-SYS-03	The system shall be capable of traversing the beach autonomously.
REQ-USER-03-SYS-06	The system shall navigate autonomously.
REQ-USER-04-SYS-01	The power subsystem shall provide a minimum power of 320 W at the average wind speed to fulfill its functions.
REQ-USER-04-SYS-02	The structure shall generate at least 60% of its power from wind.
REQ-USER-05-SYS-01	The system exterior shall be safe to touch when stationary.
REQ-USER-05-SYS-02	The system shall pose no physical harm to the public outside of a 1-metre radius when in motion.
REQ-USER-05-SYS-03	The noise produced by the structure shall not exceed 60 dB during operation.
REQ-USER-05-SYS-04	The system shall be able to make an immediate emergency stop when given an external input.
REQ-USER-08-SYS-01	The structure shall be manufacturable by moulding, pressing, and 3D printing.
REQ-USER-09-SYS-01	The total cost of manufacturing shall not exceed 30% of the total unit cost.
REQ-USER-09-SYS-02	The total cost of electronics shall not exceed 30% of the total unit cost.
REQ-USER-17-SYS-01	The wind turbine and the legs shall allow for disassembly during transportation.
REQ-USER-17-SYS-02	The entire structure shall fit within a 40 ft sea container of 12.03 x 2.40 x 2.70 m (internal dimensions LxWxH).
REQ-MAI-01-SYS-01	The maintenance of the structure shall be feasible with commercially available off-the-shelf (COTS) tools.
REQ-MAI-03-SYS-01	The system shall be designed to ensure that all critical parts shall be easily accessible to the maintenance crew.

Continued on next page

Table 4.3 – continued from previous page

System REQ Identifier	System Requirement
REQ-MAI-03-SYS-03	Maintenance shall be performed every 6 months at most.
REQ-EoL-01-SYS-01	The system shall be designed such that at least 70 % of its components are reusable at the end of its lifecycle.
REQ-EoL-02-SYS-01	The system shall able to be disassembled within 4 hours using commercially available off-the-shelf (COTS) tools.
REQ-GOV-03-SYS-02	The system shall not produce excessive lighting in accordance with EU regulation.
REQ-GOV-03-SYS-04	The system shall not operate in the vegetated areas of the beach.

4.5. Subsystem Description

The subsystem requirements flow from the mission and system requirements. In this section a brief description of these subsystems is provided.

Aerodynamics (AR) The wind turbine is the central component of the aerodynamic subsystem. This subsystem encompasses all elements related to the wind turbine, including the axle, aerofoil design, turbine blade design, and force distribution along the aerofoil.

Kinematics (KIN) The kinematics subsystem comprises the Jansen's linkage, number of legs, joints, feet, crankshaft, transmissions and gears and braking system.

Structures (STR) The structures subsystem includes all parts of the system that provide strength to withstand internal and external loads. This subsystem concerns all processes from analysing the decommissioned wind turbine blade material analysis, designing and manufacturing, and up to the end-of-life of the system.

Payload (PAY) The payload subsystem includes all parts that fulfil functions; waste collection and weather data collection. The waste system concerns collection, storage, and disposal of waste. The weather data system includes all sensors and communication module such as transceiver.

Control (CTR) The control subsystem encompasses all elements related to controlling the structure. This includes sensors, the actuators to regulate the speed and turning, mechanical and/or electrical energy storage and navigation.

4.6. Subsystem Requirements

This section shows the subsystem requirements flowing from the mission and system requirements.

Table 4.6: Structure, Control and Kinematics Subsystem Requirements ('key'=green, 'driving'=yellow), both=orange

Identifier	Subsystem Requirement
Structure Subsystem	
REQ-USER-02-SYS-01-STR-03	The natural frequency of the structure shall be higher than the frequency induced by external loads.
REQ-USER-02-SYS-02-STR-01	The structure shall retain at least TBD % of its original properties from erosion caused by rain.

Table 4.6 – continued from previous page

Identifier	Subsystem Requirement
REQ-USER-02-SYS-03-STR-01	The toughness of the material shall be higher than TBD J/m^3.
REQ-USER-02-SYS-03-STR-02	The stiffness of the material shall be higher than TBD N/m.
REQ-USER-02-SYS-04-STR-01	The structure shall retain at least TBD % of its original properties from corrosion caused by saline water.
REQ-USER-02-SYS-05-STR-01	The structure shall retain at least TBD % of its original properties from corrosion caused by sand particles.
REQ-USER-02-SYS-06-STR-01	The structure shall retain at least TBD % of its original properties from photodegredation caused by UV rays.
REQ-EoL-01-SYS-01-STR-01	The structural parts shall retain at least TBD % of the original material strength and properties at end of life.
Control Subsystem	
REQ-USER-03-SYS-01-CTR-01	The system shall be able to update its 2D position with a frequency of 1 Hz.
REQ-USER-03-SYS-01-CTR-02	The system shall be able to determine its 2D position with an accuracy of 1 m.
REQ-USER-04-SYS-01-CTR-01	The energy storage unit shall supply a minimum of TBD J during operation.
REQ-USER-04-SYS-01-CTR-02	The energy storage unit shall have a minimum lifetime of 3 years.
REQ-USER-04-SYS-01-CTR-03	The energy storage unit shall have a minimum capacity of 100 Wh.
REQ-USER-05-SYS-02-CTR-01	The system shall be able to detect obstacles within a 5-metre distance from the structure.
REQ-USER-05-SYS-02-CTR-02	The structure shall have a maximum speed of 1 m/s.
REQ-USER-09-SYS-02-CTR-01	The control subsystem shall not exceed 50 % of the total cost.
REQ-MAI-03-SYS-01-CTR-01	All electronics components shall be easily accessible to the maintenance crew.
REQ-EoL-01-SYS-01-CTR-01	The sensors used shall retain at least TBD % of the original accuracy when disassembled at end of life.
Kinematics Subsystem	
REQ-MAI-03-SYS-01-KIN-01	All linkages shall be easily accessible to the maintenance crew.

5
Material Analysis

This section provides the material analysis that serves as the foundation for the rest of this report. First, the rationale behind replacing GFRP (Glass Fibre Reinforced Polymer) with thermoplastics reinforced by NFs is explained in Section 5.1. The material likely to be used for next-generation wind blades is discussed in Section 5.2. Next, the mechanical properties of the composite are detailed in Section 5.3. Finally, the properties of the material at the EoL of the blades are examined in Section 5.4.

5.1. Justification for New Materials

The materials currently used in the manufacturing of wind turbine blades are GFRP and to a lesser extent, CFRP (Carbon Fibre Reinforced Polymer). These composites are favoured for superior stiffness and strength. However, the production of these materials is energy-intensive and presents challenges at the end of their lifecycle due to limited recycling options.

In contrast, NF-reinforced composites offer a sustainable and circular alternative. These materials leverage the high specific properties of NFs and their natural abundance, providing substantial benefits such as lower costs and a reduced carbon footprint [19]. For example, producing one tonne of NF results in a net emission of approximately -900 kg of CO_2 equivalents (CO_2 eq), due to the carbon uptake during growth. In comparison, producing one tonne of glass fibres results in nearly 2,600 kg of CO_2 eq emissions [20].

To illustrate the potential environmental benefits of this switch, consider the 1.5 GW Hollandse Kust wind farm, the largest offshore wind farm in the Netherlands. If this wind farm had used NFs instead of glass fibres, it would have resulted in a reduction of approximately 75,000 tonnes of CO_2 equivalent. This saving equates to the annual emissions of almost 8,000 Dutch residents. Given the rapid expansion of the wind energy sector, the impact of such a switch on reducing carbon footprints is substantial and underscores the need for serious consideration of NF composites.

High-performance NF composites have traditionally been produced using epoxy (EP) matrices. These matrices offer low porosity, high stiffness, low creep, and efficient stress transfer between fibres [21, 22]. However, EP matrices come with notable drawbacks, including the need for careful storage and handling, high defect sensitivity, brittleness, and poor recyclability. Thermoplastics present a promising alternative to epoxy-based systems. They offer several advantages, including simpler storage, lower-cost processing, and higher intrinsic toughness. Most importantly, they can be easily recycled with minimal degradation of their properties, enhancing their sustainability and making them a viable option for circular material use.

Considering these factors, it is plausible that the next generation of wind turbine blades will be manufactured using NF-reinforced thermoplastics. Supporting this intuition, ongoing research projects, such as the LICHEN Blades project, which focuses on designing next-generation wind blades, and the SSUCHY project, which aims to develop bio-based composites for various applications, highlight significant progress in this area.

5.2. Determining the Material for Next-Generation Wind Blades

This section will determine the optimal combination of NFs and thermoplastics for the next generation of wind turbine blades. Firstly, the type of NF is determined as it drives the mechanical

properties of the composite. Then, the thermoplastic is chosen.

5.2.1. Choosing the Natural Fibre

As there is no consensus yet on the specific NF to be used, it is essential to identify the most suitable ones based on their material properties, as these properties will drive the design process. Four common types of NFs often considered in research are bamboo, flax, hemp, and coir, each illustrated in Figure 5.1.

(a) Flax fibre[1] **(b)** Hemp fibre[2] **(c)** Bamboo fibre[3] **(d)** Coir fibre[4]

Figure 5.1: Illustrations of the sources from which flax, hemp, bamboo, and coir fibres are derived.

The properties of these fibres have been investigated, as displayed in Figure 5.2. Based on these properties, flax fibres stand out as the best reinforcement due to their robustness across all evaluated aspects. While their mechanical properties are inferior to glass fibres, flax fibres have a lower density and cost, making their specific properties comparable to those of glass fibres.

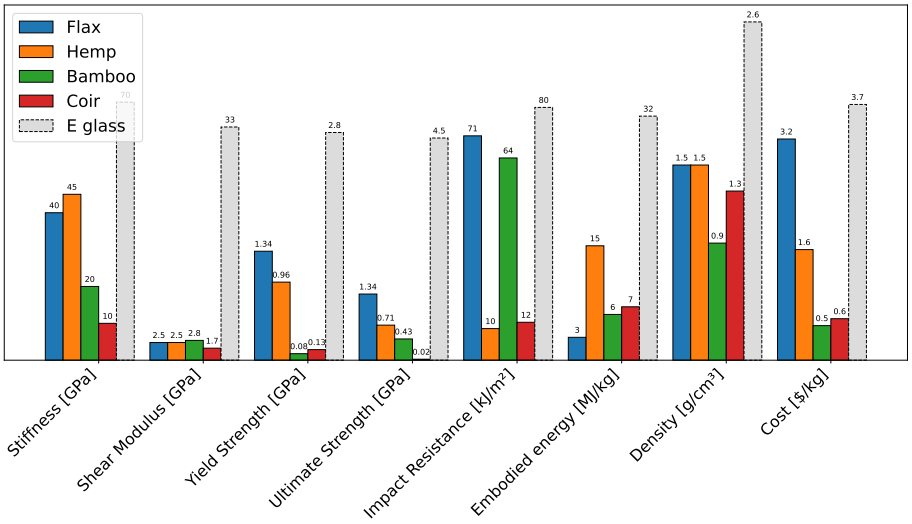

Figure 5.2: Properties of flax, hemp, bamboo, and coir fibres. The scales of each plot have been normalised.

Additionally, flax is cultivated in the Netherlands, Belgium, and France [23]. This regional availability contrasts with bamboo and coir, which would require transportation from other parts of the world, thereby undermining the sustainability goal of this project.

5.2.2. Choosing the thermoplastic

The next step is to determine the thermoplastic that would best complement these flax fibres. Van de Velde and Kiekens [24] have investigated multiple potential thermoplastics for this purpose.

[1] Flax, *URL* https://colossustex.com/flax-fiber/
[2] Hemp, *URL* https://www.manitobacooperator.ca/news-opinion/news/untangling-the-future-of-hemp-fibre/
[3] Bamboo, *URL* https://textileengineering.net/properties-flowchart-and-uses-of-bamboo-fibre/
[4] Coir, *URL* https://www.amazon.in/Natural-Coconut-Fiber-Street-Studio/dp/B0BGMKQ6M3

Based on their work, three categories of properties are analysed. The analysis is performed for the following thermoplastics:

- Polypropylene (PP)
- Low-density polyethylene (LD-PE)
- High-density polyethylene (HD-PE)
- Polyamide 6 (PA-6)
- Polyamide 66 (PA-66)
- Polycarbonate (PC)
- Polybutylene Terephthalate (PBT)
- Polyethylene Terephthalate (PET)
- Polyether Ether Ketone (PEEK)
- Polyphenylene Sulfide (PPS)
- Polyetherimide (PEI)
- Polyamide Imide (PAI)
- Polyoxymethylene (coPOM)

Characteristic temperature Flax fibres are known to degrade at temperatures above 220°C, making it imperative that the selected thermoplastic allows for processing below this degradation threshold [25]. Referring to Table 5.1, LD-PE and HD-PE are the most suitable options, as they have processing temperatures well below 220°C. PP and coPOM are close alternatives, while PA-6 is less ideal due to its higher processing temperature. Other thermoplastics exhibit processing temperatures above 220°C, rendering them unsuitable for use with flax fibres.

Table 5.1: Processing temperature T_p of thermoplastics [24]

Properties	Limits	PP	LD-PE	HD-PE	PA-6	PA-66	PC	PBT	PET	PEEK	PPS	PEI	PAI	coPOM
$T_p(°C)$	**Lower**	200	150	150	215	250	260	246	256	370	300	330	340	190
	Upper	290	230	290	270	320	330	290	310	400	340	420	400	230

Physical properties Two physical properties are investigated: density and water absorption. The latter is particularly important because the blades will be exposed to a humid environment throughout their service life, especially for offshore wind turbines.

Density is crucial for determining the specific properties of a composite, primarily influenced by the mechanical properties of the fibres and the matrix density. As shown in Figure 5.3a, PP and LD-PE are the best options for density. However, other materials remain viable, as their superior mechanical properties can balance out higher densities when considering specific properties.

Regarding water absorption, it is crucial to have the lowest possible value, as water intrusion in the composite can disturb the fibre/polymer interface, reducing the overall composite strength. This issue is even more critical for flax fibres due to their strong hydrophilic behaviour, leading to high moisture sorption and swelling deformations [26]. The swelling of flax fibres also induces stress on the surrounding matrix material, causing micro-cracks in the composites [27]. The results for the different thermoplastics are shown in Figure 5.3b. From the five thermoplastics deemed suitable after the temperature analysis (PP, LD-PE, HD-PE, PA-6, coPOM), only PA-6 is unsuitable due to excessively high water absorption.

Mechanical properties The last four thermoplastics (PP, LD-PE, HD-PE, coPOM) are then compared based on their mechanical properties. Two cases should be distinguished depending on the fibre ratio [24].

1. **High Fibre Ratio:** When the fibre ratio is relatively high, the mechanical properties of the composite are predominantly influenced by the fibres. In this scenario, the choice of thermoplastic only marginally affects the composite properties. Therefore, one can freely choose the desired thermoplastic. However, since the fibres are heavier than the thermoplastic, this solution is not preferred as it negatively impacts the specific properties of the

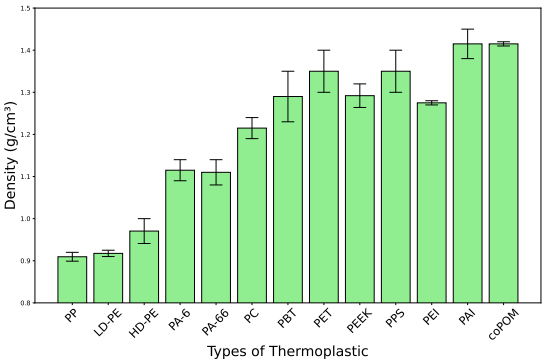

(a) Density ranges of various thermoplastics. The bar charts indicate average values. Adapted from data in [24]

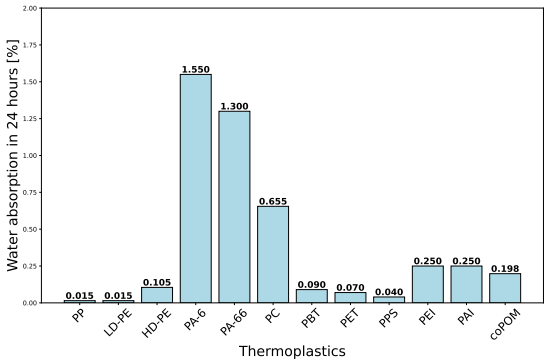

(b) Water absorption percentages for different thermoplastics. The bar charts indicate average values. Adapted from data in [24]

Figure 5.3: Comparison of density ranges and water absorption percentages of various thermoplastics

composite.

2. **Low Fibre Ratio:** When the flax fibre ratio is lower, the mechanical properties of the thermoplastic play a more significant role. In such cases, stronger thermoplastics should be preferred to enhance the overall performance of the composite. As demonstrated by Woigk et al. [28], coPOM is an appropriate choice in this scenario, as coPOM matrix composites have high longitudinal properties and excellent transverse properties.

Given the analysis conducted, coPOM emerges as the best matrix material option. Therefore, this project will focus on recycling flax-reinforced coPOM composites. For the rest of this report, a fibre fraction of 50% will be chosen to ensure proper impregnation while maximising the properties.

5.3. Mechanical Properties of the Flax-Reinforced coPOM Composite

With next-generation blades expected to use a combination of flax fibres and coPOM, the focus shifts to determining the properties of this composite. Utilising the properties of both coPOM and flax fibres, as summarised in Table 5.2, the composite properties detailed in Table 5.3 are determined using the rule of mixtures and assuming a fibre fraction of 50%.

Table 5.2: Comparison of coPOM and Flax properties [29–33]

Property	coPOM	Flax
Density [g/cm^3]	1.41	1.45 - 1.50
Young's Modulus [GPa]	3.15	52.7
Thermal Coefficient (Longitudinal) [1/K]	0.000106	-0.000008
Thermal Coefficient (Transverse) [1/K]	0.000106	0.000082
Ultimate Strength [MPa]	48.5	1339
Yield Strength [MPa]	48.5	1339
Poisson Ratio	0.44	0.4

Table 5.3: Composite Properties for 50% fibre fraction (coPOM and flax fibres)

Property	Value
Density [g/cm^3]	1.44
Young Modulus (parallel) [GPa]	28
Thermal Coefficient (Longitudinal)	0.00005
Thermal Coefficient (Transverse)	0.00009
Ultimate Strength [MPa]	694
Yield Strength [MPa]	694
Poisson Ratio	0.42
Young Modulus (transverse) [GPa]	5.9

5.4. Determining the Material Properties at the End-of-Life of the Wind Blades

Significant differences between the properties at the beginning of life (BOL) and EoL are expected due to the ageing phenomenon resulting from prolonged exposure to harsh environmental conditions. Since the material used for the structure will be recovered from the decommissioned blade, it is essential to determine the EoL properties of the composite.

Su and Kam [34] investigated how heat and humidity affect wind blades. They considered uncoated surfaces, whereas wind blade surfaces will probably have a protective coating, making their results conservative. Using their regression and a typical lifespan of 20 years [35], Young's modulus and tensile strength of wind blade materials could decrease to 60% and 58% of their initial values, respectively, with similar reductions expected for yield strength.

This study focused on current wind turbines made of GFRP. However, future turbines will use flax fibres with coPOM, and the ageing behaviour of these materials differs. Notably, flax fibres tend to swell, creating local stresses that exceed the endurance of PP, leading to micro-cracks in the matrix and reducing mechanical properties. Although no specific studies on the PP/coPOM combination exist, Pantaloni et al. [36] examined water ageing in flax/PLA composites with a 40% flax fraction.

In Pantaloni et al.'s research, a relative humidity of 98% - the most critical scenario before full immersion - resulted in a stiffness decrease of 20.3%. Additionally, yield and tensile strength dropped by up to 27%. These reductions are attributed to decohesion and micro-cracks in the matrix caused by flax fibre swelling. This swelling also reduces density by 2.3%.

Synthesising these findings and adopting conservative values, the density of the PP/coPOM composite at EoL is assumed to decrease by 2.3%, Young's modulus by 40%, and yield and tensile strength by 42%. It is also assumed that the Poisson ratio and thermal coefficients remain unaffected by ageing. These adjusted properties are summarised in Table 5.4.

Table 5.4: Composite properties for a fibre fraction of 50% (PP and Flax Fibres) considering EoL Properties

Property	Properties at BOL	Properties at EOL	Percentage Change [%]
Density [g/cm^3]	1.44	1.37	-2.3
Young Modulus (parallel) [GPa]	28	17	-40
Thermal Coefficient (Longitudinal)	0.00005	0.00005	-
Thermal Coefficient (Transverse)	0.00009	0.00009	-
Ultimate Strength [MPa]	694	402	-42
Yield Strength [MPa]	694	402	-42
Poisson Ratio	0.42	0.42	-
Young Modulus (transverse) [GPa]	5.9	3.4	-40

The limitations of applying findings from GFRP and flax/PLA composites to flax/coPOM composites are acknowledged. If more resources were allocated to this project, experiments could be conducted but the described analysis is deemed sufficient for the sake of this project.

This investigation does not address aging due to UV exposure, as it can be mitigated by integrating an anti-UV agent into the thermoplastic and applying an anti-UV coating on the surface. However, it is important to recognise that surface coating alone is not sufficient to entirely prevent the absorption of heat and moisture by the composite material. Therefore, the influences of moisture and heat absorption were considered in this analysis. Additionally, fatigue was not considered because its impact on residual strength appears to be limited [37].

Finally, it is important to interpret these results cautiously. As Pronk [37] highlighted, "no conclusions can be drawn on the residual quality of turbine blades in general" and "in practice, the blades should always be tested to approximate the real strength of the blades".

6

Material Recovery and Manufacturing Techniques

This chapter explains how decommissioned wind turbine blades can be turned into a new structure. First, Section 6.1 describes the general characteristics of wind turbine blades. Following that, Section 6.2 describes different methods to recover material from the wind blades. Next, Section 6.3 discusses the manufacturing constraints based on the requirements, helping to identify suitable manufacturing techniques. Section 6.4 then details the parts that can be made from the recovered materials. Finally, Section 6.5 outlines the methods for joining these parts.

6.1. Description of Wind Turbine Blades

Wind turbines come in two primary types: Horizontal Axis Wind Turbines (HAWT) and Vertical Axis Wind Turbines (VAWT). Since the majority of currently installed turbines are HAWTs, this report will concentrate on the recycling of HAWT blades. Their wind blades can be divided into three primary sections along their length, as depicted in Figure 6.1.

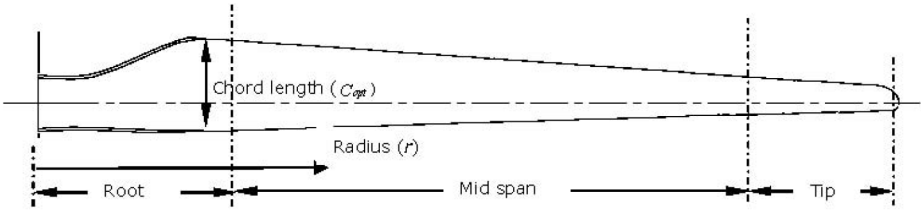

Figure 6.1: Sections of a wind turbine blade: root, mid-span, and tip [38].

- **Root**: The root end of the blade experiences the highest forces and moments. Consequently, this section is designed with thicker material and a robust profile to withstand these stresses.
- **Mid-Span**: The mid-span section of the blade features an aerodynamic profile optimised for generating movement. The height of the blade gradually decreases towards the tip.
- **Tip**: The blade's tip is where velocity is at its highest, and consequently, the majority of energy generation occurs. This section is crucial for maximising energy capture efficiency.

A typical wind blade cross-section is depicted in Figure 6.2a. The structural core of the blade is formed by the spar caps and shear webs. It can also be observed that wind blades utilise various fibre orientations. Typically, three primary fibre orientations are employed, as illustrated in Figure 6.2b. The extracted parts from the wind blade will inherit these fibre orientations.

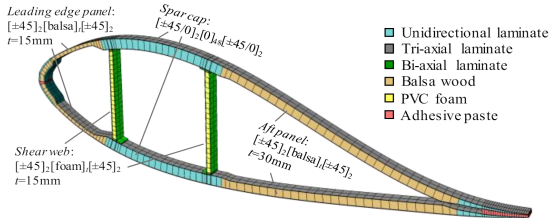

(a) Cross-section of a commercially available large utility wind turbine rotor blade [1]

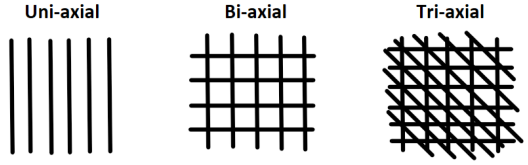

(b) Three typical fibre orientations found in traditional wind blades

Figure 6.2: Cross-section and fibre orientations of wind turbine blades

6.2. Approach for Recycling the Wind Turbine Blade

The process of reusing decommissioned wind blades can be divided into two steps. First, the elements of interest must be extracted from the blade and transported to the workshop. Second, the extracted elements need to be reshaped or remanufactured to construct the new structure.

6.2.1. Extracting the Elements

To extract elements from the wind turbine blade, a systematic approach is adopted.

Step 1: Information Gathering

Information about the blades is gathered, including the reason for decommissioning (economic, technical, or permit-related). This assists in assessing blade quality. If maintenance reports are unavailable, damages and repairs are inspected to evaluate strength and stiffness.

Step 2: Geometry Determination

The blade geometry is obtained, either from existing databases or by requesting documentation from the manufacturer. Based on the geometry, the ideal nesting pattern is determined to extract all the required elements.

Step 3: Element Extraction

Using the known geometry, elements suitable for manufacturing the new structure are extracted. Techniques such as abrasive water jet, plain water jet, or laser cutting, are known to be effective for composite materials, are employed [39]. Depending on the requirements, post-processing such as sanding, coating, or sealing may be necessary to enhance element integrity and longevity. The processed elements are then transported to the composite workshop for the construction of the new structure.

Alternatively, transporting the entire blade to the workshop is considered, but it is economically impractical. Transporting one blade, which fits on a single truck after being cut, costs about 600 € in the Netherlands. If transported as a whole blade on an exceptional convoy, the cost rises to around 30,000 €.

6.2.2. Using the Extracted Elements for the Construction of the Structure

Two primary methods exist for utilising the extracted elements. Firstly, they can be used without further modification. Alternatively, the extracted elements can be pressed to produce a flat laminate. This laminate can then be used as a raw material for various manufacturing processes, enabling the creation of more intricate pieces. Both options are explored in this section.

The thickness of the 100-meter blade varies along its span, ranging from a few centimeters at the tip to up to 16 centimeters at the root [40]. To use this material, the blade can be sectioned into rectangular pieces of different sizes [17]. This method is favored for manufacturing rectangular beams, where the thickness of the material serves as the height of the beam. After cutting, these parts can be submerged in resin to add an additional protective layer.

Another approach involves pressing the extracted elements under high temperatures, typically the melting temperature of the resin used in the composite material, to obtain a flat laminate. These flattened panels can be used to manufacture more complex shapes through press forming. However, the resulting flat laminate would still be several centimetres thick, which may not be ideal for lightweight structures. Options to reduce the thickness will be introduced in the next sections.

6.3. Manufacturing Constraints

Knowing the elements to be delivered to the composite workshop (sections of the blades to be used as-is or flattened for further processing), understanding the constraints associated with the workshop becomes crucial.

REQ-USER-08 stipulates that no highly specialised tools should be necessary during the manufacturing process. Thus, the structure must be manufacturable in a standard workshop. To meet this requirement, it is essential to initially assess the available equipment and manufacturing techniques that will constrain the design. This entails identifying the available equipment and then presenting the possible techniques based on the constraints imposed by this equipment and the materials obtained from the decommissioned wind blades, as discussed in subsection 6.3.1 and subsection 6.3.2.

6.3.1. Available Equipment

In a standard composite workshop, the following equipment is typically available:

1. **Cutting Tools**:
   - *Rotary Cutters and Scissors*: Essential for cutting composite fabrics and pre-pregs to the required shapes and sizes.
   - *CNC Cutting Machines*: Provide precision cutting for complex shapes and patterns.
2. **Layup Tools**:
   - *Layup Tables*: Flat surfaces where composite materials are layered and assembled.
   - *Rollers and Squeegees*: Used for applying and distributing resin evenly across the composite layers.
   - *Vacuum Bagging Materials*: Includes vacuum bags, sealant tape, and release films used in the vacuum bagging process to remove air and compress the layers together.
3. **Molding Equipment**:
   - *Molds and Mandrels*: Shapes around which composite materials are laid up. These can be made from various materials such as metal, wood, or high-density foam.
   - *Release Agents*: Applied to molds to ensure that the finished composite part can be easily removed.
4. **Pressing Tools**:
   - *Hydraulic Presses*: Used to apply uniform pressure during the molding and curing process, ensuring proper compaction of the composite layers.
   - *Hot Presses*: Combine heat and pressure to cure composite materials, often used for manufacturing flat or slightly contoured parts.
5. **Resin Application Tools**:
   - *Resin Mixing and Dispensing Systems*: Used for mixing resin and hardener in precise ratios and applying them to the composite materials.
   - *Brushes and Rollers*: For manual application of resin to ensure thorough impregnation of the fibres.
6. **Curing Equipment**:
   - *Ovens and Autoclaves*: Used for curing composite parts at controlled temperatures and pressures to achieve the desired mechanical properties.

- *Heat Guns and Infrared Lamps*: For localized curing and repairs.

7. **Finishing Tools**:
   - *Sanding and Grinding Equipment*: For smoothing and finishing the edges and surfaces of composite parts.
   - *Drills and Saws*: For creating holes and trimming excess material.
8. **Inspection Tools**:
   - *Ultrasonic Testing Equipment*: For non-destructive testing of the composite parts to detect internal defects.
   - *Micrometers and Calipers*: For measuring the dimensions and thickness of composite parts to ensure they meet specifications.

These tools and equipment form the backbone of a standard composite workshop. Using this equipment, the possible manufacturing techniques can be investigated.

6.3.2. Possible Manufacturing Techniques

The nature of the inputs for the manufacturing process, being elements extracted from wind blades, imposes certain constraints.

Firstly, techniques requiring fibres separated from resin or impregnated fibre filaments, such as filament winding or pultrusion, cannot be easily employed and are therefore excluded. Secondly, the plies cannot be easily extracted for re-laying, rendering all lay-up processes unsuitable. Given these limitations, the most suitable manufacturing technique is press forming, as depicted in Figure 6.3, along with other similar pressing methods. In press forming, a heated laminate is

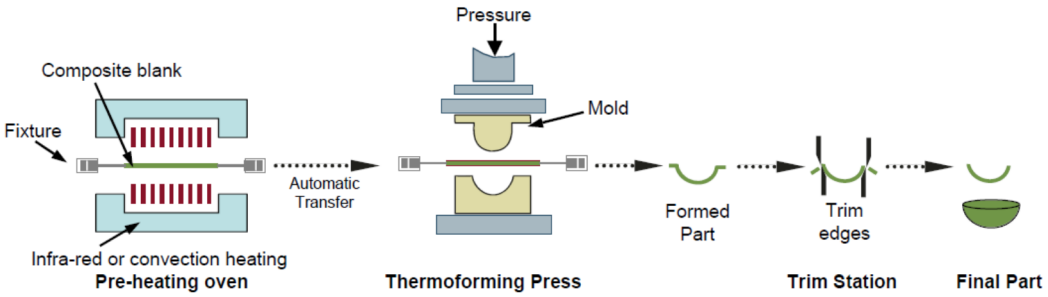

Figure 6.3: A schematic overview of the press forming process[41].

transferred between male and female dies, which press against the material to deform it. After cooling, the formed part can be removed from the press and trimmed if necessary. There are several variations to this process. For instance, in rubber forming, only a single rigid tool is required, as a rubber tool presses down to deform the material. The specific variation chosen will be determined in the manufacturing plan.

6.4. Parts that can be manufactured

In this section, the manufacturing of different parts within the constraints outlined in Section 6.3 will be discussed. Firstly, the issue of thickness reduction will be addressed. Secondly, the manufacturing processes for various shapes, including flat panels, wind turbine blades, and rectangular beams, along with their variations, will be explained.

Adjustment in thickness

As explained in Section 6.2, the thickness of 100-meter wind blades can be as large as 16 cm in some locations. Such a high thickness is unnecessary and would result in excessive mass, requiring more power to move the structure. Therefore, the first step is to reduce the thickness of the extracted element.

To reduce the thickness, the extracted element is first flattened by pressing it under the melting temperature of the thermoplastic. Once flattened, the panels can be cut in the longitudinal direction to produce thinner, straight panels, as shown in Figure 6.4.

Figure 6.4: Manufacturing process to reduce the thickness. The dotted red line indicates the cutting direction.

A limitation is acknowledged. The thickness of the panels obtained after cutting cannot be too small. Due to the initial curvature, cutting the panel will introduce delamination, which would result in poor mechanical properties if the panels are excessively thin.

Rectangular Beams

Rectangular beams will be used to construct the chassis of the structure, as they are effective at carrying loads. To manufacture these beams, the flattened panels with adjusted thicknesses will be cut to the required beam shapes.

If the structural analysis indicates a need for high moments of inertia to resist stresses, other geometries, such as C-shaped beams or variations thereof, will be considered. These can be easily manufactured by pressing the flat panels into molds at the melting temperature of the thermoplastic as shown in Figure 6.5.

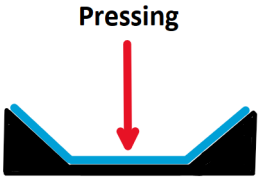

Figure 6.5: Manufacturing process of a variation of a C-shaped beam. The mold is shown in black and the beam in blue

Flat Panels

The structure contains electrical devices that are vulnerable to wet weather conditions, such as rain. To address this vulnerability, flat panels are used to provide protection. These flat panels can be produced using the previously described "Adjustment in thickness" method. Additionally, compression molding can be used to create specific shapes at the corners of the panels, ensuring complete coverage of the sensitive devices.

Wind Turbine Blades

Achieving the desired aerodynamic performance relies heavily on the shape of the aerofoil, necessitating a manufacturing process capable of producing the required shape with precision.

One effective method involves dividing the aerofoil into two sections along the chord line, as illustrated in Figure 6.6. Subsequently, a mold made of metal or a material capable of withstanding temperatures of around 200°C is created. A flax/coPOM panel with reduced thickness, prepared using the aforementioned method, is then heated and pressed into the mold.

Once both parts of the aerofoil are manufactured, they are joined together. Flanges are created for each part to facilitate the joining process. Two variations in the manufacturing process of flanges are illustrated in Figure 6.7. In both cases, the flanges are joined using adhesive. Once

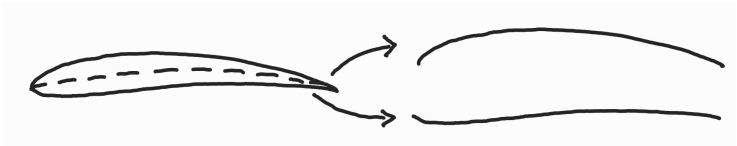

Figure 6.6: Divisions of aerofoil along the chord line

the new blades are complete, a UV-resistant and water-repellent coating is applied to the surface of the blades. If twist angles are required, they will be incorporated into the design of the mold.

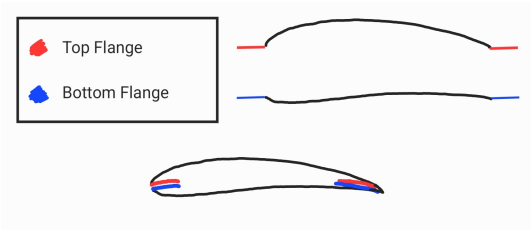

(a) The top and bottom flanges are bonded at both leading edge and trailing edge of the blade

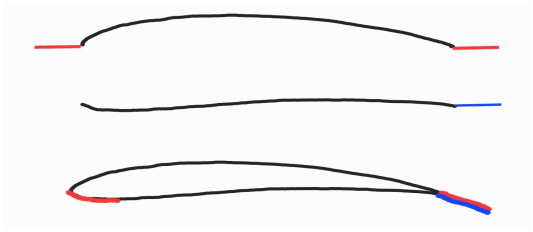

(b) The top flange is bonded to the leading edge of the bottom blade, while both top and bottom flanges are bonded together at the trailing edge

Figure 6.7: Visualisation of two methods to manufacture wind turbine blades

6.5. Joining Methods

Now that the different parts that can be manufactured have been identified, the joining methods used to link them will be explained in this section. A distinction is made between static joints, discussed in subsection 6.5.1, and dynamic joints, discussed in subsection 6.5.2.

6.5.1. Static Joints

There is a limit to the complexity of parts achievable when designing structures with recycled thermoplastic composite materials. To ensure adequate structural integrity, many parts require fixed joints. Among the methods available for statically joining two composite parts, adhesive joining and mechanical joining will be discussed. Thermoplastic welding may be a great option to consider but it is not taken into account due to the following reasons. Firstly, once a welded structure fails, it is significantly more difficult to repair compared to adhesive bonding, as the structure would be completely damaged and require extensive reworking. Secondly, maintaining the shape of structures as beams is more valuable in recycling. Adhesives can be easily removed, allowing the parts to be reused or reshaped, whereas thermoplastically welded parts cannot be returned to their original shapes (beams), reducing their recyclability and potential for reuse.

Adhesive bonding Literature research initially identified typical adhesives for bonding thermoplastic composites. Given the need to bond similar NF thermoplastic composites, the focus shifted to suitable adhesive types such as polyurethane, epoxy, and acrylics, commonly used for structural applications [42]. Polyurethane, noted for its lower hardness, was deemed softer compared to others. Since the adhesive will provide a rigid connection between beams, epoxy and acrylic emerged as preferred choices.

To decide between acrylic and epoxy, the primary selection criterion is adhesive bonding strength, critical for beams under high forces and stresses. Epoxy was chosen due to its superior bonding strength compared to acrylics, and its versatile adhesion to diverse substrates [43]. Detailed specifications of the selected epoxy adhesive are outlined in Table 6.1.

Table 6.1: Model of the epoxy adhesive [44]

Property	Bonded shear strength (MPa)	Peeling test at 22 ° C (N/mm)	Shear modulus at 22 ° C (MPa)
3M Scotch-Weld Epoxy Adhesive 2216 B/A Gray	22.063	0.175	342

Mechanical joining

Mechanical joining can be achieved by drilling holes in the composite parts and connecting them using rivets or bolts. Table 6.2 summarises the features and properties of rivets and bolts. Upon review, bolts offer numerous advantages over rivets. Therefore, bolts have been selected as the preferred mechanical joints for the final design.

Table 6.2: Features and properties of rivets and bolts

Rivets	Bolts
Simple tools	Detachable
Easy inspection and repair	Used for thick plates
Fatigue-sensitive	Increased fatigue life
Only shear loading	Loaded in shear and tension

6.5.2. Dynamic Joints

For the dynamic joints, three options are considered: off-the-shelf pivots, compliance mechanisms, and embed inserts.

Off-the-shelf pivot point

A regular pin joint is undesired since cutting or drilling a hole in a composite panel may lead to various defects, like delamination, fibre fraying or spalling [45]. Instead, methods allowing for load-bearing and 1 DOF rotation without a need to drill in the material were investigated. A straightforward solution is to use off-the-shelf joints that can be connected to the leg mechanism parts. An example of such a joint can be seen in Figure 6.8.

(a) Example of a stainless steel pivot joint **(b)** Pivot joint connected to two wooden parts

Figure 6.8: Off-the-shelf pivot joint mechanism which can be integrated between two different parts[1]

A wide range of pivot joints is available, designed for different loads and deflection angles. A fitting option could be picked once the exact requirements are known. They are a simple, robust and cheap solution. However, such joints are commonly made from steel, meaning that the leg mechanism would not be fully constructed from recycled WTB material.

Compliance mechanism

[1]AWR Solutions URL: *https://www.awrsolutions.com.au* accessed: 05 June 2024

A significant drawback of off-the-shelf joints is the additional weight they impose on the structure. To address this issue, compliant joints present a viable alternative. These flexible mechanisms achieve force and motion transmission through elastic body deformation, deriving some or all of their motion from the relative flexibility of their members rather than from rigid-body joints alone. Compliant joints can be monolithic (single-piece) or jointless structures, resulting in significant mass savings for each joint. When applied across the entire structure, this can lead to a notable reduction in overall mass.

However, a possible issue arises with these linkages. Their load-bearing capacity is not proven. To date, they have only been tested under their weight, which is relatively small. In this project, the legs will need to support additional loads from the batteries, the wind turbine, and the overall structure. It is uncertain whether these compliant mechanisms can handle such loads, and given the project's limited time frame, it is prudent not to take the risk.

Embed inserts

To prevent delamination, inserts can be effectively utilized. Figure 6.9 illustrates the steps involved in embedding an insert into a composite. Initially, the thermoplastic composite part is heated above the polymer's melting temperature. Once heated, the part is positioned in an open compression mold. The mold is then closed and a tapered pin tool is pressed through the composite, displacing the reinforcing fibres without cutting them, to create a hole. This process eliminates voids and local delaminations, reorients fibres towards the counterpunch direction, and ensures uniform part thickness, thereby enhancing joint strength. Finally, the composite cools to solidify, and the part is demoulded [46]. Subsequently, excess composite edges are trimmed, and a bolt is inserted into the hole. This method is preferred for dynamic joints, so the joints in the legs will be manufactured using this technique.

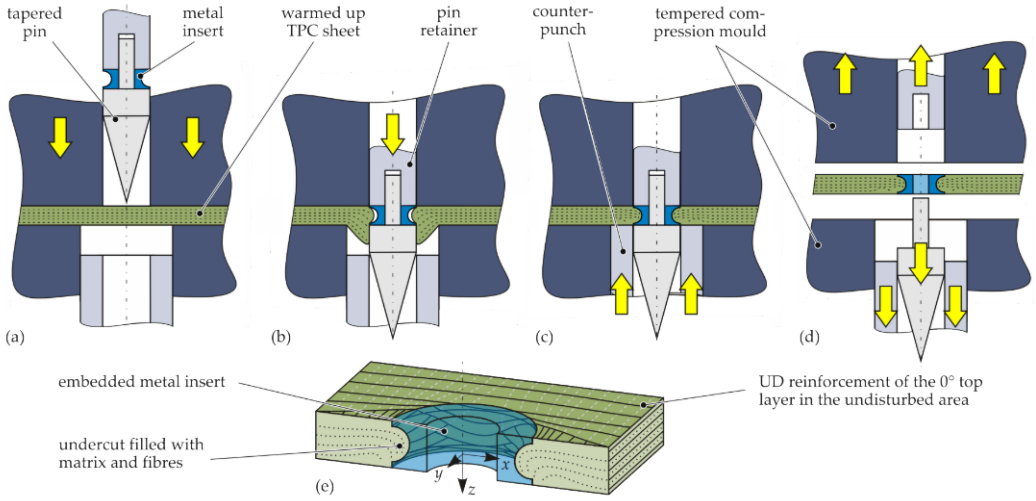

Figure 6.9: Embed the metal inserts into the parts of the legs to serve as dynamics joints[2]

[1]Insert, *URL* https://www.mdpi.com/1996-1944/15/15/5454, accessed 06 June 2024

7

Preliminary Power Estimation

The power required for the final design and power supplied from an additional source heavily influence the design of the wind turbine and supporting structure. The power estimation is based on two key components and divided as such in sections. The power needed for structural movement is assessed in Section 7.1, and the power required to execute the designated function is assessed in Section 7.2. Finally, the total power budget and how the power will be generated is discussed in Section 7.3.

7.1. Power for Motion Mechanism

This section focuses on the power needed for the motion of the structure. First, subsection 7.1.1 presents the original profile of Theo Jansen's Strandbeest linkage. Subsection 7.1.2 explains the mass estimation of the structure that is needed in subsection 7.1.3 for the power estimation.

7.1.1. Theo Jansen's original linkage

The Jansen linkage is visualised in Figure 7.1. This is a single degree of freedom, 8-link planar linkage with set ratios. The ratios were optimised for an organic, smooth walking motion using a simple rotary input[1]. A crankshaft is connected to the Jansen linkage which rotates it around the blue circle to make a motion.

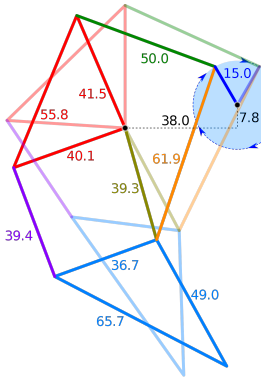

Figure 7.1: The original Jansen's linkage with the ratios of the individual bars indicated[2]

7.1.2. Preliminary Mass Estimation

To estimate the power for the motion of the Jansen legs, an estimation of the total mass of the structure is needed. The mass is 440 kg and is the accumulation of the following masses:

Body Mass The mass of the body of the structure is estimated to be 100 kg. For the estimation, a box of $4m$x$2m$x$0.5m$, with a panel thickness of 0.5 cm and the composite density of 1370 kg/m^3.

Total Leg Mass The total mass of the legs is estimated to be 60 kg. The dimensions of standard PVC electricity pipes were used for the estimation, based on the original Strandbeast design of Theo Jansen. The total height of the leg was assumed to be 2.7 m with a material density of 1320 kg/m^3.

Wind Turbine Mass The total mass of the wind turbine is estimated to be 130 kg. This estimation is based on the power requirement production of 500 W that was found in the Midterm Report of this DSE [18].

[1]Strandbeest, *URL* `https://www.strandbeest.com/explains`, accessed 5 June 2024

[2]Wikimedia, *URL* `https://upload.wikimedia.org/wikipedia/commons/thumb/b/b4/Jansen27s_Linkage.svg/`, accessed 5 June 2024

Safety Factor Mass A safety factor of 1.5 is introduced for the mass estimation to account for the mass of the functionality module, batteries, electric motor, cranks, gears and other structural components. This safety factor adds 150 kg to the weight.

7.1.3. Power Estimation of the Jansen's Linkage Structure

Initially, the power estimation is based on the reference of power of the robots with the Jansen linkages [47]. Equation 7.1 is for evaluating the energy efficacy where P is the output power, m is the total weight of the structure and v is the velocity.

$$\epsilon = \frac{P}{mgv} \tag{7.1}$$

The specific resistance with respect to the walking speed is provided in Figure 7.2. The walking speed can be modified by the angular velocity, ω of the crank shaft. From this figure, the specific resistance of the Jansen's linkage is determined to be $\epsilon = 0.31$ at $v = 0.1\ m/s$. [48]

The structure's velocity is set at 0.1 m/s. As shown in Equation 7.1, the power required for motion is linearly dependent on velocity, assuming it is below 1.5 m/s and other parameters remain constant. A higher velocity requires more power, leading to a larger wind turbine and increased mass, potentially causing a snowball effect. Therefore, the velocity is kept at 0.1 m/s to minimise power requirements. With the specific resistance of $\epsilon = 0.31$, a walking speed of 0.1 m/s, and a mass of 440 kg, the power for motion is calculated using Equation 7.1 to be 140 W.

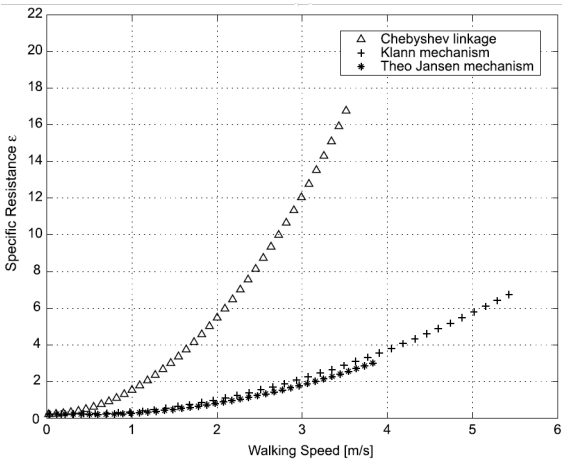

Figure 7.2: Specific resistance analysis of three closed-loop linkages with respect to the angular velocity ω and the walking speed v[48]

7.2. Power to Fulfill a Function

Estimating the power required involves considering three main functions: waste collection, desalination, and providing a beachside cinema experience.

7.2.1. Waste Collection

To minimise power usage, a robotic arm will be used to pick up beach waste. When waste is detected by a sensor or camera, the arm picks it up and places it in the compartment. A commercially available arm capable of picking up objects has a power requirement of approximately 40 W [3].

7.2.2. Desalination

As the structure will operate on the dutch coast, drinking water will not always be within reach for beach goers. As salt water is always in the vicinity, the structure could possibly fulfill the function of providing drinking water by desalination of the sea water.

[3]Kinova *URL* `https://www.kinovarobotics.com` accessed 05 June 2024

The power requirement for a desalination system, good for providing 30 L of drinking water every hour, is 110 W [4]. This system includes everything required for the desalination process. A tank shall be in place where the structure can store the sea water that is pumped up into the structure.

7.2.3. Beachside Cinema Experience

Enhancing visitor interaction, a portable cinema mounted on the structure could offer an engaging experience by broadcasting movies at the touch of a button.

This feature necessitates two key pieces of equipment: a projector and speakers. The power requirement for an outdoor projector typically averages around 45 W [5]. For speakers, maximum power generally reaches about 60 W. In total, approximately 100 W of power is necessary for operation.

7.2.4. Power Requirement for Functionality

From these three functions, the desalination has the highest power requirement. To allow for different functionalities in the same order of magnitude, and to reserve some power for the placement of sensors for the control system, a safety margin has to be in place. Therefore, it is decided that the structure shall be designed for a power requirement of 130 W for the functionality.

7.3. Power From Solar Energy

Combining the power estimation for the motion mechanism and the power estimation to fulfil a function, the total power requirement is 270 W. In addition, the efficiency of the electrical components also needs to be considered. The total electrical efficiency of the system is estimated at 50%, with back of the envelope calculations. Therefore, the total power of 540 W is required by the power source.

Following user requirement *REQ-USER-04-SYS-02*, the structure shall generate at least 60% of its power from wind energy. A smaller proportion of wind power in the power budget reduces constraints on the operational profile and enhances the stability of the structure. The minimum wind power requirement of 60% was taken as a baseline, being equal to approximately 320 W. Due to its availability in remote areas and ease of integration with the structure, solar energy has been chosen for the remaining 40% of the power budget, being equal to approximately $P_{Solar} = 215\ W$.

A preliminary calculation is performed for the required solar panel area on the structure. The average annual solar irradiation in The Netherlands is 1000 kWh/m^2. However, to account for clouded conditions the diffuse horizontal irradiance (DHI) is used, which averages approximately 560 kWh/m^2 [6]. This number can be converted to a DHI of 155.56 W/m^2. A conservative solar panel efficiency of 20% is assumed for this calculation. The solar panels will most likely experience shading from the wind turbine during part of the day. To account for this shading, the solar panel efficiency is multiplied by 0.75, resulting in a total efficiency of $\eta = 0.15$. Plugging in the values in Equation 7.2, the required solar panel area is calculated to be approximately $A_{Solar} = 9$ m^2.

$$A = \frac{P_{Solar}}{DHI * \eta} \tag{7.2}$$

[4] Watermakers *URL* `https://schenkerwatermakers.com/products/zen/#product-zen-30` accessed 05 June 2024

[5] https://www.amazon.com/BenQ-GS50-Projector-Bluetooth-Chromecast/dp/B09BTTVJLX?tag=p00935-20&ascsubtag=02GezW803YaHICZZUNer9tT&th=1

[6] Global Solar Atlas `https://globalsolaratlas.info/map?c=52.358829,3.90564,9&s=52.24462,4.424744&m=site` accessed 12 June 2024

8

Wind Turbine Design

This chapter details the design of the wind turbine, which serves as the main power system. Section 8.1 discusses the wind model, which incorporates atmospheric boundary layers and wind direction. Subsequently, in Section 8.2 trade-offs related to rotor orientation and rotor configuration are evaluated. In Section 8.3, the design of the rotor is presented, considering aspects such as the determination of rated wind speed, aerofoil profile selection, aspect ratio, and safety structure. A static loading analysis will be conducted in Section 8.4, showing the internal shear loads and bending moments. The determination of thrust and torque informs the design of the shaft and the rest of the structure. To verify the design, a sensitivity analysis based on aspect ratio (Section 8.5), comparison to similar wind turbines and verification in simulation (Section 8.6) was performed. A compliance matrix in Section 8.8 concludes the chapter to verify that requirements are met.

8.1. Wind Model

Before diving into the design of the wind turbine, it is essential to investigate the environment where the wind-propelled structure will operate, focusing on wind speed and direction. The environment introduces many variables, some too complex to solve numerically. Necessary assumptions have been included for precisely this reason, including a detailed explanation as well as its validity for the model.

8.1.1. Wind Model Assumptions

Modelling aerodynamic effects proves to be difficult analytically or numerically without establishing certain assumptions to simplify the physical problem. For preliminary design, these assumptions enable the possibility to use analytic expressions which ease computations. The simplifications relevant to the wind model are detailed below.

Wind speeds are normally distributed over a year. The normal distribution have been used in earlier models based on the historical data with an acceptable accuracy. Other models make use of Weibull distributions which look similar to a normal distribution but allow for skewness.

Wake effects do not influence turbine performance. Three-dimensional effects from wake and turbulence reduce the performance of the rotor. Advanced numerical methods such as CFD or QBlade provide a more accurate analysis of the performance of a rotor, but they require additional resources that are unavailable within the given time span. Incorporating three-dimensional effects into the model is left as a recommendation, as it would improve the credibility of the model.

Lift, drag, power, and thrust coefficients remain constant along the height of the turbine for a specified free stream velocity. Under the absence of a pitch distribution along the height of the turbine, the non-uniform velocity profile would affect the relative wind speed and consequently, the power and thrust coefficients experienced at each cross-section along the span of the rotor. The aerofoil twist section can be (partially) designed to keep those coefficients constant, however, this assumption will simplify the initial sizing of the turbine.

Sizing for average speed ensures continuous, year-long operation. While the design cannot ensure sufficient power generation in the presence of long periods of low wind speeds, it can be sized for the most probable conditions, the average wind speed. Sizing for a lower wind speed would increase the likelihood of the system operating over the entire year, but would

significantly complicate the design as it would require a larger, and heavier turbine.

Viscous effects are negligible. This simplifies the aerodynamic analysis significantly. Turbulence is ignored, equations can be solved analytically and Reynold's number does not influence aerofoil choice. This also means wake effects are removed, which is a phenomenon inherently ignored in this analysis, as it requires powerful computational models. However, neglecting viscous effects means ignoring boundary layer conditions, which this analysis does consider.

8.1.2. Wind Speed

Sizing a wind turbine depends largely on its operational wind speed. This follows from statistical data provided by eight local weather centers along the Dutch coast: Domburg, Burgh-Haamstede, The Hague, Wassenaar, Noordwijk, IJmuiden, Wijk aan Zee and De Kooy. The model initialises with over 70 thousand historical data points at a height of $10m$ between 1991 and 2019, plotted in Figure 8.1, and subsequently extracts the necessary parameters to begin sizing of the wind turbine [49]. The mean and standard deviation of the data are $6.49m/s$ and $1.38m/s$ respectively. The average wind speeds do not significantly change over the years.

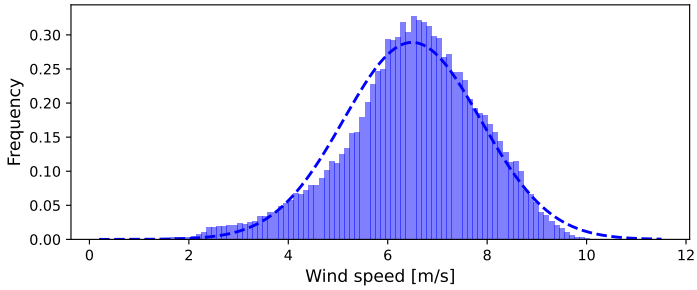

Figure 8.1: Average wind speed frequency distribution along the Dutch coastline between 1991 and 2019

Seasonal effects suggest that wind speeds are higher in the colder months and lower in warmer months [50]. The structure must be capable of executing its functions year-round, as defined by the user. With this in mind, the model does not lose credibility for neglecting wind speed variations over seasons.

8.1.3. Atmospheric Boundary Layer Corrections

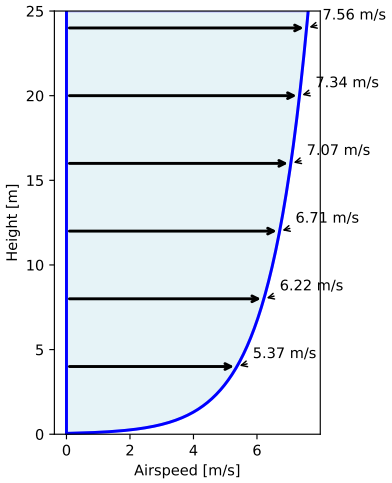

Figure 8.2: Wind shear effects following the logarithmic wind profile with surface roughness length $0.05m$

Wind shear is caused by the presence of a boundary layer on Earth; the wind profile is not uniform but changes at various heights above the surface. Because of that, the maximum power density varies along the height. The wind model follows the method outlined by Wieringa and Agterberg which includes a logarithmic correction factor defined by Equation 8.1 to account for surface roughness [51] (below $60m$). Figure 8.2 takes a reference height of $10m$ corresponding to the mean velocity of $6.49m/s$.

$$v(h) = v(h_{ref}) \frac{\ln \frac{h}{z_0}}{\ln \frac{h_{ref}}{z_0}} \tag{8.1}$$

Wieringa and Agterberg also classify various roughness levels depending on the surrounding terrain with a distinction between various landscapes. The factor accounting for surface roughness is z_0 and is assumed to equal 0.05 m (open landscape) for coastal conditions.

8.1.4. Wind Direction

It is crucial to assess the wind directions since the mission involves operating at various locations along the North Sea coastline. The wind roses, which characterise the wind direction and speed at two potential locations where the structure may travel, are shown below.

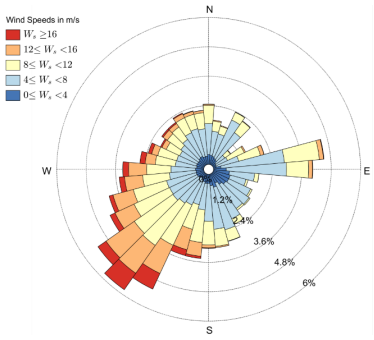

Figure 8.3: Wind rose from the IJmuiden weather station (at 2m) maintained by the Royal Netherlands Meteorological Institute KNMI (2011–2016)[52]

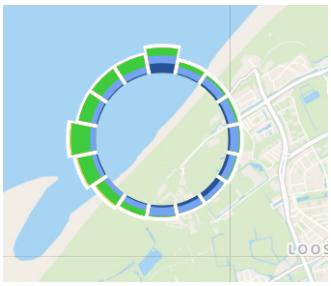

Figure 8.4: Wind rose from Kijkduin/The Hague weather station (at 7m) computed by Windfinder in a year [1]

As presented in Figure 8.3, the wind direction at IJmuiden is predominantly from the south-west. According to multiple wind roses derived from WindFinder statistical data, the dominant winds shift to the northwest direction when moving to the southern part of the Dutch coastline (see Figure 8.4). Therefore, the wind turbine needs to be designed to accommodate different dominant wind directions.

8.1.5. Environmental Loading

It is critical to design the wind turbine for the optimal performance, even under the extreme weather conditions. Table 8.1 outlines the reference wind speeds and gusts for different wind turbine classes. The wind turbine in question falls within the fourth class, with annual average wind speeds around 6 m/s.

Table 8.1: Wind Class defined by The International Electrotechnical Commission.[2]

	I	**II**	**III**	**IV**
Reference wind speed $[m/s]$	50	42.5	37.5	30
Annual average wind speed $[m/s]$	10	8.5	7.5	6
50-year gusts $[m/s]$	70	59.5	52.5	42
1-year gusts $[m/s]$	52.2	44.6	39.4	31.5

Gusts, defined as sudden wind speed increases lasting 3 seconds, can be detrimental to the wind turbine. Designing the wind turbine structure should consider the loading under these gust

[1] WindFinder, *URLhttps://nl.windfinder.com/windstatistics/kijkduin_den_haag*, accessed 05 June 2024

[2] Wind Class, *URLhttps://www.lmwindpower.com/en/stories-and-press/stories/learn-about-wind/what-is-a-wind-class*, accessed 06 June 2024

speeds. However, according to initial estimations, 50-year gusts and 1-year gusts in Class IV are too high for a moving structure on the beach to withstand. As Figure 8.1 shows, the hourly average wind speed on the beach rarely reaches 12 m/s. But based on the observation of live Dutch weather conditions, the wind speed can go beyond 15 m/s on certain days. Therefore, the wind turbine's cut-out speed is set to 20 m/s and the loading analysis will be based on this value. A corresponding operation plan and a maintenance plan will be established to account for higher wind speeds.

8.2. Wind Turbine Design Trade-offs

Following a better understanding of the wind conditions on the Dutch coastline, this section determines the orientation and the configuration of the rotor in subsection 8.2.1 and subsection 8.2.2. The performance of the design options is summarised in the trade-off table. The trade-off scores are represented by the following colours: Bad, Average, Good, Exceptional.

8.2.1. Rotor Orientation Trade-offs

Two types of wind turbines are commonly used today: vertical axis wind turbines (VAWT) and horizontal axis wind turbines (HAWT). When considering the installation of a wind turbine on a moving structure at the beach, the following criteria have been identified:

- **Mass**: A lightweight wind turbine design is essential to minimise the total mass.
- **Integrability**: The wind turbine can be easily installed on the structure without affecting its overall elegance.
- **Operation** The wind turbine should be able to adapt to changing wind directions as the structure moves along the Dutch coastline.
- **Centre-of-Gravity**: A low centre-of-gravity wind turbine contribute to the stability.
- **Peak Efficiency**: The wind turbine should efficiently extract energy from the wind.
- **Maintenance**: The wind turbine should be easily maintainable.
- **Noise**: The wind turbine should produce low noise on the beach, which is sustainable for the environment.

These criteria are considered equally important. Table 8.2 presents a comparison between the two orientations of wind turbines. It can be concluded that VAWT is a better option for the final design.

Table 8.2: Comparison between horizontal axis wind turbine and vertical axis wind turbine [53][54]

Properties / Type	**HAWT**	**VAWT**
Mass	Higher	Lower
Integratibility	Low	High
Operation	Need yaw control systems	Adapt to all wind directions
Centre of Gravity	High	Low
Peak Efficiency	50 %	40 %
Maintenance	Hard	Easy
Noise	High	Low

8.2.2. Rotor Configuration Trade-offs

VAWT are divided into two categories according to the main acting force: Savonius using drag and Darrieus driven by lift. In the Midterm Report, the low-efficiency of the Savonius was investigated. Here, the trade-off is only performed on four main configurations of Darrieus type (see Figure 8.5).

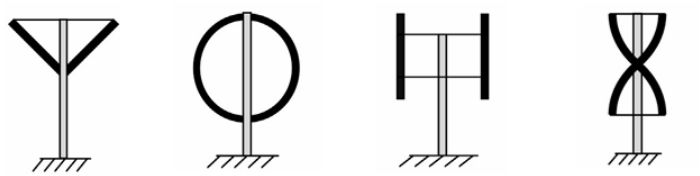

Figure 8.5: Four Darrieus-type VAWT (left to right): V-Rotor, Phi(ϕ)-Rotor, H-Rotor and Helical-Rotor [55]

The trade-off criteria include the following aspects:

- **Manufacturability (Weight 2/5)**: Considering the manufacturing process of wind turbine blades from recycled material, the curvy design of blades significantly increases the difficulty, as seen in the blades of phi-rotor and helical-rotor.
- **Performance (Weight 2/5)**: This criterion evaluates the quantity of power and thrust generated from wind energy. The V-rotor is underdeveloped, while the other three vertical wind turbines have the potential for high-capacity wind farms. Stability of performance is also considered; helical-rotor has the least C_p fluctuation during rotation, followed by the h-rotor, with the phi-rotor having the most fluctuation in unsteady wind conditions[56].
- **Space Efficiency (Weight 1/5)**: This criterion indicates how well the wind turbine utilises the given space. The preliminary design of the upper surface of the body features a platform on top. The V-rotor structure is less compact than other VAWTs and cannot utilise space close to the structure, a similar issue seen with the phi-rotor.

The results are presented in Table 8.3. That scores such as 'very high' indicate better performance compared to other options, not the exact performance compared to existing wind turbines. The h-rotor is selected as the configuration of the final design.

Table 8.3: Trade-off table of four vertical axis wind turbine (VAWT) based on manufacturability, performance and space efficiency

	V-rotor	**Phi-rotor**	**H-rotor**	**Helical-rotor**
Manufacturability	High	Low	High	Very low
Performance	Very low	Very high	High	High
Space Efficiency	Low	High	Very high	Very high

8.3. Rotor Detailed Design

Due to the limited time frame, trading-off for each element is not feasible. Designs are selected based on the rated wind speed, aerofoil, the number of blade and the number of rotor.

8.3.1. Load Assumptions

Below are the assumptions relevant to the loading analysis and structural design of the turbine.

Bending moments due to rotor mass are negligible From preliminary analysis, the bending

moments due to the rotor mass are much smaller than those induced by aerodynamic effects.

The thrust over the cross-sectional area is uniform For load determination purposes, this assumption removes the need to analyse 3D effects, and reduces the rotor to a simple cylinder.

The supporting tower carries only bending moments This assumption concerns the load distribution over the supporting structure. Where the rotating shaft carries torque loads and the weight of the turbine, the supporting tower carries the bending moments.

The rotating shaft carries the turbine weight See explanation above.

8.3.2. Rated Wind Speed

The wind turbine must generate the required power at the average wind speed to ensure year-round operation. The rated wind speed is the speed for which the aerodynamic surfaces are designed and can exceed the average wind speed. The rated wind speed is set to 10 m/s to reflect the current market of VAWT. The excess power will be stored in the battery to power the structure when wind speeds are below the average wind speed. The power scheme relating to the wind speed is shown in Figure 8.6.

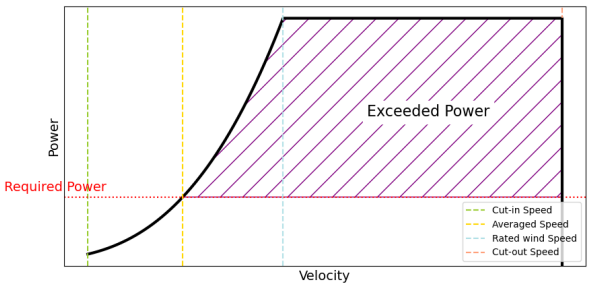

Figure 8.6: Power Scheme

8.3.3. Aerofoil Profile Selection

Various tailored aerofoil in NACA 4-series, natural laminar flow (NFL) aerofoil and SAND aerofoil were investigated for Darrieus VAWT [55]. These aerofoils are customised for higher turbine reliability and longer lifetime when operating at high TSR. In that study, Selig S 1046 emerged as the best-performing aerofoil in the simulation, with a peak C_p of 0.4051. Meanwhile, other studies found that the aerofoil profile in DU17-series had a higher power coefficient C_p at a lower TSR and with reasonable solidity (see Figure 8.7), making it preferable for this design.

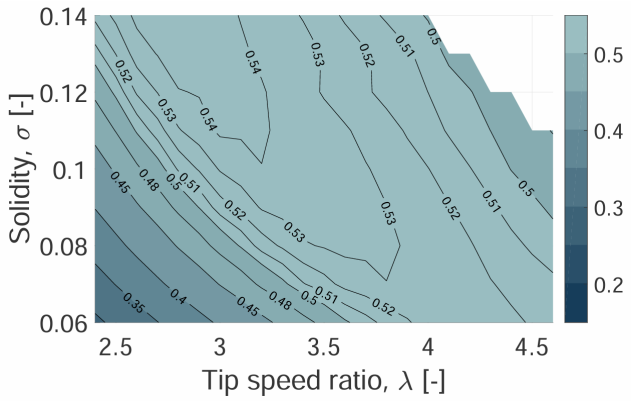

Figure 8.7: Performance coefficient C_p versus tip speed ratio λ at different solidifies for a DU17VAWT200, variable pitch aerofoil [57]

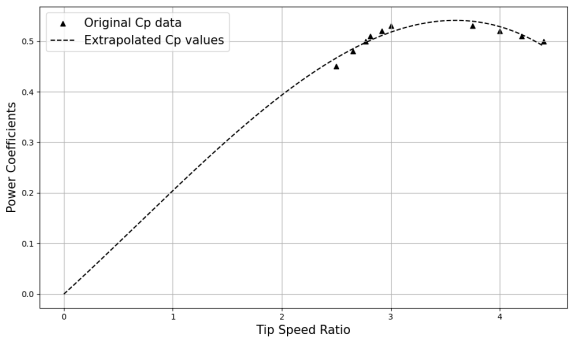

Figure 8.8: Power coefficient C_p as a function of tip speed ratio (λ)

Given the wind turbine operational environment, a lower rotating speed is desirable for safety. Additionally, low solidity (σ) is required for manufacturability (lower chord length of the aerofoil

to manufacture at a fixed radius of wind turbine) and good aerodynamic performance. Therefore, the solidity is chosen to be 0.1 and TSR 2.5, resulting in a peak C_p of around 0.45. With these selected parameters, C_p can also be described as a function of TSR. The generated power will be restricted after reaching the rated wind speed by changing the pitch angle of the wind blades to reduce the TSR and C_p. The available data from Figure 8.7 only includes TSR above 2.5. To present TSR and C_p relation in a lower range, the values are extrapolated in Figure 8.8. Although the selected aerofoil may not achieve its best performance in actual application, it is believed that higher power and lift coefficients for wind turbine aerofoils are possible in the coming years.

8.3.4. Number of Rotors and Blades

VAWT can be designed in a multi-rotor configuration to reduce total weight and total cost [58]. However, multiple sets of rotors will dramatically increase the loading a relatively small structure needs to withstand. Since structural considerations are bound to constrain the design the most, one rotor is chosen as the design configuration.

The number of blades directly influences the initial performance of a Darrieus-type VAWT. The ability of a two-blade rotor to start depends on its initial position, often requiring external assistance. In contrast, three-bladed rotors can self-start regardless of its starting position [59]. According to the 3D modelling results, as the aspect ratio is close to 1, C_p does not change significantly among three blades and five blades [57]. Therefore, a three-blade rotor is selected.

8.3.5. Pitch Control System

The pitch of the blades will be controlled during different phases of power generation as following:

1. Start-up phase: At low wind speeds, the blade pitch is adjusted to ensure the highest torque, facilitating the turbine to self-start.
2. Optimisation phase: At wind speeds between the cut-in speed and the rated wind speed, the pitch is tuned to maximise power output by reaching the optimal λ.
3. Constant power phase: From the rated wind speed until the cut-off wind speed, the pitch is controlled such that the produced power does not exceed the rated power. This is achieved by using decreasingly optimal pitch angles as wind speed increases.
4. Minimum force phase: When wind speeds exceed the cut-off speed, each blade is turned to the angle that minimises the force on the turbine.

The pitch control system uses the wind speed, wind direction, and output power as inputs to output the suitable blade pitch.

8.3.6. Strut Connection

Three common methods for spanwise connecting positions of struts are middle span, quarter span, and end span, presented in Figure 8.9. In terms of aerodynamic performance, middle span and

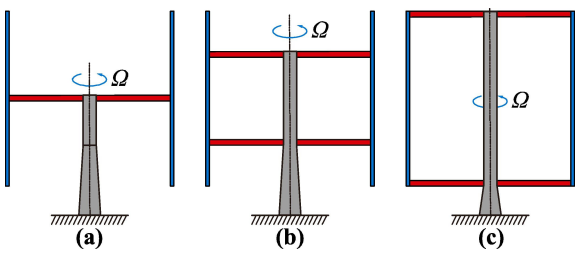

Figure 8.9: Three strut spanwise connecting positions. (a)Middle Span. (b)Quarter Span. (c)End Span. Ω is the rotating speed.

quarter span cause more interruption to the high-performance region of the blades. Nevertheless, end span struts must withstand high bending stress due to the weight of wind blades, leading to potential structural risks. To balance aerodynamic and structural performance, the quarter span is a better option [60]. The quarter span is not fixed exactly at 1/4 of the wind blade. In this design, the struts will be connected to the $0.5c$ of the blades, following the common design of h-rotors. The same aerofoil as the wind turbine blades will be used. The connecting angle, connecting chordwise position, and strut aerofoil profile can be further optimised in the future.

8.3.7. Safety Structure

With a TSR of 2.5 and a foreseeable small wind turbine, the rotating speed can exceed 160 rpm. Although the whole structure is very tall, having a high-speed rotating structure in an open environment may pose risks to nearby tourists and animals. Designing a protective structure around the wind turbine is indispensable. This safety structure should not cause any noticeable interference to the upwind inflow and downwind wake of the wind turbine. A wired fencing structure will be installed on the structure, similar to the one designed by Racing Aeolus Hardliner for their wind car in Figure 8.10. The illustration of the safety structure can refer to Figure 8.11. The safety structure will be purchased from the external supplier because the mesh shape is hard to manufacture from the recycled wind turbine blade.

Figure 8.10: Racing Aeolus Hardliner wind car with vertical axis wind turbine (VAWT) and protection structure

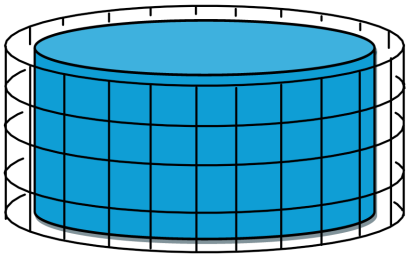

Figure 8.11: Safety structure illustration. Blue cylinder represent rotating wind turbine.

8.3.8. Aspect Ratio

Sizing the wind turbine is done through an iterative procedure. The procedure initiates with a fixed C_p (0.45) and power requirement (320 W from Chapter 7). With four different aspect ratios, the first iteration can be performed by first calculating the power density.

$$Pd = C_p \frac{1}{2} \rho v^3 \tag{8.2}$$

The first maximum height (H_0) follows from the turbine size derived from the average wind speed $6.49 m/s$ and is therefore the same starting point for all iterations. The wind speed, however, is an overestimate of the actual wind speed as a result of wind shear. Considering the design space of the turbine is below $10m$, the wind speed decreases considerably along the cross-section. Following Equation 8.2 one arrives at an initial frontal area of $6.71 m^2$.

$$H_i = \sqrt{AR \cdot A_i} + h_0 \tag{8.3}$$

The height found previously corresponds to the maximum height that the turbine reaches and is not the dimensional height of the turbine, hence the addition of the base height of the turbine.

The maximum height is of interest when determining the wind speed profile along the cross-section of the turbine, the average of which is calculated using Equation 8.4.

$$\bar{v}_i = \frac{1}{H_i - h_0} \int_{h_0}^{H_i} v_{ref} \frac{\ln h/z_0}{\ln h_{ref}/z_0} \, dh \tag{8.4}$$

In the above case, the turbine is assumed to rotate according to the average wind speed, as opposed to the maximum or minimum speed within its design space. The area follows straightforwardly from the power density formula. Rewriting it for area as a function of the average wind speed, one arrives at a new size for the wind turbine which is readily translated to its maximum height using the same aspect ratio as before.

$$A_{i+1} = \frac{2P}{\rho C_p \bar{v}_i^3} \tag{8.5}$$

$$H_{i+1} = \sqrt{AR \cdot A_{i+1}} + h_0 \tag{8.6}$$

The procedure undergoes four iterations for all aspect ratios before converging within two percent of the final value. The results are summarised in Table 8.4.

Table 8.4: Class II turbine frontal area estimation for different aspect ratios and a performance coefficient of 0.45

	Iteration 1			Iteration 2			Iteration 3			Iteration 4		
Aspect ratio	**Maximum height** $[m]$	**Average velocity** $[m/s]$	**New size** $[m^2]$	**Maximum height** $[m]$	**Average velocity** $[m/s]$	**New size** $[m^2]$	**Maximum height** $[m]$	**Average velocity** $[m/s]$	**New size** $[m^2]$	**Maximum height** $[m]$	**Average velocity** $[m/s]$	**New size** $[m^2]$
0.5	5.06	5.36	7.53	4.94	5.35	7.60	4.95	5.35	7.59	4.95	5.35	7.59
1	5.06	5.36	7.53	5.74	5.46	7.15	5.67	5.45	7.19	5.68	5.45	7.18
2	5.91	5.48	7.07	6.76	5.58	6.68	6.66	5.57	6.73	6.67	5.57	6.72
3	6.57	5.56	6.76	7.50	5.66	6.40	7.38	5.65	6.44	7.40	5.65	6.44
4	7.12	5.62	6.54	8.12	5.72	6.19	7.98	5.71	6.23	7.99	5.71	6.23
5	7.61	5.67	6.36	8.64	5.78	6.03	8.49	5.76	6.07	8.51	5.76	6.07

8.4. Static Loading Analysis

In this section, the loading model applied is static, without considering dynamic effect over the cross section of the wind turbine and the turbulence and the wake. At the upwind and downwind part of the wind turbine, the load is uniform.

8.4.1. Optimum Energy Conversion

Both horizontal and vertical axis wind turbines must obey energy conservation as a part of the Momentum Theory. While a maximum energy conversion would result in a downstream wind velocity of $0m/s$, this is not physically possible. There exists a physical maximum, and thus optimal ratio of wind speeds such that power conversion is maximised.

A non-dimensional factor known as the induction factor defines the total loss of velocity induced by the turbine rotor, defined by the difference in wind speed over the free stream velocity. Maximising this factor results in the most optimal design. The two coefficients of interest are those for thrust and power, defined in terms of the induction factor by Equation 8.7 and Equation 8.8 respectively. Their distributions have been plotted in Figure 8.12 along with the normalised mass flow distribution. Note that the product of the mass flow and thrust results in the power distribution.

$$C_T = 4a(1-a) \tag{8.7}$$

$$Cp = 4a(1-a)^2 \tag{8.8}$$

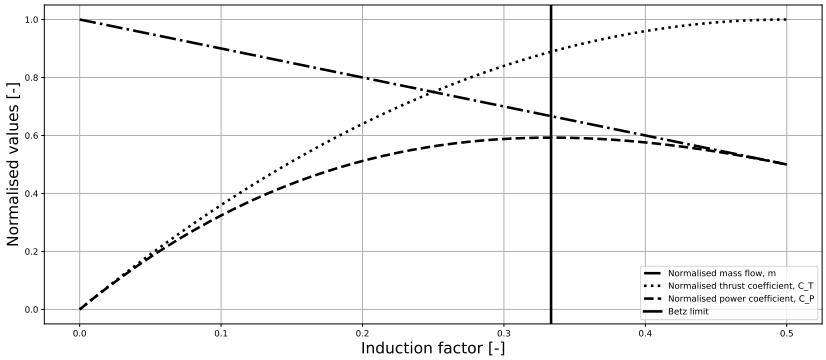

Figure 8.12: Dimensionless performance coefficients as a function of induction factor for optimum energy conversion including the Betz limit at $a = 1/3$

From this plot it is apparent that the the mass flow rate passing through the rotor decreases while the thrust increases. This leads to an optimal combination of thrust force and mass flow rate that optimises the power.

For a design C_p of 0.45 as defined previously, one can inverse to arrive at an induction factor of 0.159 which is well below the Betz limit. Following these relations, the thrust coefficient equals 0.535.

8.4.2. Thrust and Internal Loading Distribution

The turbine must be capable of operating in all conditions below the cut-out speed of $20m/s$. Sizing the supporting structure must therefore be done according to the thrust resulting from this maximum speed. Two distributions are of importance, those being the shear load distribution and the bending moment distribution. Concerning the design, these distributions lead to the sizing and design of VAWT structural elements including the rotating shaft and load bearing tower. The latter shall be discussed in more detail within the Structures chapter. In order to compute the shear load distribution one must know how thrust varies along the rotor.

Following from the induction factor it is possible to compute the thrust distribution as a function of height as illustrated by Figure 8.13.

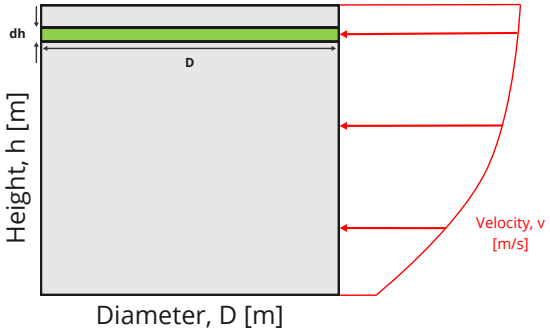

Figure 8.13: Turbine height discretisation for loading analysis

The thrust distribution as a function of height can be found in Figure 8.14. Reflecting Table 8.4,

different loading distributions are visualised for varying aspect ratios. It is noteworthy how the distributions scale significantly for decreasing aspect ratios, where the differential loading at each height is much larger for low aspect ratios. This follows directly from the combined fact that the maximum height of the VAWT scales with the square root of the aspect ratio and area as well as the average velocity decreasing exponentially. Integrating the thrust distribution yields the total thrust over the entire structure, and thus the total shear force at the root of the VAWT.

$$dT = C_T \frac{1}{2} \rho v^2 D dh \tag{8.9}$$

$$T = \int_{h_T} dT \tag{8.10}$$

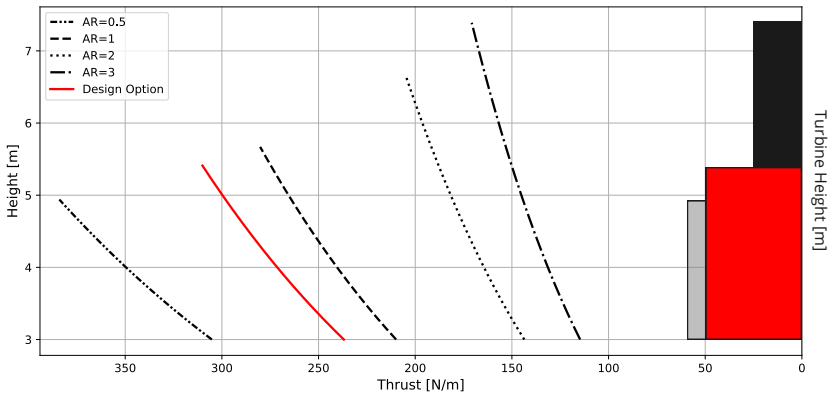

Figure 8.14: Internal thrust distribution at cut-out speed as a function of turbine height for different aspect ratios including the design option in red and turbine heights for illustration purposes, assuming constant thrust coefficient

As explained previously, the internal shear distribution follows straightforwardly from the loading distribution as it equals the summation of differential thrust forces above a specified height, with the top of the rotors being load free. Note that the internal loading diagrams of Figure 8.15 display magnitudes and analyse the influence of the free stream and not that of the struts. These distributions play an important role in determining the placement of the struts and thus it is not yet known where the strut forces will apply on the turbine blade.

The internal bending moment follows similarly from the differential thrust method. In this case, however, the force per infinitesimal area is multiplied by the height of the element to obtain the bending moment. Mathematically speaking, this results in Equation 8.11. With the total bending moment at the root of the turbine determined by Equation 8.12.

$$dM = h dT \tag{8.11}$$

$$M = \int_{h_T} dM = \int_{h_T} C_T \frac{1}{2} \rho v^2 D h dh \tag{8.12}$$

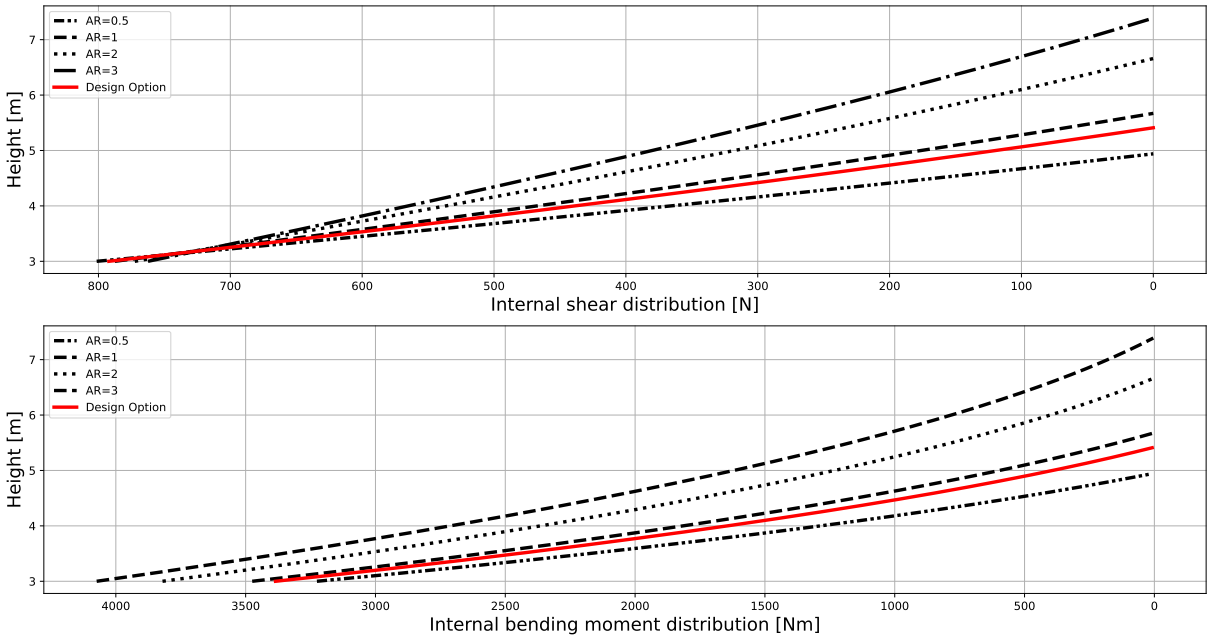

Figure 8.15: Internal loading diagrams as a function of turbine height for different aspect ratios at cut-out speed including the design option in red, assuming constant thrust coefficient

Determining Aspect Ratio The turbines of Figure 8.14 and Figure 8.15 have been sized such that they generate the same theoretical amount of power, yet they differ in performance. Small aspect ratio, and thus short turbines, require a larger swept area to compensate for the lower wind velocities. Conversely, high aspect ratio turbines require additional support at the root to carry the large bending loads. A compromise must be made between performance and structural integrity.

As will be discussed in more detail in a later chapter, the bending moment deemed to be a more limiting factor than the reduced performance of a low aspect ratio turbine. Requirements on the transportation and stability of the structure dictate that the total height must be minimised. For this reason, the chosen aspect ratio is 0.8. Table 8.7 defines the turbine sizing and loading.

Chord Length Design With the aspect ratio determined as 0.8 and a σ of 0.1, the chord length can be calculated.

$$\sigma = \frac{Bc}{2R} \tag{8.13}$$

Thus, the chord length is 0.1 m and the thickness is 0.02 m at 0.025 m position. The illustration of the dimension of the aerofoil is in Figure 8.16.

8.4.3. Rotor Performance

It is assumed that the cut-in speed is 3 m/s[3]. And the rated wind speed and the cut-out speed has been defined as 10 m/s and 20 m/s in subsection 8.3.2 and subsection 8.1.5, respectively. With all the necessary parameters determined, λ, C_p, C_T, power and thrust relations with the wind speed are presented Figure 8.17 to Figure 8.19.

[3] `https://theroundup.org/wind-turbine-power-curve/`

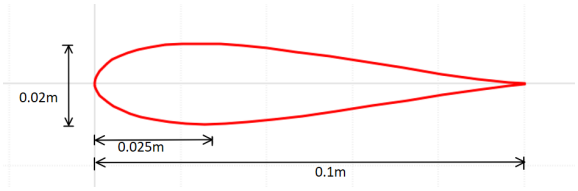

Figure 8.16: Illustration of the chord design of DU17VAWT200

Table 8.5: VAWT parameters according to the static loading analysis model

Parameter	Value
Aspect Ratio [–]	0.8
Swept Area $[m^2]$	7.32
Height $[m]$	2.42
Diameter $[m]$	3.02
Chord Length $[m]$	0.1
Tip Height $[m]$	5.42
Root Shear Load $[N]$	666.1
Root Bending Moment $[Nm]$	2846
Maximum Power Generation $[W]$	1171

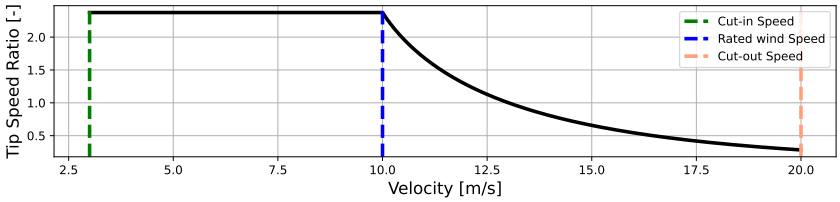

Figure 8.17: Tip speed ratio, λ with respect to velocity

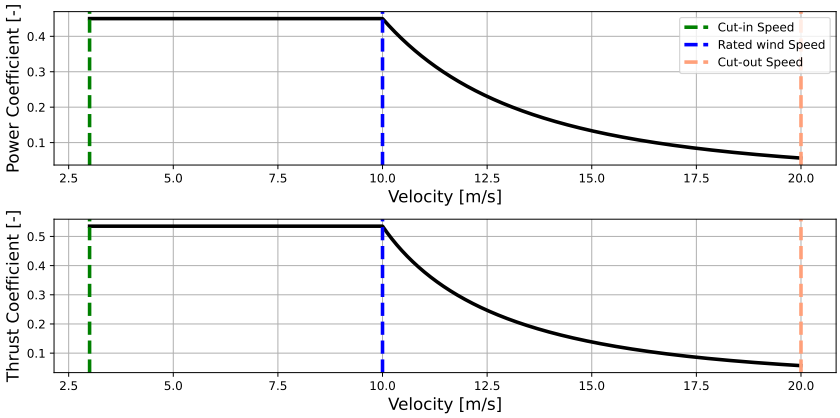

Figure 8.18: Power and thrust coefficients, C_p C_T versus velocity curve assuming uniform free stream

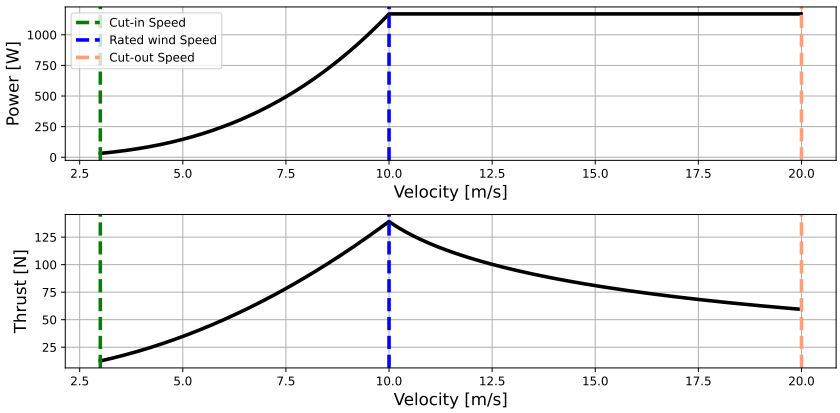

Figure 8.19: Power, P and thrust, T distributions versus velocity assuming uniform free stream

8.4.4. Torque

The wind energy is extracted to mechanical power, which means the torque making the wind turbine rotate. The mechanical torque can be determined by the Equation 8.14 as following:

$$T = \frac{P}{\omega} \tag{8.14}$$

P indicates the power generated and ω represents the rotational speed. From Figure 8.17, the relation between wind speed and the rotational speed and estimated torque are computed. The results are in Figure 8.20.

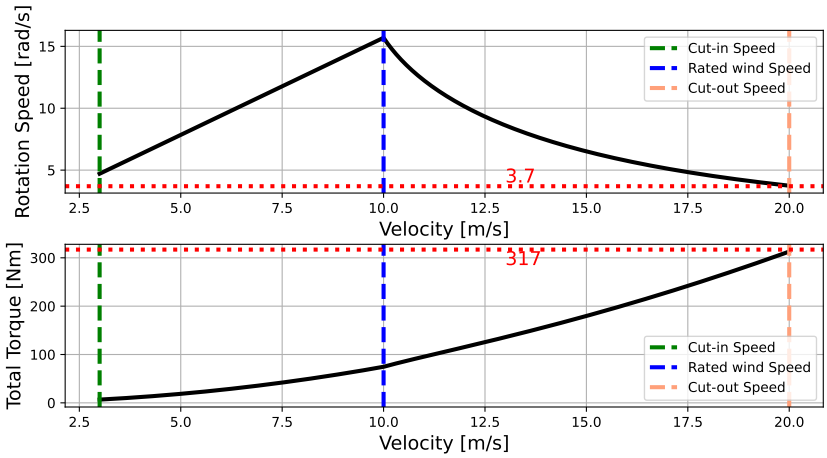

Figure 8.20: Rotational speed, ω and estimated total torque provided by the wind blades, T vary with the coming wind speed

From Figure 8.20, it can also be concluded that the rotor frequencies ranges from the lowest 0.59 Hz to the highest 2.63 Hz. It is recommended to optimise the structure to avoid overlapped natural frequencies between different subsystems.

8.4.5. Torque Analyses and Shaft Design

After estimating the total torque, the torque analyses and the shaft design can be performed. One of the assumptions is that there is no internal torque in the shaft during accelerating and decelerating of the wind blades, and the resistance of the gearbox and the generator will be neglected. Thus, the rotor shaft only carries the weight of the wind turbine and the torque of the rotor caused by the braking system when reaching the cut-out speed. The structure bearing other loading, such as the bending moment caused by the thrust, is designed in Section 12.5.

Generally, the rotor shaft in the tower connects to the struts at the top, and the gearbox at the bottom, which followed by the generator. Besides, the braking system mechanism needs to be clarified. It has been proposed that the h-rotor has the potential to effectively utilise this aerodynamic braking mechanism by adjusting the pitching angle in the strong wind[55]. For instance, the slots can be incorporated into the blade design, supporting a higher decelerating rate [61]. Beyond this, a disc brake can be connected the shaft before the gearbox. The actual mutual effects of aerodynamic braking and disc brake to high-speed VAWT are not cleared currently and lack of relevant literature. Moreover, braking mechanisms affect the design of the shaft and the rest of the structure. The shear stress of shaft should not go over the shear strength of the shaft material, which here is assumed to the stainless steel with shear strength approximately 200 MPa [4]. The resultant internal torque is related to the torque to slow down the rotating wind

[4]Matweb,https://www.matweb.com/search/datasheet_print.aspx?matguid=71396e57ff5940b791ece120e4d563e0

turbine. Related formula are Equation 8.15 and Equation 8.16:

$$\tau = \frac{Tr}{J_{shaft}} \tag{8.15}$$

$$T = I_{windturbine}\frac{d\omega}{dt} \tag{8.16}$$

For the analyses, it is assumed that the stopping time is 1.3 seconds [62] and it is a steady braking. From Figure 8.20, the rotational speed at the cut-out speed is 3.7 rad/s, resulting the decelerating rate of 2.84 rad/s^2. To simplify the torque model, the torsion analyses consider aerodynamic braking and disc braking separately as following. Besides, $I_{windturbine}$ is based on a simplified hollow cylinder.

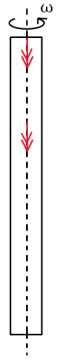

Figure 8.21: Braking torques applying to the rotating shaft by the wind blades

Figure 8.22: Braking torque applying to the rotating shaft provided by the disc braking system

Aerodynamic Braking
Following increasing wind speed, the wind blades will be adjusted to reduce the torque or produce an anti-torque to stop the rotation. In this case, the model only considers the anti-torque (see Figure 8.21). With the designed braking time, the anti-torque is calculated as 365.7 Nm. The radius of the shaft should be at least 0.0104 m.

Disc Braking
If there is only disc brake stopping the rotation, the internal torque it caused at the end of the shaft (see Figure 8.22) should be at least 682.7 Nm as the wind turbine still tries to rotate. To withstand this torque, the radius of the shaft should be at least 0.0129 m.

With a safety factor 1.5, the radius finally is decided as 0.02 m. With this radius, the shaft can also withstand the compressive load due to the weight. It is noted that the disc brake system will introduce a torque to the moving structure, which is not a stable foundation. High-torque transmission also easily leads to gearbox failure [62]. Therefore, only having a disc brake is not desirable. Apart from sizing, the material of the shaft needs further study for its performance in the humid environment and its sustainability.

8.4.6. Aerofoil Pitch and Blade Twist

The thrust and internal loading diagrams of Figure 8.14 and Figure 8.15 assume a constant thrust coefficient at the cut-out speed. For initial sizing and load determination, this assumption is acceptable as it is a conservative one. However, one must not ignore the fact that the turbine rotates at a constant angular velocity and the generated power cannot be discretised over the height as it is linked to the rotational speed. The power and thrust coefficients from above, which have been determined using the rated wind speed, do not remain constant under the variable wind speed model. However, incorporating non-uniform wind speeds leads to power and thrust coefficients that vary over the height and over the cross-sectional area when considering 3D effects. Such an analysis is far beyond the scope of this exercise, yet designing for this effect is much more straightforward.

The variable airspeed profile can be compensated for by introducing variable pitch in the rotor

aerofoil. Varying pitch changes the angle of attack, and angle of attack is a variable for the coefficient of lift and drag. The latter two influence the normal and tangential forces, which in turn influence the thrust produced by the turbine. More on this will be discussed later. Varying the blade pitch therefore ensures that the power and thrust coefficients remain constant over the entire turbine.

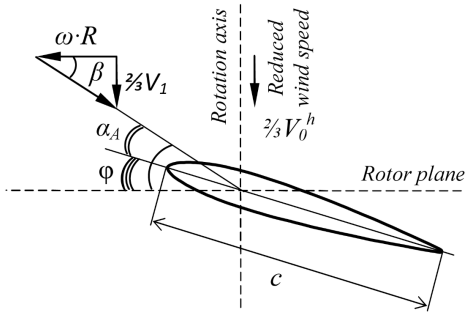

Figure 8.23: Incoming airflow as a function of angle of attack, α and pitch angle φ for a HAWT [63]

The incoming airflow vector, β depends on the rotational velocity and free stream velocity. Its incidence angle can be divided into the aerofoil pitch angle φ and angle of attack α as illustrated by Figure 8.23. Note that the figure is for a horizontal wind turbine, although its angles apply for VAWT as well. Rearranging for angle of attack and expressing the incoming airflow as an inverse tangent function of the velocity components results in Equation 8.23.

$$\alpha_h = \beta - \varphi = \arctan\left(2a\frac{v_{\infty,h}}{R\omega}\right) - \varphi_h \tag{8.17}$$

Here, the subscript h in the angle of attack and free stream velocity relate to a specific height. R is the turbine radius and ω the rotational velocity. Substituting in the log law from before yields a relation of angle of attack with height.

$$\alpha(h) = \arctan\left(\frac{2a}{R\omega} \cdot v_{ref} \cdot \frac{\ln h/z_0}{\ln h_{ref}/z_0}\right) - \varphi \tag{8.18}$$

Keeping the angle of attack constant as desired for increasing (turbine) height means setting its derivative with respect to height equal to zero. Additionally defining a constant term Z and rewriting for the change of pitch angle in height yields Equation 8.20.

$$Z = \frac{2a}{R\omega} \cdot v_{ref} \cdot \frac{1}{\ln h_{ref}/z_0} \tag{8.19}$$

$$\frac{d\varphi}{dh} = \frac{1}{(Z \ln h/z_0)^2} \cdot \frac{Z}{hz_0} \tag{8.20}$$

Finally, integrating Equation 8.20 yields the distribution of pitch angle as a function of turbine height.

$$\varphi(h) = \left[\frac{1}{z_0}\arctan\left(Z \ln h/z_0\right)\right]_3^h + \varphi(3) \tag{8.21}$$

Equation 8.21 yields a maximum relative twist of 10.4 $[deg]$ which is illustrated in Figure 8.24 (blade length not to scale).

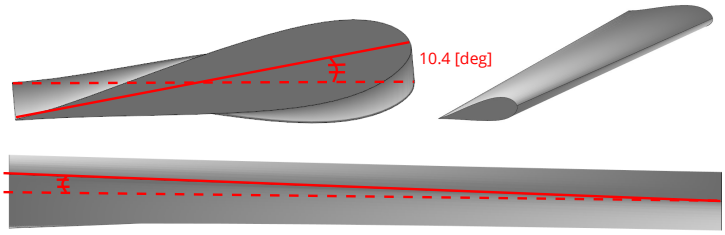

Figure 8.24: Aerofoil twist over blade span, blade length not to scale

Manufacturing of the aerofoil blade would be more difficult for a twisting aerofoil. The main difference between manufacturing a twisted blade and a uniform-pitch one is the mould. As explained in the manufacturing chapter, however, this is possible with little additional effort. In addition to this, the twist of the decommissioned wind turbine blades can be harnessed for this twist design. Its effect on the other hand is that its performance and reliability to perform in the intended way is increased considerably. Figure 8.25 outlines how the angle of twist is distributed over the total height of the chosen configuration. It is plotted against a linear twist distribution to better understand the nature of twist.

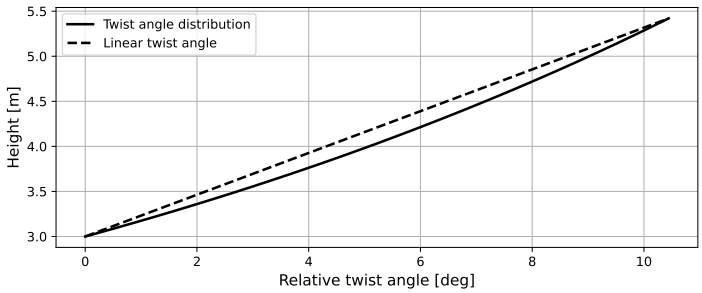

Figure 8.25: Aerofoil twist distribution over turbine height plotted against a linear twist

8.5. Sensitivity Analysis

The aspect ratio was established through iteration under certain conditions with the help of established research on its influence on performance. Additionally, the structure is constrained in its dimensions due to stability and the fact that it must fit within a standard shipping container. The analysis on loading under the influence of the ABL defined the preference for a tall turbine to exploit high airspeeds at increasing heights.

Maximum height dimensions result from transportation requirements and stability. Minimum dimensions, however, result from optimisation on aerodynamic front. Changes in the configuration could have a significant effect on the other sub-systems, particularly structures and materials (a low aspect ratio turbine a requires a larger rotor). Understanding the magnitude of the aspect ratio's influence on rotor dimensions and loading is, for the reasons stated above, necessary.

The objective of this sensitivity analysis is to remind the reader of the variables influencing the rotor design and quantitatively understand how small differences in aspect ratio affect rotor dimensions and turbine loading.

Wind model and loading variables

- Performance coefficient, C_p
- Thrust coefficient, C_T
- (Reference) wind speed, v
- Frontal area, A
- **Aspect ratio,** AR
- Air density, ρ
- (Reference) height, h
- Base height, h_0
- Surface roughness level, z_0

Table 8.6: Wind turbine variations in dimensions, loading and performance for incremental changes in rotor aspect ratio

Aspect Ratio [-]	Rotor size $[m^2]$	Height $[m]$	Diameter $[m]$	Rotor size difference	Shear load difference	Bending moment difference	Maximum power difference
0.6	7.5	2.12	3.53	2.5%	0.7%	3.1%	0.9%
0.7	7.40	2.28	3.26	1.1%	0.5%	1.2%	0.3%
0.8	7.32	2.42	3.02	-	-	-	-
0.9	7.25	2.56	2.84	1.0%	0.5%	1.1%	0.2%
1.0	7.19	2.68	2.68	1.8%	0.6%	2.7%	0.3%

It is evident from Table 8.6 that incremental changes in aspect ratio of ± 0.2 minimally change the shear loads and bending moments. The size of the rotor changes within a maximum of 2.5% which is an acceptable amount.

8.6. Verification of Wind Turbine Design

Beyond sensitivity analysis, other methods to verify the design of the wind turbine are included in this section, such as comparing its performance to other micro-scale wind turbines and verifying it with the simulation software QBlade.

8.6.1. Comparison to Historical Data

Manufacturing and assembling the designed wind turbine for field tests on the Dutch coastline are not feasible within the limited time frame. However, the estimated performance of the designed wind turbine can be verified by comparing it to the performance of other micro-scale wind turbines in low-wind, near-ground areas. According to a study conducted in the UK [64], wind turbines with a rated power of 1.5 kW, a rotor diameter of 2.1 m, and a cut-in wind speed of 2.4 m/s in areas with an average wind speed of 4.9 m/s yield an annual energy output of approximately 2500 kWh, which translates to a power output of around 285 W. The similarity in performance levels suggests that the design falls within a reasonable range.

8.6.2. Dynamic Thrust Discussion and 2D Model Verification

The model applied to the design only considers static thrust and assumes uniform loading over the cross-sectional area of the wind turbine, which is sufficient for primary sizing and analysis. The strength of this analysis lies in including the wind shear effect to optimise the aspect ratio determination and loading computation. The plan for including height-level thrust variation has also been designed for the twist in subsection 8.4.6, but dynamic pitch control to accommodate flow variation over a 2D plane has not yet been considered. To delve into the neglected aspects of this model and investigate the effects of these assumptions, it is necessary to examine the flow and force variation with blade location from a 2D blade element perspective. The forces applied to the wind blade in relation to the blade location are described in Figure 8.26 and Equation 8.22 to Equation 8.27.

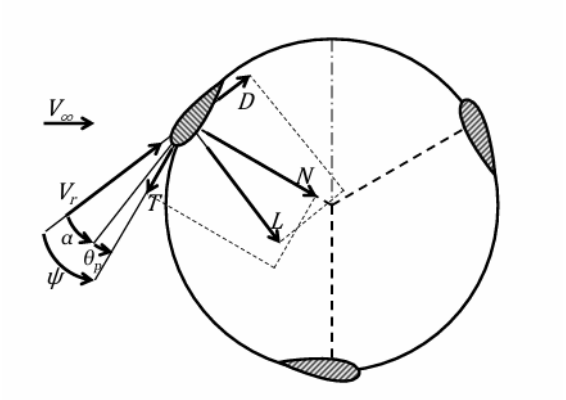

Figure 8.26: Forces acting on a 2D blade element. Clockwise rotation.[57]

$$\vec{V_{\text{rel}}} = \vec{V_\infty} + \vec{V_{\text{rot}}} + \vec{V_{\text{ind}}} \tag{8.22}$$

$$\alpha = \tan^{-1}\left(\frac{V_n}{V_t}\right) - \theta_p \tag{8.23}$$

$$L_{2D} = \frac{1}{2} C_L(\alpha) \rho V_{\text{rel}}^2 c \tag{8.24}$$

$$D_{2D} = \frac{1}{2} C_D(\alpha) \rho V_{\text{rel}}^2 c \tag{8.25}$$

$$F_N = L_{2D} \cdot \cos(\Psi) + D_{2D} \cdot \cos(\Psi) \tag{8.26}$$

$$F_T = L_{2D} \cdot \sin(\Psi) - D_{2D} \cdot \sin(\Psi) \tag{8.27}$$

Angle of attack α, defined in Equation 8.23, is positive in the upwind part and negative in the downwind part (see Figure 8.27). As simulation results in Figure 8.28, relative velocity V_{rel} become largest at θ = zero because the incoming flow velocity V_∞ and the rotational velocity V_{rot} are in the same direction. From Equation 8.26 and Equation 8.27, it can be concluded that the normal force and the tangential force vary over a cycle (see Figure 8.29). To calculate the

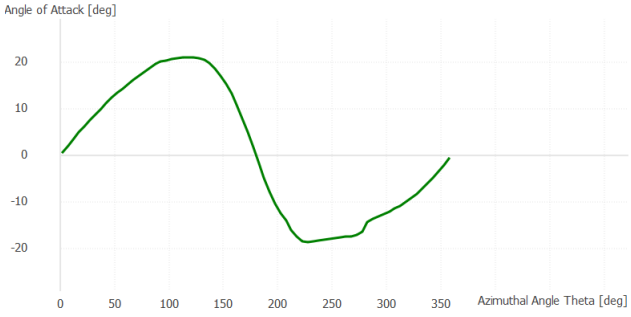

Figure 8.27: Angle of Attack α varies with the Azimuth Angle θ (without defining pitch angle). Radius $R = 1.5125\ m$, chord length $c = 0.1\ m$, number of blades $B = 2$, incoming velocity $V_\infty = 10\ m/s$, Tip speed ratio $\lambda = 2.5$

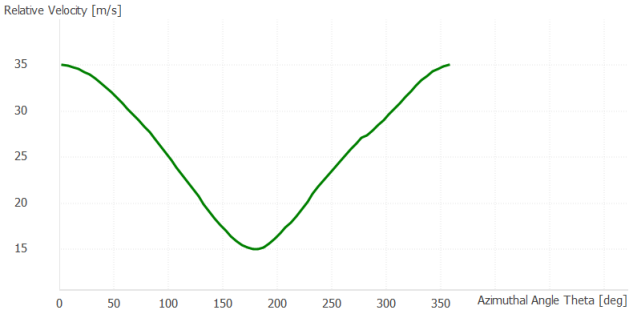

Figure 8.28: Relative velocity V_{rel} varies with the Azimuth Angle θ. Radius $R = 1.5125\ m$, chord length $c = 0.1\ m$, number of blades $B = 2$, incoming velocity $V_\infty = 10\ m/s$, Tip speed ratio $\lambda = 2.5$

resulting averaged power, thrust and torque in a 2D plane, force components will be integrated over θ as Equation 8.28, Equation 8.29 and Equation 8.30.

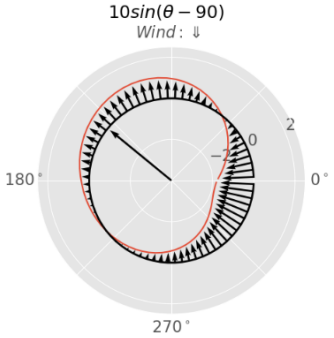

Figure 8.29: An example of normal force distribution over azimuth angles θ. Pitch angle θ_p setting for each θ: $10sin(\theta - 90)$ [65]

$$P_{2D} = \frac{1}{2\pi} \int_0^{2\pi} B \cdot F_T(\theta) \cdot \omega R d\theta \tag{8.28}$$

$$T_{2D} = \frac{1}{2\pi} \int_0^{2\pi} B \cdot (F_T \cdot cos(\theta) - F_N \cdot sin(\theta)) d\theta \tag{8.29}$$

$$T = \int_0^{2\pi} R \frac{1}{2} \rho V^2 c (C_L sin(\Psi) - C_D cos(\Psi)) d\theta \tag{8.30}$$

Incorporating flow and force variation, the simulation based on the double-multiple-streamtube (DMS) model was performed using the wind turbine simulation software QBlade. The DMS model sections the 2D cross-sectional area of the wind turbine into a series of adjacent aerodynamically independent streamtubes, enabling calculations of different induced velocities for the upwind and downwind halves separately [57].

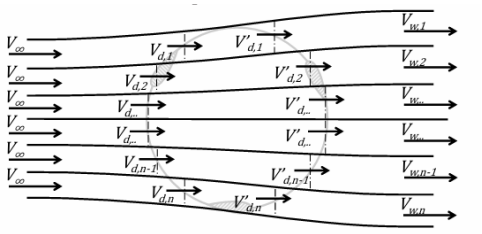

Figure 8.30: Double-multiple-streamtube model illustration [57]

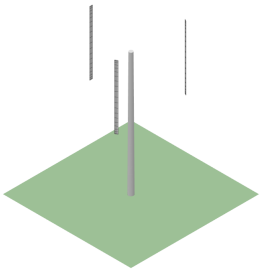

Figure 8.31: Simulation model in Qblade. Blade length = 2.24 m, shaft length = 4.68 m, calculated twist angle applied to corresponding cross sections.

The simulated C_p and C_T at a λ of 2.5 are 0.38 and 0.533, respectively. Corresponding power, thrust and torque performances of the wind turbine between cut-in speed and rated wind speed, from the simulation are at high Reynolds number Re, are shown in Figure 8.32. The results of

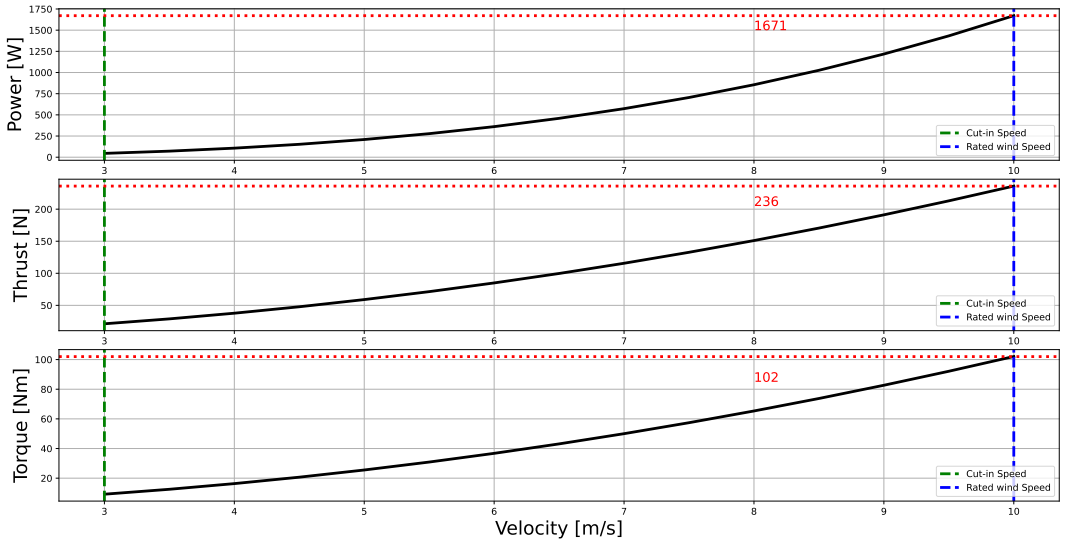

Figure 8.32: Simulated power, thrust and torque from cut-in speed to rated wind speed assuming uniform free stream. Reynolds number Re = 1700000, swept area = 7.32 m^2, tip speed ratio λ = 2.5.

the simulation are subject to viscous effects. However, without the correction of the wind field (mainly through the wind shear effect and updated swept area implemented concurrently), the simulated power and thrust are larger than the estimated results in Figure 8.19. Apart from the force variation at different positions, the 2D model does not include turbulence and wake effects. Additionally, when choosing an aspect ratio lower than 1, the power loss becomes significant between a 2D model and a finer 3D model, i.e. C_p performs worse than the design. Although this was considered in selecting the number of blades, choosing a low aspect ratio was inevitable

for the stability of the entire structure, resulting in less satisfactory performance. Due to these consequences of the simplified design model, optimisation and iteration are recommended for future work.

8.7. Summary

Table 8.7: Designed VAWT key parameters

Parameter	Unit	Values
Wind Turbine Type	-	VAWT
Rotor Configuration	-	H-rotor
Turbine Class	-	IEC Class IV
Aerofoil	-	DU17VAWT200
Number of Rotor	-	1
Number of Blade	-	3
Strut Connection	-	Quarter span
Solidity	-	0.1
Designed Tip Speed Ratio	-	2.5
Aspect Ratio	-	0.8
Swept Area	m^2	7.32
Height	m	2.42
Diameter	m	3.02
Chord length	m	0.1
Tip Height	m	5.42
Shaft Radius	m	0.02
Shaft Material	-	Stainless Steel
Maximum Relative Twist	deg	10.4
Cut-in Speed	m/s	3
Rated Wind Speed	m/s	10
Cut-out Speed	m/s	20
Rated Power	W	1171
Estimated power output	W	320
Pitch Control System	-	Yes
Braking System	-	Aerodynamic Braking & Disc Braking
Safety Structure	-	Yes

8.8. Compliance Matrix

This section presents the list of requirements and the degree to which the wind turbine sub-system adheres to them. Requirements can be fully met, partially met, not met, or to be investigated where the current analysis techniques are insufficient and they require physical testing. In the interest of saving space, only requirement identifiers have been added which correspond to the requirements listed in the first chapter.

Table 8.8: Wind turbine subsystem compliance matrix

Requirement	Status	Requirement	Status
REQ-USER-01-SYS-01	Fully met	**REQ-USER-05-SYS-03**	To be investigated
REQ-USER-02-SYS-03	To be investigated	**REQ-USER-17-SYS-01**	Fully met
REQ-USER-02-SYS-07	To be investigated	**REQ-USER-17-SYS-02**	Fully met
REQ-USER-04-SYS-01	To be investigated	**REQ-EoL-01-SYS-01**	Fully met
REQ-USER-04-SYS-02	Fully met	**REQ-EoL-02-SYS-01**	To be investigated
REQ-USER-05-SYS-02	Partially met	**REQ-USER-02-SYS-02-STR-03**	To be investigated

9

Kinematics

This chapter is dedicated to investigate on the kinematic motion of the design. The order of the chapter follows: Section 9.1 delves into the modified Jansen's linkage that is used in the structure. Section 9.2 lays out how the structure is going to steer and brake while operating. The design and analysis of the feet of the legs is provided in Section 9.3. The sizing of the legs is performed in Section 9.4 and finally, the power estimation of the leg system is given in Section 9.5.

9.1. Jansen Linkage Configuration

From the original Jansen linkage introduced in subsection 7.1.1, it is modified to improve the stability of the overall design [66]. Figure 9.1 shows the original linkage and the modified linkage, Table 9.1 presents the ratios, respectively.

(a) Original Jansen Linkage

(b) Modified Jansen Linkage

Figure 9.1: Visual differences in the modified Jansen Linkage compared to the original [66]

Table 9.1: Differences in link ratios from the Jansen Linkage

Parameter	Jansen linkage	Modif. Jansen	Parameter	Jansen linkage	Modif. Jansen
A_0A/l_2	15.0	15.0	DE/l_8	36.7	36.7
AB/l3	50.0	59.0	EM/l_81	49.0	49.0
B_0B/l_4	41.5	40.0	x_{A_0}	-38.0	-45.0
B_0C/l_41	40.1	41.5	y_{A_0}	-7.5	0
AE/l_5	61.9	63.0	α_0	90.0°	86.4°
B_0E/l_6	39.3	39.3	β_0	90.0°	99.1°
CD/l_7	39.4	43.0			

The first noticeable change is to make the fixed points collinear to create a stable horizontal platform for a walking structure. The distance between the fixed points (x_{A_0}) has also been increased to create more clearance between the feet when they are at the closest point to each other. Furthermore, other links are carefully adapted to maintain a smooth motion.

It is necessary to verify the effect that the modification of the mechanism has on the footpath (also called coupler curve) and the stability of a walking structure using this link. Therefore, both

mechanisms are analysed using a python program adopted from DIY Walkers [1]. This program uses a circle intersection algorithm to determine the joints' positions one by one for different crank angles (ϕ in Figure 9.1). Using an adaptation of this kinematic simulation program, Coupler curves of the leg are created for both the original (Figure 9.2a) and the modified Jansen linkage (Figure 9.2b).

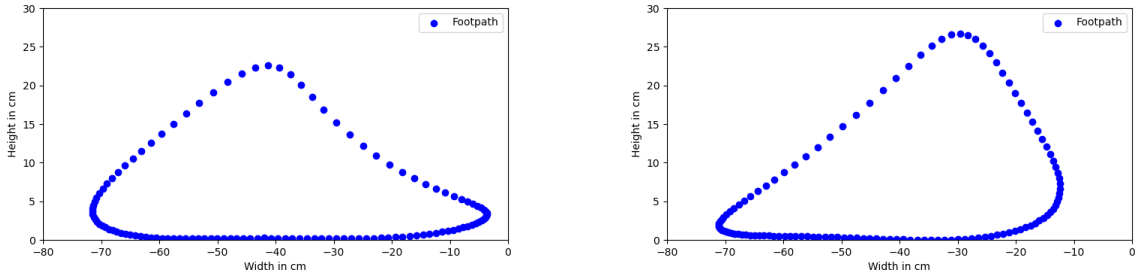

(a) Coupler Curve Original Jansen Linkage **(b)** Coupler Curve Modified Jansen Linkage

Figure 9.2: Differences in the footpath of the modified Jansen Linkage compared to the original

From the curves, two observations can be made; the step height of the modified Jansen linkage is higher, and the step length is shorter. This modification helps navigating on a rough terrain and limits how much the structure will get stuck.

For stability, it is useful to observe a foot in contact with the ground. Using the simulation and defining it to be in contact with the ground below 3 $[cm]$, it is found that both versions of the Jansen Linkage are in contact about 56% of the time. The amount of legs also influence the stability; at least three legs should be on the ground at all times to maintain stability, however four legs on the ground effectively doubles the base of support. Therefore, at least four pairs of legs are necessary; two pairs on each side to ensure at least two legs on the ground at each side. Six pairs of legs might improve stability as more legs are in contact with the ground, and therefore the movement will be smoother. This is further investigated by looking at the heights of the feet for two pairs and three pairs of feet on each side.

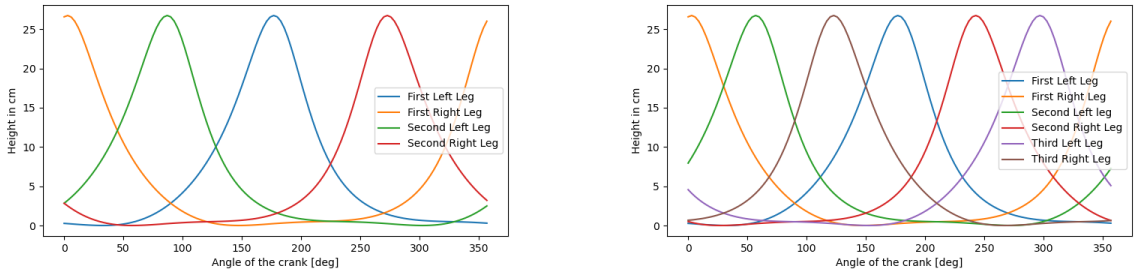

(a) Footheigth at specific crank angles for two pairs of legs at one side **(b)** Footheight at specific crank angles for the three pairs of legs

Figure 9.3: Footheight at specific crank angles for two and three pairs of legs

From Figure 9.3a a transition can be noted for two pairs on one side: one leg is moving down to the ground, while the other leg is already being relieved from the ground pressure. Three pairs of legs on each side provide more stability; by ensuring at least two feet are on the ground at each side it provides smoother motion. Therefore three pairs of legs on each side are chosen.

[1] DIY Walkers.com, *URL* `https://www.diywalkers.com/linkage-simulation.html`, accessed 31 May 2024

To analyse stability and loads, the most critical leg situation must be identified and quantified. The most critical loading situation arises when a large moment is induced by aerodynamic forces, causing the loads to be carried by one side of the legs to counteract the moment, just before tipping over. This occurs when one leg on that side is in contact with the ground, just before a second leg touches the ground (as shown by the left leg in light grey in Figure 9.4). At this point, the moment arm is minimal, and all forces must be carried by one set of legs. This assumes that the legs on the left and right sides of the structure are in the same phase, the most critical scenario.

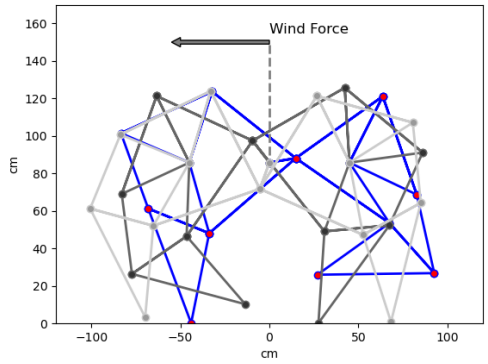

Figure 9.4: Critical situation for stability and loading

Joint	x	y	Joint	x	y
1	0	85.79	5	-83.43	101.46
2	-45	85.79	6	-33.83	48.11
3	14.82	88.14	7	-68.09	61.28
4	-32.26	123.71	8	-43.98	0.17

Table 9.2: Relative location of the joints for the critical scenario

The location of the joints of the most critical scenario serves as input for the structural analysis in Section 12.2. Therefore the relative position of the joints of a critical leg were computed. For a crank angle ϕ of 9° a critical situation was found for the first leg on the left. The joint locations for the critical situation of this leg can be found in Table 9.2.

Verification and Validation of Simulation Code

Since the simulation code is adapted from an external source, it needs to be verified to ensure correct functioning of the simulation which also verifies the results retrieved from this simulation. The verification consists of two parts; verification of the circle intersection algorithm and visual check of the linkage output.

The circle intersection algorithm works by computing the next joint from two known joint locations and the lengths of the two bars connecting them. This results in two possible locations for the joint. Therefore knowledge about the connection is necessary to choose the right one. The implemented circle intersection algorithm was verified by testing it with two joints and links and the verification was successful.

Lastly the simulation of the linkage with crank angle as an input was checked visually by comparing the created animation of an original Jansen Linkage to a stock animation of the linkage of the internet. This verification procedure was also carried out successfully. Therefore the program was accepted as an analysis tool.

9.2. Steering and Braking

In this section, the possible mechanisms for steering and braking will be explained first. Then, the most suitable mechanism will be determined based on engineering decisions.

9.2.1. Steering

The structure will be able to steer using differential steering. In this way, the structure can steer in two ways, with a zero-turn radius while standing still or by differential steering while walking. In a zero-turn radius turn, one side of the legs of the structure are moving forward while the other side of the legs walk backwards. When differential steering is used while walking, one side of the legs walk slower than the other side, initiating a turn to the side of the slower walking legs.

The structure is able to move the legs slower or in opposite direction between the two sides with legs because of the layout of the crank shaft. A schematic topview of this layout is provided in Figure 9.5a. Two separate electric motors are used. These electric engines are both attached via a rotational rod to a crank shaft (indicated in orange and red). Each crank shaft has three Jansen linkage legs attached to it. These crank shafts are connected to their respective parallel crank shaft with a coupling rod (indicated in green). This linkage was inspired by coupling rods that trains use as can be seen in Figure 9.5b. This layout enables the two crank shafts on each side of the structure to rotate with the same angular velocity making the legs on each side walk with the same velocity.

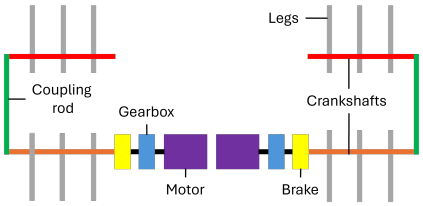

(a) Schematic topview of the crankshaft layout with the different elements indicated in the figure. Not to scale

(b) Coupling rod on a train[2]

Figure 9.5: Crank shaft layout of the structure

9.2.2. Braking

Although the structure is designed with a philosophy that it can move constantly without stopping, it still has to be able to stop. There are two cases in which it is necessary to brake: when an emergency stop has to be performed or when the structure has to stop because of the wind.

The brakes of the system are placed on the rotational shaft as indicated in yellow in Figure 9.5. For braking systems on the structure, there are two options: friction brakes or magnetic brakes.

Friction brakes are brakes that are typically seen in cars like disc brakes and drum brakes. Both of these types of brakes are not suitable for the structure because disc brakes lose their braking capabilities when in park mode because the disc expand or contract when exposed to temperature changes. Drum brakes require a hydraulic system and a complicated shaft design because their brake shoes expand to touch the inside of the drum. Because the shaft in the system is relatively small, this is not convenient [67].

For the structure, magnetic brakes are chosen as braking system because of the ease of integration and their reliability. Permanent magnet brakes are designed to stop or hold a load when electrical power is turned off. They are typically used in braking applications that require fast response times and precise tension control and use a permanent magnet to attract a single face armature. When the brake is activated, the magnets generate magnetic flux lines that pull the armature towards the brake housing. To release the brake, power is supplied to the coil, creating an alternative magnetic field that neutralises the magnetic flux of the permanent magnets. These

[2]Entertainment Junction, *URL* `https://entertrainmentjunction.com/trains-and-autism`, accessed 12 June 2024

brakes engage when power is not applied, ensuring they can hold or stop a load if power is unavailable [67].

In case of an emergency brake, the power to the engines and the permanent magnet brakes will be cut off to bring the structure to an immediate complete stop. When the structure has to initiate a preservation manoeuvre, the structure has to be put in parking mode. This is where a braking system based on permanent magnet brakes is convenient because they do not require power when in hold [67].

Adding a regenerative braking option to the braking system is not viable. The rotating crank shaft is powered by electric motors and these could be used for regenerative braking. However, the angular velocity of the crank shaft is low. Next to that, as mentioned before, the structure is designed to be constantly moving without any braking. So the power you would recover with regenerative braking, while operating, would be very low. [67]

For the designed structure, a permanent magnet brake that torques up to 2 Nm is sufficient. A good fit forthe brakes is the off-the-shelf magnet brake 'Combistop M' from 'KEB America'[3]. This small and compact brake weights 0.4 kg and uses 15 W at 48 V.

9.3. Feet Design

The designed structure needs to have feet attached to leg to prevent it from sinking too far in the sand. The Strandbeast structures that Theo Jansen builds have feet that are semicircles (Figure 9.6a) or skis (Figure 9.6b). The team explored nature-inspired options with embodied intelligence to find a better foot design for the structure. This section discusses the design of the feet for the structure. One of the user requirements is that the structure needs to have embodied

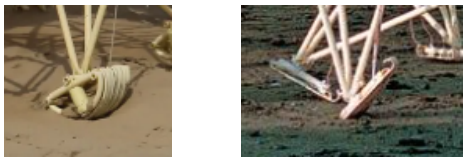

(a) Semicircle Feet **(b)** Ski Feet

Figure 9.6: Feet Design for the Structure[16]

intelligence. The feet are one of the parts of the structure in which embodied intelligence can be implemented. The main inspiration for the feet are the original semicircle feet design and camel feet. Badawy[68] discusses that camel feet expand in soft sand to increase support. The cushioned pads spread when the camel places its foot on the ground. This spread allows the weight of the camel's body to act on a bigger surface area reducing the pressure exerted on the ground. This concept of increasing surface area can be applied to the feet of the structure. The schematic design of the feet is provided in Figure 9.7a. The bottom rods of the Jansen's linkage are indicated in blue, a pin with rigidity that allows for some deflection is indicated in orange, the two beams that connect the pin with the feet plate are indicated in black and the plate that touches the ground and is able to deflect is indicated in green. In Figure 9.7b, the feet in deflection is illustrated. With this deflection, the area of the feet that is touching the ground increases, inspired by the feet of a camel.

[3]KEB America, *URL https://www.kebamerica.com/products/permanent-magnet-brakes/*, accessed 17 June 2024

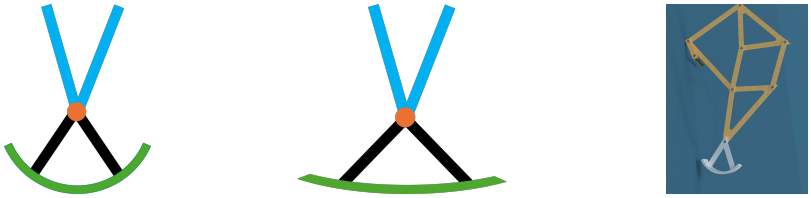

(a) Undeflected Feet **(b)** Deflected Feet **(c)** Render of the feet

Figure 9.7: Feet Design for the Structure

9.3.1. Feet Analysis and Material Selection

For the feet analysis, the design is simplified to a beam structure. The feet plate, indicated in green, is split into two beams that are clamped to the ground as can be seen in Figure 9.8. This way, the deflection of the beams can only be found with using finite element method (FEM), resulting in an estimation of the deflection of the plate. From this deflection one can derive the material properties needed for the feet.

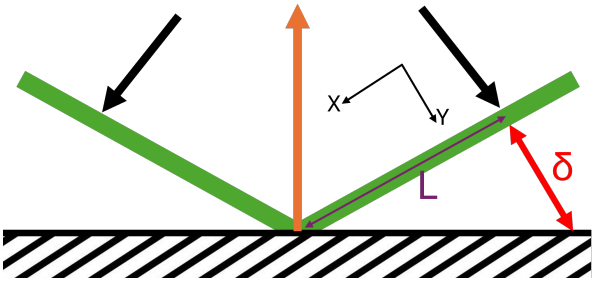

Figure 9.8: The plate was simplified to two clamped beams for the analysis of the feet

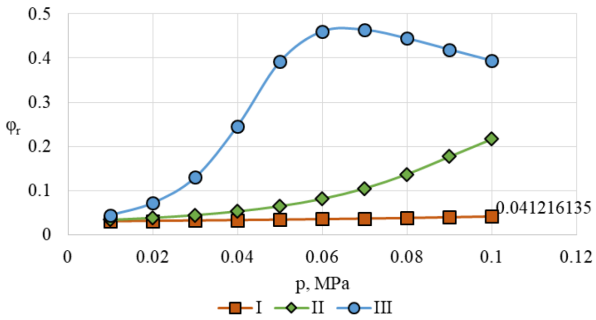

Figure 9.9: Resistant coefficient as a function of vehicle ground pressure and soil category. I = bearing soil, II = moderate soil and III = weak soil [69]

The area of the feet that is touching the ground depends on the type of soil, the power transferred and the weight of the structure. A method using different types of hardness of the ground developed by G.V. Grigorev et al [69] was used to size the feet.

$$\phi_r = \frac{P \cdot \eta}{v \cdot W} \tag{9.1}$$

With P = 220 W, η estimated at 0.8, a moving velocity v of 0.1 m/s and the mass of the structure of 710 kg, the rolling resistance, ϕ_r was calculated using Equation 9.1 and is 0.25.

Using Figure 9.9, the ground pressure, p, of the two types of sand can be found. For soft sand, category III, the ground pressure is 40 kPa. For hard, wet sand, category, II, the ground pressure is 100 kPa.

With these two ground pressures the minimal effective area of the feet can be found using Equation 9.2. The minimum amount of feet of the structure, n, that are on the ground is 6. Using the same mass and the two ground pressures, effective area per leg for soft sand is 290 cm^2 and for hard sand 116 cm^2.

$$A = \frac{W}{p \cdot n} \tag{9.2}$$

The formula for a bending beam is given in Equation 9.3. With F being the decomposed force on the legs and L the length indicated in Figure 9.8, this equation is used to find the flexural rigidity, EI, for the plate. The L can be found using the effective area of the feet found previously, using a width of the feet of 20 cm, a circle radius of the feet plate of 30 cm and a force on the legs of 2653 N. Using these numbers leads to a required EI of 406 Pam^4.

$$F = \frac{3 \cdot E \cdot I}{L^3} \cdot \delta \tag{9.3}$$

Material Selection The plate material needs a flexural rigidity of 406 $Pa\ m^4$. It must be withstand high loading cycles and have a low Young's modulus, making recycled wind turbine blade material unsuitable due to its high Young's modulus of 17 GPa and yield strength of 402 MPa.

Rubber, particularly from old car tires, is a viable alternative. Tire rubber has an average Young's modulus of 2.1 MPa, resulting in a required plate thickness of 2.3 cm. Using recycled tire rubber enhances sustainability, as recycling old tires is challenging due to their complex composition. Recycled tires can be repurposed into new tires, synthetic turf, or playground floors[4].

9.4. Sizing

The sizing of the legs is not straightforward because the only requirement related to sizing is *REQ-MAI-03-SYS-01-KIN-01 All linkages shall be easily accessible to the maintenance crew.* It was decided to size the legs according to the step height. The team chose 30 cm based on the levelness of the beach. If there are big objects present on the beach, the structure has obstacle avoidance.

With this step height of 30 cm, the leg ratios that are given in Table 9.1, have to be converted with a factor of 1.1 cm. With this sizing, the body's platform, that is at the same height as the crankshaft of the linkage, is at 94 cm. This leg sizing will be used to iterate the design on e.g. stability, and the final sizing after iteration will be presented in Chapter 13.

9.5. New Power Estimation

The power estimation for the modified Jansen's linkages uses the method explained in subsection 7.1.1. The specific resistance is dependent on the velocity and because the velocity is kept at 0.1 m/s, the specific resistance is kept at 0.31. The design mass of the structure increased from 440 kg to 710 kg. This increase in mass led to an increase of the power for motion. The preliminary power estimation led to a power requirement of 140 W. The new power estimation for the kinematic motion is 220 W. This new power requirement is used to iterate the design and the final power estimation after iteration will be presented in Chapter 13.

9.6. Compliance Matrix

This section presents the list of requirements and the degree to which the kinematic subsystem adheres to them.

Table 9.3: Compliance matrix of the kinematic subsystem requirements

Requirement	Status	Requirement	Status
REQ-USER-17-SYS-01	Fully met	**REQ-MAI-03-SYS-01-KIN-01**	Fully met
REQ-USER-17-SYS-01	Fully met		

[4]Sensoneo, *https://sensoneo.com/waste-library/how-to-recycle-tires/*, accessed 18 June 2024

10

Control and Navigation

The functional structure is required to move autonomously on the Dutch coast. This chapter details how this functionality will be achieved. The requirements for control and navigation are provided in Section 10.1. Path planning methods and the division of the Dutch coast into sections for waypoint placement are discussed in Section 10.2. Obstacle avoidance is detailed in Section 10.3. Section 10.4 and Section 10.5 describe the decision-making process and sensors for navigation. Section 10.6 presents the verification of the subsystem. Finally, Section 10.7 shows the compliance matrix for verification of the requirements.

10.1. Subsystem Requirements

REQ-USER-03-SYS-01-CTR-01	The system shall be able to update its 2D position with a frequency of 1 Hz.
REQ-USER-03-SYS-01-CTR-02	The system shall be able to determine its 2D position with an accuracy of 1 m.
REQ-USER-05-SYS-02-CTR-01	The system shall be able to detect obstacles within a 5-metre distance from the structure.
REQ-USER-05-SYS-02-CTR-02	The structure shall have a maximum speed of 1 m/s.
REQ-USER-09-SYS-02-CTR-01	The control subsystem shall not exceed TBD% of the total cost.
REQ-MAI-03-SYS-01-CTR-01	All electronics components shall be easily accessible to the maintenance crew.
REQ-EoL-01-SYS-01-CTR-01	The sensors used shall retain at least TBD% of the original accuracy when disassembled at end of life.

10.2. Navigation

Navigation of an autonomously moving structure is often performed with global and local route planning. Global planning is laying out the rough path of the structure by using predetermined waypoints. Local planning is the path from waypoint to waypoint while avoiding obstacles. It is not efficient to plan the path of the structure completely globally because that would involve a lot of small steps. This results in a very high data storage requirement and computational load because the waypoints and headings have to be updated much more frequently.

10.2.1. Global Path Planning

The structure has to be capable of performing different functionalities. Different path planning is required to perform well in each functionality. That is why, for the global path planning, three different use cases related to functionalities were identified: travel, waste collection and display:

Travel The first identified use case is travel, as shown in Figure 10.1a. In this mode, the structure travels to a distant waypoint. Once this waypoint is reached, the structure can start performing a functionality like waste collection. This use case is important to the less frequently visited parts of the Dutch coast, where there is less waste to collect and fewer visitors who can engage its entertaining function.

Waste Collection The second use case for the structure is waste collection(see Figure 10.1b). In this use case, the structure loops through the beach to comprehensively cover the designated area, effectively removing waste. This use case is necessary at busy parts of the Dutch coast, where a large number of people go and leave waste, or when a significant amount of waste is washed ashore.

Display Another use case for the structure is displaying itself along the Dutch coast, illustrated in Figure 10.1c. In this mode, the structure moves along the coast and stops for a certain time at waypoints in busy areas. At these points, people can approach the structure and view it from up close. The structure fulfils entertaining purposes and enables people to learn about the

(a) Travel **(b)** Waste Collection **(c)** Display

Figure 10.1: Three different path planning cases. The waypoints are indicated in yellow, the path in cyan. Note: Image and waypoint placement are meant as reference, this is not to scale.

sustainable design of wind turbine recycling solutions in this way.

10.2.2. Limitations on the Dutch Coast

Several big obstacles exist on the uncontinuous Dutch coast, like harbours and rivers, that the structure cannot overcome. That is why the Dutch coast was split up in four sections, as can be seen in Figure 10.2.

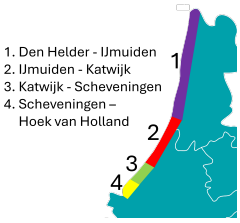

Figure 10.2: The Dutch coast split in four sections for deployment of the structure.

Figure 10.3: An example of predetermined obstacle avoidance using waypoints.

The four sections are separated by physical barriers, requiring the structure to stay and operate within its designated section. To fulfill its function in another section of the Dutch coast, the structure must either be disassembled and transported in parts or additional structures must be deployed in those sections.

Fixed obstacles, such as the harbours, and smaller obstacles, such as beach restaurants, must be avoided. This can be managed by placing waypoints in the right place so that the structure does not encounter these obstacles on its regular path. An example of this waypoint placement is shown in Figure 10.3.

10.3. Obstacle Avoidance

The beach is a vast space that is mostly empty, but there are still objects that have to be detected so that the structure can avoid them. These objects include temporary, mobile, or previously unaccounted-for items such as people, holes, large sandcastles, cars, and garbage bins. In Figure 10.5, the path around an obstacle is shown. An obstacle is first detected at a certain angle α with respect to the movement direction in Figure 10.4. When the obstacle comes within 5 m of the outside of the structure, the structure will steer 90 degrees minus the absolute value

of α to the opposite side of the obstacle.

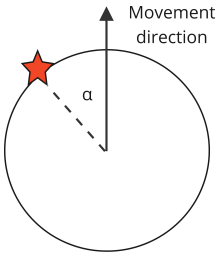

Figure 10.4: Illustration of the detected obstacle angle

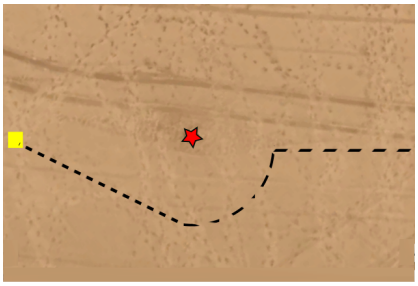

Figure 10.5: A path around obstacle

The structure shall keep moving around the obstacle until it reaches a point where it steers directly to the waypoint again. This point is reached when the heading directly to the waypoint no longer has the obstacle in the front 180 degrees of the vision field. After that, the path will be a straight line to the original waypoint again.

10.4. Navigation Control

The navigation of the structure is done in the hierarchy that is shown in Figure 10.6. Obstacle avoidance, being the most urgent factor in navigation, overrules path planning and the preservation manoeuvre. Then the preservation manoeuvre, which positions the structure safely for weather conditions in which it cannot operate, overrules the regular path planning for which the options are described above.

Obstacle avoidance uses the aforementioned mechanism to decide whether any steering manoeuvre has to be performed. Meanwhile, it uses the weather forecast and live wind speed to estimate whether the wind speed will reach levels at which the structure cannot operate in the immediate future. In this case, the structure shall seek refuge near the dunes and position itself in the most stable way. When there is no danger from wind conditions, the structure continues to follow its regular path, which is made with predetermined waypoints.

10.5. Sensors

This section describes the different sensors needed for the structure to navigate using the control decisions described in Section 10.4.

Obstacle detection For obstacle avoidance, three different types of active sensors can be used: Radar, LiDAR and Sonar. LiDAR is preferred over Radar due to its higher accuracy at short distances [70], and over Sonar due to Sonar's susceptibility to sound-absorbing materials and limited range [71]. Therefore, LiDAR is chosen for obstacle detection. It performs well in low lighting conditions and is less affected by environmental factors like fog and dust.

The LiDAR sensor creates a point map that charts all the points where the LiDAR reflections occur, forming a 3D representation of the environment, as shown in Figure 10.7. This environmental map enables the use of SLAM (Simultaneous Localisation and Mapping) to track the structure's location. Point cloud mapping employs LiDAR to emit laser pulses that reflect off surrounding objects. The returning pulses are measured to calculate distances, generating a dense set of 3D coordinates, or a point cloud, which accurately represents the environment's surface geometry.

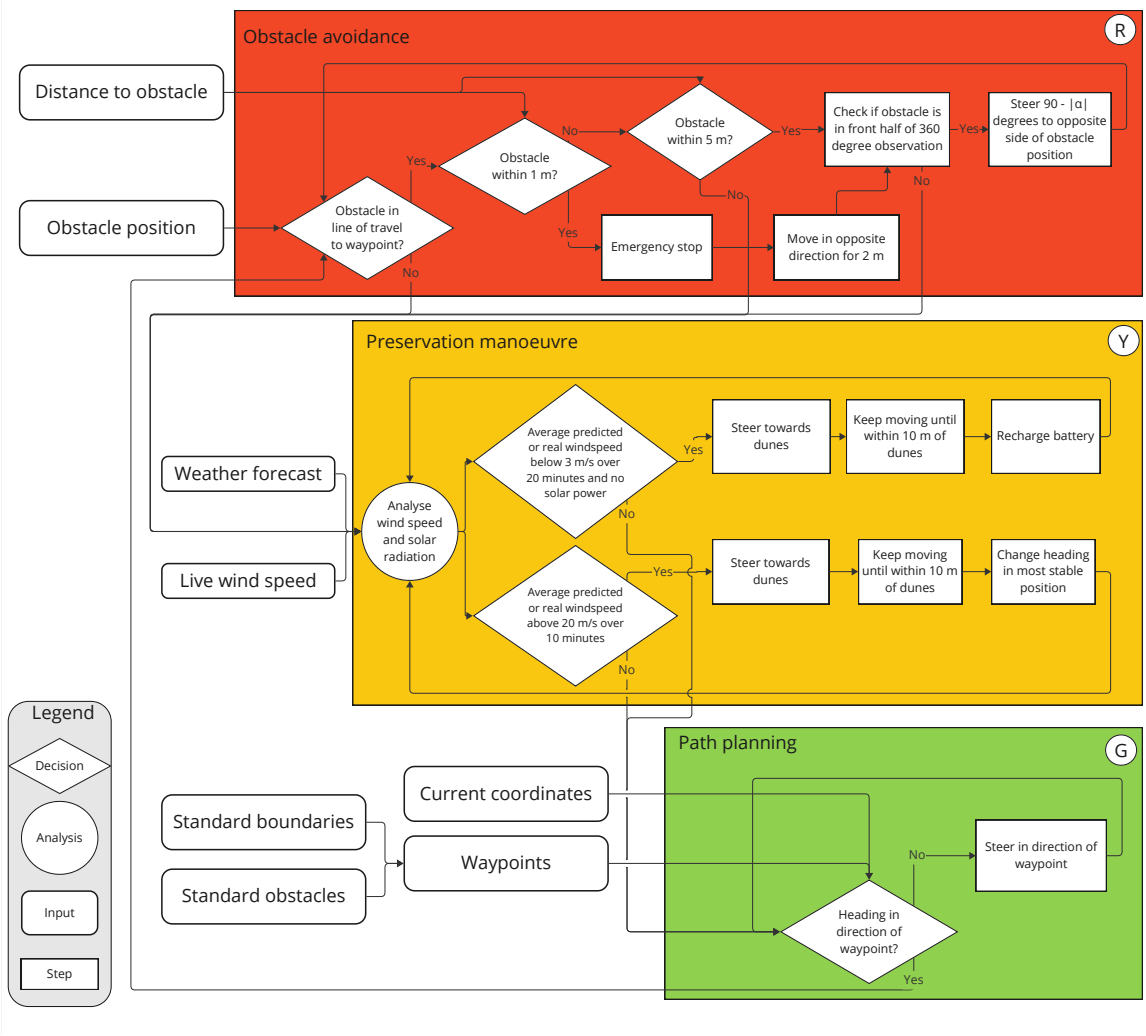

Figure 10.6: Navigation control diagram showing the hierarchy of decision-making. Path planning is overruled by preservation manoeuvre which is again overruled by obstacle avoidance (colour indicated on top right of blocks).

A 360° view around the structure can be created by using two LiDAR cameras.[1] The chosen rotating LiDAR is the Unitree 4D LiDAR L1, which has the specifications shown in Table 10.1. To ensure a 360° view around the structure, two of the LiDAR sensors will be placed on the structure as shown in the following Figure 10.8.

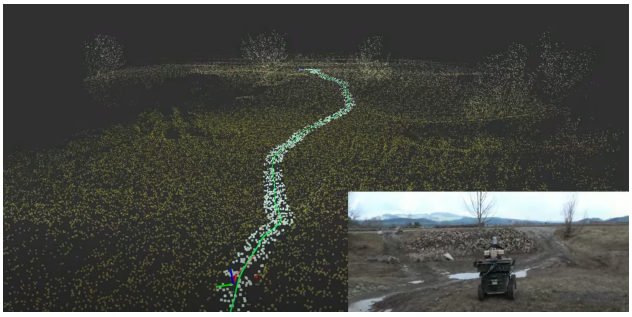

Figure 10.7: LiDAR point cloud with reference visual environment[2]

[1]Unitree, *https://www.unitree.com/LiDAR/*, accessed 11 June 2024

[2]ETH Zürich, *URL www.youtube.com/watch?v=eOoMwWEyERQ*, accessed 12 June 2024

Table 10.1: Specifications of selected LiDAR

Parameter	Value
Range	10 m
Sampling points	21600
Field of View	360° horizontal, 90° vertical
Sampling rate	2 Hz
Mass	230 g
Input power	6W

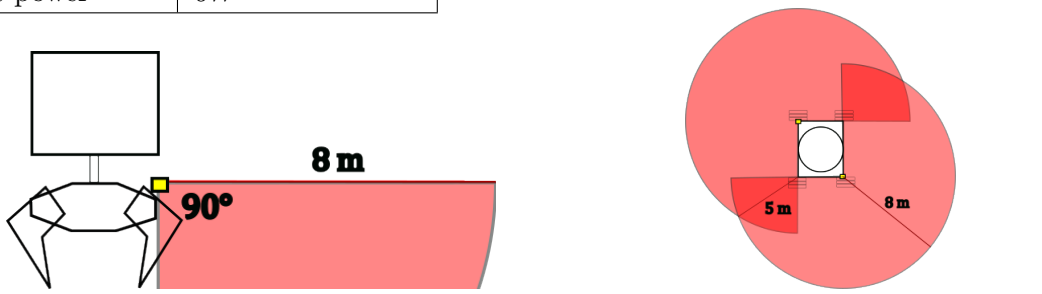

(a) Side view of the LiDAR field of view **(b)** Top view of the LiDAR field of view

Figure 10.8: LiDAR field of view and placements

Since the structure has to detect obstacles within 5 metres of the structure boundaries, the sensor resolution is evaluated at 8 metres. Using the 21600 sampling points, this results in a resolution at 8 metres of 14 cm horizontally and vertically. This is sufficient to detect all objects that can be hazardous to the structure. The resolution also linearly increases when the obstacles gets closer.

Telecommunication The structure uses predicted wind speeds to determine when to initiate the preservation maneuver. Weather data is obtained via a 5G internet connection, which covers the entire Dutch coast [3]. A controller equipped with a 5G modem, antenna, and SIM card is necessary to receive the 5G telecommunication signal. In the Netherlands, a maximum data rate of 600 $Mbit/s$ is achievable, with 50 $Mbit/s$ being sufficient for the structure. The weather forecast for the next hour is downloaded every 10 minutes to ensure the structure can promptly respond to changing conditions. The 5G receiver is mounted on the flat top section of the structure.

GPS The structure navigates between predetermined waypoints using GPS satellites to determine its longitude and latitude. To receive and process the GPS signal, a controller equipped with a GPS module and antenna is used. The accuracy that can be obtained with GPS in this autonomous use case is 1-3 m with a frequency of 1 Hz[72]. Because the velocity of the structure is 0.1 m/s, and given the accuracy of GPS, the structure will be updating its location every 10 seconds. It is designed to be mounted on the flat part on top of the body.

IMU To navigate towards pre-set waypoints, the structure relies on a magnetic IMU (Inertial Measurement Unit) to determine its heading relative to the direction of each waypoint. The IMU integrates magnetometers, accelerometers, and gyroscopes to provide a precise estimate of the structure's orientation. Magnetometers measure the orientation relative to Earth's magnetic field, assumed to be constant. Gyroscopes monitor angular accelerations and continually update orientation accuracy. Accelerometers track linear acceleration. By combining data from these sensors, the IMU accurately determines the structure's heading. The IMU is housed inside the body of the structure, ensuring it remains well-protected.

[3] 5G Coverage map KPN, *URL* `www.kpn.com/netwerk/dekkingskaart.htm`, accessed 12 June 2024

Anemometer The anemometer is crucial for measuring wind speed and direction, influencing decisions on the operational safety of the structure. Wind direction is particularly significant; during high wind speeds, the structure can orient itself to the most stable direction. Mounted on the flat section of the body, the anemometer accounts for a safety margin due to potentially higher wind speeds at the turbine's height. This ensures prudent operational decisions are made based on accurate wind data.

In summary, the selected products and their specifications are in Table 10.2.

Table 10.2: Specifications of selected sensors and instruments

Parameter	5G-receiver	GPS	IMU	Anemometer
Product	Zyxel NR7101 – Nebula [1]	Navilock NL-281GG	Bosch BNO055[2]	BRESSER 5-in-1 [3]
Mass	1.2 kg	0.15 kg		1.3 kg
Size	255 x 245 x 58 mm	44 x 37 x 14.5 mm	3.8 x 5.2 x 1.1 mm	39 x 39 x 34 cm
Input Power	6 W	< 1 W	< 1 W	< 1 W

10.6. Verification

The control and navigation subsystem are verified by ensuring that all functions shown in Figure 10.6 are enabled by the sensors. Additionally, an analysis of the Dutch coastline identifies sections suitable for navigation by the structure. Sensor placement is carefully considered to match the structure dimensions and ensure performance according to the requirements.

Verification was also performed by consulting an expert on control and navigation of the TU Delft. This expert checked the method used for navigation, control and obstacle avoidance. Next to that, only proven technology is used for control and navigation. All components are off the shelf so it can be assumed that these work as indicated in their product information sheet.

For the control and navigation subsystem, a sensitivity analysis is not very useful to perform because the functions that the structure has to perform are already set and thus the sensors and actuators will be similar for changing parameters.

10.7. Compliance Matrix

To see if the design meets the requirements that are set for the control subsystem, the compliance matrix in Table 10.3 is created. For every requirement, it is indicated if the requirement is fully met, partially met, not met, or needs to be investigated later.

Table 10.3: Compliance matrix of the control subsystem requirements

Requirement	Status	Requirement	Status
REQ-USER-03-SYS-01-CTR-01	Fully met	**REQ-USER-09-SYS-02-CTR-01**	To be investigated
REQ-USER-03-SYS-01-CTR-02	Fully met	**REQ-MAI-03-SYS-01-CTR-01**	Fully met
REQ-USER-05-SYS-02-CTR-01	Fully met	**REQ-EoL-01-SYS-01-CTR-01**	To be investigated
REQ-USER-05-SYS-02-CTR-02	Fully met		

[1]Zyxel NR7101 – Nebula, URL: *https://capestone.com/product/zyxel-nr7101-nebula/* accessed 18 June 2024

[2]Bosch BNO055, URL: *https://cdn-learn.adafruit.com/assets/assets/000/125/776/original/* accessed 18 June 2024

[3]BRESSER, 5-in-1 outdoorsensor 7002520 URL: *https://www.bol.com/nl/* accessed 18 June 2024

11

Power Transmission and Management

The designed system has two sources of power and multiple output components; some require a majority of the delivered power and many need only a fraction of that. This chapter outlines the power transmission and management of the system that effectively links the power input and output components. Section 11.1 first introduces a set of power subsystem requirements and system-level requirements that entail power management. Section 11.2 mainly deals with electrical and data handling block diagrams and explains the components related to power transmission. Sensitivity analysis on the designed power transmission system is performed in Section 11.3, and the system is verified in Section 11.4. Finally, compliance with the earlier introduced requirements is checked in Section 11.5.

11.1. Subsystem Requirements

The power management subsystem shall conform to the list of following requirements:

REQ-USER-02-SYS-08 The system shall be able to travel at least 100 m in case of windless conditions.

REQ-USER-04-SYS-01 The power subsystem shall provide a minimum power of TBD kW at a wind speed of 10 m/s to fulfil its functions.

REQ-USER-04-SYS-01-POW-02 The energy storage unit shall have a minimum lifetime of 3 years.

REQ-USER-04-SYS-01-POW-03 The energy storage unit shall have a minimum capacity of 100 Wh.

REQ-USER-09-SYS-02 The total cost of electronics shall not exceed TBD % of the total unit cost.

11.2. Electrical and Data Handling Block Diagram

The electrical block diagram shows interconnections of major electrical components of the entire system. The purpose of this diagram is to provide a general overview of the electrical system and is not intended to portray the exact circuitry of the system. In the diagram, each component is represented with a labeled block and the connections are shown with lines and arrows to indicate the direction of electrical flow. [73]

The data handling block diagram shows the data connections and flow between the system components. As there are many overlaps between the components described by the electrical block diagram and those presented by the data handling diagram, the two diagrams were merged into one. The electrical and data handling block diagram is shown in Figure 11.1.

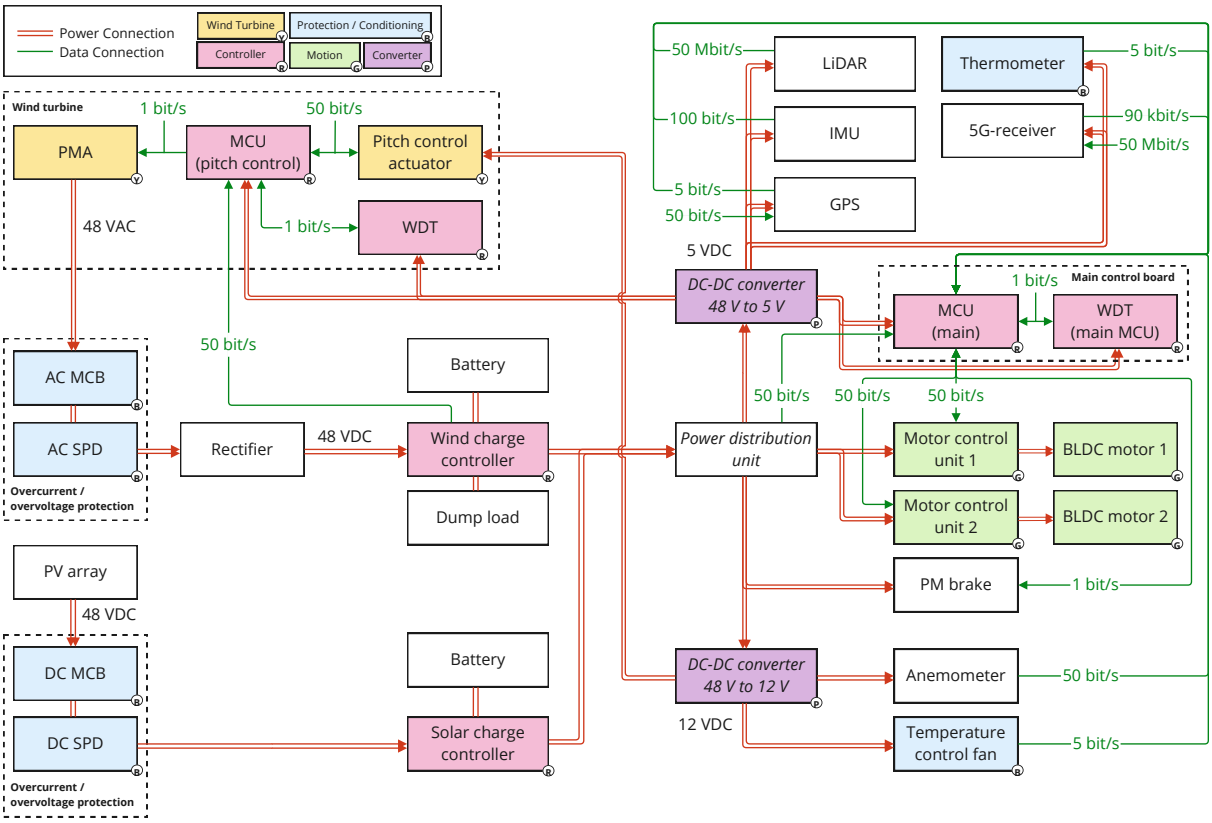

Figure 11.1: Electrical and data handling block diagram showing power and data transmission of the system. The double lines indicate power connections and the single line indicates data connections. Data connection includes the expected bitrate. The abbreviations are explained in the text.

The data rates are estimated based on the type of data that has to be transmitted, the frequency at which it has to be transmitted and the accuracy of the data. The most demanding data rates are compared to those of products that are on the market to verify that they are realistic.

The largest data rates come from the LiDAR and the 5G receiver. The LiDAR has to estimate 43200 points in the pointcloud per second, which all have three coordinates. If we estimate their accuracy at 1 cm within a range of 10 metres, that means that each coordinate needs to be able to take 1000 different values. This requires eleven bits per coordinate when including a sign. When considering that there are two LiDARs this results in around 3 $Mbit/s$. A very large safety factor is taken to ensure that this is not underestimated.

The 5G receiver will receive a weather forecast every 10 minutes. The relatively large data rate of 90 $kbit/s$ ensures that this forecast can be as detailed as desired.

The smallest data rates of only 1 bit/s such as the signal from the main MCU to the brake and from the pitch control MCU the PMA are only on/off signals that can thus have very small data rates.

11.2.1. Overview of Power Transmission

The power transmission begins with Permanent Magnet Alternator (PMA) and photovoltaic (PV) array as shown on the leftmost side of the Figure 11.1. PMA is a type of generator widely used for small stand-alone wind turbines for its high efficiency and absence of gearboxes or brushes that require regular maintenance [74]. PMA is directly connected to the wind turbine shaft and converts mechanical energy from the rotation of the wind blade into electricity. The output of

the chosen PMA is three-phase 48 VAC. The rest of the system components require DC voltage, thus the electricity generated from PMA gets fed into a rectifier that converts AC voltage to DC. The PV array of the solar panel converts sunlight into electricity. The output of the chosen solar panel is 48 VDC, and no conversion is required.

The outputs of the PMA and solar panel fluctuate since the intensity of the sources of the electrical power, wind and sunlight, vary by the seasons and even the times of the day. This fluctuation in power can easily lead to overcharging of the batteries, the selected energy storage method of the system. Charge controllers, therefore, are placed between the power sources and batteries to minimise the effect of the fluctuation. The charge controllers monitor the respective batteries and regulate the charging and discharging processes. The wind charge controller, in particular, is also responsible for discharging excess energy generated by the wind turbine during high-wind periods [74]. This excess energy gets transferred into a dump load, or a resistor, which releases this energy in the form of heat. This is quite beneficial when it comes to ensuring electronics performance during winter when the average wind speed is high on average since the efficiencies of most electronics drop significantly at low temperatures.

The power generated by the PMA and the solar panel is then fed into a single power distribution unit. This unit is responsible for dividing and supplying power to different components. Power is directly delivered to components with a rated input voltage of 48 V by the power distribution unit while others with different rated input voltage require a converter. As shown in Figure 11.1 two DC-to-DC step-down converters are in place; one that converts 48 V to 5 V and the other to 12 V. Power then can be safely delivered to these components.

11.2.2. Electrical System Protection

There are several components shown in the Figure 11.1 for protecting and conditioning the system. Miniature circuit breaker (MCB) and surge protection device (SPD) are connected to the PMA and the PV array to protect the rest of the electrical system from overcurrent and overvoltage. A watchdog timer (WDT) is put next to each MCU to watch over its operation. A thermometer and temperature control fans are located near the PMA and the rectifier to cool them down in case of overheating. It is also important to accommodate sufficient airways by placing vents near them.

11.2.3. Power Component Efficiencies

As discussed in Chapter 8 and Chapter 9, 320 W and 214 W are to be generated from wind and solar panels, respectively, and 220 W is required for the motion. The required power for each component shown in Figure 11.1 is tabulated in Table 11.1.

Table 11.1: Required power per component

Component		**Power** $[W]$
Control and Navigation	LiDAR	12
	GPS	0.25
	IMU	0.33
	PM brake	10
Weather data collection	Anemometer	0.03
	5G-receiver	6
Active cooling	Temperature control fan	3
	Thermometer	0.03
Motion		220

It is important to consider the electrical components' efficiencies to determine whether this required power for motion can successfully be delivered. The effect of the efficiencies on power throughout the system is illustrated in Figure 11.2.

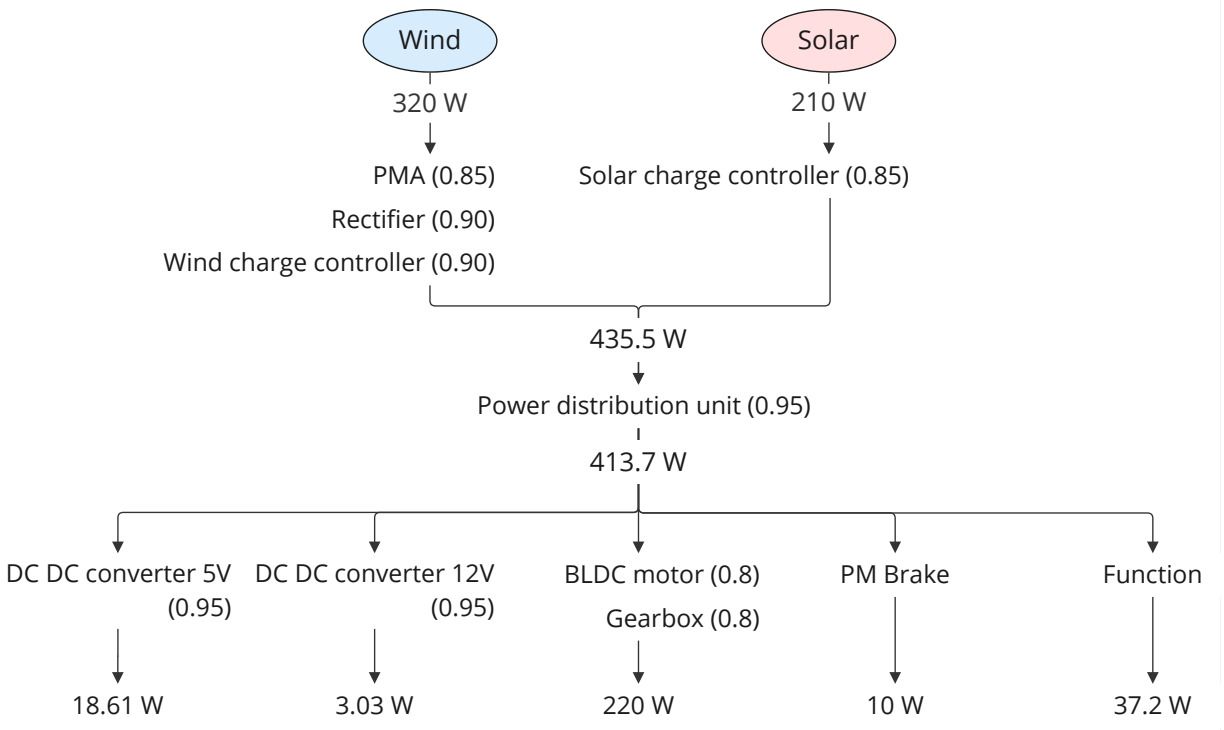

Figure 11.2: Efficiencies of main components (shown in parentheses) and change in delivered power through the system

Previously in Chapter 7 approximately 130 W was set as the power required to perform a "function". Besides control and navigation, weather data collection, and active cooling, this requirement was also to be used for one of the three possible functionalities discussed in that chapter. However, it is clear from the Figure 11.2 that only a fraction of the original power can be delivered for the function. The possibility of increasing this power shall be investigated during iteration.

11.2.4. Motor and Generator Selection

The motion of the system is delivered by two brushless DC motors (BLDC) connected to the leg shafts. BLDC motors are generally more compact and have higher efficiencies than brushed motors. Torque is the driving factor in the motor selection for motion as the chosen nominal speed of the structure is a mere 0.1 m/s while the total mass of the structure is in the range of hundreds of kilograms. High-torque BLDC motors require high voltages of at least 24 V. However, as voltage and current are directly related to power, a low voltage equals a high current for a given required power. The higher the current the thicker the cables and the heavier the system gets. Furthermore, the difference between the efficiencies of the voltage step-down converters for an input voltage of 24 V and 48 V is negligible. Therefore, 48 V BLDC motors were chosen and the PMA and the PV arrays rated at 48 V were selected to avoid using loss-introducing converters as much as possible. Possible off-the-shelf selection of BLDC motors and PMA are presented in Table 11.2.

Table 11.2: Possible off-the-shelf BLDC motors and PMA models

	Model	**Rated Power** $[W]$	**Max Power** $[W]$	**Rated Current** $[A]$	**Rated Speed** $[rpm]$	**Rated Torque** $[Nm]$	**Mass** $[kg]$
BLDC	ATO-D5BLD200 [1]	200	-	5.21	3000	0.83	3
	BL34E27-02 [2]	200	-	5.06	4000	0.48	1.56
	ATO-D5BLD250 [3]	250	-	6.51	3000	0.83	3
PMA	ATO-PMG-600M2 [4]	600	636	-	500	11	10
	ATO-PMG-1kW [5]	1000	1500	-	500	19.1	14.5

11.2.5. Energy Storage: Battery Selection

Previously in Chapter 3, lithium-ion and lead-acid batteries were determined to be the possible energy storage options based on a preliminary sizing and trade-off. However, a further investigation into the characteristics of each battery type revealed great downsides that motivated the consideration of alternative battery types.

The factor that makes lithium-ion a great contender is its high energy density. It typically ranges between 80 and 250 Wh/kg, but it was found that certain lithium-ion batteries can even have up to 300 Wh of energy storage per kilogram [75]. In contrast, lead-acid has extremely low energy density ranging between 30 and 40 Wh/kg [76]. This means around four kilograms of lead-acid battery is required to achieve the same energy storage capacity as one kilogram of lithium-ion battery with 140 Wh/kg which makes lead-acid battery not an ideal choice for the structure.

Lithium-ion batteries, however, are made of critical materials including lithium and cobalt. These raw materials are known to be very scarce due to the high energy demand for mining and the limited number of reserves. Lead is not necessarily considered rare although it makes up a smaller percentage of the Earth's crust (0.0014%) than lithium (0.0020%) and cobalt (0.0025%) do because its mining processes are less demanding and as it is much more spread out throughout the world. [77, 78]

Sodium-ion battery is a possible alternative to lithium-ion and lead-acid batteries. Although its

[1] ATO-D5BLD200, URL: *https://www.ato.com/1-4-hp-200w-24v-brushless-dc-motor* accessed 18 June 2024

[2] BL34E27-02, URL: *https://www.linengineering.com/products/brushless-motors/standard-bldc-motors/bl34-series/bl34e27-02/BL34E27-02*accessed 18 June 2024

[3] ATO-D5BLD250, URL: *https://www.ato.com/250w-bldc-motor* accessed 18 June 2024

[4] ATO-PMG-600M2, URL: *https://www.ato.com/600w-alternator* accessed 18 June 2024

[5] ATO-PMG-1kW, URL: *https://www.ato.com/1-kw-alternatorr* accessed 18 June 2024

technology readiness level is low and thus is yet to be commercialised, it is expected to perform better than lead-acid and to be comparable to lithium-ion [75]. Moreover, sodium is more than 1000 times more abundant than lithium and lead, and it is much less demanding to extract making it a more sustainable choice [79]. An overview of the characteristics of the three batteries is shown in Table 11.3 below.

Table 11.3: Overview of the lead-acid, lithium-ion, and sodium-ion batteries [75–81]

	Lead-acid	**Lithium-ion**	**Sodium-ion**
Energy density (Wh/kg)	Low; 30-40	High; 100-300	Moderate; 100-160
Material scarcity	Moderate	Scarce	Abundant
Toxicity	High	Moderate	Moderate
Cycling stability	Low	High	High
Cost (battery cost only)	Low	High	Moderate
Technology maturity	High	High	Low

The sodium-ion battery technology is expected to have matured and become more established by the time the next-generation wind turbine blades become widely implemented. Therefore, the structure will be designed with sodium-ion batteries as its energy storage component.

11.2.6. Energy Storage: Battery Sizing

During the majority of the operation, the required power for motion and functions will be directly delivered by the two power sources: wind turbine and solar panel. However, the structure shall be designed to travel at least 100 m even during windless conditions to escape possible high tide areas as specified by *REQ-USER-02-SYS-08*. It was further assumed that no solar power would be generated during this condition to make the estimation conservative. The battery thus shall be capable of supplying the total required power for the escape manoeuvre.

All batteries experience degradation in energy storage capacity after charge and discharge cycles. It is important to ensure that even at its EOL the battery can store and provide the required amount of energy. The mass of the battery is calculated using the Equation 11.1.

$$M_{BAT_{EOL}} = \frac{E_{BAT_{EOL}}}{E_{sp_{BAT}}} = \frac{P_{BAT} \cdot t_{discharge}}{E_{sp_{BAT}} \cdot DOD \cdot \beta_{EOL} \cdot \eta_{BAT}} \cdot SF \tag{11.1}$$

A total of 370 W is to be delivered to the motors, control and navigation, and active cooling from the power distribution unit during the escape manoeuvre. The structure would take around 17 minutes to travel 100 m at its normal operating speed of 0.1 m/s. According to existing studies, some 160 Wh/kg-rated sodium-ion battery cells have been proven to retain around 80% of their original capacity (β_{EOL}) after 4000 cycles at 80% depth of discharge (DoD) [82]. Assuming battery power is required every twelve hours, the battery will last around five and a half years until its capacity falls below 80% of the original. Battery efficiency η_{BAT} of 0.7 was assumed for energy loss during charge and discharge. Furthermore, a hefty safety factor of 4 was implemented to account for the low technology readiness level and other battery-related component mass. The total required mass was then determined to be around 5.75 kg.

11.3. Sensitivity Analysis

The main factor of the required power is the mass of the structure. As the mass increases, the required power for motion increases respectively. Therefore, a sensitivity analysis on the effect of

the weight was performed. The results are tabulated in Table 11.4.

Table 11.4: Change in required power due to 10% point decrease and 10 percentage point increase in total system weight.

	10%pt. decrease	**No change**	**10%pt. increase**
Mass $[kg]$	639	710	781
Power for motion $[W]$	200	220	240
Power delivered to motors $[W]$	312.5	343.8	375.0
Wind turbine required power $[W]$	295.8	320.0	344.2
Required wind velocity $[m/s]$	6.3	6.5	6.6
Solar panels required power $[W]$	197.5	213.6	229.8
Required solar panel area $[m^2]$	8.5	9.2	9.8
Total power required $[W]$	493.3	533.6	573.9
Efficiency [-]	0.547	0.543	0.540

Mass and the power required have a linear relationship. A 10 percentage point increase in total mass leads to a 40 W increase in the total required power and a 3 percentage point decrease in the electrical system efficiency. It also increases the required wind velocity by 10 percentage points which may very well be a negligible difference in the grand scheme of the design. On the other hand, some issues may arise from the positive linear relationship between the total mass and the required solar panel area, since the panel area is also directly correlated with the solar panel mass and thus to the total mass. To avoid a situation of ever-increasing mass, some adjustments in the power ratio between the wind turbine and the solar panel may need to be implemented.

11.4. Verification

No specific code was involved in the calculation of the power. Therefore, the verification mainly focused on finding small-scale implementations of wind and solar energy systems in real life and checking the performed hand calculations. Renewable energy community forums such as DIY Solar Power Forum and NAZ Solar Electric Forum were the main sources used to verify the feasibility of the electrical set-up. The hand calculations were verified by deriving the output powers from the required power values.

To ensure that the components used are actually feasible, off-the-shelf products were chosen for them. Finally, the power management diagram has been verified by Dr. H Vanedi who is an assistant professor at the Electrical Engineering faculty of Delft University of Technology.

11.5. Compliance Matrix

The compliance with the earlier introduced subsystem requirements is shown in Table 11.5.

Table 11.5: Compliance matrix of the control subsystem requirements

Requirement	**Status**	**Requirement**	**Status**
REQ-USER-02-SYS-08	Fully met	**REQ-USER-04-SYS-01-POW-03**	Fully met
REQ-USER-04-SYS-01	Fully met	**REQ-USER-09-SYS-02**	Fully met
REQ-USER-04-SYS-01-POW-02	Fully met		

12

Structural Analysis

This chapter details the structural analysis of the entire system, aiming to achieve three main objectives: ensuring structural integrity to prevent failure, determining critical dimensions, and predicting the lifespan of the structure. To address this topic comprehensively, the chapter is divided into four parts:

Firstly, the structural analysis focuses on the main load-carrying body. This begins with an overview of idealisation and load cases, detailed in Section 12.1, followed by stability, stress, and deflection analyses in subsequent sections.

Secondly, attention shifts to the analysis of the legs. In Section 12.6, stress assessments using both static and dynamic analyses inform the sizing of the legs. Additionally, the selection and sizing of leg joints will be discussed.

Thirdly, the chapter delves into failure considerations. Beginning with an exploration of four potential failure modes in Section 12.9, it then introduces a fuse-like design concept in Section 12.10 to facilitate maintenance scheduling. This is followed by a detailed lifetime analysis in Section 12.11.

Lastly, the chapter concludes with verification and validation procedures specific to the structural analysis. Section 12.12 includes checks for compliance with requirements, a sensitivity analysis to ensure process robustness, and a detailed account of verification and validation methods employed throughout the structural assessment.

12.1. Structural Body Design: Idealisation and Load Cases

This section outlines the foundation required for the analyses. First, an overview of the structure is given in subsection 12.1.1. Next, the idealisation of the structure is explained in subsection 12.1.2. Then, the load cases are presented in subsection 12.1.3, followed by a discussion of the assumptions in subsection 12.1.4.

12.1.1. Overview of the body

The general design of the body consists of a load-bearing structure, shown in Figure 12.1. Thin panels will be attached to this load-bearing structure to protect the critical components and provide space for solar panels.

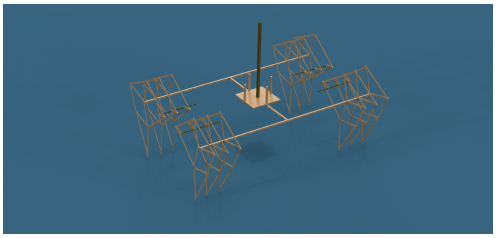

Figure 12.1: Main body frame of the structure, with a wind turbine support pole (in black)

The sizing of the body depends on three constraints. The first is that the body of the structure needs to fit within a sea container with dimensions 12.03 x 2.40 x 2.70 m, as specified in *REQ-USER-17-SYS-02*. Secondly, the sizing of the body needs to be such that it allows for sufficient

ground clearance for smooth operation. The third constraint is that the sizing of the body shall allow for sufficient solar panel area on the structure. As elaborated in Section 7.3, the required area of solar panels on the structure is approximately $A_{Solar} = 9$ m^2.

12.1.2. Idealisation of the Body

The first step is to idealise the structure by identifying its key elements. These include the two beams that connect the legs and the central beam that links these two beams together. At the centre of this central beam is a pole that supports the vertical axis wind turbine. It is important to note that the legs are excluded from this idealisation as they will be analysed separately. With these elements defined, the structure can be idealised as shown in Figure 12.2.

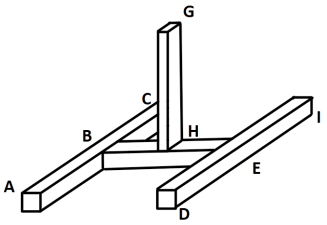

Figure 12.2: Idealisation of the body structure. The figure is not to scale and is for illustration purposes only.

12.1.3. Load cases

With the structure defined, the next step is to investigate the different load cases to consider.

First, when the wind turbine operates, it generates a force that creates a bending moment in the structure, as shown in Figure 12.3. Only the case where the wind blows in the y-direction is considered, as it is the most critical. The bending moment might cause the structure to tip over. Additionally, the bending moment introduces significant stresses within the body, which should be resisted by the beams.

Another loading case to consider is torsion. As shown in Figure 12.4, the vertical axis turbine relies on torque (shown in red) transmitted to the generator (shown in green) via a rotating shaft (shown in blue). Since the torque is not resisted by the generator but is instead used to produce energy, no torsion is introduced into the body. However, the generator will introduce vibrations into the structure that need to be accounted for.

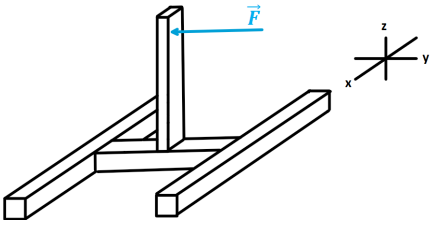

Figure 12.3: Force introduced on the structure when the wind blows on the wind turbine.

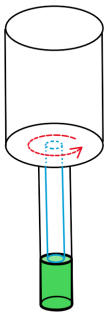

Figure 12.4: Representation of the VAWT. The blue section is the rotating shaft that carries the torque and transmits it to the generator shown in green.

In summary, the body must be designed to handle the introduced stresses, ensure stability, and accommodate vibrations. Therefore, a stability analysis will be conducted in Section 12.2 to

ensure the structure remains stable. Then, a stress analysis will be conducted in Section 12.3 to ensure the body can withstand the introduced stresses, and solutions to damp vibrations will be addressed.

12.1.4. Assumptions

Before conducting the analyses, it is essential to introduce and explain the assumptions that will be used throughout. They are as follows:

- The force due to the wind turbine and the pole is assumed to be a point force.
- The mass of the body, combined with the equipment for energy storage, sensors, and electrical systems, is considered a point force acting through the CG of the structure.
- The joints at points B and E in Figure 12.2 are pin joints.
- Out of the twelve legs, a minimum of four legs are in contact with the ground at all times.
- The horizontal reaction forces at the leg locations are assumed to be equal.
- All beams share the same rectangular cross-section to ease manufacturing.
- The aerodynamic force acting on the body is neglected as it is negligible in comparison to the force generated by the wind turbine.

12.2. Stability Analysis

This section focuses on performing a stability analysis to prevent the structure from tipping over. To begin, the mass of each component will be determined in subsection 12.2.1. Then, the stability calculations will be detailed in subsection 12.2.2.

12.2.1. Mass Estimation

To ensure the stability of the structure, the normal reaction force of the legs is crucial as it counteracts the moments generated by the wind turbine and the friction of the legs. Therefore, meeting the stability requirement hinges on two factors: the total mass of the structure and the moment arm of the normal force, which is influenced by the width of the body. Thus, the initial step in the stability analysis is to estimate the total mass of the entire structure accurately.

The mass estimation is divided into components corresponding to the wind turbine, the body, and other parts, with their respective masses provided in Table 12.1.

Table 12.1: Mass estimation for the components of the structure

Wind turbine	*Mass [kg]*	**Body**	*Mass [kg]*	**Other**	*Mass [kg]*
Turbine	60	Beams	70	batteries	6
generator	40	Panels	200	payload	50
Shaft of WT	10	Solar panels	100	motors	10
Pole of WT	20	Legs total	120		
Cage of WT	20				

12.2.2. Stability Calculations

The critical load case for stability is when the wind turbine generates its maximum force, causing the highest moment on the structure. For analysis, the scenario where the rear legs have just lifted off from the ground is considered, leaving all the load supported by the front legs alone. For this critical scenario the stability can be analysed in 2D as illustrated in Figure 12.5.

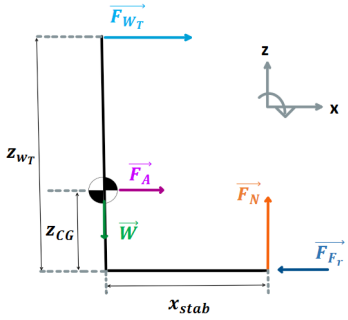

Figure 12.5: Stability analysis of the structure

The entire weight of the structure is distributed over the front legs in contact with the ground, resulting in Equation 12.1. The friction force on the feet is computed with Equation 12.2, for which the friction coefficient is assumed to be $\mu = 0.31$ [-].

$$F_N = m_{tot} \cdot g \tag{12.1}$$

$$F_{Fr} = \mu \cdot F_N \tag{12.2}$$

The moment equilibrium is analysed around the CG of the structure. The required distance to maintain stability is defined as the horizontal distance in the x-direction, denoted by x_{stab} in Figure 12.5. This distance is calculated using Equation 12.3.

$$x_{stab} = \frac{F_{W_T} \cdot (z_{wt} - z_{c.g}) + F_{Fr} \cdot z_{c.g}}{F_N} \tag{12.3}$$

The sum of moments can be plotted to visualise the bottom and upper limit on x_{stab}, as can be seen in Figure 12.6. To allow for a sufficient safety margin for the wind turbine force and adequate spacing in the container, the stability distance, x_{stab}, is chosen to be 1.6.

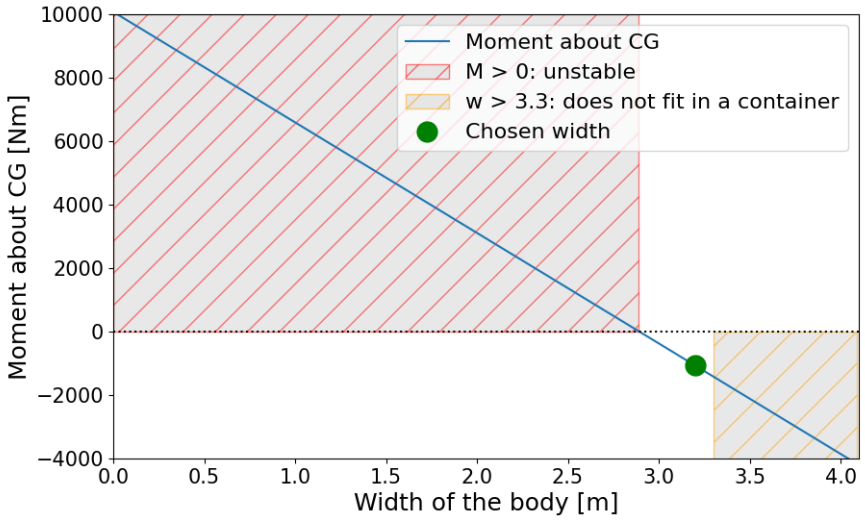

Figure 12.6: Sum of the moments about the CG of the structure. A negative moment is stabilising.

Achieving this stability requirement with a single turning shaft for one pair of legs would require each leg to be 8.5 m high. However, such large leg sizes are undesirable because they significantly increase the total mass of the structure and raise its center of gravity. Moreover, larger legs would complicate maintenance of structural components. Therefore, a new shaft-leg configuration was developed. Instead of having one turning shaft for one pair of legs, the design now incorporates two shafts for each leg pair. These shafts are connected by a coupling rod to ensure synchronous rotation. A visualisation of this configuration is depicted in Figure 12.7.

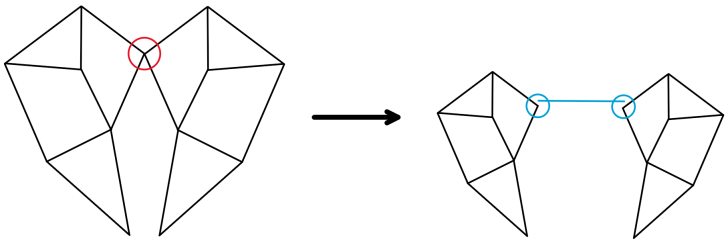

Figure 12.7: High-level comparison between one shaft (in red) and two shafts design (in blue).

This way, the required spacing can be achieved without an excessive increase in leg size. The sizing for this scenario was determined as follows. The team decided that to efficiently function at the beach, the structure should be able to step over obstacles up to 0.3 m, such as sand castles. Following that, legs in the new configuration would be 1.4 m high, with the fixed point at 0.93 m, which is also the height of the main body platform.

The shafts, being hollow cylinders and not load-bearing, will be made of bamboo for sustainability, as composite materials are not suitable for this purpose.

12.3. Stress Analysis

With stability ensured, the next step is to verify that the stresses within the body do not exceed the material strength. Specifically, since the cross-section of the beams in the structure has not been determined yet, this section focuses on determining an appropriate cross-sectional size that ensures the structure can withstand the stresses imposed upon it.

12.3.1. Loading of the body

The first step consists in determining the loading on the body, as shown in Figure 12.8. Six forces are distinguished:

- The vertical reaction of the legs on the body on the right side: $\vec{F_F}$ in orange.
- The vertical reaction of the legs on the body on the left side: $\vec{F_B}$ in yellow.
- The horizontal reaction force of the legs on the body: $\vec{F_H}$ in blue.
- The force due to the wind turbine: $\vec{F}$ in light blue.
- The aerodynamic force acting on the body: $\vec{F_A}$ in purple
- The weight of the whole structure: $\vec{W}$ in green.

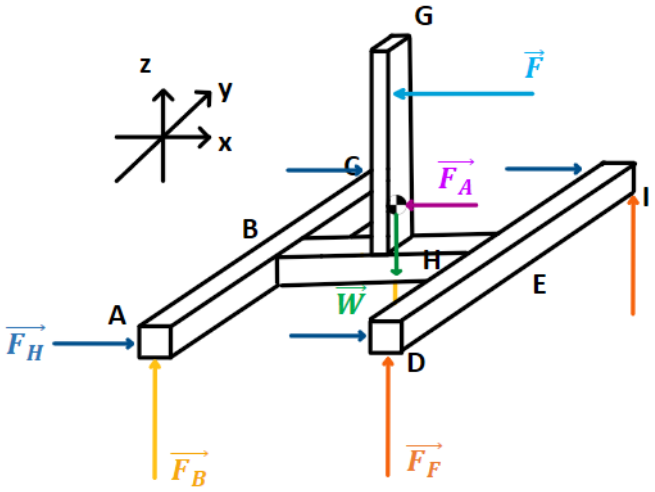

Figure 12.8: Free-body diagram of the body

After examining the kinematic linkage, it was determined that at each moment at least four out of the twelve legs are in contact with the ground. Multiple combinations of four legs can be in contact with the ground, but the most critical case occurs when the four legs at the edges of beams AC and DI are in contact with the ground. This configuration leads to the highest bending moment at the center of beams AC and DI.

12.3.2. Inputs and outputs of the stress analysis

With the loading determined, the inputs and outputs of the stress analysis can be defined as shown in Figure 12.9. The goal of this analysis is to determine the cross-section of the structural beams of the body, assuming that all beams have the same cross-section.

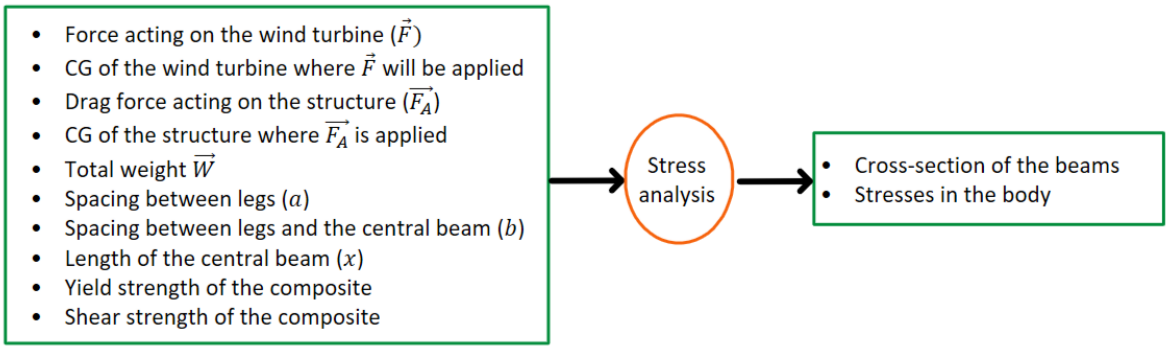

Figure 12.9: Inputs and outputs of the stress analysis

To determine the values for each input, the preliminary analyses (kinematic, aerodynamic, etc.), initial body sizing, and stability analysis output are utilised. Material properties, including yield strength at end-of-life from Chapter 5 and a shear strength assumed to be 17.5 MPa [83], reported for a flax/epoxy composite, are considered. A summary of the inputs is provided in Table 12.2.

Table 12.2: Table of Inputs

Input	Symbol	Value	Units
Force acting on the wind turbine	$\vec{F}$	2362	N
CG of the wind turbine where $\vec{F}$ is applied	z_{T}	3.275	m
Drag force acting on the structure	$\vec{F_A}$	0	N
CG of the structure where $\vec{F_A}$ is applied	z_{CG}	0.35	m
Total weight	$\vec{W}$	6975	N
Spacing between legs	a	0.5	m
Spacing between legs and the central beam	b	2.1	m
Length of the central beam	x	3.2	m
Yield strength of the composite	σ_y	397	MPa
Shear strength of the composite	τ_s	17.5	MPa

12.3.3. Determining the beams' cross-section

Using the FBD defined in Figure 12.8 along with the given inputs, the internal loading in the body can be determined. To accomplish this, the following steps were followed:

- Determine the reaction forces through equilibrium ($\vec{F_H}$, $\vec{F_B}$, $\vec{F_F}$).
- Split the body into straight beams (AC, DI, BE, GH).
- Determine the internal loading of each beam (shear force, normal force, and internal bending moment).

The output of this process includes NVM diagrams for all the beams. However, for clarity, only the diagram for the most heavily loaded beam is presented in Figure 12.10.

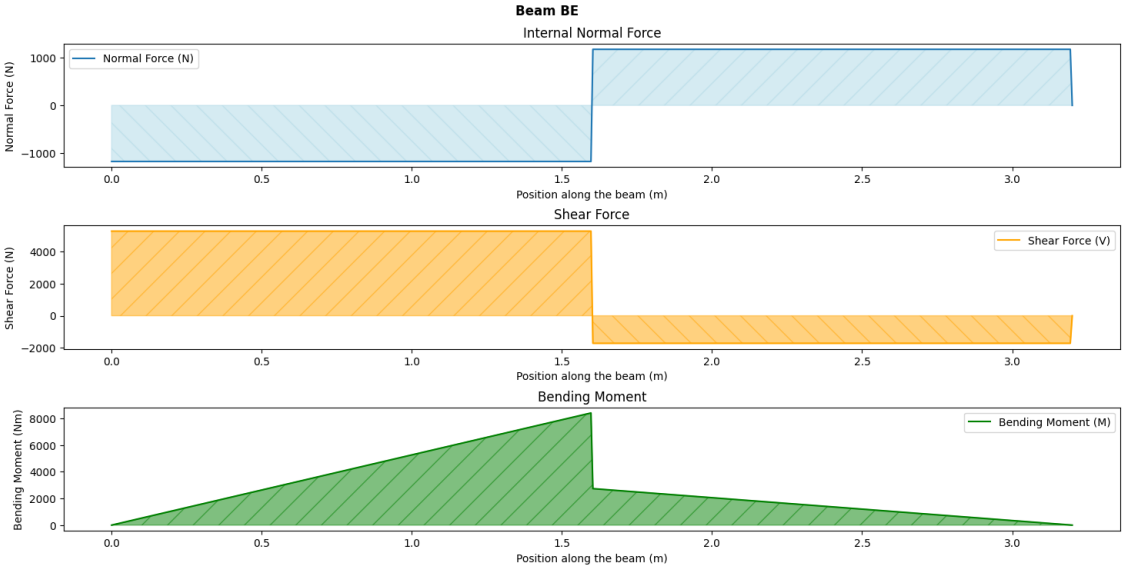

Figure 12.10: Internal normal force, shear and bending moment diagrams for the beam BE

Based on the internal loading in beam BE, the cross-section can be determined. To achieve this, certain constraints need to be applied. Specifically, all beam cross-sections are assumed to be identical and rectangular for ease of manufacturing. The cross-section is illustrated in Figure 12.11.

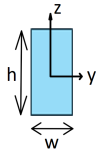

Figure 12.11: Cross-section of the beam BE. Note that all the other beams have the same cross-section

The initial step in sizing the cross-section involves correlating the stresses in the beam with the internal loading. This entails considering two types of stresses: shear and axial stresses. As the cross-section is symmetrical, the maximum axial and shear stresses can be determined using Equation 12.4 and Equation 12.5, respectively.

$$\sigma_{\text{axial}} = \frac{N}{w \cdot h} + \frac{6 \cdot M}{w \cdot h^2} \tag{12.4}$$

$$\tau = \frac{3 \cdot V}{2 \cdot w \cdot h} \tag{12.5}$$

In these equations, the internal loads (N, M, and V) are known from the NVM diagrams, and the stresses (σ_{axial} and τ) can be calculated using the yield and shear strength of a composite, with a safety factor of 1.5. The only unknowns are the width and height of the cross-section. Those two variables influence various properties of the beam, the most important being the area and the moment of inertia. Optimising both width and height separately would be impractical. To simplify the problem, the aspect ratio of the cross-section (width to height) was set at 0.5. This limits the design space while ensuring reasonable bending performance. To determine the dimensions, the margin of safety (MS) was calculated using Equation 12.6 for different combinations of width and height. The results can be seen in Figure 12.12.

$$MS = \frac{\text{Max allowable stress}}{\text{Safety factor} \cdot \text{Applied stress}} - 1 \tag{12.6}$$

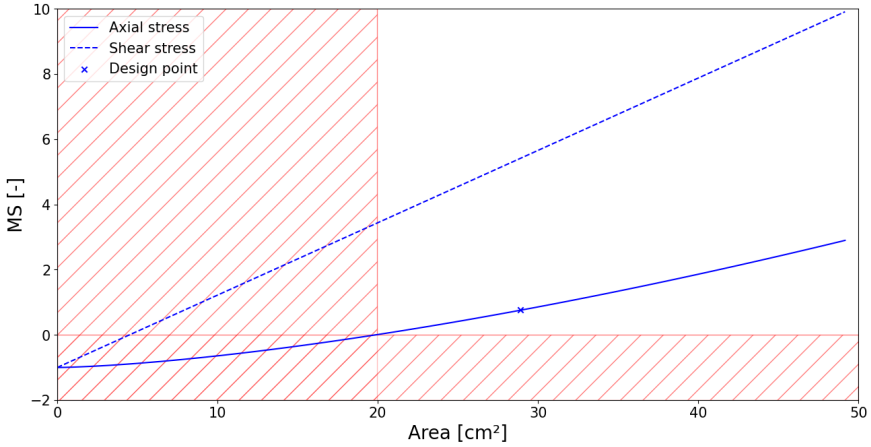

Figure 12.12: Safety margin for the beams in an initial configuration, plotted against beam cross-section area

The red hatches indicate the unfeasible design areas, where one of the MS is below 0. The chosen cross-section area is 29 cm^2, corresponding to width w of 3.8 cm and height h of 7.6 cm.

12.3.4. Analysis of the results

Given the stresses along all beams, analysing the margin of safety, as defined in Equation 12.6, is a good way to assess how optimised the cross-sections are. The margin of safety for both axial and shear stresses is plotted for all beams in Figure 12.13.

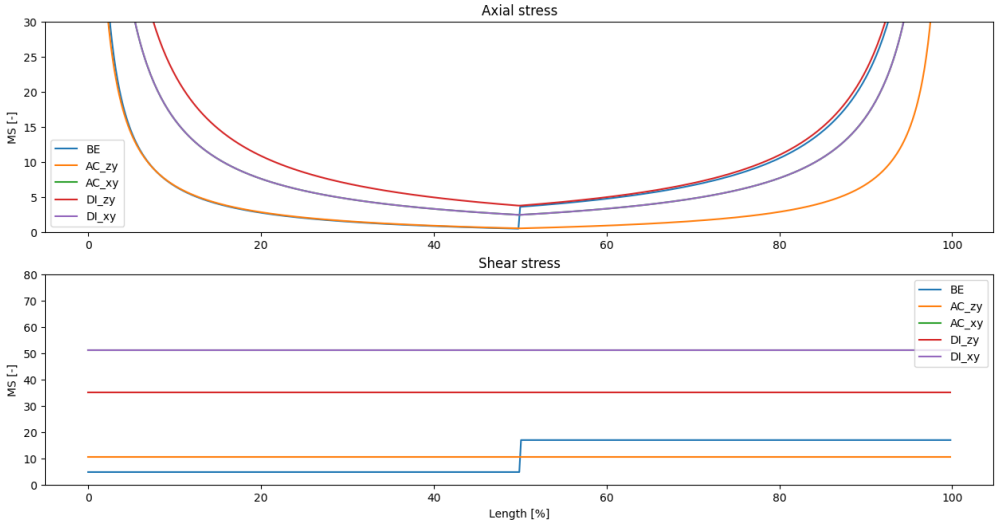

Figure 12.13: Safety margin for all the beams in the initial configuration, plotted against the percentage of length

As expected, the minimum margin of safety is for beam BE, as it was sized accordingly. It can be

seen from those plots that the beam DI and beam AC have been optimised to a lesser extent as their margin of safety is (much) larger than zero. This leads to unnecessary mass and increased power requirements for motion.

Another issue with the current body design is its inability to handle vibrations introduced by the wind turbine and generator. Additionally, the design is driven by the large bending moment in the middle of beam BE, as shown in Figure 12.10, resulting in an oversized cross-section primarily designed to resist this moment.

Considering these aspects, introducing another design option is necessary to address the following issues:

- Reduce vibrations introduced by the wind turbine and generator.
- Reduce the internal bending moment at the center of beam BE.
- Optimise the cross-section to avoid oversized beams.

12.3.5. Introducing a new design for the frame

Considering these factors, the updated frame shown in Figure 12.14 is introduced. The wind turbine is mounted on a platform with springs to dampen vibrations. To better distribute the bending moment along beam BE, beams JK and HI are added with springs to more effectively distribute the loads. To optimise the cross-sections and reduce mass, three cross-sections are used: beams BE and OP, beams JK and HI, and beams AC and AG each share the same cross-section.

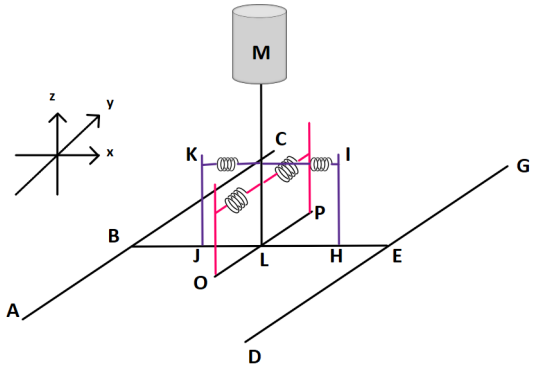

(a) New design option, including springs to damp vibrations and reduce the bending stress of beam BE. Note that the springs are not considered in this figure for clarity

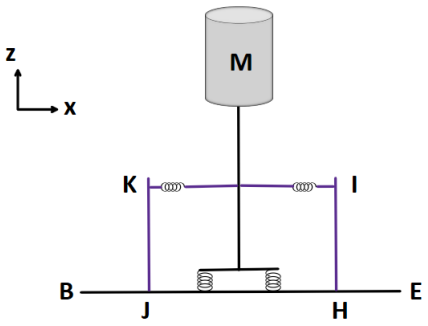

(b) Side view of the central view to display the platform used to dampen the vibrations. Note that the drawing is not to scale

Figure 12.14: The new design option and its side view

For this new design, the same analysis is performed to determine the stresses along each beam and from that determining their cross-sections (h and w). In addition to the inputs explained in Table 12.2, additional inputs are required. They are listed in Table 12.3.

Table 12.3: Table of inputs for the new design using springs

Inputs	Symbol	Value	Units
Height of the support springs on beams JK and HI	h_s	0.65	m
Width of the foundation	w_f	0.5	m
Distance between the springs and the wind turbine	x_{sup}	0.5	m
Stiffness of the top support springs	k_s	20	kN/m
Stiffness of the bottom springs	k_f	20	kN/m

Performing the same analysis as for the case without springs, the cross-sections of the beams can be determined. The resulting plot can be seen in Figure 12.15.

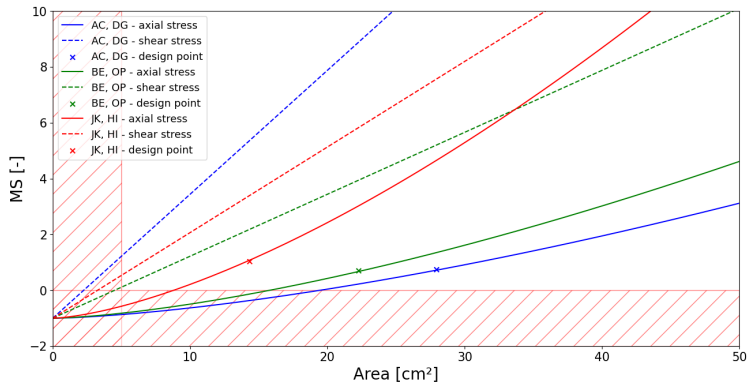

Figure 12.15: Safety margin for all the beams in the spring configuration, plotted against the area of the beams

Red hatches indicate areas that are not feasible. Please note that the vertical right-hand-side hatches for MS below 0 have not been added for clarity. Instead, an area of 5 cm^2 was chosen as the smallest manufacturable one. The design points corresponding to different beams were chosen to have small positive MS. This results in the cross-sections presented in Table 12.4.

Table 12.4: Cross-sections of the beams for the new design of the frame

Beams	Height [cm]	Width [cm]
JK and HI	5.35	2.68
BE and OP	6.67	3.34
AC and DG	7.47	3.74

Considering the cross-sectional data, the impact of the new design can be assessed in two ways. Firstly, the design change's effect on beam BE is evaluated. Table 12.5 displays the results before and after the design modification for this beam. From this table, it is evident that the design change decreases the maximum internal bending moment in BE but significantly increases the maximum internal axial force. Nevertheless, the combined effect on the cross-section leads to a significant (>20%) reduction in the cross-sectional area of beam BE.

Table 12.5: Properties of beam BE

	Old design	**Design with springs**
Maximum normal force [N]	**1181**	**4002.6** (+239%)
Maximum shear force [N]	**5904**	**5904** (-0%)
Maximum bending moment [Nm]	**9428**	**6475** (-31%)
Mass of the frame [kg]	**66.1**	**59.8** (-9.5 %)
Cross-section [cm^2]	**28.5**	**22.3** (-21.8%)

Finally, comparing the masses of the two design options is insightful. On the one hand, the second option has smaller cross-sections but, on the other hand, includes more beams. Referring to the figures in Table 12.5, it appears that the second design option is lighter by almost 6.5 kg.

With the impact of this design change on beam BE and the mass of the frame established, the next step is to investigate how this change has affected the margin of safety for all beams. Figure 12.16 illustrates the margins of safety for the updated design. Comparing it with Figure 12.13, it is apparent that the margins of safety are closer to zero, indicating a more optimised cross-section than in the initial design of the structure.

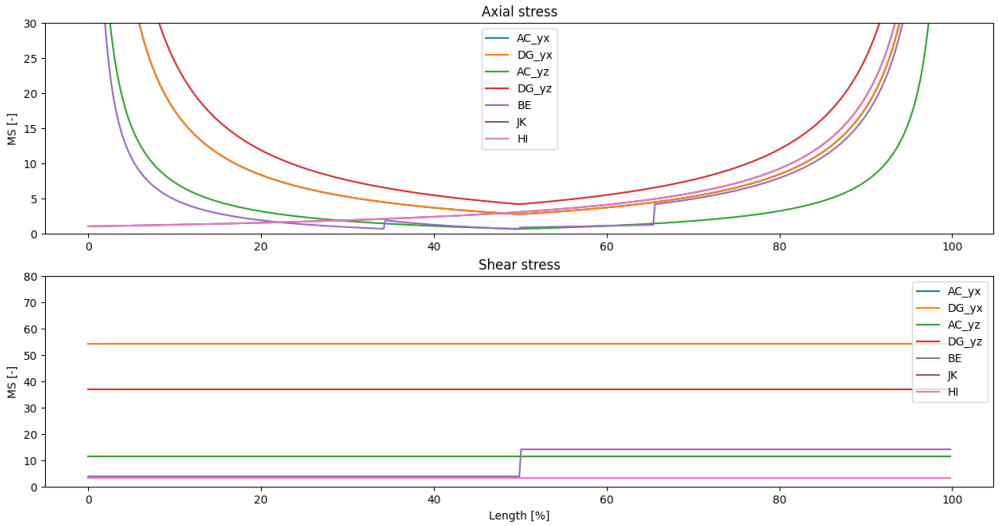

Figure 12.16: Safety margin for all the beams in the spring configuration, plotted against the percentage of length

12.4. Deflection Analysis

Another critical failure mode to consider is excessive deflection of the beams under applied loads. If deflections exceed acceptable limits, the structure may sag excessively or come into contact with other components, which is undesirable.

Two specific cases are of particular interest. Firstly, the beam that undergoes the most deforma-

tion should not come into contact with the ground and must maintain adequate clearance beneath the central box. Secondly, it is crucial to ensure that beams J-K and H-I in Figure 12.14a do not deform excessively, as this could potentially interfere with the box, as illustrated in Figure 12.17.

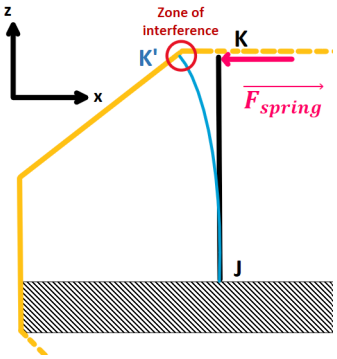

Figure 12.17: Interferences between the protective boxes shown in yellow and beam J-K when the spring force is applied

12.4.1. Deflection to ensure sufficient ground clearance

Firstly, priority is given to ensuring adequate ground clearance. The deflection analysis of the beams will use Macaulay's method, focusing on the critical loading scenario considered in the stress analysis. Among all beams, beam AC (refer to Figure 12.14a) has been identified with the highest deflection and thus warrants detailed examination.

To determine its deflection in the y-z plane, the beam is modeled assuming support by a pin joint at point B. This modeling approach is depicted in Figure 12.18a. The analysis reveals a maximum deflection of approximately 1.3 meters, as can be seen in Figure 12.18b.

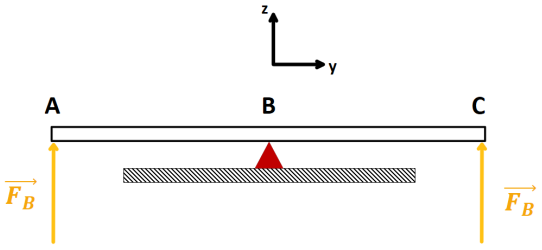

(a) Model of beam AC with its loading case

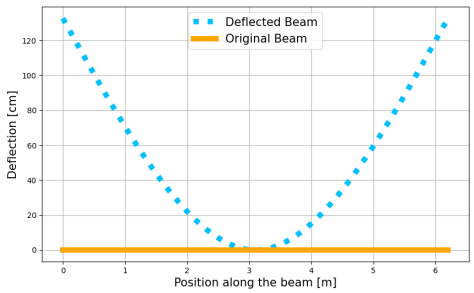

(b) Deflection of the AC beam in the z-y plane

Figure 12.18: Caption for both figures

This deflection is too extreme, potentially causing the protective box to contact the ground. Therefore, adjustments are necessary to address this issue. Namely, the following changes have been decided upon:

- Increasing the height of the legs by multiplying all leg dimensions by 1.9 to provide more clearance.
- Modifying the cross-sections of beams AC and DG to limit the maximum deflection to 30 cm, ensuring a ground clearance of 1.2 m, as depicted in Figure 12.19.

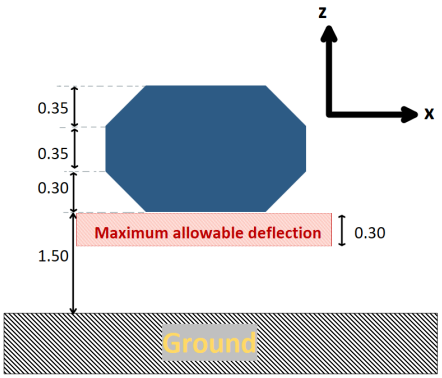

Figure 12.19: Maximum allowable deflection to ensure sufficient ground clearance for the protective box (shown in blue). All dimensions are provided in meters

Following these changes, the structural analysis needs to be repeated due to the altered geometry. The process for conducting the revised structural analysis is illustrated in Figure 12.20. The process involves repeating the previously executed steps, which will not be re-explained. Only the results are presented.

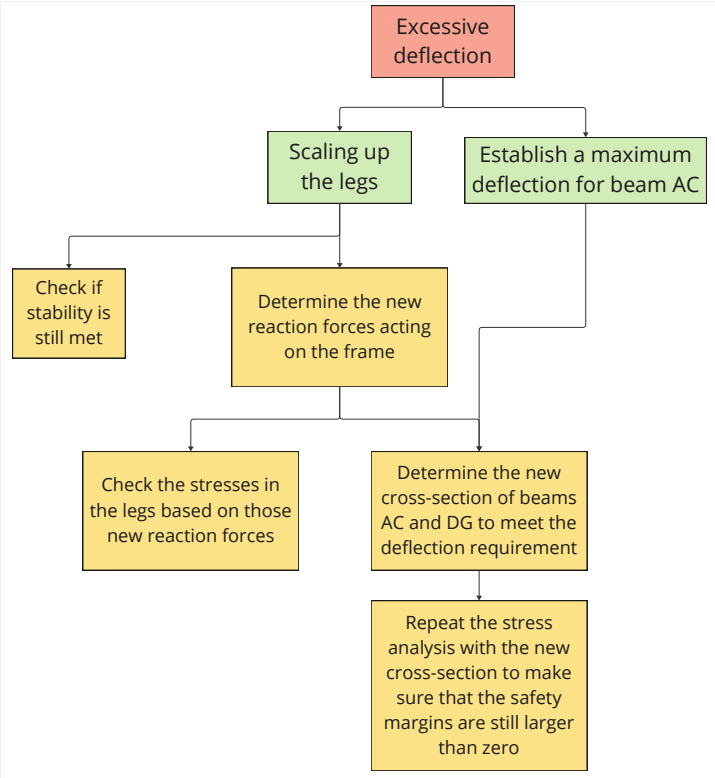

Figure 12.20: Structural analysis process accounting for larger leg size and deflection constraints on beams. The red box highlights the issue, the green boxes show chosen solutions, and the yellow boxes outline the steps for analysis

To find the new required moment of inertia, Figure 12.21 is constructed. From this figure, it can be seen that the minimum I to meet the requirement of 30 cm is $5 \cdot 10^{-6}$ m^4. Therefore, the cross-sections for beams AC and DG have been adjusted to a width of 5.0 cm and a height of 10.6 cm.

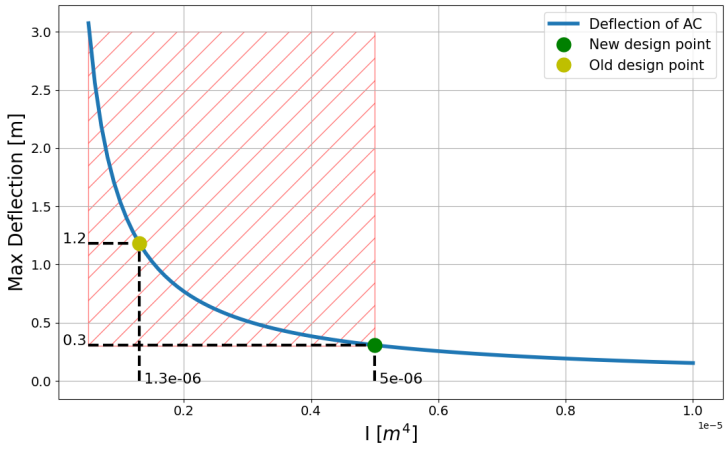

Figure 12.21: Deflection of the AC beam in the z-y plane as a function of its moment of inertia

Based on the larger dimensions of the legs and the updated cross-sections of beams AC and DG, stability and stress analyses were revisited. The results confirm that this new geometry ensures the frame will not experience failure due to stability issues or excessive stresses. Therefore, these revised cross-sections and increased leg dimensions constitute the final design.

12.4.2. Deflection of beams J-K and I-H

To conclude the section on deflections, it is necessary to examine the deflection of beams JK and HI, as this will impact the design of the protective box for the equipment. The beam model is shown in Figure 12.22a. In the most critical scenario, the spring force is approximately 3800 N. For this force and the selected cross-section detailed in Table 12.4, the deflection is plotted in Figure 12.22b. The maximum deflection observed is 3 cm.

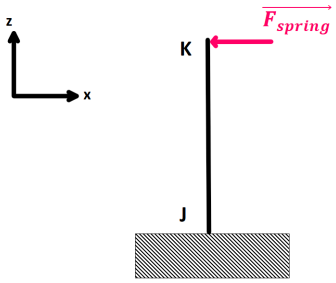

(a) Modelisation of the spring, with a spring force of 3806 N for the new configuration

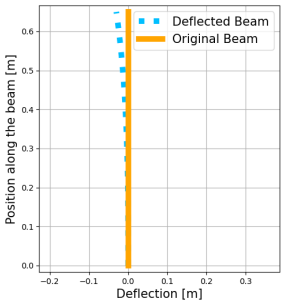

(b) Deflection of beam JK.

Figure 12.22: Spring model and deflection

To accommodate this deflection, the panel will be elongated by 5 cm to provide clearance for maximum deflection, as shown in green in Figure 12.23.

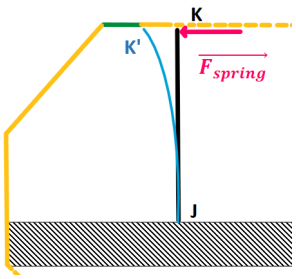

Figure 12.23: Adjustment of the box dimensions to provide clearance, with the extension shown in green.

12.5. Tower design

Now that the stability and stress analyses have been performed on the load-bearing frame, one must design the tower that will support the vertical axis wind turbine. The tower consists of two elements: a circular shaft that will transmit the torque to the generator and a tower that will carry the loads, shown in blue and in green respectively in Figure 12.24. This section will focus only on the design of the pole, as the design of the shaft is explained in Chapter 8.

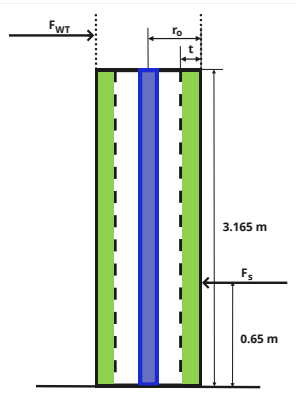

Figure 12.24: Visualisation of the tower, with the load-bearing tower shown in green and the shaft to transmit the torque in blue.

The tower is a hollow circular shaft, but as discussed in Section 6.4, manufacturing hollow circular shafts using the provided composite panels is challenging. Consequently, an alternative material is needed. The focus is on finding a sustainable material that can withstand high loads and harsh environmental conditions. Considering these factors, bamboo has been selected for the tower. The mechanical properties of bamboo are summarised in Table 12.6.

Table 12.6: Key properties of bamboo to design the tower [84]

Tensile Yield Strength [MPa]	**Shear Strength [MPa]**	**Density** $[g/cm^3]$
217	7.8	1

The next step is to determine the required geometry of the pole to resist the load case shown in Figure 12.24. The outer radius of the tower is set to 10 cm for structural reasons. To determine the thickness of the pole, the stresses are calculated, and the minimum thickness required to withstand these stresses is found, using a safety factor of 1.5. The results of this analysis are presented in Table 12.7.

Table 12.7: Dimensions of the tower

Outer radius of the tower (cm)	Required thickness (cm)	Inner radius of the tower (cm)	Mass of the tower (kg)
10	2.512	7.488	43.68

12.6. Stresses in the Legs

In Chapter 9, the sizing of the leg system was addressed, but the cross-section of the legs was not determined. This section aims to establish the required cross-section of the leg components to withstand the forces acting on them. A static analysis is conducted in subsection 12.6.1, followed by a dynamic analysis in subsection 12.6.2 to assess stress levels during motion.

12.6.1. Static analysis

To determine the stresses in the legs, the leg configuration of the scenario considered in the stability analysis will be employed, as shown in Figure 12.25a. This is considered the most critical case stress-wise. Although this linkage is intrinsically dynamic, it will be addressed here as a static case. The goal is to find the stresses and deformations in the linkage system due to the loads introduced at point 2 which are consistent with those used in the stress analysis.

To model the situation, the node in contact with the ground (node 8) is constrained in the x and y directions. The y direction is constrained because the node is on the ground, and the x direction is constrained to prevent slipping. No constraints are imposed on nodes 2 and 1, as their only support is the beams underneath in the considered case. Considering these aspects, the model shown in Figure 12.25b can be built.

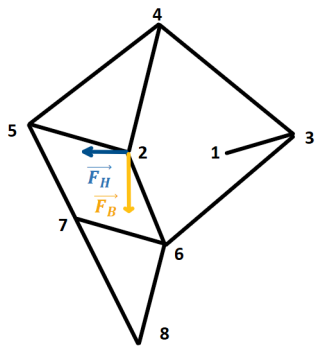

(a) Representation of the leg model structure with the applied forces. Note that the locations of the points are illustrative and not to scale.

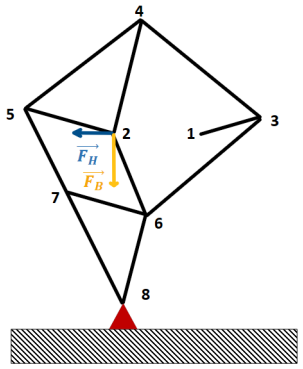

(b) Leg model with the constraints and the forces applied. The red triangle indicates a pinned connection.

Figure 12.25: Leg configuration and modeling

Two approaches can be used to determine the forces in each member: treating the structure either as a beam or a truss. The decision hinges on whether the joints are considered pinned (truss) or have solid connections (beam). While the majority of joints are pinned, the connections corresponding to triangles 2-4-5 and 6-7-8 are solid. These triangles always remain the same shape, so they can be manufactured as a single piece (hollow triangle) instead of three separate components. Given that in the analyzed configuration the remaining joints provide significant resistance to bending when a force is applied to the linkage in a static position on the ground,

the structure should be treated as a beam-type structure.

Solving the problem by hand is impractical, so a simple FEM analysis was implemented to determine the stresses. The results are shown in Figure 12.26, where the stresses in each element are displayed. This figure uses the Young's modulus of the flax/coPOM composite, as that is the material that will be used for the legs. The cross-section of the beams that will compose the legs is chosen to be rectangular with a width of 1 cm and a height of 5 cm.

The deflections are minimal (less than one millimetre) and therefore not a concern. As seen in the figure, the stresses are much lower than the yield strength of the composite (402 MPa), so failure is unlikely.

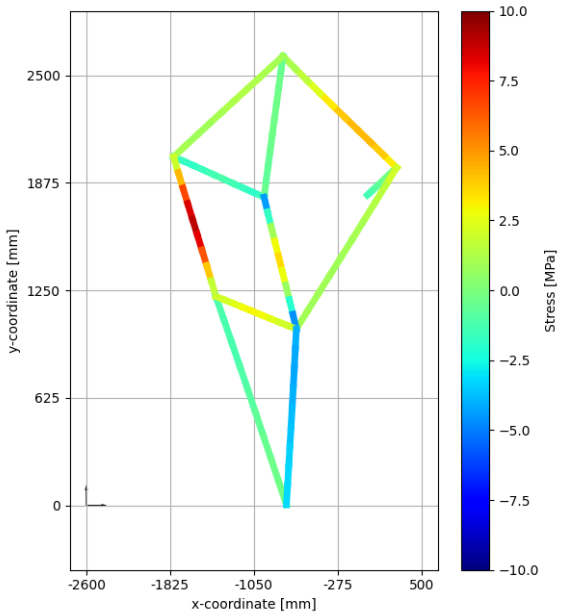

Figure 12.26: Stresses in the elements of Jansen's linkage for the critical case considered in the stability analysis. The loading and the boundary conditions are defined in Figure 12.25b.

Additionally, it is possible to optimise the cross-section further to have actual stresses closer to the yield stress. However, this is not advisable as it would require reducing the thickness of the panels below 1 cm, which is unsuitable manufacturing-wise. Indeed, reducing the thickness could lead to significant delamination in very thin panels, significantly reducing their mechanical properties.

12.6.2. Dynamic analysis

After conducting the static analysis, it is crucial to examine the dynamic behavior of the legs because the stresses evaluated in subsection 12.6.1 may not represent the peak stresses experienced during motion.

To solve the dynamic problem, Equation 12.7 can be used. It is similar to the equation used in the static analysis, except for the added acceleration term.

$$\mathbf{M}\ \ddot{\mathbf{x}}(t) + \mathbf{K}\ \mathbf{x}(t) = \mathbf{F}(t) \tag{12.7}$$

In practice, implementing this equation would typically involve defining the mass matrix of the legs. However, a back-of-the-envelope analysis can provide an initial assessment of its significance.

For instance, considering the mass of the heaviest element (beam 6-3), which is 0.52 kg, and a particularly high acceleration for this element (10 m/s^2), the contribution of the acceleration remains very small compared to the forces applied on the legs (order of magnitude of a thousand times smaller). Therefore, the contribution of the acceleration accounts for less than 1%, allowing its neglect.

By assuming the mass matrix can be neglected, the analysis returns to the static case, allowing the analysis of multiple frames as static cases and then combining the frames to obtain the dynamic analysis. The resulting analysis can be found by clicking on the following link: `https://youtube.com/shorts/KAwaBgjkn3A`.

From this dynamic analysis, it can be seen that the maximum stress during one period is 8.95 MPa, whereas the maximum stress in the static analysis was also 8.95 MPa. Therefore, it is proven that the considered case in the static analysis is indeed the most critical one. It can also be observed that the legs experience no stress when they are not touching the ground, as expected.

12.6.3. Joints for the Legs

With the forces in the legs determined for the most critical case, the joining method to prevent failure will be chosen. As determined in Chapter 6, compliant mechanisms are not suitable, so traditional joining methods are considered. Shear joints are preferred over tension joints due to their higher load-carrying capacity.

The four potential failure modes shown in Figure 12.27 will be analyzed: net-section failure, bearing failure, shear tear out, and bolt shear. Based on this analysis, the joint's geometry will be defined, and the most critical failure mode identified.

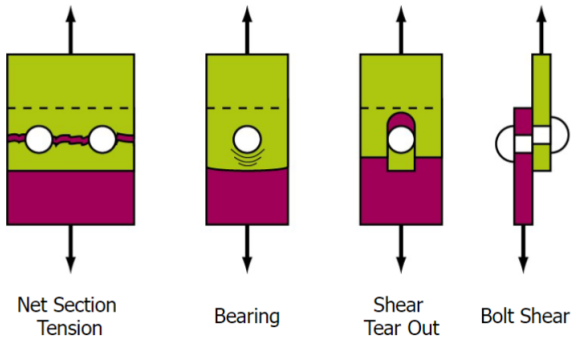

Figure 12.27: The four potential failure modes of shear joints.

For each failure mode, the failure load can be computed, given relevant stress and dimensions. Then, this failure load is compared to the design load. The MS is calculated using Equation 12.6, however loads are considered, instead of stresses.

Net-Section Failure

The net-section failure load (F) can be computed by rearranging Equation 12.8, with the number of joints $n = 1$. The calculated stress is compared to the ultimate tensile strength of the sheet material (402 MPa for flax/coPOM, as determined in Chapter 5).

$$\sigma_u = \frac{F}{t \cdot (W - n \cdot d)} \tag{12.8}$$

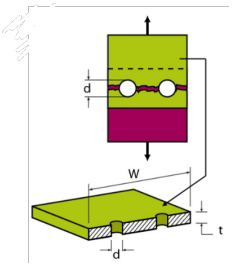

Figure 12.28: Dimensions relevant to the net-section failure.

Bearing failure

For bearing failure, a similar procedure is followed. The actual stress is computed using Equation 12.9 and then compared to the allowable bearing strength of the sheet material (flax/coPOM). Although the specific bearing strength of the composite is unknown and no literature could be found on the bearing strength of this combination, it is typically around 1.5 times the ultimate strength. Therefore, using the ultimate strength as the bearing strength is a conservative approach.

$$\sigma_{br} = \frac{F}{t \cdot d} \tag{12.9}$$

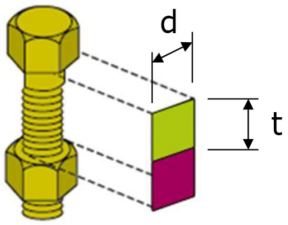

Figure 12.29: Dimensions relevant to bearing failure.

Shear tear out

For shear tear out, Equation 12.10 is employed. The resulting value will be compared to the ultimate shear stress of the composite. The shear stress of the composite is assumed to be 17.5 MPa [83], as this value is reported for a flax/epoxy composite, given the absence of specific data for the flax/coPOM composite. For more precise designs, conducting a test on the flax/coPOM composite to determine this property is recommended.

$$\sigma_{su} = \frac{F}{2 \cdot b \cdot t} \tag{12.10}$$

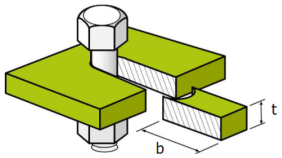

Figure 12.30: Dimensions relevant to the shear tear out failure.

Bolt shear

Finally, the stress to be considered for the bolt shear is defined in Equation 12.11. The result will be compared to the ultimate shear stress of the material of the bolt. Typically, the shear stress of the bolt material is approximated to be around 60% of its tensile strength. Assuming a medium carbon steel; quenched and tempered joint, the shear strength is 480 MPa. For this

analysis, n is assumed to be 1 as one sheet will be used per leg, and using more sheets would result in an undesired addition of mass.

$$\sigma_s = \frac{F}{n \cdot \frac{\pi}{4} \cdot d^2} \tag{12.11}$$

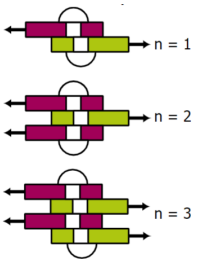

Figure 12.31: Dimensions relevant to the bolt shear failure.

Results

The most critical loading case determined in subsection 12.6.2 was used for all failure modes, in combination with the parts sizes and their properties. The input (predefined) values are summarised in Table 12.8 below.

Table 12.8: Predefinded inputs for leg joint sizing analysis.

Variable	**Value**	**Unit**
Sheet thickness (t)	10	mm
Sheet width (W)	50	mm
Ultimate stress of the sheet (σ_u)	402	MPa
Bearing stress of the sheet (σ_{br})	402	MPa
Ultimate shear stress of the sheet (σ_{su})	17.5	MPa
Ultimate shear stress of the bolt (σ_s)	480	MPa
Design load (F_d)	5500	N

Considering the width of the panel and ease of manufacturing, a feasible bolt size range was determined from 10 mm to 40 mm. To find a precise diameter value, the failure load was determined for each failure mode and then the corresponding MS was calculated. The obtained values are plotted against the diameter sizes in Figure 12.32. The red hatches indicate not feasible design areas (MS below 0 or difficult manufacturing).

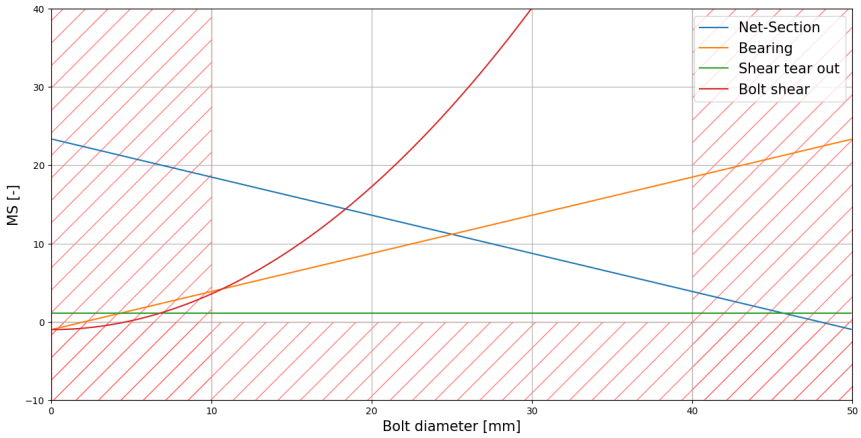

Figure 12.32: Margin of Safety of the joints for different failure modes, plotted versus bolt diameter.

From Equation 12.10, the shear tear out failure load does not depend on the bolt diameter, but rather on the fastener edge distance. To ensure that MS is above 0, a value of 50 mm was used for this variable. Considering the rest of the failure modes, it can be seen that MS stays above 0 for all feasible diameter sizes. Therefore, the 10 mm diameter was chosen to avoid adding unnecessary weight. For this size, the MS are 18.4 (net-section), 3.8 (bearing), 1.1 (shear tear out), and 3.5 (bolt shear).

12.7. Body panels

The frame will be covered with panels that also provide space for solar panels. Based on calculations performed in subsection 12.1.1, an area of 9 m^2 is required. Additionally, the panels should protect the sensitive payload and cover the spring system. With this in mind, a set of 8 panels was designed. The dimensions are summarised in Table 12.9.

Table 12.9: Table summarising body panels dimensions.

Panel	**Size [cm] (w x t x l)**	**Quantity**
Front and back	35 x 0.5 x 400	2
Top and bottom	110 x 0.5 x 400	2
Angled top	111 x 0.5 x 400	2
Angled bottom	100 x 0.5 x 400	2

The panels are not load-bearing, therefore a small thickness of 5 mm was chosen.

12.8. Element extraction the wind turbine blade

In the previous sections, the design was made keeping available geometries in mind. Now, extracting the needed elements from the WTB can be planned in more detail.

The 100 m blade has properties and geometry varying along the length, therefore not all of it can be efficiently used. The area near the root has highly curved geometry and big thickness and therefore is not suitable for obtaining flat panels and straight beams. A similar issue is present at the tip of the blade. To account for that, the first 20% and the last 10% of the blade length

will not be used.

Wind turbines often suffer from leading edge erosion and lightning strikes, which may lead to delamination of the material. To account for the unknown edge damage, a margin of 30% will be applied to the leading edge, and a margin of 20% to the trailing edge. Visualisation of those constraints can be seen in Figure 12.33. The planform was derived from available literature on existing 100 m blades [85].

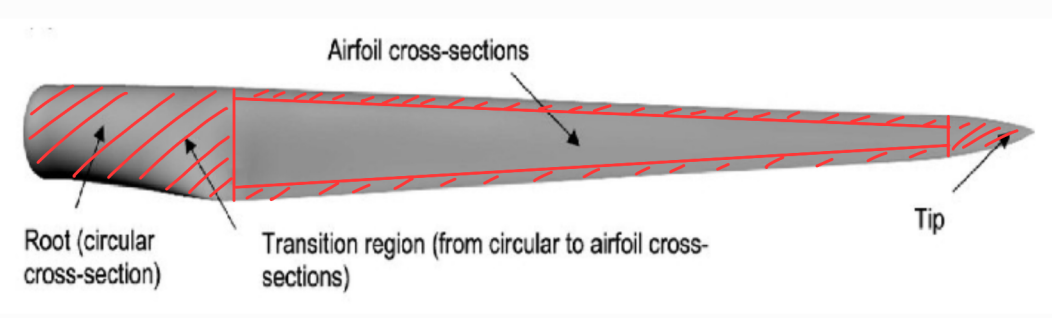

Figure 12.33: Available design space on the wind turbine blade.

The unused parts of the blade still can be recycled. EoL wind blade components too damaged to be used in the structure can be recycled similarly to EoL structure parts. Please see Section 16.5 for possible solutions.

Summarising the sections above, the main structural elements needed are eight load-carrying beams and eight thin panels. Overall, 82% of all structural components (mass percentage) can be extracted from the WTB. The dimensions should be rounded to the nearest millimetre as this is the expected ply thickness (therefore, a manufacturing constraint) [86].

It is favourable to position the elements longitudinally, as this aligns better with the shape of the blade. Load-bearing beams should be cut out of thicker structural elements, while the panels should be acquired from thinner sheets. Ideally, the thickness of the material would align with the required thickness of the parts to minimise the manufacturing effort. When reusing the blade, different fibre arrangements of different parts can be used as an advantage. The spars are commonly made of composite with uni- or bidirectional fibre, which is favourable considering axial loads, bending and shear resistance. Those are the prevalent loading for the beams, so reusing the spars would be beneficial. Keeping the above in mind, the arrangement presented in Figure 12.34 was planned.

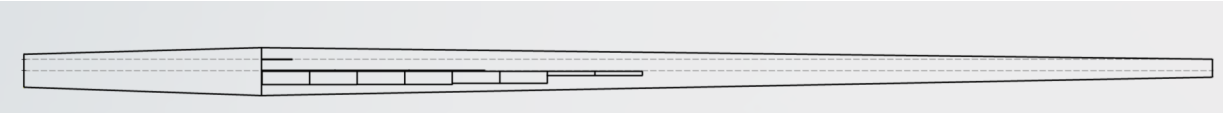

Figure 12.34: Blade geometry with parts overlaid on it.

Thicker beams will be cut out from the rear spar, while the thinner ones can be extracted from the front one. The thin panels will be cut out from the flat panels on the side of the blade. Figure 12.35 shows the arrangement in more detail.

The thickness reduction procedure may be additionally needed, based on the exact dimensions of the blade. However, if the discrepancies are in order of a few millimetres it is advised to accept them, for the sake of minimising the manufacturing resources needed (as will be done for this design). All cut-out parts need to undergo the sanding process and have a protective resin

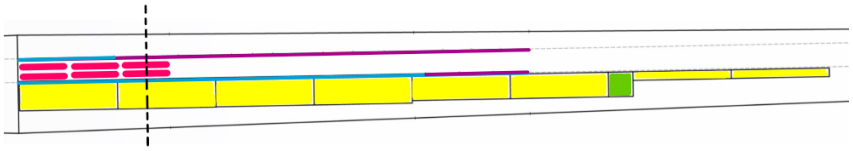

Figure 12.35: Parts arrangement (yellow: panels used for the body; green: foundation; blue: beams for the body; purple: beams for legs; pink: aerofoil)

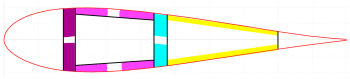

Figure 12.36: Parts arrangement in cross-sectional view indicated by a dotted line in Figure 12.35

applied to the newly exposed edges to ensure satisfactory edge quality.

Based on initial estimations, up to 4 structures can be produced from a single WTB.

Finally, a discussion on the fiber direction for each element can be based on the cross-section shown in Figure 12.36. Biaxial fibers are used for the beams in the legs and body to provide multidirectional strength and load distribution. For the aerofoil, unidirectional panels are employed to maximize strength along the primary load-bearing direction. For the panels, the non-load bearing parts of the blade can be utilized effectively.

12.9. Failure Mode Analysis

Having completed the sizing of the structural elements, the next step involves conducting a failure mode analysis. This analysis aims to determine the potential failure modes of the structure.

First, the potential failure modes should be identified and considered. The identified failure modes are as follows:

- Buckling of structural elements
- Failure of adhesive bonds
- Failure of mechanical joints
- Exceeding material's ultimate strength (tension/compression)

12.9.1. Buckling of structural elements

Given the relatively large cross-sections and the relatively small loads involved, buckling is unlikely to occur in the structure. Additionally, there are no thin-walled load-carrying elements, further reducing the risk of buckling. Therefore, it can be concluded that buckling is not a critical failure mode for this design.

12.9.2. Failure of adhesive bonds

There are three types of failure modes in composite adhesive joints: substrate failure, cohesive failure of the adhesive, and adhesive failure. Adhesive failure is preferred because it is the only failure mode that preserves the properties of both the composite and the adhesive, and it is also easier to repair.

Figure 12.37 displays the area where the adhesive is applied. Those locations will be analysed.

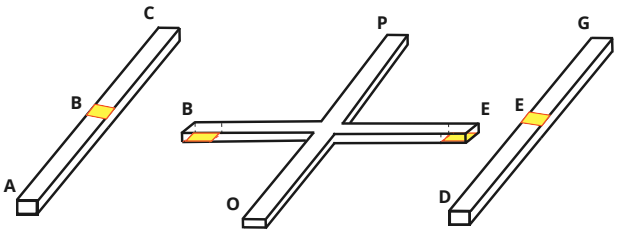

Figure 12.37: Visualisation of area of adhesive bond applied at beam AC

Referring back to subsection 6.5.1, the epoxy model '3M Scotch-Weld Epoxy Adhesive 2216 B/A Gray' is selected as the adhesive bond. Calculations will be performed to ensure stresses do not exceed the epoxy specifications.

The peak stress applied at the joint will be analysed and compared with the shear strength of the composite and adhesive [87]. Volkersen's theory serves as a foundation for understanding the distribution of shear stresses in the adhesive layers of a lap joint [88]. Since the same composite materials are to be bonded, the following equations can be used [89]:

$$\tau_{avg} = \frac{F_{shear}}{A} \tag{12.12}$$

$$\frac{\tau}{\tau_{avg}} = \frac{\omega}{2} \pm \frac{t_1 - t_2}{t_1 + t_2} \tag{12.13}$$

$$\omega = (1 + \frac{t_1}{t_2}) \frac{Gl^2}{Et_1 t_{adhesive}} \tag{12.14}$$

With the values in Table 12.10, the peak stresses at the bonding area are 0.97 MPa and -0.43 MPa. Assuming a safety factor of 1.5 is applied to the shear strength of the composite and adhesive, these strengths are 14.71 MPa and 11.67 MPa, respectively. Since the shear strengths of the composite and adhesive are both greater than the expected peak stresses at the bonding area, it can be concluded that substrate failure and cohesive failure of the adhesive are unlikely to occur. Adhesion failure may be possible, but this is highly dependent on the pre-preparation of the adhesive bonding.

Table 12.10: Values required to calculate the peak stress

$\tau_{avg}[MPa]$	$\mathbf{t_1}$**[cm]**	$\mathbf{t_2}$**[cm]**	$\mathbf{G_{adh}}$ **at 22°C[MPa]**	**l[cm]**	$\mathbf{E_{adherent}}$**[GPa]**	$\mathbf{t_{adh}}$**[mm]**
2.106	6.67	3.34	342	3.74	28	3

12.9.3. Failure of mechanical joints

As extensively discussed in subsection 12.6.3, the mechanical joints have been sized such that they would mot fail under any of the four considered failure modes. Looking at Figure 12.32, the MS for all failure modes is above 0. Therefore, the joints should withstand the stresses even if the applied loading exceeds the design value. Under extreme unexpected conditions, the leg may fail by shear tear out as this failure mode has the lowest MS.

12.9.4. Exceeding material's ultimate strength

Since the cross-sections of the legs and of the frame have been sized such that they will withstand the loads with a safety factor of 1.5, no failure is expected due to loads exceeding the ultimate strength of the composite.

12.10. Learning from Failure: Fail-Safe Design

Despite using a considerable safety margin, a failure may occur during the operational lifetime as some adverse effects cannot be fully mitigated. Being deployed all year round, the structure will face a harsh beach environment and unexpected conditions. Therefore, adequate maintenance will be needed. One method for determining when maintenance should be performed is through a controlled failure of one of the components. When a chosen part fails, it indicates that the material properties of the structure have deteriorated to the point where maintenance is required. Such a part should be dispensable, visible and easy to repair.

After careful consideration, it was decided that the element to fail first should be a non-critical bolt in the outer leg linkages. Such failure is easy to spot and repair, while not endangering the structure or its surroundings. Judging from stresses in legs, bolt 4 (most top one, see Figure 12.25a for joints indexing) was chosen to be intentionally weaker than others. When bolt 4 fails, part 4-3 will not carry any loads (note that parts 4-5 and 2-4 are still connected). The leg will be weakened but still functional such that the structure will not collapse. To further ensure that bolt 4 will fail before the rest of the linkages, the cross-section of part 4-3 was decreased to 3 cm by 1 cm (instead of the regular 5 cm by 1 cm). In this way, part 4-3 will experience slightly higher stresses than the parts around it. Figure 12.38 compares stress distributions for three scenarios: original leg design (Figure 12.38a), leg with one weaker part (Figure 12.38b) and leg after failure (Figure 12.38c, note the scale difference for this case).

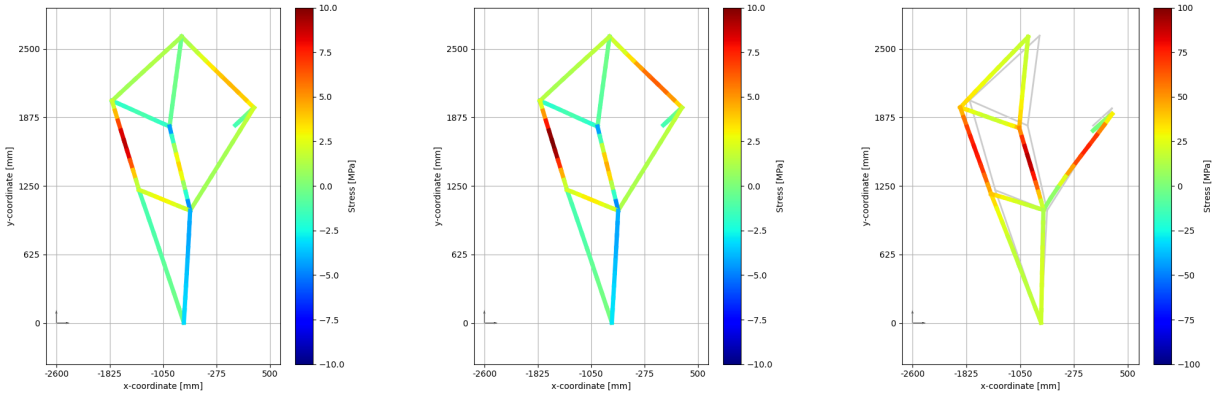

(a) Stress distribution in the original leg design (all parts have the same cross-sections).

(b) Stress distribution in the new leg design (part 4-3 has smaller cross-section).

(c) Stress distribution in the leg after failure of bolt 4 (non-load bearing part 4-3 is not present).

Figure 12.38: Stresses in the leg for different scenarios.

One can notice that with one weaker linkage, the overall maximum stress is slightly higher, but it is still an acceptable value. After failure, the leg cannot function as usual, but the stresses stay below the ultimate strength of the composite. Therefore, the other legs will not fail.

The new diameter of bolt 4 was chosen based on the new stress in part 4-3. The preferred failure mode is bolt shear, as it is the easiest to repair. Therefore, it should have the lowest MS value. Following the procedure outlined in subsection 12.6.3, 4.5 mm was found to be a suitable diameter. The safety margins for the weakened bolt 4 are 33.8 (net-section), 2.4 (bearing), 2.33 (shear tear out), and 0.45 (bolt shear). Compared to the entire structure, the bolt 4 shear failure MS value is the lowest, meaning that it should fail first. The time period estimation can be found in Section 12.11.

12.11. Lifetime Analysis

Finally, the lifetime of the structure should be determined. In Section 12.9, the failure behaviour of the structure was assessed assuming no deterioration of the properties of the materials. In reality, it is known that the properties will drop over time due to fatigue and to the harsh environment the structure has to operate in. This section addresses those issues. For this section, a distinction is made between the degradation of the composite and of the metal that is used for the joints.

Composite: flax/coPOM

For composites, degradation occurs due to two main factors: fatigue and environmental degradation. Liang et al. [90] investigated the fatigue behavior of flax fiber composites, determining the fiber fraction. The results for the composite are shown in Figure 12.39a. To determine the lifetime of the composite, one should relate the number of cycles to the time. One cycle is estimated to be a full revolution of one of the linkages. From the kinematic analysis, the frequency is known to be 0.044 Hz, which allows relating the number of cycles to the time. The results are shown in Figure 12.39b. Note that shear strength is not considered here as from the previous analysis, it is known that failure will occur in the axial direction.

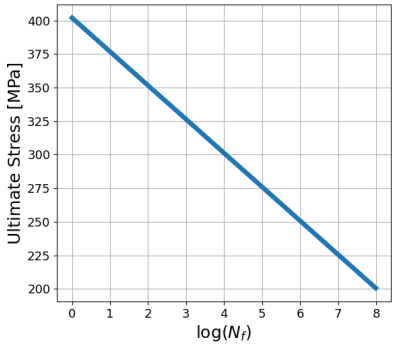

(a) S-N curve of a flax fiber reinforced composite with a 50% fiber fraction.

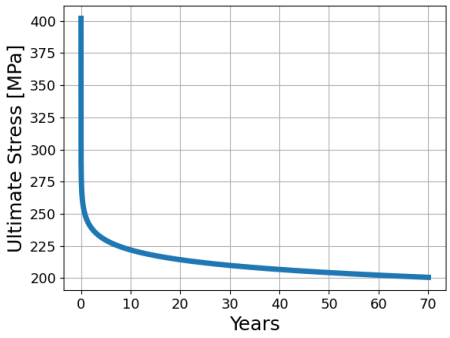

(b) Ultimate stress of the composite as a function of the number of years.

Figure 12.39: Curves concerning the fatigue performance of the composite.

The structure will operate in a succession of dry and wet conditions at varying temperatures. Therefore, it is of interest to study the cyclic hygrothermal ageing of flax fiber composites. Cadu et al. [91] have investigated the impact of humidification/drying cycles on such composites (3.5 days at 90% RH and 3.5 days at 40% RH, both at 55°C). Decreases of about 10% for the modulus and about 14% for the ultimate tensile stress have been recorded after 1 year of exposure and 52 cycles of ageing.

For a preliminary estimate of the lifetime, it is assumed that the material properties decrease by a certain percentage each year (14% for strength properties and 10% for the Young's modulus [91]). This assumption allows one to project the composite's properties over time, as illustrated in Figure 12.40. Using those values, one can determine the point at which the structure will no longer be able to support the stresses in the legs and in the structural frame.

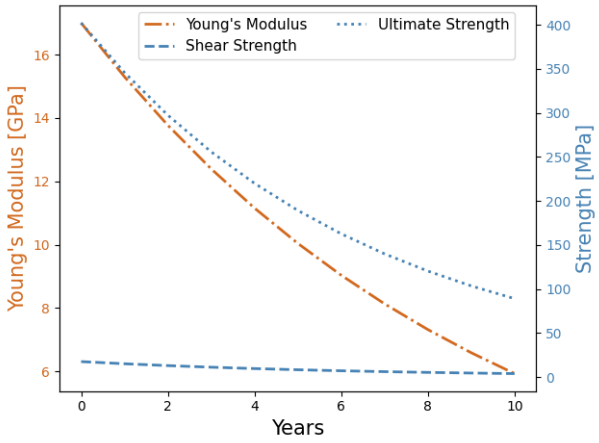

Figure 12.40: Degradation of the flax fibre composite over time, with the Young's modulus decreasing by 10% annually and the shear and ultimate strengths decreasing by 14% annually [91]

As the leg linkages were designed with big MS, it is expected that the frame will fail first due to material properties degradation. To investigate the lifetime, the safety margins of each beam were recalculated using lower (degraded) material properties. The process was repeated until any of the MS fell below 0. This happened when using material properties after 4 years. The corresponding MS plot can be seen in Figure 12.41. For better clarity, only MS close to 0 are shown.

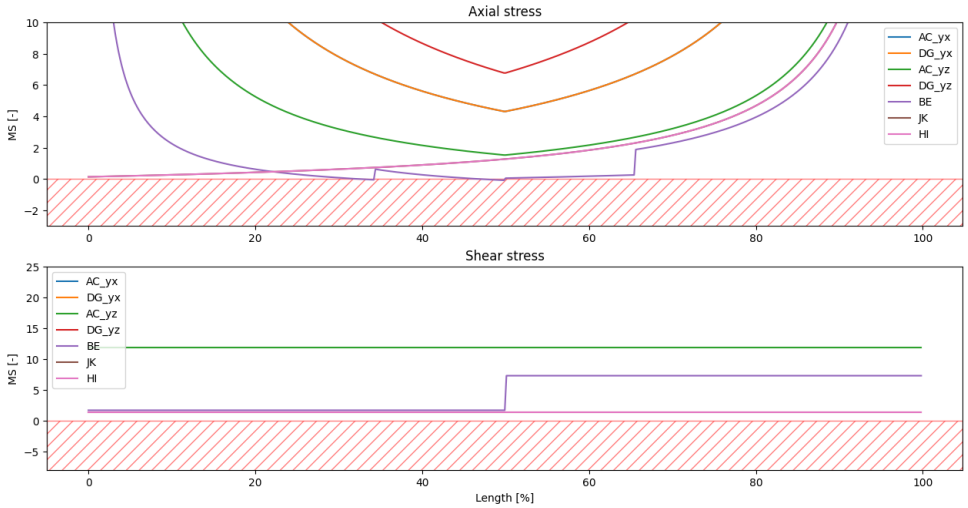

Figure 12.41: Margin of safety plot for the frame after 4 years of operations.

After 4 years, the axial stress in beam BE will be larger than the ultimate strength of the composite, leading to failure. At this point, beam HI is also close to failure.

An unaccounted factor in the lifetime analysis of the composite is the presence of salt aerosols along the coastline. These aerosols, containing dissolved salt, are known to impact the composite. Fiore et al. have extensively studied the effects of marine environments on flax fiber composites [92–96]. Through investigations involving salt-fog/dry cycles, they have demonstrated that the composite's strength and stiffness properties deteriorate during wet cycles due to exposure to salt.

Although the material partially recovers its strength during dry phases, the stiffness degradation remains irreversible.

Thus, while the degradation in strength during wet salty periods and the permanent loss in stiffness in such environments should ideally be incorporated into the analysis, the lack of generalised quantification prevented their inclusion in this report. Therefore, a safety factor of 1.5 has been applied to the estimated lifetime to stay on the side of caution. Therefore, the projected lifetime is 2.5 years when considering the composite material alone.

Metal

In addition to the lifetime of the composite, the lifetime of the joints should also be considered. These joints are made of carbon steel and are therefore susceptible to corrosion. This section examines how corrosion affects the mechanical properties of the joints, specifically focusing on the evolution of the metal's tensile strength over time in a corrosive environment (coastline). Since shear strength is approximately 60% of tensile strength, any changes in tensile strength will directly affect shear strength.

Research by Kumar et al. [97] predicts the corrosion behavior of steel by exposing samples to a simulated marine environment. Steel samples were corroded for varying durations (5, 10, 20, 30, 45, and 60 days) in a salt spray chamber, and their properties were tested. They found that the tensile strength of steel follows a linear degradation trend over exposure time, with a 3% reduction after 60 days.

Assuming this trend holds for longer periods, the shear strength of the bolt over time can be plotted as shown in Figure 12.42.

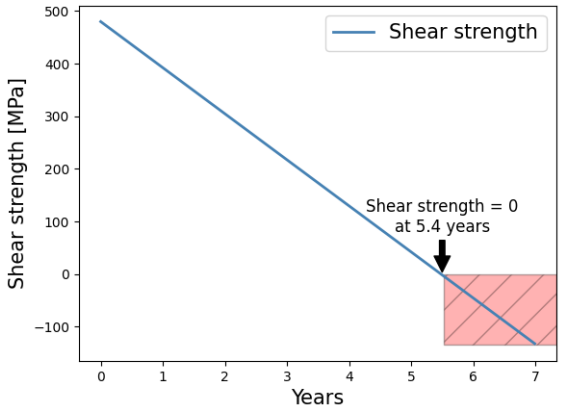

Figure 12.42: Shear strength degradation over time of the carbon steel joints due to corrosion

To determine when the weaker bolt would fail, bolt shear MS was calculated using carbon steel shear strength at different stages of degradation. The MS fell below 0 while using the shear strength value corresponding to 627 days (or 1.7 years) of degradation. Therefore, bolt 4 is expected to fail after this period and maintenance should be scheduled accordingly, ideally even before the failure happens. Considering unexpected environmental conditions and possible inaccuracies of the analysis, a safety factor of 1.5 will be used to remain on the safe side of the estimation. Thus, the maintenance should occur every 418 days (or 1.14 years).

12.12. Verification and Validation of Structure

To conclude this chapter, the verification and validation process will be outlined. First, compliance with the requirements will be assessed in subsection 12.12.1. Following that, a sensitivity analysis of the structures will be conducted in subsection 12.12.2, and the V&V procedures will be detailed in subsection 12.12.3.

12.12.1. Compliance with the requirements

The initial step involves verifying if the designed structure aligns with the requirements, which are reiterated in Table 12.11.

Table 12.11: Structure subsystem requirements

Identifier	Structure Subsystem Requirement
REQ-USER-02-SYS-01-STR-03	The natural frequency of the structure shall be higher than the frequency induced by external loads.
REQ-USER-02-SYS-02-STR-01	The structure shall retain at least TBD % of its original properties from corrosion caused by rain.
REQ-USER-02-SYS-03-STR-01	The toughness of the material shall be higher than TBD J/m^3.
REQ-USER-02-SYS-03-STR-02	The stiffness of the material shall be higher than TBD N/m.
REQ-USER-02-SYS-04-STR-01	The structure shall retain at least TBD % of its original properties from corrosion caused by saline water.
REQ-USER-02-SYS-05-STR-01	The structure shall retain at least TBD % of its original properties from corrosion caused by sand particles.
REQ-USER-02-SYS-06-STR-01	The structure shall retain at least TBD % of its original properties from photodegredation caused by UV rays.
REQ-EoL-01-SYS-01-STR-01	The structural parts shall retain at least TBD % of the original material strength and properties at end of life.

None of these requirements were quantified, so a simple yes or no regarding compliance is not possible; a detailed discussion is necessary for each.

Concerning **REQ-USER-02-SYS-01-STR-03**, the frequency of the structure was not evaluated. Determining the natural frequency of the structure would have required a time-demanding analysis that was not considered a priority for this project. Therefore, this requirement still needs to be assessed.

Regarding **REQ-USER-02-SYS-02-STR-01** and **REQ-USER-02-SYS-04-STR-01**, it was demonstrated that corrosion would notably affect both composite and metal joints. This impact was quantified, influencing the assessment of their lifetimes, thus fulfilling these requirements.

Concerning **REQ-USER-02-SYS-03-STR-01**, the structural analysis did not explicitly include the composite's toughness. However, based on known properties of flax fiber-reinforced composites, which are recognised for their high toughness [98], the likelihood of failure due to insufficient toughness is deemed low. Hence, this requirement is considered adequately addressed.

Regarding **REQ-USER-02-SYS-03-STR-02**, stiffness was thoroughly considered during the structural analysis, ensuring all components were sized accordingly. Therefore, this requirement has been accounted for.

Concerning **REQ-USER-02-SYS-06-STR-01**, it was demonstrated that UV aging poses no threat to the structure, as it can be effectively mitigated by incorporating an anti-UV agent into the resin and applying a UV-resistant coating to the surface.

Regarding **REQ-EoL-01-SYS-01-STR-01**, mechanical properties have been projected over time. Hence, based on desired end-of-life mechanical properties, the lifetime can be determined.

12.12.2. Sensitivity analysis

To ensure safety, it is essential to analyze the sensitivity of the structure to changes in key inputs. Given the large number of inputs considered in this chapter, only the three leading inputs will be addressed: the width of the structure (length of beam BE), the force from the wind turbine, and the weight of the structure.

The impact of changes in these inputs on stability, frame stress analysis, leg stress analysis, potential joint failures, and deflection will be assessed. It is important to note that the margins of safety in the legs are currently very large. With a safety factor of 1.5, these margins remain above 25, indicating that small input changes will not lead to leg failure due to stress. Therefore, stress-induced failure in the legs will not be discussed further.

Width of the Structure

The current width of the structure (length of beam BE) is 3.2 m. This section investigates the impact of changing this length by ±0.1 m. When the variations are acceptable, the boxes are colored green; otherwise, they are colored red. The results are displayed in Table 12.12.

Table 12.12: Sensitivity analysis for a variation of length BE by ± 0.1 m. Green indicates an acceptable variation in opposition to red boxes.

	Lower margin	**Actual design**	**Upper margin**
Length of beam BE [m]	**3.1**	**3.2**	**3.3**
Stability	OK	OK	OK
Lowest MS for the stresses in the frame	0.72	0.67	0.62
Maximum deflection downward	31	30	30
Lowest MS for the joints	1.26	1.28	1.32

This sensitivity analysis suggests that the structure is not highly sensitive to variations in the length of beam BE, as these variations still result in functional failures according to the four indicators investigated. It is likely that the most critical failure mode will involve the frame when the length of beam BE is varied.

Force Generated by the Wind Turbine

Another critical input is the force generated by the wind turbine, represented by F in Figure 12.8. Currently, the force considered is 2632 N, as this is the maximum expected force. If the wind blows faster, the wind turbine stops operating, causing the force to decrease. However, the braking system of the wind turbine might not be very accurate. Therefore, variations of 10% in the force will be examined to determine their impact. The results of this analysis are shown in Table 12.13.

Table 12.13: Sensitivity analysis for a variation of the wind turbine force by ± 10%. Green indicates an acceptable variation in opposition to red boxes.

	Lower margin	**Actual design**	**Upper margin**
Force on the wind turbine [N]	**2125**	**2362**	**2598**
Stability	OK	OK	OK
Lowest MS for the stresses in the frame	0.68	0.67	0.66
Maximum deflection downward	29	30	32
Lowest MS for the joints	1.55	1.12	1.07

Once again, variations of 10% in length still result in a fully functional structure. In this case, the most critical factor is stability. The structure will become unstable if the force generated by the wind turbine exceeds 2690 N.

Total weight

The influence of weight variations should be considered. From the mass analysis performed in subsection 12.2.1, the mass used was 710 kg. Variations of 10% are deemed sufficient to check the sensitivity. The results are displayed in Table 12.14.

Table 12.14: Sensitivity analysis for a variation of the total mass by ± 10%. Green indicates an acceptable variation in opposition to red boxes.

	Lower margin	**Actual design**	**Upper margin**
Total mass [kg]	**639**	**710**	**781**
Stability	OK	OK	OK
Lowest MS for the stresses in the frame	0.84	0.67	0.53
Maximum deflection downward	28	30	32
Lowest MS for the joints	1.5	1.28	1.09

Variations in mass of 10% still result in a functional design. However, stability remains the most critical factor. If the mass drops below 623 kg, the structure will become unstable. Therefore, one should ensure that the mass remains above this value by adding additional weight if necessary.

12.12.3. Verification and Validation Procedures

Firstly, a Python routine was developed to determine the internal loading of the beams and construct the NVM diagrams. To ensure accuracy, the internal loading was manually verified, and NVM diagrams were created for a series of critical cases, demonstrating that the Python code worked as expected.

For stress determination, a Finite Element Method approach was used. This method relies on an extensively verified and validated FEM code developed as part of the Simulation, Verification, and Validation project, ensuring its reliability. Other methods in this chapter relied on basic calculations, which were double-checked for accuracy but did not require formal validation procedures beyond manual verification.

For recommendation, one can perform experiments to determine the fatigue behavior of the composite, which could not be included in this analysis. To verify the degradation over time in a coastline environment, conducting experiments over a longer period (order of years) is suggested.

13
Final Design

This chapter gives an overview of the final design and describes essential design elements that ensure that it is a complete and fully integrated design. Section 13.1 describes the general design and shows a rendering of the CAD model. Section 13.2 details the mass, cost and power budgets. The design is of course not complete without a plan to actually produce it, this is described in Section 13.3. To give an overview of interactions between subsystems, the hardware and software diagrams are shown in Section 13.4. Finally, Section 13.5 describes the logistics and operation plan.

13.1. System Overview

After analysing all the subsystems, they can be combined to form the final design concept. This section aims to provide a general summary of the final design concept, highlighting its most important characteristics. A general overview of the final design concept is provided in subsection 13.1.1. The external dimensions are provided in subsection 13.1.2 and the operating of the structure is elaborated in subsection 13.1.3.

13.1.1. General Overview

A render of the final design concept is presented in Figure 13.1. Based on this visualisation of the final design concept, important aspects can be elaborated.

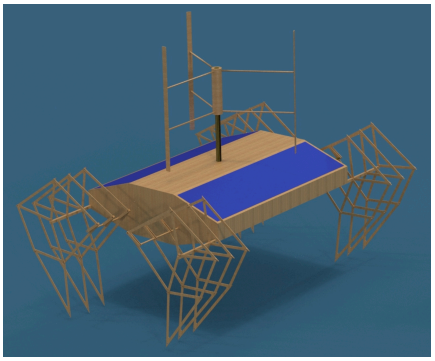

Figure 13.1: Render of the final design concept

This render visualises the world's first walking wind turbine. The walking mechanism allows it to roam the beach and perform various functions, ranging from litter collection to water desalination. The mechanism consists of 12 Jansen linkages powered by crankshafts, enabling the structure to walk organically over the beach. Each side of the structure has its own electric motor, providing both motion and steering capabilities.

The power of the structure is provided by a combination of a vertical axis H-shaped wind turbine and solar panels. The wind turbine is the main power source and is good for 60% of the power budget. The remaining 40% of the power budget is provided by solar panels. These solar panels enable the generation of power on wind still days and reduce the size of the wind turbine. The vertical pole that supports the wind turbine is connected to the body. The body is covered by composite panels that house the electrical components and enable the placement of solar panels.

13.1.2. Dimensions

With the final design concept in place, an overview of the relevant external dimensions is presented in Table 13.1.

Table 13.1: External dimensions of the final design concept

Parameter	Value	Unit
WT diameter	3.025	m
Height of structure	5.1	m
Width of structure	6.2	m
Length of structure	3.2	m
Ground clearance	1.5	m
Leg height	2.6	m

13.1.3. Operations and performance

The structure will be deployed on the beach where it will encounter variable soil substrate and varying terrain roughness. Therefore, the walking mechanism is designed for a step height of 0.56 m to walk over sand castles and other obstacles encountered on the beach. The feet of the structure are designed to adapt their contact area with the ground, depending on the ground pressure.

The structure has the ability to perform all its functions autonomously and it navigates the coastline by using path planning and obstacle avoidance. The structure has a low operating speed of 0.1 m/s, which helps extend its operational lifespan.

13.2. Budget Breakdown

This section provides a detailed description of the various budgets associated with the final design. The aim is to offer potential future customers clear specifications regarding power requirements and distribution, structural mass, and anticipated costs. All the budgets include contingency margin.

13.2.1. Mass Budget

The mass budget is a crucial component of the design. Initially, a preliminary mass estimation was conducted during the stability analysis phase, as this information was essential (refer to Section 12.2). This preliminary mass breakdown was based on analyses of other components such as aerodynamics and control systems.

Following the structural analysis, the exact cross-sections of the beams were determined, allowing for a more accurate calculation of the frame's mass and the legs' mass. The updated and precise mass budget is presented in Table 13.2, reflecting the final mass estimations for all components.

Table 13.2: Mass estimation for the components of the structure and their associated uncertainty, with preliminary results shown in brackets when applicable

Wind turbine	*Mass [kg]*	**Body**	*Mass [kg]*	**Other**	*Mass [kg]*
Turbine	60 ± 30	Beams	60 ± 1 (70)	Batteries	6 ± 1
Generator	40 ± 2	Panels	200 ± 5	Payload	50 ± 5
Shaft of WT	10 ± 2	Solar panels	100 ± 10	Motors	10 ± 1
Tower of WT	20 ± 2	Legs total	90 ± 2 (120)		
Cage of WT	20 ± 2				

The final mass of the structure has been calculated to 666 ± 63 kg. During the initial sizing of structural elements, a conservative estimate of 710 kg was used, resulting in slightly oversized cross-sections. Despite this, the design process was not repeated because the mass variation is minimal (<2%), and is unlikely to significantly impact the final results. Moreover, considering the manufacturing tolerances achievable with the pressing techniques employed, the cross-sections determined before and after iteration would likely remain the same when rounded.

Finally, a comment on the uncertainty of this result is necessary. All uncertainties are relatively small except for the wind turbine mass (±50%). This is because all other masses are determined from off-the-shelf components or known dimensions and materials, allowing for accurate mass estimation. The wind turbine mass, however, is based on a regression from turbines with much larger power generation capacity, making it less reliable and thus having a larger uncertainty.

The lower and upper mass estimations are provided in Figure 13.2a and Figure 13.2b, respectively. The upper limit falls within the range investigated in the sensitivity analysis, and it was demonstrated that this would lead to a fully functional structure.

However, the lower mass estimation does not fall within the range investigated in the structural analysis, and it is smaller than the lower limit of 623 kg required to ensure the structure's stability. Therefore, this lower margin is not acceptable. If such a low mass is achieved, additional ballast must be added to reach a minimum of 650 kg to provide a safety margin.

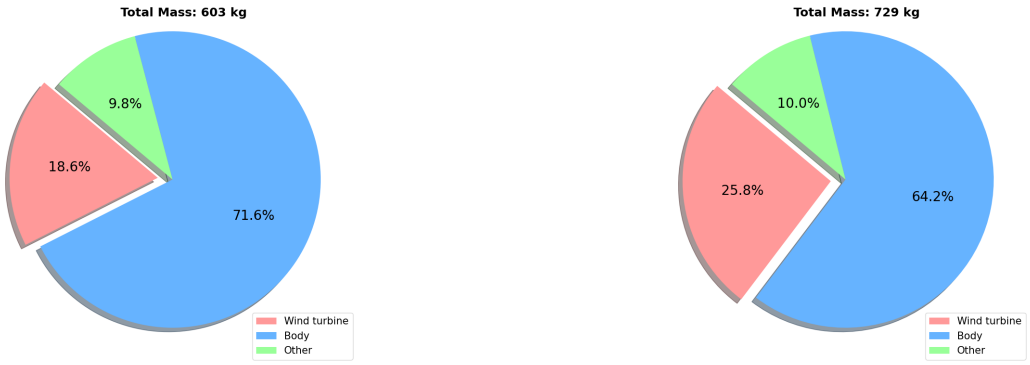

(a) Lower mass estimation

(b) Upper mass estimation

Figure 13.2: Mass estimations

13.2.2. Power Budget

The power budget using the final mass of 666 kg is presented in Table 13.3. With this iterated power, waste collection discussed in Chapter 7 becomes a feasible option.

13.2.3. Cost Budget

The cost budget breakdown considers components cost, manufacturing cost, transportation cost, operation cost, maintenance cost, verification and validation activities cost and EoL cost. A contingency margin of approximately 10% is included.

Components Cost The cost of key components that need to be purchased from suppliers are shown in Table 13.4. Notably, except for certain components with specific requirements, such as LiDAR (see Section 10.5), the costs are selected mainly from the median value among different levels of existed products, which requires a cost contigency margin of ±10%. The total estimated cost is therefore 9000 ± 900 EUR.

Manufacturing and Transportation Cost The intensively discussed topic in the market

Table 13.3: Power budget of the entire system, with η_{elec} from Section 11.3

Element	**Power** $[W]$
Motion	210
Control and navigation	23
Weather data collection	6
Active cooling	3
Function to be performed	53
Subtotal with η_{elec} **= 0.554**	534
of which generated by wind turbine	320
of which generated by solar panel	214

Table 13.4: Component cost for various subsystems

Subsystems	**Components**	**Price [EUR FY24]**
Wind Turbine	Safety Structure	200
	Torque Shaft	300
	Tower	20
Electrical System	MCU	10 X 2
	Disc Brake	300
	PMA	1000
	Gearbox (high gear ratio)	500
	PM Brake	100
	High Torque BLDC Motors	600
	Charge Controller	200 X 2
	Battery	50 X 2
	Power distribution unit	300
	DC DC converter	100 X 2
Structure	Crankshaft	25 X 4
	Springs	50 X 8
	Adhesive	10
	Bolt	10
Kinematic System	Bearing	10
	Gearbox (low gear ratio)	200 X 2
Solar Panels		2500
Control and Navigation System	LiDAR	2 X 350
	GPS	50
	IMU	40
	5G-receiver	375
	Thermometer	2 X 20
	Anemometer	80
	Temperature Control Fan	30
	Total (Margin $\pm 10\%$**)**	**9000** $\pm$ **1000**

currently is the recycling of wind turbine blades made from glass fibre-reinforced composites. Handling blades made from new materials has not yet been clearly investigated. To make a

preliminary estimation of manufacturing and transportation costs, this analysis uses the recycling glass fibre reinforced polymer (GFRP) as a reference, providing some insights into those costs. The cost of relevant recycling GFRP activities are presented in Table 13.5. Please note that the processing fee includes the material cost in this analysis. The maximum cost is charged for high-quality processing instead of residual material, acting as a gate fee for environmentally responsible and permitted processing.

Table 13.5: Cost for various glass fibre reinforced polymer (GFRP) processing activities [99]

Activity	**Minimum [EUR/tonne FY20]**	**Maximum [EUR/tonne FY20]**
Cutting (80x80 cm) and Transport	20	50
Shredding	55	55
Depositing	120	120
Incineration	100	200
Cement kiln processing [a]	200	300

[a]The charge of cement kiln processing in Germany reaches 450 $EUR/tonne$ in 2020, including reduction, shredding, transport and gate fee. (information from interview with Albert ten Busschen, 30 June 2020).

First, it is assumed that cutting and transportation are necessary for every recycling approach. Based on the costs for different steps of processing GFRP, the manufacturing cost of moulding can be determined, which is the main manufacturing method of the structure and wind turbine blades. Incineration and cement kiln processing both requires high-temperature processing, which is both energy and cost-demanding. Moulding at approximately 200 $°C$ should cost less than incineration and cement kiln processing but more than shredding, resulting in an conservative estimation of 80 $EUR/Tonne$.

Additionally, considering the rising demanding of recycling decommissioned wind turbine blades, it is foreseeable that positive regulations and environmental initiatives will allow a lower gate fee for reusing blades in the coming years.

Other cost for manufacturing can not be overlooked, such as hiring staff for assembly, transmission and deployment, which is estimated at 100 EUR per person per hour. A budget of 5000 EUR is considered.

According to **REQ-USER-17-SYS-01** and **REQ-USER-17-SYS-02**, a vehicle capable of carrying a sea container to transport the partially assembled structure to different locations is required. Within the Netherlands, a 24-$tonne$ curtain truck costs approximately 7 EUR/km for middle-range distance transportation.

Operation and Maintenance Cost The cost estimation for hiring staff is the same as in manufacturing, estimated at 100 EUR per person per hour. The budget of operation and maintenance are 1000 EUR and 2000 EUR, respectively.

Other Cost In the Midterm Report [18], several verification and validation activities of the whole system have been investigated. The costs of these activities are shown in Table 13.6.

At the end of the mission, if the broken parts of structure made of NF composite can not be recyclable, landfill is the final solution. This may cost the same as depositing, as shown in Table 13.5, incurring a relatively high gate fee due to regulations in the Netherlands.

Summary of Cost Budget

Table 13.6: Verification and validation activities with estimated costs

REQ Identifier	Verification and Validation Activities	Estimated cost [USD FY24]
REQ-USER-03-SYS-02, REQ-MAI-03-SYS-01, REQ-EoL-02-SYS-01	Building and testing the medium fidelity prototype	7500 [a]
REQ-EoL-01-SYS-01	Testing and inspecting recycled content, obtaining certificates	2500 [b]
REQ-USER-02-SYS-01, REQ-USER-04-SYS-01	Wind tunnel testing	2000 [c]
REQ-USER-05-SYS-03	Noise level testing	250 [d]

[a]Design 1st, *URL* `https://design1st.com/how-much-do-hw-prototypes-cost/`, accessed 17 May 2024
[b]ISCA, *URL* `https://eservices.isca.org.sg/CourseDetailClone?courseMasterId=a0g2t000001sFl1AAE&_ga=2.46938350.819554548.1716812066-1673518802.1715947444`, accessed 27 May 2024
[c]UWAL Service and Rate, *URL* `https://www.aa.washington.edu/AERL/KWT/rateguide`, accessed 17 May 2024
[d]Spec Scientific Direct, *URL* `https://sperdirect.com/collections/sound`, accessed 17 May 2024

Table 13.7: Cost breakdown summary

Activities	Price [FY24]	Estimated cost [EUR]
Purchasing components	-	9000 ± 1000
Cutting and Transportation of Decommissioned Wind Blades	35 [EUR/Tonne]	15 ± 2
Moulding	80 [EUR/Tonne]	35 ± 5
Other manufacturing activities	100 [EUR/(hour · staff number)]	5000± 500
Other transportation	7 [EUR/km]	500 ± 50
Verification and Validation	-	9750 ± 1000 USD
Certificate	-	2500 ± 250 USD
Operation	100 [EUR/(hour · staff number)]	1000 ± 100
Maintenance	100 [EUR/(hour · staff number)]	2000 ± 200
EoL	120 [EUR/Tonne]	50 ± 2
	Total	30000 ± 5000

13.2.4. Carbon Budget

The carbon emissions related to the structure can be split up into the following emission categories, which cannot be elaborated further than discussing the effects without the actual product.

1. Transport: it had been estimated in the Baseline Report that using long-haul trucks generates 56.6 gCO_2/t−km[1].
2. Manufacturing: the significant source of CO_2 emissions arises from moulding, while NF captures CO_2 in the production. Meanwhile, the team will ensure that the chosen workshop is supplied by green electricity (wind or solar energy), thereby mitigating this aspect in the carbon budget.

[1]CO_2 emissions from trucks in EU, `https://theicct.org/publication/co2-emissions-from-trucks-in-the-eu-an-analysis-of-the-heavy-duty-co2-standards-baseline-data/`, accessed 18 June 2024

3. Maintenance: Maintenance is another consideration, wherein the advantage of thermoplastics lies in their ease of repair. Patches can be heated and applied using equipment akin to hairdryers, requiring minimal energy and emitting negligible carbon. Hence, this aspect can also be disregarded in the carbon budget.
4. EoL: the impact on the carbon budget hinges on the new material performance with the corresponding end-of-life solution, which will be determined in the future.

The carbon payback period depends on the functionalities the structure will perform. If waste collection is the primary functionality, the carbon payback period estimation will be based on the carbon emissions of general waste collection approaches. Given that the structure will be zero-emission during its operation and that carbon emissions during the four stages outlined above will be minimised, the structure has the advantage of counteracting emissions. The exact performance will be investigated further in future studies

13.3. Production Plan

This production plan consists of three levels of steps to describe the procedures of production. The top level, level 2, and level 3 are highlighted in blue, yellow, and green, respectively. Levels 2 and 3 break down the steps of the top-level approach to provide more context for each step. It is important to note in advance that this production plan will mainly focus on the procedures of manufacturing and assembly of the components, rather than focusing on the precise application of various joints such as adhesive bonding, bolts, or other types of joints.

Top level

Figure 13.3 presents the top-level approach. In the process of obtaining materials required to manufacture the structure, this part is divided into materials that can be retrieved from a wind blade and off-the-shelf components. Step 1.0 is not discussed in the production plan as subsection 6.2.1 already covers a detailed procedure on extracting material from the WTB. Once all components are prepared, the steps 4.0, 5.0, and 6.0 are performed individually to assemble the main body frame, leg linkages, and wind turbine, respectively. Finally, they are all combined, and the electronic components are mounted in the body frame at the end.

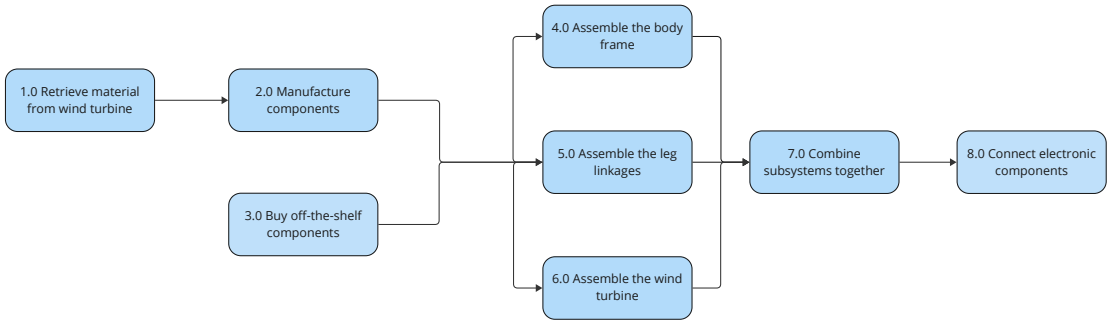

Figure 13.3: Production plan at top level

2.0 Manufacture components

Components that can be recycled from the WTB are extensive, so they have been divided into multiple parts. In Figure 6.7a, struts, frame support platform, and body panels have similar manufacturing procedures, differing only in the dimensions of the components. From the composite

panel, the thickness is reduced to the desired level for each component. The panel is then cut into thin struts and panels according to the desired size. For each strut, frame support platform, and body panel, appropriate finishing processes such as sanding and dipping in protective resins are applied to protect the structures. All panels and struts are iterated in steps 2.1.2 and 2.1.3 using the panels from step 2.1.1. Frame beams can be directly obtained by cutting out beams from the blade, and they also follow the finishing process. All frame beams follow the same procedure.

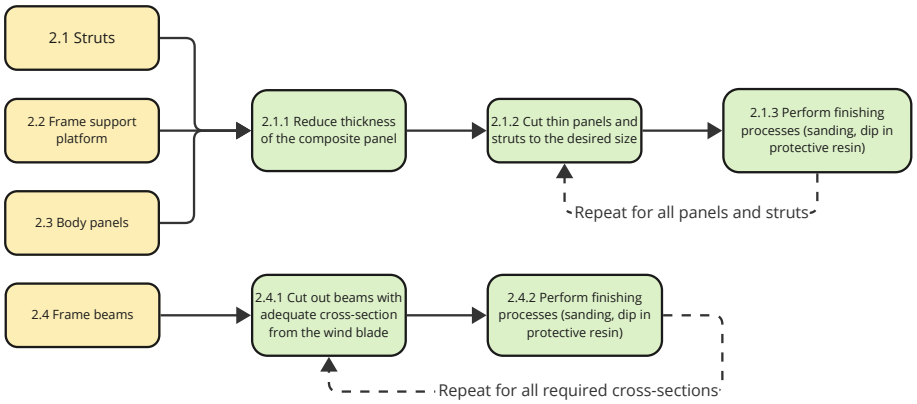

Figure 13.4: Manufacture components - part 1

In Figure 13.5, linkage parts, aerofoils and foot are introduced. Starting with the linkage parts, they are the parts of the leg which require dynamic joints at the ends to allow free rotation. Similar to the previous process, the thickness of the panel is adjusted to the right dimension and cut into rectangular and triangular pieces. Inserts are embedded into these pieces using the method mentioned in subsection 6.5.2. As additional space is required to clamp the pieces, the redundant parts are trimmed after insertion. Finally, the finishing process is applied.

Manufacturing aerofoils requires processing top and bottom halves of the aerofoil separately, but the procedure is the same for both. Initially, the metal mould is manufactured for both the top and bottom halves using CNC. Then, the composite panel is processed to the appropriate dimensions, heated, and pressed into the molds. Once cooled down, the flanges at each end of the parts are bonded together, and a finishing process is applied to protect the surface.

Finalising this subsection with the 'foot,' the initial stages are similar to other procedures up to step 2.7.3. Once the struts are prepared, the elastic membrane is extracted from an off-the-shelf component and cut into the desired shape. The membranes are then attached to the struts, and pin joints are used to connect the struts together.

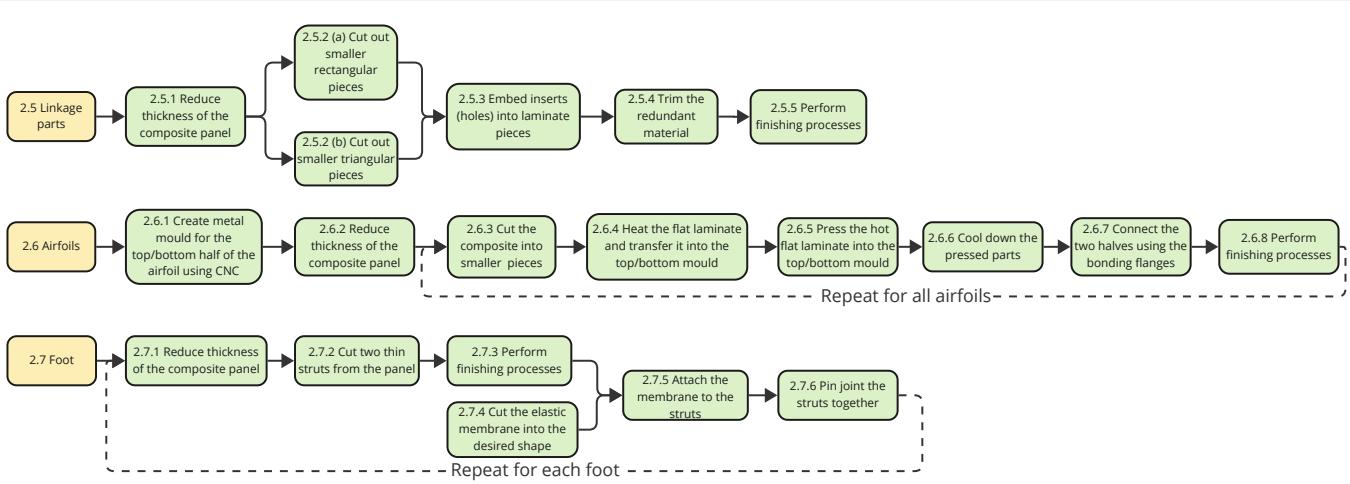

Figure 13.5: Manufacture components - part 2

3.0 Buy off-the-shelf components

Being able to serve multiple functions from the structure requires more than the recycled materials from WTB. This subsection will briefly mention the off-the-shelf components that need to be bought from a market.

- Adhesive bond (Epoxy)
- Mechanical insert
- Solar panel
- Generator
- Motor
- WT shaft
- Spring
- Electric wires
- Bamboo
- Electronic devices
- Bearing
- Crank shaft
- WT cage
- Elastic membrane

4.0 Assemble the body frame

Starting from this subsection, components from **Manufacture components** are used for assembly, and there will be no further discussions on manufacturing parts. Initially, the bamboo shafts (beams AC and DG) are adhesively bonded to the cross-shaped beam BOEP. The procedure is divided into two parts. Step 4.3 (a) involves attaching a flat panel on top of the beam BOEP with adhesive bond. Following this, in step 4.4 (a), a damping panel is bonded above the flat panel. Step 4.3 (b) involves attaching vertical beams at points J, O, H, and P. For each beam, thin composite plates are adhesively bonded to connect the beam BOEP to the vertical beams. In step 4.4 (b), the springs are attached to the vertical beams as shown in Figure 12.14a. Recalling the dimensions of the panel, it is 0.5 m wide. Since the lengths of sides BE and OP are 1 m respectively, the panel fits within the boundaries of the vertical beams. After setting the placement for the WT, step 4.5 involves attaching the WT to the damping plate and springs. Since this step depends on the assembly of the WT, step 4.5 will not be immediately performed after step 4.4. The detailed order of assembling the WT will be discussed in a later subsection. Lastly, plates are attached to beams AC and DG to form the main body.

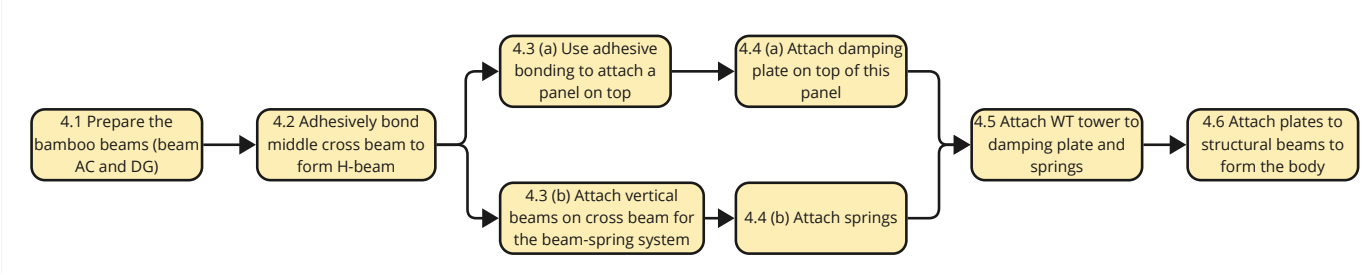

Figure 13.6: Assemble the body frame

5.0 Assemble the leg linkages

Assembly of leg linkages are relatively simple due to the use of dynamic joints to connect parts together. In step 5.1, bolts are used to join linkage parts from step 2.5 to assemble into a full leg. Once the leg is fully assembled, it is connected to the pin joint of the foot as shown in Figure 9.7. After step 5.2, the leg is fully assembled and it is connected to the frame beams of AC and DI.

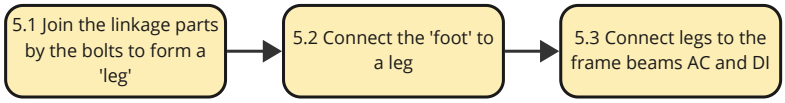

Figure 13.7: Assemble the leg linkages

6.0 Assemble the wind turbine

A careful consideration of the order of assembly is required in this subsection due to the enclosed part (tower) covering the turbine shaft. Initially, in step 6.1, the 'head' of the wind turbine is assembled first. The 'head' consists of the WTBs, struts, and a hub to connect the struts. The blades are joined to the struts, which are then connected to the hub to form the 'head'.

In step 6.2, the bearing is installed onto the turbine shaft at the desired height. Then, the shaft is connected to the generator. The generator is an exceptional case of an electronic component being connected in step 6.0 due to the engineering intuition that it is easier to connect the shaft to the generator at an earlier stage rather than connecting the whole wind turbine to the generator later. Around the bearing, the tower is installed to protect the shaft. Step 4.5 can be continued here simultaneously. Finally, the hub of the 'head' is mounted on the turbine shaft to complete the assembly.

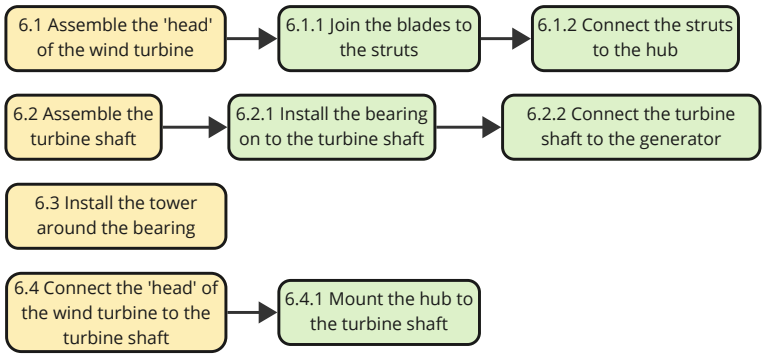

Figure 13.8: Assemble the wind turbine

7.0 & 8.0 Combine subsystems and Connect electronic components
Starting from steps 4.0, 5.0, and 6.0, the body frame, leg linkages, and wind turbine are retrieved, respectively. All subsystems are then mounted into a single structure following the previously mentioned steps. Electronic components are stored in the main body frame, and the solar panel is mounted on the panels of the main body, equipped with sensors such as LiDAR, anemometer, 5G receiver, and GPS.

13.4. Block Diagrams

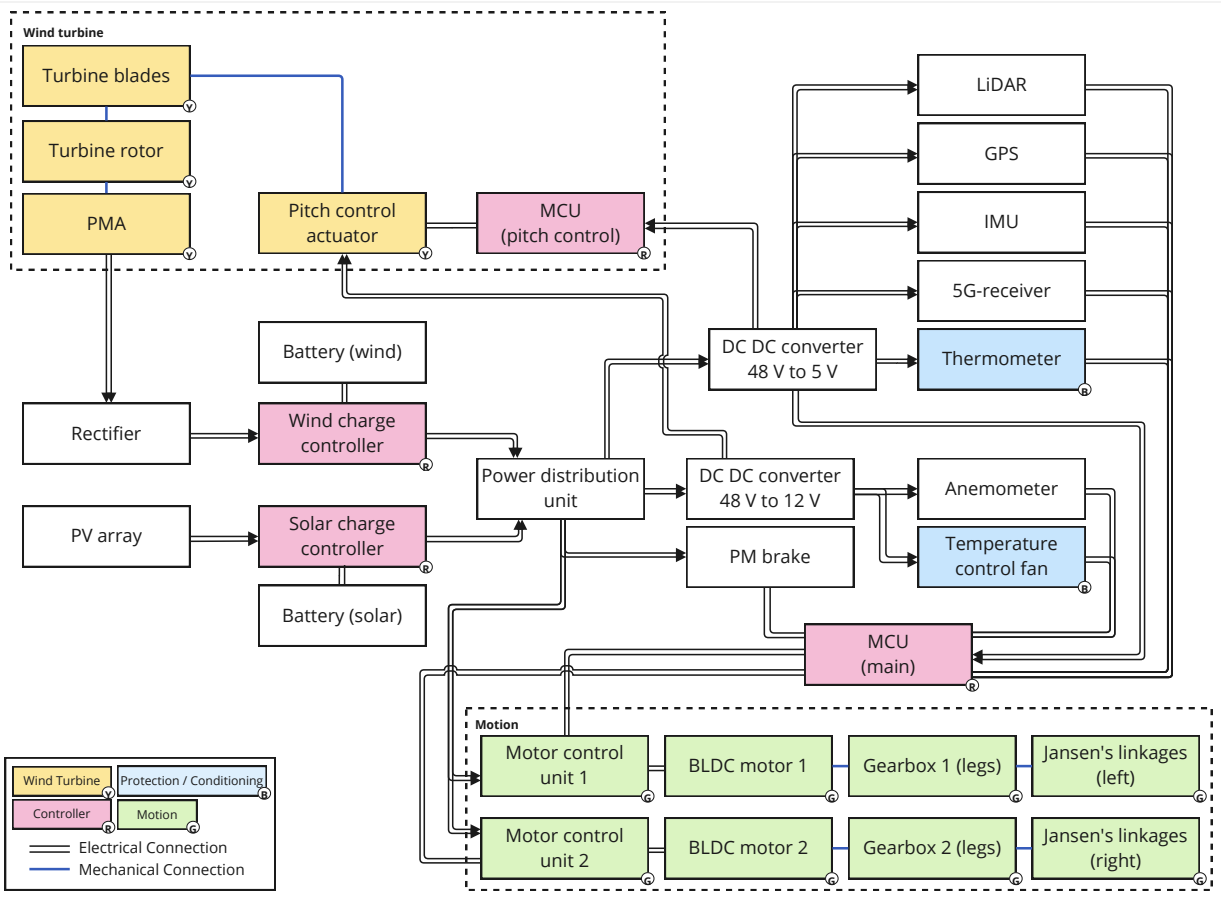

Figure 13.9: Hardware diagram showing the interconnections between all major physical components of the system. The double lines indicate electrical connections and the single line indicates mechanical connections

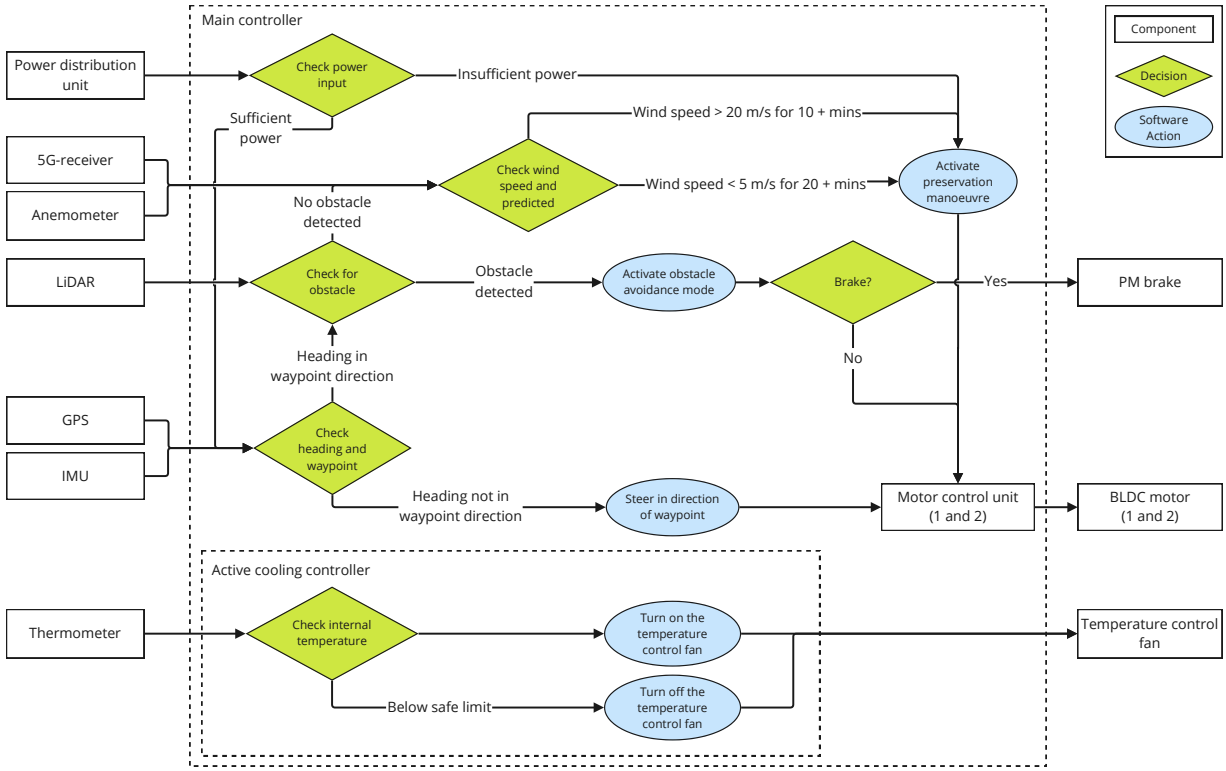

Figure 13.10: Software diagram of the main controller showing interactions between physical components (represented with rectangular blocks) and software (represented with ovals), and the deciding factors (represented with diamond blocks)

13.5. Logistics and Operations Plan

This section introduces the logistics of recycling decommissioned wind turbine blades, the operational process of the structure, the maintenance procedure, and the end-of-life (EoL) process. Figure 13.11 shows the outline of aforementioned procedures.

The logistics segment outlines arrangements for transporting segmented or partially assembled wind turbine blades. Additionally, an operational plan is detailed for deploying the functional structure. In Chapter 7, three different functionalities were investigated: waste collection, desalination station, and beachside cinema that are summarised here under 'perform functionalities'. If there is gust condition, the structure needs to perform preservation manoeuvre to avoid catastrophic damage. In the event of damage to the functional structure that remains maintainable, distinct maintenance strategies are provided based on the severity of the damage. Otherwise, if the structure is deemed irreparable, it will proceed to an EoL process, with the expectation that most parts will be utilised. For more details about the EoL solutions, refer to Section 16.5.

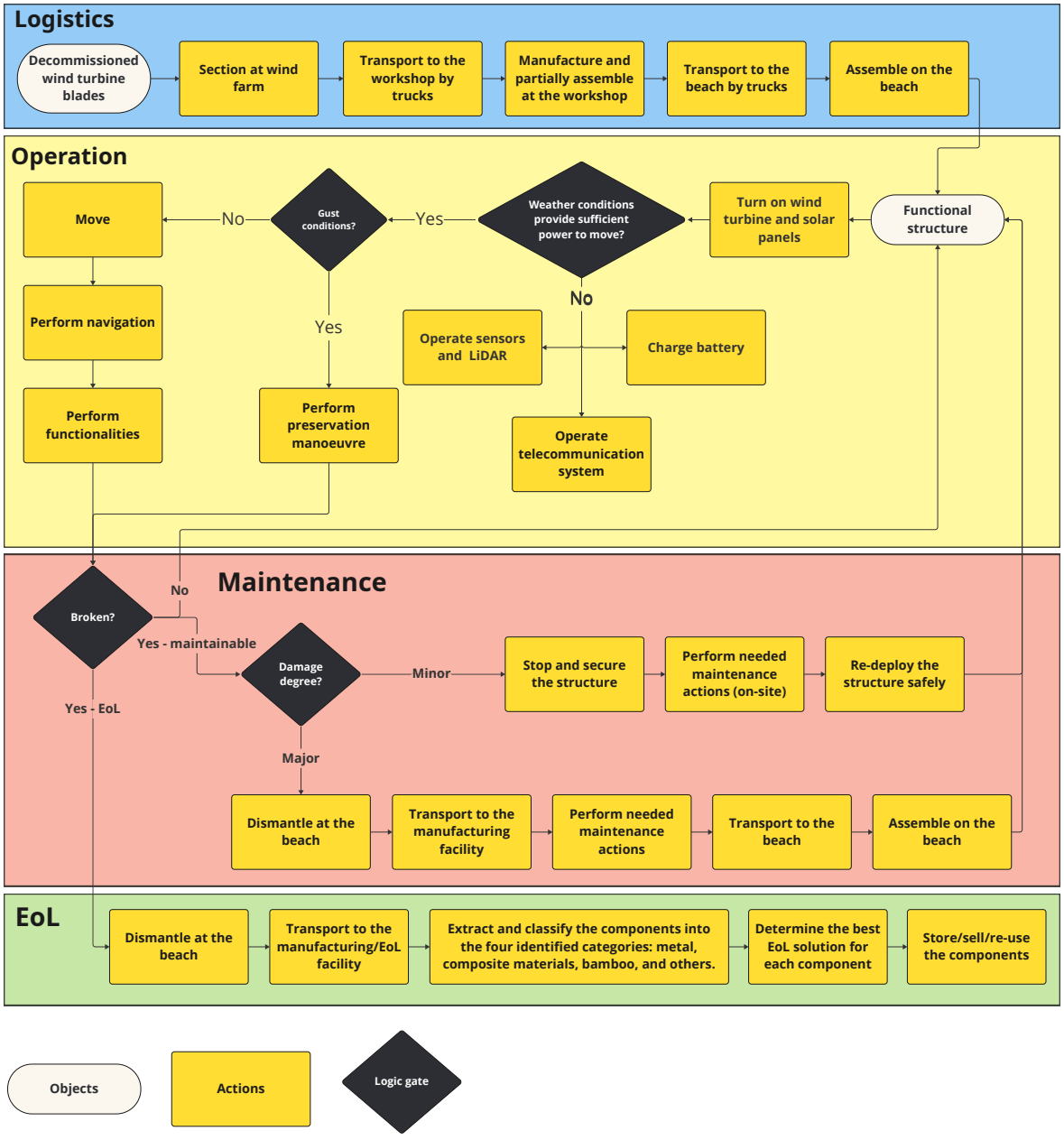

Figure 13.11: Logistics and operation plan, starting from recycling the wind blades and ending at the EoL solution

14

Technical Risk Assessment

Similar to Theo Jansen's Strandbeests, various risks are encountered when bringing the designed structure to life. The risks associated with the production of the structure are discussed in Section 14.1, while Section 14.2 addresses the risks during its operational life. Mitigation strategies are in place for the most critical risks. All risks and the effects of their mitigation strategies are visualised in the risk maps in Section 14.3.

14.1. Production Risks

Before the risks can be classified, the identifiers that are used throughout this chapter need to be defined.

Identifiers

- *PD*: Parts manufacturing related risks
- *AS*: Assembly related risks
- *AR*: Aerodynamic Related risks
- *PR*: Power Related risks
- *SR*: Structure Related risks
- *NAV*: Navigational risks
- *PL*: Payload related risks

The assessment of the production risks is based on their likelihood and consequences, for which the scaling is explained in Table 14.1. Risk (R) is an index assigned to different hazards, calculated as the product of the likelihood of occurrence (L) and the severity of the consequence (C). Identifiers highlighted in red represent risks without mitigation because they are either very unlikely to occur or their consequences are relatively insignificant.

Table 14.1: Likelihood and consequence scales for production risks

Likelihood (L)	**Explanation**	**Consequence (C)**	**Explanation**
5.Very high	Guaranteed to happen instantly	5.Catastrophic	Flaw can not be repaired, production must restart
4.High	Will happen repeatedly during production	4.Critical	Significant flaw that needs repairing
3.Moderate	Likely to happen once during production	3.Moderate	Flaw worsens performance measurably
2.Low	Unlikely to happen	2.Low	Flaw has minor effect on performance
1.Very low	Will practically never happen	1.Negligible	Flaw is negligible

14.1.1. Classification of Production Risks

An overview of the identified production risks is provided in Table 14.2. It covers risks related to the direct manufacturing of risks related to the assembly of the structure.

Table 14.2: Risk classification of production risks

Identifier	Hazard	Explanation	R = [L,C]
PD-01	Fibre layer cutting	Risk of cutting through fibre layers during the panel thinning process, leading to reduced material properties	R=[4,3]
PD-02	Finishing imperfections	Risk of insufficient component finishing, resulting in increased environmental degradation	R=[3,3]
PD-03	Undesired curvature of parts	The curvature of wind blades after flattening can still be significant for larger parts, imposing the risk of misalignment between components	R=[3,2]
PD-04	Non-linear behaviour of flax fibre	Flax fibre introduces non-linear behaviour, making the properties of the composite harder to predict, introducing the risk of unexpected failure	R=[2,2]
PD-05	Damaged wind blade sections	Damaged section of the recycled wind blade can have a significant influence on components with small cross-sections, imposing the risk of unexpected failure	R=[4,3]
PD-06	Delamination during production	The steps in processing the wind blade to obtain the desired component introduce the risk of delamination of the composite	R=[4,4]
AS-01	Failure of adhesive bonding	Risk of adhesive bonding failure at critical connections in the structure, imposed by the bonding sensitivity to temperature changes and uneven stress distributions across the joint.	R=[2,5]
AS-02	Failure of metal inserts	Embedding the metal inserts in the parts for the legs, introduces the risk of unexpected behaviour at these joint locations due to the reorientation of the fibres	R=[2,4]

14.1.2. Mitigation Strategies for Production Risks

Critical production risks can have a major influence on the reliability of the structure. Therefore, the mitigation strategies explained in Table 14.3 will be implemented for the risks with the highest risk factor. The right column gives the new risks, showing the effect of the mitigation strategies.

Table 14.3: Mitigation strategies for production related risks

Identifier	Explanation	R = [L,C]
PD-01	While the likelihood of cutting through fiber layers during the thinning process is difficult to mitigate, the consequences can be minimised. These consequences become more critical as the desired thickness decreases. To minimise the impact of cutting through fiber layers, a minimum thickness of 0.005 m shall be maintained for non-load-bearing components	R=[4,1]
PD-02	Flax fibre is very sensitive to direct environmental exposure, requiring special attention to ensure proper coating. This can be achieved by entirely submerging the component in a protective resin, which minimises the likelihood of imperfections in the coating.	R=[1,3]

Identifier	Explanation	R = [L,C]
PD-05	The potential consequences of manufacturing components from damaged wind blade sections cannot be mitigated. However, the likelihood of occurrence can be minimised by using damaged sections only for components with sufficient safety margins and using flawless sections for critical components. Additionally, the leading edge, which contains the most damage, is not used in the manufacturing of any components.	R=[2,3]
PD-06	Delamination shall be addressed in the design by selecting appropriate volume fractions of both the fibres and the thermoplastic, thereby decreasing the likelihood of occurrence. Additionally, suitable processing methods for composite components shall be implemented, such as redirecting fibres to create holes and using compression cutters for sectioning	R=[2,4]
AS-01	Adhesive bonding at critical connections of the beam can have catastrophic consequences. To reduce the consequences, large safety margins shall be in place and the joint shall be be mechanically supported to allow for redundancy	R=[2,2]
AS-02	These mechanical inserts are difficult to analyse and therefore, large safety margins and sufficient redundancy shall be in place to minimise the consequences	R=[2,2]

14.2. Operational Risks

With mitigation strategies in place for the risks related to production, a reliable structure can be brought to life. However, during the operative lifetime of the structure, it will again encounter several risks. For the operational risk assessment, the scaling of the risks is defined based on different scaling compared to the production risks, shown in Table 14.4.

Table 14.4: Likelihood and consequence scales for operational risks

Likelihood (L)	Explanation	Consequence (C)	Explanation
5.Very high	Likely to happen very soon	5.Catastrophic	Damage to surroundings and destruction of the designed structure
4.High	Likely to happen within the first operative weeks	4.Critical	Structure is incapable of fulfilling its functions but is still in one piece
3.Moderate	Likely to happen once in the structure's lifetime	3.Moderate	Designed structure continues with a handicap
2.Low	Unlikely to happen	2.Low	Designed structure is slightly affected
1.Very low	Will practically never happen	1.Negligible	Mission is practically unaffected

14.2.1. Classification of Operational Risks

An overview of the identified operational risks is provided in Table 14.5. It covers general operational risks and how these risks relate to the different subsystems of the structure.

Table 14.5: Risk classification of operational risks

Identifier	Hazard	Explanation	R = [L,C]
AR-01	Affected Aerodynamic Shape	Risk of damage to the wind turbine imposed by weather conditions	9=[3,3]
PR-01	Absence of wind	Windless days impose the risk of the structure to generate insufficient energy from wind	16=[4,4]
PR-02	Battery Malfunction	Using batteries in harsh environmental conditions poses various risks, affecting performance, safety, and length of life	12=[3,4]
PR-03	Clouded Conditions	Clouded conditions impose the risk of insufficient energy being generated by the solar panels	4=[4,1]
SR-01	Structural Damage	Harsh weather conditions can potentially damage structural elements	5=[5,1]
SR-02	Variable Soil Substrate	Differences in soil substrates could result in the structure getting stuck in the sand	12=[4,3]
SR-04	Exposure to Salt Water	Salt water exposure could influence the degradation of mechanical parts in the structure	12=[4,3]
SR-05	Lightning Strike	Large objects in an open area have the risk of being hit by lightning, having catastrophic consequences	10=[2,5]
NAV-01	Small Operating Area	Variable beach area imposes a risk on the successful autonomous navigation of the control system	6=[3,2]
NAV-02	Trapped by Sea Water	Tidal changes could cause the structure to get trapped on an elevated area on the beach	16=[4,4]
NAV-03	Collision	There are a lot different objects on the beach that the structure can potentially collide with, including people	20=[4,5]
PL-04	Payload-related risks	Payload risks related to fulfilling its function, sensors and telecommunication systems malfunctioning	12=[3,4]

14.2.2. Mitigation Strategies for Operational Risks

To improve the reliability and operational lifetime of the structure, critical operational risks shall be limited through the mitigation strategies describes in Table 14.6.

Table 14.6: Mitigation strategies for operational risks

Identifier	Explanation	R = [L,C]
AR-01	Aerodynamic surfaces are sized to account for 60 % of the power budget. To mitigate the consequences of damage to these systems, a suitable safety factor must be imposed on the sizing	6=[3,2]

Identifier	Explanation	R = [L,C]
PR-01	Mitigating the likelihood of this risk is not possible as environmental conditions cannot be influenced. To reduce the consequence of this risk, a battery system shall be in place to allow for energy storage in convenient conditions	8=[4,2]
PR-02	While the consequences of a complete battery malfunction are difficult to mitigate, the likelihood can be reduced by placing them in side the body where they are protected form harsh environmental conditions. During operations, the temperature of the batteries must be monitored and acted on accordingly. The batteries must also be concealed in separate water- and dust proof casings in order to protect them	8=[2,4]
SR-02	Once the structure gets stuck in the sand it is hard to recover. The focus should therefore be on decreasing the likelihood of it getting stuck. Concerning the pressure distribution, the weight of the design must be minimised with the contact surface being maximised. Sufficient ground clearance shall be in place to overcome rough terrain	9=[3,3]
SR-04	Minimising exposure to salt water can be achieved by keeping the distance to the sea line at a specified level. Selection of corrosion-resistant materials and the application of coatings can help the structure be able to withstand salt water without severe degradation. Proper ventilation and drainage prevent water from accumulating in the structure and reduce moisture build up	8=[4,2]
SR-05	The most effective way to to reduce the likelihood of lightning strike is by avoiding large open areas during thunderstorm. Therefore a program shall be in place that instructs the designed structure to move to surrounding beach houses or other high objects when a thunderstorm occurs	5=[1,5]
NAV-02	Getting trapped by sea water can have similar consequences as SR-04. Decreasing the risk of getting trapped by sea water is most effectively done by minimising the likelihood. This can be achieved by making the designed structure aware of tidal changes. When the tide is at its lowest point and it starts to increase, the minimum distance to the sea line shall be increased	4=[1,4]
NAV-03	In order to limit the likelihood of a collision, an obstacle avoidance mechanism should be in place to detect obstacles and take avoiding actions by correcting the course or warn the public. It should also be able to slow down in unexpected events, and thus a braking mechanism should be included	10=[2,5]

14.3. Risk Maps

With all risks identified, the effect of their corresponding mitigation strategies can be clearly visualised in a risk map. There are two risk maps in place, the production related risk map is provided in Figure 14.1, and the operational risk map is given in Figure 14.2. Mitigation strategies are applied to all the risks that are located in the high risk area, for which their old risk classification is shown in grey.

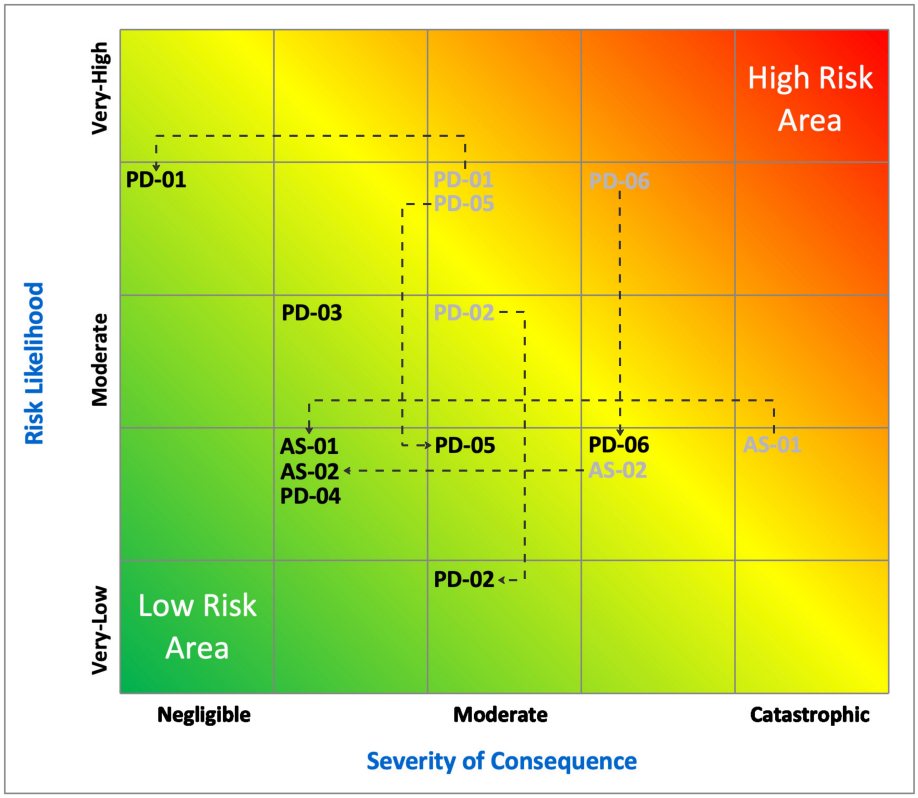

Figure 14.1: Technical risk map for production related risks.

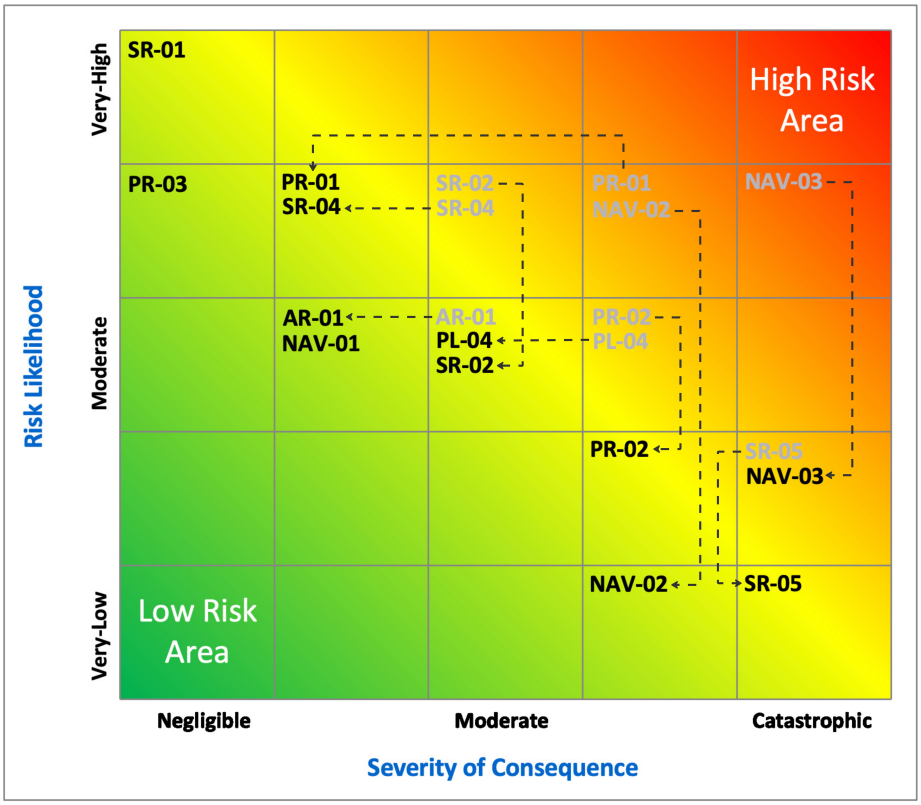

Figure 14.2: Technical risk map for operational risks.

15

Verification and Validation of the Final Design

In this chapter the final design is verified and validated. In Section 15.1, the methods for the verification of all system requirements is layed out. Section 15.2 provides the compliance matrix of all mission and system requirements. The validation of the mission is given in Section 15.3 and finally, the sensitivity analysis of this mission validation is done in subsection 15.3.1.

15.1. System Verification

In this section, all the system requirements are given with their respective verification procedure. Four methods are used for this process:
Test (T) The compliance can be tested using a representative model in realistic conditions.
Analysis (A) The compliance can be analysed by a mathematical tool or another analysis tool.
Demonstration (D) The compliance can be established by a demonstration.
Inspection (I) The compliance can be inspected (visually).

In Table 15.1, all requirements listed with their assigned method. Next to that, a few examples of verification methods are provided.

Table 15.1: Verification method of the mission and system requirements.

Requirement	Method	Requirement	Method
REQ-USER-10-MIS-02	I	**REQ-MAN-02-MIS-02**	D
REQ-MAN-02-MIS-01	I	**REQ-GOV-01-MIS-02**	D
REQ-USER-01-SYS-01	A	**REQ-USER-05-SYS-03**	T
REQ-USER-02-SYS-01	T	**REQ-USER-05-SYS-04**	D
REQ-USER-02-SYS-02	T	**REQ-USER-08-SYS-01**	A
REQ-USER-02-SYS-03	T	**REQ-USER-09-SYS-01**	D
REQ-USER-02-SYS-04	A	**REQ-USER-09-SYS-02**	D
REQ-USER-02-SYS-05	A	**REQ-USER-17-SYS-01**	T
REQ-USER-02-SYS-06	A	**REQ-USER-17-SYS-02**	A
REQ-USER-02-SYS-07	I	**REQ-MAI-01-SYS-01**	I
REQ-USER-02-SYS-08	D	**REQ-MAI-03-SYS-01**	I
REQ-USER-03-SYS-03	D	**REQ-MAI-03-SYS-03**	T
REQ-USER-03-SYS-06	A	**REQ-EoL-01-SYS-01**	A
REQ-USER-04-SYS-01	T	**REQ-EoL-02-SYS-01**	D
REQ-USER-04-SYS-02	A	**REQ-GOV-03-SYS-02**	T
REQ-USER-05-SYS-01	D	**REQ-GOV-03-SYS-04**	T
REQ-USER-05-SYS-02	D		

For example, *REQ-USER-02-SYS-01 The system shall withstand wind up to 100 km/h* needs to be tested to verify the requirement. A (prototype) structure needs to be tested under adequate conditions in an aerodynamic facility.

REQ-USER-02-SYS-04 The operation of system shall not be hindered by corrosion due to saline water for at least 52 weeks needs analysis to be verified. This analysis has to prove compliance by modelling the corrosion effects.

REQ-MAI-03-SYS-01 The structure shall be designed to ensure that its critical components are easily accessible to the maintenance crew requires a demonstration to be verified. This demonstration has to show that (prototype) structure's critical components can be accessed fast and without needing special tools or training.

15.2. System Compliance Matrix

To finalise the design process, the compliance matrix of all the mission and system requirements is checked. This compliance matrix is provided in Table 15.2.

Table 15.2: Compliance matrix of the mission and system requirements

Requirement	Status	Requirement	Status	Requirement	Status
REQ-USER-10-MIS-02	Fully met	**REQ-USER-05-SYS-01**	Fully met	**REQ-USER-02-SYS-07**	To be investigated
REQ-MAN-02-MIS-01	To be investigated	**REQ-USER-05-SYS-02**	Fully met	**REQ-USER-02-SYS-08**	Fully met
REQ-MAN-02-MIS-02	To be investigated	**REQ-USER-05-SYS-03**	To be investigated	**REQ-USER-03-SYS-03**	Fully met
REQ-GOV-01-MIS-02	Fully met	**REQ-USER-05-SYS-04**	Fully met	**REQ-USER-03-SYS-06**	Fully met
REQ-USER-01-SYS-01	Fully met	**REQ-USER-08-SYS-01**	Fully met	**REQ-USER-04-SYS-01**	Fully met
REQ-USER-02-SYS-01	Partially met	**REQ-USER-09-SYS-01**	Fully met	**REQ-USER-04-SYS-02**	Fully met
REQ-USER-02-SYS-02	Fully met	**REQ-USER-09-SYS-02**	Fully met	**REQ-MAI-03-SYS-03**	Fully met
REQ-USER-02-SYS-03	Fully met	**REQ-USER-17-SYS-01**	Fully met	**REQ-EoL-01-SYS-01**	Fully met
REQ-USER-02-SYS-04	Fully met	**REQ-USER-17-SYS-02**	To be investigated	**REQ-EoL-02-SYS-01**	Fully met
REQ-USER-02-SYS-05	Fully met	**REQ-MAI-01-SYS-01**	Fully met	**REQ-GOV-03-SYS-02**	To be investigated
REQ-USER-02-SYS-06	Fully met	**REQ-MAI-03-SYS-01**	Fully met	**REQ-GOV-03-SYS-04**	To be investigated

The system requirement *REQ-USER-02-SYS-01 The system shall withstand wind up to 100 km/h* is partially met because the wind turbine stops operating at 20 m/s but the structure will not get damaged buy the wind. Some requirements still need to be investigated in more detail. The compliance with those requirements will be reassessed in a future stage of the design process.

15.3. Mission Validation

The mission validation is performed by simulating the performance of the structure on a data set of real-time wind speed at Amsterdam from June 15, 2024, to June 16, 2024, which includes both windy and calm days. By retrieving the irradiance and sun elevation angle at Amsterdam on June 24, 2024, a relatively ideal sunny day, the solar power estimation can be determined. The simulated results are in Figure 15.1.

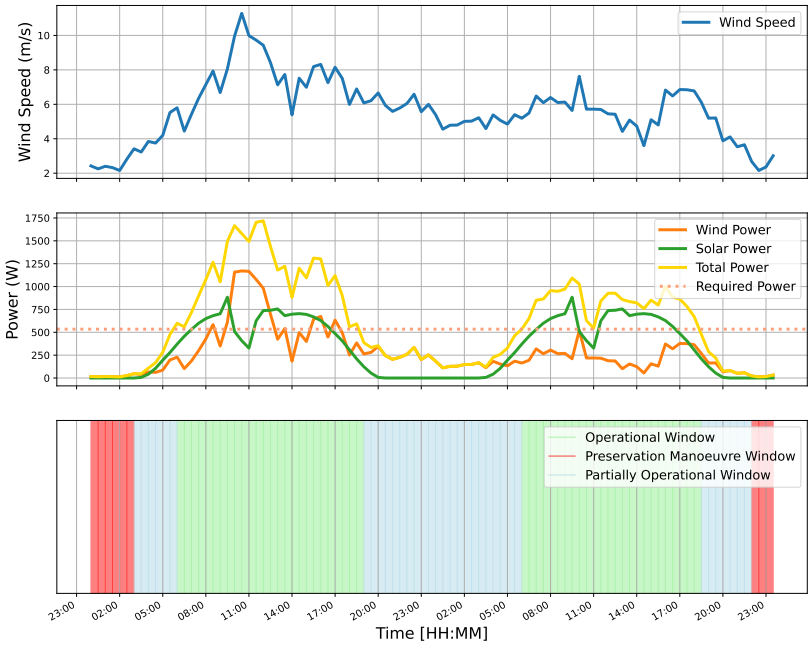

Figure 15.1: Real-time wind speed at Amsterdam from June 15, 2024 to June 16, 2024. The wind power and solar power generation simulation and resulting possible operational windows.

According to the operation strategy, the structure will fully operate if the required power is generated. This operation period is highlighted in Figure 15.1 as operational windows, which can be calculated that in this scenario the total fully operational time is 1580 min in two days. The preservation manoeuvre window starts when the wind speed is lower than 3 m/s and for the rest of the time, the structure will partially operate as the operational plan in Figure 13.11.

15.3.1. Sensitivity Analysis

To evaluate the robustness of the designed system and validation results, a sensitivity analysis is indispensable. Three conditions in Amsterdam (location 1) are included: an ideal situation and no solar power available. Additionally, two other locations are chosen: Loobos (location 2) and Veenkampen (location 3). The results of the sensitivity analysis are presented in Figure 15.2.

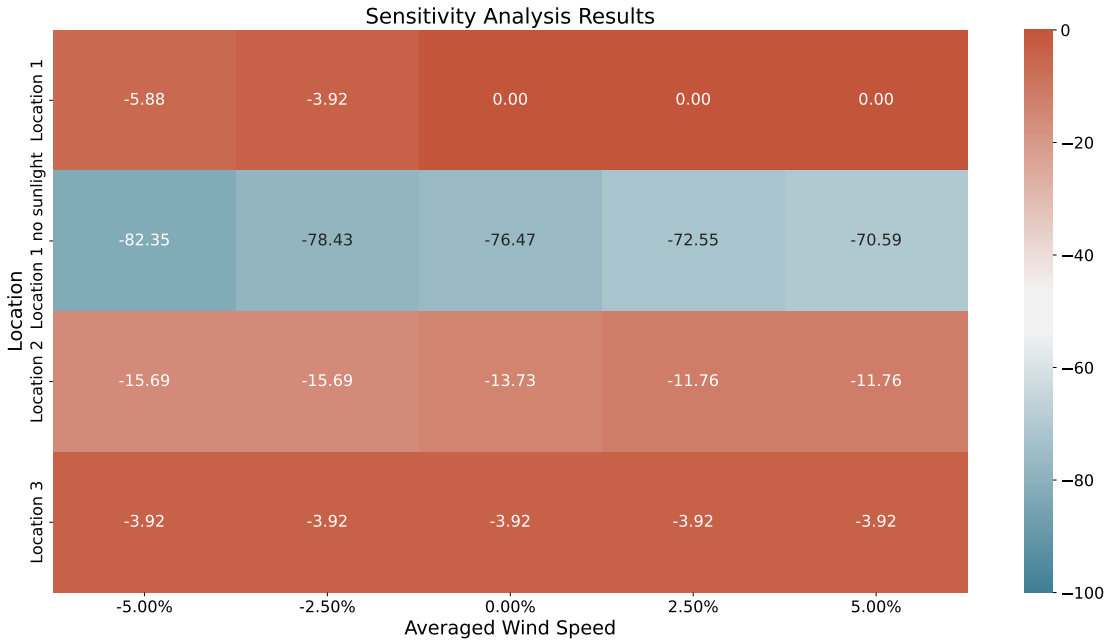

Figure 15.2: Sensitivity analysis results showing the impact of varying the averaged wind speed by ±5.00%, ±2.50%, 0.00% on the operational time under different weather conditions at Amsterdam (location 1), and at different locations such as Loobos (location 2) and Veenkampen (location 3)

The negative values in the red cells indicate a relatively small decrease in operation time compared to 1580 min, while the negative values in the blue cells represent a dramatic decrease in the operational period percentage. From the results, the operational window seems to be sensitive to changes in the average wind speed at some places while remaining unchanged at other places. It can be concluded that the functioning time is highly dependent on the locations and weather conditions. The completion of the mission needs a thorough investigation of the implement field and detailed backup plans for various conditions. Therefore, a better operation strategy and corresponding system optimisation are necessary to enable long-term stable operation.

Although these locations are not the designated areas, accessible wind and solar data from these sites can help conduct the preliminary simulations. It is recommended to perform a more comprehensive sensitivity analysis with detailed real-time data collected from the beach areas.

16

Sustainable Development

This chapter discusses the ways sustainability is taken into account in the final design. The chapter is divided into five sections which correspond with the different phases of the system lifecycle; material sourcing in Section 16.1, manufacturing in Section 16.2, logistics in Section 16.3, operation and maintenance in Section 16.4, and finally, end-of-life of the system in Section 16.5

16.1. Materials

To analyse the impact of the use of resources, these elements are categorised based on their material: flax/coPOM composite elements, bamboo elements, electrical components, and metal components. Each category of material is analysed separately.

The recycled next-gen composite is the material used for the main structural elements and the wind turbine. Reusing an already existing processed material eliminates the environmental impact and energy consumption from extracting raw materials and processing them into half fabricates. These elements are responsible for a high fraction of the total structure mass, and thus the overall impact due to used resources is greatly reduced.

Bamboo, used for shafts and the pole, is known to be one of the fastest-growing, most abundant plant in the world. Although they are mostly available in tropical regions, there are several bamboo nurseries in Europe that supply the material for construction. During their lifetime, bamboo plants absorb carbon dioxide from the atmosphere, making bamboo a carbon-neutral material. [100, 101]

The electrical components are the least sustainable out of all elements. All components are to be purchased off-the-shelf and the majority of the components are difficult to recycle. Nonetheless, some efforts were made to incorporate sustainability into the electrical component selection, including revising the sodium-ion battery selection, which involves a less energy-consuming and less environmentally harmful production process.

Metal parts also need to be purchased off-the-shelf. However, the parts are made of a single material and therefore are easily recycled. Furthermore, metal recycling points are widely available across the world.

16.2. Manufacturing

This subsection is dedicated to assessing sustainability in the manufacturing process. The main contribution to sustainability is the production of simple and similar parts to minimise the manufacturing resources required.

Lean manufacturing is a manufacturing process aiming at eliminating non-essential activities while adding value to the product [102]. Following the lean manufacturing principle, a step-by-step production plan was created to ensure that waste is minimised. All parts were designed in forms of relatively simple shapes as discussed in Section 6.4. Frame beams have rectangular shapes that allow the materials to be directly derived by cutting them consecutively without spacing. In another case, the moulds used to create aerofoils can be re-used for the entire WTB as they have the exact same dimensions. The simplicity of part shapes and the same or similar dimensions of parts allow for minimising waste, thereby maintaining the value of sustainability within the process.

16.3. Logistics

As discussed in Figure 13.11, sectioning the WTB at a wind farm indicates that the large turbine blades can be cut into smaller pieces. This step reduces the required size of trucks needed to transport the pieces to the workshop. Smaller trucks release less carbon dioxide and consume less fuel. It could also be possible to utilise electrically powered trucks to eliminate emissions created during material transportation.

Ideally, the workshop is designed to operate on green energy during manufacturing processes. Electricity is to be generated by solar panels installed on the roof of the workshop and wind turbines located outside the workshop.

16.4. Operation & Maintenance

At the stage of operation, one of the key contributions to sustainability is the functions served by the final design. As discussed in Chapter 7, the final function of the designed system is to be selected, and the available power for this function presented in Chapter 13 suggests that waste collection would be a feasible option. Currently, waste on the Dutch coast is collected by people, which takes a lot of manpower, or by raking and sifting machines dragged by large tractors. These tractors require traditional fuels and emit large sums of carbon dioxide. The designed system is entirely run by renewable energy, wind and solar, and therefore is much more sustainable than the existing solution.

Regarding maintenance, minor damages to the final design can be repaired on-site. This approach supports sustainability by eliminating the need to transport the entire structure to a workshop for repairs thus ultimately eliminating the emissions that otherwise would have been created.

16.5. End-of-life of the Structure

An important consideration regarding sustainability is the end-of-life of the structure. This section aims to describe the end-of-life scenario for the structure and explain how it could be re-used, whilst maintaining as much of the material properties as possible. End-of-life solutions are highly dependent on the usage and operational duration of the structure. As explained in Section 12.11, the mechanical properties of the structure can vary greatly due to the harsh environment, significantly affecting the possibilities of end-of-life.

Therefore, two scenarios are investigated here for the operational life of the structure:

- The structure is used for a relatively short period, such as for educational purposes during events or to meet a specific, short-term need (e.g., a desalination system on a beach for three months during the summer).
- The structure is used for its maximum operational life, fulfilling its intended functionality until failure (e.g., collecting trash along the Dutch coastline).

The end-of-life scenarios for these two operational lifespans are examined in subsection 16.5.1 and subsection 16.5.2, respectively.

16.5.1. End-of-life Solutions: Short Operational Life

Since the operational life has been short, the flax/coPOM composite elements are likely to retain most of their original mechanical properties. Thus, these composite elements can be reused in load-bearing applications to avoid downgrading their utility. The beams from the load-bearing frame and legs can be extracted and resized for various structural applications where a high safety factor is acceptable. Examples of reuse include constructing partitions in homes or building bed frames. Additionally, the panels from the structure can be re-used as wall panels or bike shelters,

retaining their original form and function.

The aerofoils present a unique challenge due to their specific shapes and twist angles, which limit their reusability in other applications. However, two solutions are conceivable. First, the aerofoils can be reused in vertical axis wind turbines (VAWT) Alternatively, they can be melted and reshaped into desired structures.

The shaft and crankshaft made of bamboo can also be reused as such for multiple applications, ranging from garden structures to lightweight construction support poles.

The electrical equipment and metal components can be safely extracted and re-used in other contexts. These components typically have longer lifespans and can be integrated into new systems without significant loss of functionality.

16.5.2. End-of-life solutions: maximum operational life

Towards the end of its lifecycle, the composite structure experiences a significant decline in its load-bearing capabilities. Despite this limitation, there are viable recycling avenues available. One approach involves grinding the beams into small particles, which can then serve as filler material in the production of new composite products. Another method leverages the thermoplastic properties of the material, allowing it to be melted and reshaped into items like composite boards. These boards find practical uses in non-load-bearing applications such as interior decoration, furniture backing, or signage.

At the end of the structure's maximum operational life, bamboo elements, such as the shaft and crankshaft, may exhibit signs of wear and deterioration. However, due to bamboo's natural durability and biodegradability, they can still be repurposed in various ways. Repurposing options include using it for creating garden structures such as trellises and fencing, enhancing outdoor aesthetics with their natural strength. Additionally, bamboo can be employed in diverse craft and DIY projects, from home decor to small furniture items. If these elements are no longer suitable for reuse, they can be composted and naturally decomposed to enrich soil quality and support eco-friendly disposal practices.

Given that the electrical components were protected by the composite panel box, they should remain functional even after the structure's maximum lifetime. However, a precautionary check-up should be implemented to inspect the electrical components before reintegrating them on the market.

At the end of life, the metal components will be significantly corroded by the saline environment. Therefore, they cannot be used for their primary functionality anymore. Corroded metal can be broken down into scrap, melted, and reprocessed into lower-grade products for construction reinforcement, manufacturing new metal alloys, or industrial applications where high-grade properties are not essential.

17

Post DSE Activities

After this DSE project is finished, many tasks still have to be performed to end up with a functioning structure on the beach. These tasks involve detailed designing, testing and production. All these tasks are layed out in this chapter. In Section 17.1, the project design and development logic is discussed. Then, the Gantt chart, that follows from the logic diagram is provided in Section 17.2.

17.1. Project Design and Development Logic

After this DSE project is over and the proposed design has been approved, the implementation phase will begin. The post DSE activities are planned out in five main phases, as shown in the project design and development logic in Figure 17.1a.

The first phase is research and development, as there are still some requirements that need further investigation. Iterations should take place until the design converges. Then, the proposed improvements are taken into the production phase. This step aims at maufacturing subassemblies of the structure that can be tested in the third phase, testing.

During the testing phase, the improved subassemblies are evaluated against the requirements. In case the performance is not satisfactory, the complete design needs to be revised starting at the analysis of the subsystems in the first phase. If the components pass the tests, the next phase takes place.

The fourth phase is assembly, where the tested subassemblies are transported to the operating location and integrated with the functional module into the full structure. At the end of this phase, the complete structure is tested once again to ensure that it meets the system requirements. After those, the structure is fully operational and can be deployed.

The last phase is life cycle management. During the life time of the structure, maintenance needs to be performed and when the structure is at its End-of-Life, the adequate procedure should be applied.

17.2. Gantt Chart

From the project design and development logic diagram follows the timeline of the project. This timeline is visualised in a Gantt Chart and is provided in Figure 17.1b. In the Gantt Chart, the five phases with the different tasks can be seen with their approximate duration in months. The task called 'Perform maintenance' is indicated with a striped bar because this task continues till the structure is EOL and this date is unknown.

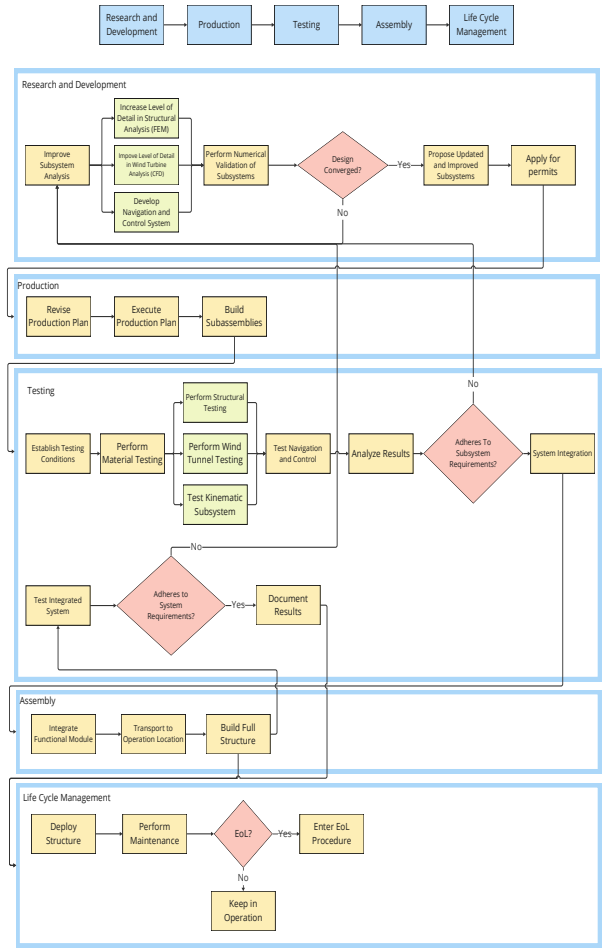

(a) Project Design and Development Logic

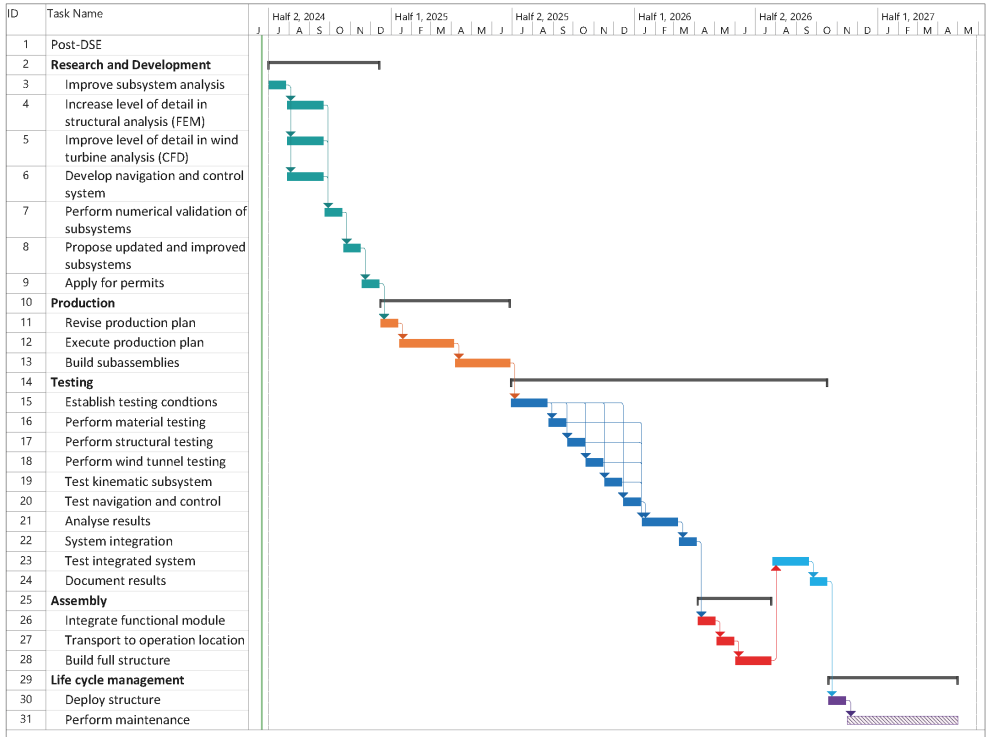

(b) Gantt chart of the project design and development phase of the DSE project. Colors indicate different phases of the project.

Figure 17.1

18

Conclusions

In recent years, researchers have investigated the potential of using natural-fiber reinforced thermoplastics to replace GFRP in wind turbine blades. One of the key arguments advanced by the scientific community to justify this shift is the recyclability of natural-fiber reinforced thermoplastics at the blades' end-of-life stage. However, the literature still lacks design cases demonstrating this recycling potential. Acknowledging this gap, the team embarked on a project aimed at transforming concepts as abstract as "circularity" and "recyclability" into an impactful, concrete, and viable design.

To make this case as powerful as possible, the team chose to combine the challenges associated with recycling composites, wind energy, and autonomous navigation. This resulted in the design of an autonomous wind-powered structure capable of performing a societally impactful function.

Given the project's multiple facets and lack of precedents, it offered a vast, unexplored playground with almost no prior constraints. Echoing Michelangelo's insight that "art lives on constraint and dies of freedom", the first phase focused on initial investigations to establish constraints and limit the design space, paving the way for deeper exploration and innovation in the second phase of the project.

This first phase began with a market analysis to demonstrate the growing need to recycle decommissioned wind blades and explore the potential of wind-powered structures. Following this, a trade-off analysis was conducted to determine the concept to be further investigated. The outcome of this first phase was a structure powered by a vertical axis wind turbine, supplemented by solar panels, utilizing Jansen's linkage to facilitate motion, and designed to perform a set of different functionalities to allow for modularity.

The second phase involved the detailed design of the concept, as explained in this report. To address this phase comprehensively, the prerequisite was to determine the constraints imposed by the material recovered from decommissioned wind blades. Material analysis revealed that Flax/-coPOM, though not the most popular combination, was ideal for its mechanical performance and sustainability. Notably, flax fibers capture CO2 during growth, and the use of thermoplastic allows for easy reshaping. Assessing this reshaping potential alongside manufacturing constraints, the best options were identified as reshaping the recovered material into panels or beams. Furthermore, the melting behavior of thermoplastics was explored to design joints by reshaping the fibers, thereby creating new load paths. This innovative approach deserves more attention from researchers, as it has the potential to be generalized to many structures.

With these prerequisites discussed, the focus shifted to integrating all the technical aspects into the design: wind turbine design, kinematics mechanism, control and navigation systems, power system, and structural analysis.

Key outcomes can be highlighted:

From the wind turbine design, it was demonstrated that sufficient power could be generated by a moving wind turbine. Unlike the current market, which designs wind turbines for the rated speed, this analysis accounted for the lower airspeed due to the atmospheric boundary layer and the actual weather conditions on the Dutch coastline, providing a robust power supply for most wind conditions found on the coastline.

In the kinematics chapter, advancements were made to the traditional legs employed in the "Strandbeest" concept through two key improvements. Firstly, the leg geometry was modified to enable smoother motion and achieve a greater step height, addressing current challenges faced by "Strandbeest" structures in overcoming obstacles. Furthermore, an intelligent feet system was developed to passively adapt to various soil conditions.

In the structural analysis phase, extensive investigations were conducted on stress, deflection, and stability. These analyses encompassed dynamic stress analysis in linkage-type legs, marking a pioneering endeavor in this field. Additionally, a comprehensive failure analysis was undertaken for the first time in strandbeest-inspired design. This led to modifications enabling controlled failure after a predetermined period, a novel approach in advancing the durability and reliability of the design.

By integrating all these system analyses, it was shown that an ambitious design could be fabricated using a decommissioned wind blade. The final design consists of 80% recycled composite material, with a total cost estimated at 30,000 ± 5,000 €. This design is capable of generating 534 W under average Dutch weather conditions, operating effectively 55% of the time, and experiencing complete downtime less than 10% of the time.

This project has introduced several challenges that warrant further research. A primary recommendation is to delve deeper into the extraction of materials from wind turbines. In this study, it was determined that flattening the extracted elements from wind blades for use in structural inputs is more practical and can be applied universally across various blade geometries, irrespective of their curvature. However, there may be a more cost-effective approach by directly reusing the extracted elements without flattening them, thereby eliminating the reshaping process. To achieve this, a more precise determination of wind blade geometries is essential, which is currently hindered by limitations in research on next-generation blades. Moreover, companies involved in this sector often hesitate to disclose their advancements. Therefore, collaboration with major industry players is recommended to facilitate significant advancements in extracting necessary thermoplastic elements from wind blades.

Considering the cost-driven nature of the wind energy sector, it is advisable to conduct a thorough, quantified assessment of this design. Such an analysis could potentially incentivize the industry to embrace these solutions, as they promise cost savings and enhance public perception.

Reflecting on this project, it has illustrated that integrating end-of-life considerations into wind blade design can make a circular model achievable for the wind energy sector. This demonstration aims to inspire a paradigm shift throughout the entire aerospace industry.

"Setting an example is not the main means of influencing others, it is the only means." – Albert Einstein

References

[1] X. Chen and M. A. Eder. "A critical review of damage and failure of composite wind turbine blade structures". In: 2020.

[2] Ralph EH Sims, Hans-Holger Rogner, and Ken Gregory. "Carbon emission and mitigation cost comparisons between fossil fuel, nuclear and renewable energy resources for electricity generation". In: *Energy policy* (2003).

[3] Kumar et al. "Wind energy: Trends and enabling technologies". In: *Renewable and Sustainable Energy Reviews* (2016).

[4] Dennis G Shepherd. *Historical development of the windmill*. Tech. rep. NASA, 1990.

[5] European Court of Auditors. *Special report 22/2023: Offshore renewable energy in the EU*. 2023. URL: https://www.eca.europa.eu/en/publications?ref=SR-2023-22.

[6] G. Lichtenegger et al. "Offshore and onshore wind turbine blade waste material forecast at a regional level in Europe until 2050". In: *Waste management* (2020).

[7] M. Khalid et al. "Recycling of wind turbine blades through modern recycling technologies: A road to zero waste". In: *Renewable Energy Focus* (2023). DOI: https://doi.org/10.1016/j.ref.2023.02.001.

[8] Chen J., Wang J., and Ni A. "Recycling and reuse of composite materials for wind turbine blades: An overview". In: *Journal of Reinforced Plastics and Composites* (2019). DOI: 10.1177/0731684419833470.

[9] Shuaib N. Ai. and Mativenga P. T. "Energy demand in mechanical recycling of glass fibre reinforced thermoset plastic composites". In: *Journal of Cleaner Production* (2016).

[10] Beauson et al. "Recycling of shredded composites from wind turbine blades in new thermoset polymer composites". In: *Applied Science and Manufacturing* (2016).

[11] L. Hartman. *Wind Turbines: the Bigger, the Better*. 2023. URL: https://www.energy.gov/eere/articles/wind-turbines-bigger-better.

[12] L. Hartman. *Haliade-X offshore wind turbine*. URL: https://www.gevernova.com/wind-power/offshore-wind/haliade-x-offshore-turbine.

[13] European Commission. *More circular, less carbon: chemical recycling holds promise for wind-turbine blade waste*. URL: https://environment.ec.europa.eu/news/.

[14] "WindEurope". In: (June 2021). URL: https://windeurope.org/newsroom/press-releases/wind-industry-calls-for-europe-wide-ban-on-landfilling-turbine-blades/. (accessed: 14-05-2024).

[15] Z. Janipour. *Beyond design life: What to do with aging wind turbines in Europe?* URL: https://www.rabobank.com/knowledge/d011409804-beyond-design-life-what-to-do-with-aging-wind-turbines-in-europe.

[16] Theo Jansen. *Strandbeest*. URL: https://www.strandbeest.com/strandbeest.

[17] S. Pronk. *"Repurposing wind turbine blades as a construction material"*. Sept. 2021.

[18] DSE group 17. *Functional Structure from Recycled Wind Turbine Blades - Midterm Report*. Tech. rep. Delft University of Technology, 2024.

[19] K. N. Keya et al. "Natural fiber reinforced polymer composites: history, types, advantages and applications". In: *Materials Engineering Research* (2019).

[20] M. Barth and M. Carus. "Carbon footprint and sustainability of different natural fibres for biocomposites and insulation material". In: (2015).

[21] C. A. Fuentes et al. "Effect of physical adhesion on mechanical behaviour of bamboo fibre reinforced thermoplastic composites". In: *Colloids and surfaces A: physicochemical and engineering aspects* (2013).

[22] H. Brodowsky and E. Mäder. "Jute fibre/epoxy composites: Surface properties and interfacial adhesion". In: *Composites science and technology* (2012).

[23] D. Jones et al. *Performance of bio-based building materials*. Woodhead Publishing, 2017.

[24] K. Van de Velde and P. Kiekens. "Thermoplastic polymers: overview of several properties and their consequences in flax fibre reinforced composites". In: *Polymer testing* (2001).

[25] J. George, E.T.J. Klompen, and T. Peijs. "Thermal degradation of green and upgraded flax fibres". In: *Advanced Composites Letters* (2001).

[26] M. M. Lu, C. A. Fuentes, and A. W. Van Vuure. "Moisture sorption and swelling of flax fibre and flax fibre composites". In: *Composites Part B: Engineering* (2022).

[27] Z. Azwa et al. "A review on the degradability of polymeric composites based on natural fibres". In: *Materials and Design* (2013).

[28] W. Woigk et al. “Interface properties and their effect on the mechanical performance of flax fibre thermoplastic composites”. In: *Applied Science and Manufacturing* (2019).
[29] M. Le Gall et al. “Recommended flax fibre density values for composite property predictions”. In: *Industrial Crops and Products* (2018). DOI: https://doi.org/10.1016/j.indcrop.2018.01.065.
[30] G. Coroller et al. “Effect of flax fibres individualisation on tensile failure of flax/epoxy unidirectional composite”. In: *Composites Part A: Applied Science and Manufacturing* (2013). DOI: https://doi.org/10.1016/j.compositesa.2013.03.018.
[31] J. Thomason et al. “Characterisation of the Anisotropic Thermoelastic Properties of Natural Fibres for Composite Reinforcement”. In: *Fibers* (2017). DOI: 10.3390/fib5040036.
[32] J. Zhu et al. “Recent Development of Flax Fibres and Their Reinforced Composites Based on Different Polymeric Matrices”. In: *Materials* (2013). DOI: 0.3390/ma6115171.
[33] M. Haris et al. “Preliminary analysis of hybrid laminate composite for aircraft radome application”. In: *IOP Conference Series: Materials Science and Engineering* (2019). DOI: 10.1088/1757-899X/697/1/012032.
[34] H. M. Su and T. Y. Kam. “Reliability analysis of composite wind turbine blades considering material degradation of blades”. In: *Composite Structures* (2020).
[35] P. Majewski et al. “End-of-life policy considerations for wind turbine blades”. In: *Renewable and Sustainable Energy Reviews* (2022).
[36] D. Pantaloni et al. “Influence of water ageing on the mechanical properties of flax/PLA non-woven composites”. In: *Polymer Degradation and Stability* (2022).
[37] S. Pronk. “Repurposing wind turbine blades as a construction material: A method to extract valuable elements from a decommissioned wind turbine blade for applications in the construction industry”. In: (2022).
[38] P. J. Schubel and R. J. Crossley. “Wind turbine blade design”. In: *Energies* (2012).
[39] D. K. Shanmugam et al. “Comparative study of jetting machining technologies over laser machining technology for cutting composite materials”. In: *Composite Structures* (2002).
[40] D. T. Griffith and T. D. Ashwill. *The Sandia 100-meter All-glass Baseline Wind Turbine Blade: SNL100-00*. accessed 03 June 2024. 2011. URL: https://energy.sandia.gov/wp-content/gallery/uploads/.
[41] F. Da Cunha Saraiva. “Development of press forming techniques for thermoplastic composites: Investigation of a multiple step forming approach”. In: 2017.
[42] “Joining and Bonding of Composite Parts – The Structural Adhesive Advantage”. In: (). accessed 14 June 2024. URL: https://multimedia.3m.com/mws/media/1586280O/iatd-joining-and-bonding-structural-adhesives-white-paper.pdf.
[43] Sastry V.R. *Plastics in Medical Devices*. Elsevier, 2022.
[44] accessed 14 June 2024. URL: https://www.3m.com/3M/en/US/p/d/b40066446/.
[45] J. Feito et al. “Experimental Analysis of the Influence of Drill Point Angle and Wear on the Drilling of Woven CFRPs”. In: *Materials* 7 (2014). DOI: 10.3390/ma7064258.
[46] J. Troschitz et al. “Joining Processes for Fibre-Reinforced Thermoplastics: Phenomena and Characterisation”. In: *Materials* 15 (2022). DOI: 10.3390/ma15155454.
[47] Gabrielli G. and T. von Kármán. “What price speed? Specific power required for propulsion of vehicles”. In: *Mech. Eng. 72* (1950).
[48] K. Komoda and H. Wagatsuma. “Energy-efficacy comparisons and multibody dynamics analyses of legged robots with different closed-loop mechanisms”. In: (2016).
[49] *”Meteorological data portal”*.
[50] R. Hoxha et al. “Influence of seasonal air density fluctuations on wind speed distribution in complex terrains in the context of energy yield”. In: *Energ. Ecol. Environ* (2024).
[51] R. Agterberg and J. Wieringa. “Mesoscale terrain roughness mapping of the Netherlands”. In: (1989).
[52] J. Donker, M Van Maarseveen, and G Ruessink. “Spatio-Temporal Variations in Foredune Dynamics Determined with Mobile Laser Scanning”. In: *Journal of Marine Science and Engineering* (2018). DOI: 10.3390/jmse6040126.
[53] M. A. Al-Rawajfeh and M. R. Gomaa. “Comparison between horizontal and vertical axis wind turbine”. In: *International Journal of Applied Power Engineering* (2023). DOI: 10.11591/ijape.v12.i1.pp13-23.

[54] J. Li et al. “A review on development of offshore wind energy conversion system”. In: *International Journal of Energy Research* (2020). DOI: 10.1002/er.5751.
[55] W. Tjiu et al. “Darrieus vertical axis wind turbine for power generation I: Assessment of Darrieus VAWT configurations”. In: *Renewable Energy* (2015). DOI: 10.1016/j.renene.2014.09.038.
[56] F. Scheurich and R. E. Brown. “Modelling the aerodynamics of vertical-axis wind turbines in unsteady wind conditions”. In: *Wind Energy* (2013). DOI: 10.1002/we.532.
[57] D.A.M. De Tavernier. “Aerodynamic Advances in Vertical-Axis Wind Turbines”. In: (2021). DOI: 10.4233/uuid:7086f01f-28e7-4e1b-bf97-bb3e38dd22b9.
[58] P. Jamieson et al. “Development of a multi rotor floating offshore system based on vertical axis wind turbines”. In: *Journal of Physics: Conference Series* 2275 (2022). DOI: 10.1088/17426596/2257/1/012002..
[59] D. Rominy et al. “Self-starting capability of a Darrieus turbine”. In: *Journal of Power and Energy* (2007). DOI: 10.1243/09576509JPE340.
[60] W. Miao et al. “Recommendation for strut designs of vertical axis wind turbines: Effects of strut profiles and connecting configurations on the aerodynamic performance”. In: *Energy Conversion and Management* 276 (2023). DOI: 10.1016/j.enconman.2022.116436.
[61] N. Kumar et al. “Aerodynamic braking system analysis of horizontal axis wind turbine using slotted airfoil”. In: *Materials Today: Proceedings* (2020). DOI: 10.1016/j.matpr.2020.06.334.
[62] B. P. McNiff, W. D. Musial, and R. Errichello. “Variations in Gear Fatigue Life for Different Wind Turbine Braking Stategies”. In: *AWEA Wind Power ’90* (1990).
[63] N. Afanasieva. “The Effect of Angle of Attack and Flow Conditions on Turbulent Boundary Layer Noise of Small Wind Turbines”. In: (2017). DOI: 10.1038/s43017-022-00387-5.
[64] A.D. Peacock et al. “Micro wind turbines in the UK domestic sector”. In: *Energy and Buildings* (2008). DOI: 10.1016/j.enbuild.2007.12.004.
[65] B. Leblanc and C. Ferreira. “Experimental Demonstration of Thrust Vectoring with a Vertical Axis Wind Turbine using Normal Load Measurements”. In: *Journal of Physics: Conference Series* (2020). DOI: 10.1088/1742-6596/1618/5/052030.
[66] A. Alexeev, A. Dobra, and E. Lovasz. “Walking Robot with Modified Jansen Linkage”. In: *Machine and Industrial Design in Mechanical Engineering* (2021).
[67] H. Khairnar, V. Phalle, and S. Mantha. “Comparative Frictional Analysis of Automobile Drum and Disc Brakes”. In: (2016).
[68] A. Badawy. “Computed Tomographic Anatomy of the Fore Foot in One-Humped Camel”. In: (2011).
[69] G. Grigorev et al. “Permissible ground pressure of wheeled forestry vehicles depending on the ground conditions”. In: *IOP Conf. Series: Materials Science and Engineering* (2020). DOI: 10.1088/1757-899X/817/1/012011.
[70] JOUAV. “LiDAR vs. Radar: What’s the Difference?” In: (2024).
[71] MaxBotix. “Ultrasonic Sensors vs. LiDAR: Which One Should You Use?” In: (2021).
[72] Manning C. In: (Sept. 2023). URL: https://www.nasa.gov/directorates/somd/space-communications-navigation-program/.
[73] “Module 4 - Introduction to Electrical Conductors, Wiring Techniques and Schematic Reading”. In: Naval Education, Training Professional Development, and Technology Center, 1998.
[74] D. Wood and P. Freere. “Stand-alone wind energy systems”. In: Woodhead Publishing, 2010. DOI: doi.org/10.1533/9781845699628.2.165.
[75] K. M. Abraham. “How Comparable Are Sodium-Ion Batteries to Lithium-Ion Counterparts?” In: *ACS Energy Letters* (2020). DOI: 10.1021/acsenergylett.0c02181.
[76] G. J. May, A. Davidson, and B. Monahov. “Lead batteries for utility energy storage: A review”. In: *Journal of Energy Storage* (2018). DOI: 10.1016/j.est.2017.11.008.
[77] “Abundance of Elements in the Earth’s Crust and in the Sea”. In: *CRC Handbook of Chemistry and Physics*. Ed. by Haynes W. H. CRC Press, 2016.
[78] M. L. Vera et al. “Environmental impact of direct lithium extraction from brines”. In: *Nature Reviews Earth and Environment* (2023). DOI: 10.1038/s43017-022-00387-5.
[79] M. Schirber. “Sodium as a Green Substitute for Lithium in Batteries”. In: *Physics* 17 (2024). DOI: 10.1103/Physics.17.73.

[80] D. H. Kang, M. Chen, and O. A. Ogunseitan. "Potential environmental and human health impacts of rechargeable lithium batteries in electronic waste". In: *Environmental Science and Technology* 47 (2013). DOI: 10.1021/es400614y.
[81] *Lead acid batteries*. accessed 12 June 2024. URL: https://www.safework.sa.gov.au/workplaces/chemicals-substances-and-explosives/lead-acid-batteries.
[82] accessed 13 June 2024. URL: https://faradion.co.uk/technology-benefits/strong-performance/.
[83] A. Oun et al. "Influence of elevated temperature on the mechanical properties of hybrid flax-fiber-epoxy composites incorporating graphene". In: *Polymers* (2022).
[84] Masdar A. et al. "Implementation of Connection System of Wooden Plate and Wooden Clamp on Joint Model of Bamboo Truss Structures". In: *International Journal of GEOMATE* (2019). DOI: 10.21660/2019.59.4589.
[85] D. T. Griffith and T. D. Ashwill. "The Sandia 100-meter All-glass Baseline Wind Turbine Blade: SNL100-00". In: (2011).
[86] K. Cox and A. Echtermeyer. "Structural Design and Analysis of a 10MW Wind Turbine Blade". In: *Energy Procedia* (2012). DOI: 10.1016/j.egypro.2012.06.101.
[87] J.A. Pascoe. *Lecture 6 Bonding Welding 2024*. Feb. 2024.
[88] S. Ebnesajjad. *Adhesives Technology Handbook (Second)*. William Andrew, 2009.
[89] I. Ashcroft and A. Crocombe. *Modeling of Adhesively Bonded Joints*. Springer, 2008.
[90] S. Liang, P. Gning, and L. Guillaumat. "A comparative study of fatigue behaviour of flax/epoxy and glass/epoxy composites". In: *Composites Science and Technology* (2012).
[91] T. Cadu et al. "Cyclic hygrothermal ageing of flax fibers' bundles and unidirectional flax/epoxy composite. Are bio-based reinforced composites so sensitive?" In: *Industrial Crops and Products* (2019).
[92] V. Fiore et al. "Assessment of performance degradation of hybrid flax-glass fiber reinforced epoxy composites during a salt spray fog/dry aging cycle". In: *Composites Part B: Engineering* (2022).
[93] V. Fiore et al. "On the response of flax fiber reinforced composites under salt-fog/dry conditions: Reversible and irreversible performances degradation". In: (2022).
[94] V. Fiore et al. "Effect of repeated salt fog-dry cycles on the performances reversibility of flax fiber reinforced composites". In: *Polymer Testing* (2024).
[95] L. Calabrese et al. "Performances recovery of flax fiber reinforced composites after salt-fog aging test". In: *Journal of Composites Science* (2022).
[96] L. Calabrese et al. "Flax–Glass Fiber Reinforced Hybrid Composites Exposed to a Salt-Fog/Dry Cycle: A Simplified Approach to Predict Their Performance Recovery". In: *Polymers* (2023).
[97] V. Kumar et al. "Effect of corrosion on IF-Steel in simulated-marine environment via its mechanical properties". In: *Materials Today Communications* (2023).
[98] I. Elfaleh et al. "A comprehensive review of natural fibers and their composites: an eco-friendly alternative to conventional materials". In: *Results in Engineering* (2023).
[99] T. H. van der Meulen et al. "Offshore wind farm decommissioning". In: (2020).
[100] Emamverdian A. et al. "Application of Bamboo Plants in Nine Aspects". In: *The Scientific World Journal* (2020). DOI: 10.1155/2020/7284203.
[101] DURAND C. *5 Surprising Countries That Are Growing Bamboo*. 2021. URL: https://bamboou.com/5-surprising-countries-that-are-growing-bamboo/.
[102] T. Sijpkes. *Lecture 9B. Lean Manufacturing*. Feb. 2024.